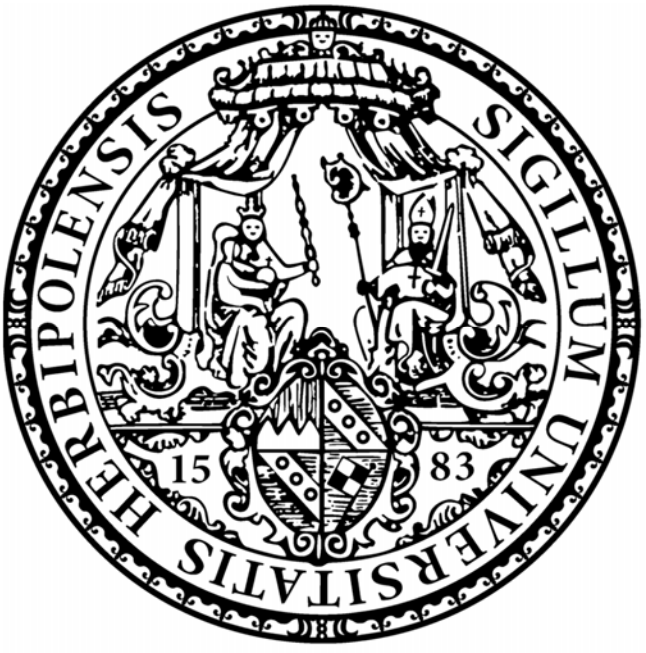

Intestinal stem cells and the Na^+-D-Glucose Transporter SGLT1: potential targets regarding future therapeutic strategies for diabetes

Intestinale Stammzellen und der Na^+-D-Glukose Transporter SGLT1: potentielle Ansatzpunkte neuartiger Therapien für Diabetes Patienten

Doctoral thesis for a doctoral degree
at the Graduate School of Life Sciences (GSLS),
Julius-Maximilians-Universität Würzburg,
Section Biomedicine

submitted by

Markus Mühlemann

From

Bern (Switzerland)

Würzburg 2018

Submitted on:

……..……..

Office stamp

Members of the Thesis committee:

Chairperson:

…….....

Primary Supervisor: PD Dr. Marco Metzger

Second Supervisor: Prof. Dr. Heike Walles

Third Supervisor: Prof. Dr. Frank Edenhofer

Date of Public Defense:

…….....

Date of Receipt of certificates:

…….....

Dedicated to my family

“Happiness is only real when shared”

-Chris Mc Candless-

Table of contents

Abstract

The pancreas and the small intestine are pivotal organs acting in close synergism to regulate glucose metabolism. After absorption and processing of dietary glucose within the small intestine, insulin and glucagon are released from pancreatic islet cells to maintain blood glucose homeostasis. Malfunctions affecting either individual, organ-specific functions or the sophisticated interplay of both organs can result in massive complications and pathologic conditions. One of the most serious metabolic diseases of our society is diabetes mellitus (DM) that is hallmarked by a disturbance of blood glucose homeostasis. Type 1 (T1DM) and type 2 (T2DM) are the main forms of the disease and both are characterized by chronic hyperglycemia, a condition that evokes severe comorbidities in the long-term. In the past, several standard treatment options allowed a more or less adequate therapy for diabetic patients. Albeit there is much effort to develop new therapeutic interventions to treat diabetic patients in a more efficient way, no cure is available so far. In view of the urgent need for alternative treatment options, a more systemic look on whole organ systems, their biological relation and complex interplay is needed when developing new therapeutic strategies for DM.

T1DM is hallmarked by an autoimmune-mediated destruction of the pancreatic β-cell mass resulting in a complete lack of insulin that is in most patients restored by applying a life-long recombinant insulin therapy. Therefore, novel regenerative medicine-based concepts focus on the derivation of bioartificial β-like cells from diverse stem cell sources *in vitro* that survive and sustain to secrete insulin after implantation *in vivo*. In this context, the first part of this thesis analyzed multipotent intestinal stem cells (ISCs) as alternative cell source to derive bioartificial, pancreatic β-like cells *in vitro*. From a translational perspective, intestinal stem cells pose a particularly attractive cell source since intestinal donor tissues could be obtained via minimal invasive endoscopy in an autologous way. Furthermore, intestinal and pancreatic cells both derive from the same developmental origin, the endodermal gut tube, favoring the differentiation process towards functional β-like cells. In this study, pancreas-specific differentiation of ISCs was induced by the ectopic expression of the pancreatic transcription factor 1 alpha (Ptf1a), a pioneer transcriptional regulator of pancreatic fate. Furthermore, pancreatic lineage-specific culture media were applied to support the differentiation process. In general, ISCs grow *in vitro* in a 3D Matrigel®-based environment. Therefore, a 2D

culture platform for ISCs was established to allow delivery and ectopic expression of Ptf1a with high efficiency. Next, several molecular tools were applied and compared with each other to identify the most suitable technology for Ptf1a delivery and expression within ISCs as well as their survival under the new established 2D conditions. Success of differentiation was investigated by monitoring changes in cellular morphology and induction of pancreatic differentiation-specific gene expression profiles. In summary, the data of this project part suggest that Ptf1a harbors the potential to induce pancreatic differentiation of ISCs when applying an adequate differentiation media. However, gene expression analysis indicated rather an acinar lineage-determination than a pancreatic β-cell-like specification. Nevertheless, this study proved ISCs not only as interesting stem cell source for the generation of pancreatic cell types with a potential use in the treatment of T1DM but alsoPtf1a as pioneer factor for pancreatic differentiation of ISCs in general.

Compared to T1DM, T2DM patients suffer from hyperglycemia due to insulin resistance. In T2DM management, the maintenance of blood glucose homeostasis has highest priority and can be achieved by drugs affecting the stabilization of blood glucose levels. Recent therapeutic concepts are aiming at the inhibition of the intestinal glucose transporter Na^+-D-Glucose cotransporter 1 (SGLT1). Pharmacological inhibition of SGLT1 results in reduced postprandial blood glucose levels combined with a sustained and increased Glucagon-like peptide 1 (GLP-1) secretion. So far, systemic side effects of this medication have not been addressed in detail. Of note, besides intestinal localization, SGLT1 is also expressed in various other tissues including the pancreas. In context of having a closer look also on the interplay of organs when developing new therapeutic approaches for DM, the second part of this thesis addressed the effects on pancreatic islet integrity after loss of SGLT1. The analyses comprised the investigation of pancreatic islet size, cytomorphology and function by the use of a global SGLT1 knockout ($SGLT1^{-/-}$) mouse model. As $SGLT1^{-/-}$ mice develop the glucose-galactose malabsorption syndrome when fed a standard laboratory chow, these animals derived a glucose-deficient, fat-enriched (GDFE) diet. Wildtype mice on either standard chow (WTSC) or GDFE (WTDC) allowed the discrimination between diet- and knockout-dependent effects. Notably, GDFE fed mice showed decreased expression and function of intestinal SGLT1, while pancreatic SGLT1 mRNA levels were unaffected. Further, the findings revealed increased isled sizes, reduced proliferation- and apoptosis rates as well as an increased α-cell and

reduced β-cell proportion accompanied by a disturbed cytomorphology in islets when SGLT1 function is lost or impaired. In addition, pancreatic islets were dysfunctional in terms of insulin- and glucagon-secretion. Moreover, the release of intestinal GLP-1, an incretin hormone that stimulates insulin-secretion in the islet, was abnormal after glucose stimulatory conditions. In summary, these data show that intestinal SGLT1 expression and function is nutrient dependent. The data obtained from the islet studies revealed an additional and new role of SGLT1 for maintaining pancreatic islet integrity in the context of structural, cytomorphological and functional aspects. With special emphasis on SGLT1 inhibition in diabetic patients, the data of this project indicate an urgent need for analyzing systemic side effects in other relevant organs to prove pharmacological SGLT1 inhibition as beneficial and safe.

Altogether, the findings of both project parts of this thesis demonstrate that focusing on the molecular and cellular relationship and interplay of the small intestine and the pancreas could be of high importance in context of developing new therapeutic strategies for future applications in DM patients.

Zusammenfassung

Das komplexe Zusammenspiel zwischen Pankreas und Dünndarm ist von großer Bedeutung für den Zucker Stoffwechsel. Während der Dünndarm Glukose aus der Nahrung absorbiert, sezerniert der Pankreas Insulin und Glukagon für die Regulation des Blutzuckerspiegels. Bereits kleinste Fehlfunktionen in einem der beiden Organe können das fein abgestimmte Zusammenspiel aus der Balance bringen und zu schwerwiegenden Begleiterscheinungen führen. Die bekannteste Krankheit bezüglich eines gestörten Blutzuckerhaushaltes ist Diabetes mellitus (DM). Die wichtigsten Formen sind Typ1 und Typ 2 Diabetes, welche beide durch chronische Hyperglykämie gekennzeichnet sind, einem Zustand der langfristig zu schweren Komplikationen führt. Derzeit ist keine Heilung möglich, jedoch vermindert eine Vielzahl von Medikamenten und Therapien die auftretenden Symptome, was die Lebensqualität der Patienten erheblich verbessert. Für die Entwicklung von neuen Medikamenten und Therapien für DM Patienten, muss der Fokus vermehrt auf die Gesamtheit der Organ-Organ Interaktionen, sowie den entwicklungsbiologischen Ursprung der einzelnen Organe gerichtet werden.

Bei Typ 1 Diabetes werden die insulinsekretierende β-Zellen vom Immunsystem zerstört, was zu einem Mangel an Insulin führt. Deshalb ist eine regelmäßige Insulingabe unabdingbar, um eine Hyperglykämie vorzubeugen. Ein vielversprechender Ansatz um fehlendes Insulin zu kompensieren besteht darin aus Stammzellen bioartifizielle, insulinsekretierende Zellen zu generieren. In diesem Zusammenhang ist der biologische Ursprung der zu differenzierenden Zellen von großer Bedeutung. In dieser Arbeit werden daher intestinale Stammzellen (ISZ) als mögliche alternative Zellquelle beschrieben, um insulinsekretierende Zellen zu generieren. Aus medizinischer Sicht eigenen sich ISZ besonders gut für regenerative Therapien, da sie patientenspezifisch durch eine minimal-invasive Endoskopie entnommen werden können. Des Weiteren haben die beiden Organe einen gemeinsamen embryologischen Ursprung, die endodermalen Darmröhre, was die pankreatische Differenzierung begünstigen könnte. Mithilfe der ektopischen Expression des pankreatischen Masterregulators pankreatischer Transkriptionsfaktors 1 alpha (Ptf1a), sollen ISZ in insulinsekretierende β-Zell-ähnliche Zelltypen differenziert werden. Zudem soll ein pankreas-spezifisches Differenzierungsmedium die Effizienz der Differenzierung erhöhen. Da ISZ normalerweise in einer 3D

Umgebung kultiviert werden, wurde für diese Arbeit eine 2D Zellkultur etabliert, um eine hocheffiziente genetische Manipulation zur ektopischen Expression von Ptf1a zu garantieren. Im nächsten Schritt wurde die bestmögliche Methode evaluiert um Ptf1a in ISZ zu integrieren, welche gleichzeitig aber das Wachstum und Überleben der Zellen nicht beeinträchtigt. Der Erfolg der angewandten Methode wurde basierend auf der Zellmorphologie, sowie der Transkription von pankreasspezifischen Genen überprüft. Die Ergebnisse dieser Studie haben gezeigt, dass die Ptf1a-induzierte Differenzierung in Verbindung mit der Applikation eines spezifischen Differenzierungsmediums das Genexpressionsprofil von Azinär Zellen induziert und nicht wie erwartet, das von endokrinen β-Zellen. Dies bedeutet, dass Ptf1a die Kapazität aufweist, ISZ in pankreatische Zellen zu konvertieren, jedoch bei der Entwicklung in Richtung insulinsekretierende β-Zellen keine Rolle spielt. Letztendlich zeigen die Ergebnisse dieser Arbeit, dass ISZ eine interessante Alternative zu pluripotenten Stammzellen darstellen.

Im Gegensatz zu Typ 1 leiden Typ 2 Diabetes Patienten an Hyperglykämie infolge von Insulinresistenz, welche oft mit blutzuckerregulierenden Medikamenten behandelt werden können. Eine gute Therapiemöglichkeit ist die Inhibition des intestinalen Glukosetransporters SGLT1, was zu einer drastisch reduzierten postprandialen Glukoseaufnahme führt und gleichzeitig die intestinale Sekretion des Inkretins Glukose-like Peptide 1 (GLP-1) erhöht. Beides wirkt sich positiv auf die Blutzuckerregulation unter diabetischen Verhältnissen aus. Obwohl SGLT1 primär im Dünndarm exprimiert ist, wurde dessen Expression auch in anderen Organen, wie dem Gehirn, dem Herz, der Lunge und in pankreatischen α-Zellen nachgewiesen. Im zweiten Teil dieser Arbeit wurde daher der Einfluss des Funktionsverlustes von SGLT1 auf die Integrität pankreatischer Inselzellcluster analysiert. Im diesem Rahmen wurde die Morphologie der pankreatischen Inseln, deren Architektur und Funktion mithilfe eines etablierten murinen SGLT1 Knockout ($SGLT1^{-/-}$) Modelles untersucht. Da $SGLT1^{-/-}$ Mäuse unter einer Standard Labordiät (SD) ein schweres Glukose-Galaktose Malabsorptions Syndrom entwickeln, erhalten die Tiere eine glukose-freie, fett-angereicherte Diät (GDFE). Um diät- und knockoutspezifische Effekte unterscheiden zu können, wurden als Kontrollen SD- und GDFE-gefütterte Wildtyp Tiere mit den $SGLT1^{-/-}$ Mäusen verglichen. Wildtyptiere unter GDFE Diät zeigten eine verminderte Expression und Funktionalität des intestinalen SGLT1 Transporters, während im Pankreas die SGLT1 mRNA Expression nicht von der Diät beeinflusst wurde. Die

Ergebnisse dieser Arbeit haben gezeigt, dass in SGLT1$^{-/-}$ Pankreata, die Inseln größer sind, aber auch die Proliferations- und Apoptoserate in den Inselzellen reduziert ist. Zudem befinden sich in SGLT1$^{-/-}$ Inseln mehr α-Zellen und weniger β-Zellen. Des Weiteren ist die typische Anordnung der endokrinen Zellen gestört. Diese Beobachtungen deuten darauf hin, dass SGLT1 in pankreatischen Inseln eine wichtige Rolle für die strukturelle Organisation der verschiedenen Zelltypen innerhalb der Inseln spielt. Ergänzend wurde gezeigt, dass isolierte SGLT1$^{-/-}$ Inseln in der Gegenwart von Glukose unfähig sind Insulin oder Glukagon zu sezernieren. Weitere Untersuchungen im Tier haben ergeben, dass auch das insulinsekretionsfördernde Hormon GLP-1 in atypischer Art und Weise sekretiert wird.

In dieser Arbeit wurde gezeigt, dass die intestinale SGLT1 Expression und Funktion durch Nährstoffe beeinflusst werden kann. Des Weiteren wurde erstmals eine neue Funktion für SGLT1 bezüglich der strukturellen und zellulären Organisation pankreatischer Inselzellcluster beschrieben. Daten zu neuen klinischen SGLT1 Inhibitoren beschreiben lediglich eine intestinale SGLT1 Blockierung, während die Wirkung in weitern Organen nicht berücksichtigt wurde. Die Daten dieser Arbeit liefern klare Indizien dafür, dass starke Nebenwirkungen und Effekte auch in anderen SGLT1-exprimierenden Geweben und Organen auftreten könnten, wenn die SGLT1 Funktion verloren geht.

Zusammenfassend konnte in dieser Arbeit gezeigt werden, dass die Regulation des Blutzuckerspiegels auf einem komplexen Zusammenspiel zwischen Dünndarm und Pankreas basiert. Daher sollten bei zukünftigen SGLT1 Inhibitions-Studien im Menschen die Interaktionen zwischen den beiden Organen unbedingt berücksichtigt werden, um die Wirksamkeit und die Sicherheit solcher Medikamente für Diabetes Patienten besser darzulegen.

List of Figures & Tables

Abbreviations

-/-	knockout
+4 LRC	label-retaining cells (2nd intestinal stem cell population)
°C	°celsius
µg	microgram
µL	microliter
µm	micrometer
µM	micromolar
ADP	adenosine diphosphate
Arx	aristaless related homeobox
Ascl2	achaete-scute complex homolog 2
ATP	adenosine triphosphate
Bmi1	B lymphoma Mo-MLV insertion region 1 homolog
BMP	bone morphogenetic protein
bp	base pair(s)
BSA	bovines serum albumin
BTC	betacellulin
cAMP	cyclic adenosine monophosphate
Cdx1	caudal type homeobox1
ChymoB1	chymotrypsinogen B1 or CTRB1
CPP	cell penetrating peptide
Cxcr4	CXC chemokine receptor 4
DAB	3,3'-Diaminobenzidine
DAPI	4',6'-diamidio-2-phylindole
DC	diet chow (glucose-deficient, fat-enriched)
Dll	delta-like ligand
DMEM	Dulbecco Modified Eagle Medium
DNA	deoxyribonucleic acid
DNase	desoxyribonuclease
E. coli	*Escherichia coli*
EGF	epidermal growth factor
eGFP	enhanced green fluorescent protein

ELISA	enzyme-linked immunosorbent assay
EMSA	electrophoretic mobility shift assay
Epac	cAMP-regulated guanine nucleotide exchange factor
ESCs	pluripotent embryonic stem cells
FACS	Fluorescent Activated Cell Sorting
FCS	fetal calf serum
FFA	free fatty acid
FGF	fibroblast growth factor
FoxA2	forkhead Box Protein A2
g	unit of gravitational force or gram
GDFE	glucose-deficient, fat-enriched diet
GIP	glucose-dependent insulinotropic peptide
GLP-1	glucagon-like peptide 1
GLUT	glucose transporter
GMEM	Glasgow's MEM Medium
GPR40	G protein-coupled receptor 40
h	hour
H&E	hematoxylin & eosin
Hb9	motor neuron and pancreas homeobox1
HbA_{1c}	hemoglobin A1c
HEPES	4-(2-hydroxyethyl)-1-piperazineethanesulfonic acid
Hes1	hairy and enhancer of split 1
Hnf	hepatocyte nuclear factor
IgG	Immunoglobulin G
IHC	Immunohistochemistry
iPSCs	induced pluripotent stem cells
ISC	intestinal stem cell
LB medium	lysogeny broth
Lgr5	leucine-rich repeat-containing G-protein coupled receptor 5
LRP	Frizzled lipoprotein receptor related protein
MafA	muscululoaponeurotic fibrosarcoma oncogene homolog A
Math1	mouse atonal (ato) homolog 1 (Math1) transcription factor
min	minute(s)

mLIF	murine leukemia inhibitory factor
Mnx1	motor neuron and pancreas homeobox1
MPP	multipotent progenitor cells
mTert	mouse telomerase reverse transcriptase
MTT	3-(4,5-dimethylthiazol-2-yl)-2,5-diphenyltetrazolium bromide
Nanog	homeobox transcription factor Nanog
Ngn3	neurogenin 3
NICD	Notch intracellular domain
Nkx6.1	homeobox protein NK-6 homolog A
o/n	over night
Oct3/4	octamer-binding transcription factor 3/4
Olfm4	olfactomedin 4
Pax4	paired Box 4
Pax6	aniridia type II protein
PBS^-	phosphate-buffered saline without bivalent ions
PBS^+	phosphate-buffered saline with bivalent ions
Pdx1	pancreatic-duodenal homeobox factor 1
PEPT1	di/tripeptide transporter 1
PFA	paraformaldehyde
PGK	phosphoglycerate kinase
PKA	protein kinase A
POD medium	pancreas organoid differentiation medium
Ptf1a	pancreatic transcription factor 1 alpha
qPCR	quantitative polymerase chain reaction
R	receptor
RA	retinoic acid
RBPJL	recombinant signal binding protein for immunoglobulin kappa J and L
RFP	red fluorescent protein
RNA	ribonucleic acid
RPMI	Roswell Park Memorila Institute Medium
RT	room temperature
s	second(s)
SC	standard chow

SD	standard deviation
SGLT	Na^+-D-glucose cotransporter
SHH	sonic hedgehog
Smad	SMA protein *C. Elegans* and MAD protein *Drosophila*
Smoc2	SPARC related modular calcium binding protein 2
Sox	SRY (Sex Determining Region Y) Box
T1DM or T2DM	type 1 or type 2 Diabetes mellitus
T1R3	taste receptor type 1 member 3
Tcf4	transcription factor 4
TF	transcription factor
TGF-β	transforming growth factor beta superfamily
TMR	tetra methyl rhodamine
Tnfrsf19	TNF receptor superfamily member 19
UTR	untranslated region
VA	valproic acid
VDCCs	voltage-dependent Ca^{2+} channels
VEGF	vascular endothelial growth factor
w/v	weight per volume
Wnt3	named after the *Drosophila* segment polarity gene wingless

1. Introduction

1.1. The small intestine

1.1.1. Structural and anatomical characteristics of the small intestine and its role for nutrient and energy absorption from food

The small intestine builds together with the large intestine the lower gastrointestinal tract. Combined with the esophagus, stomach and the duodenum characterizing the upper gastrointestinal tract, this organization represents one of the biggest organ systems in humans, rodents and other organisms.

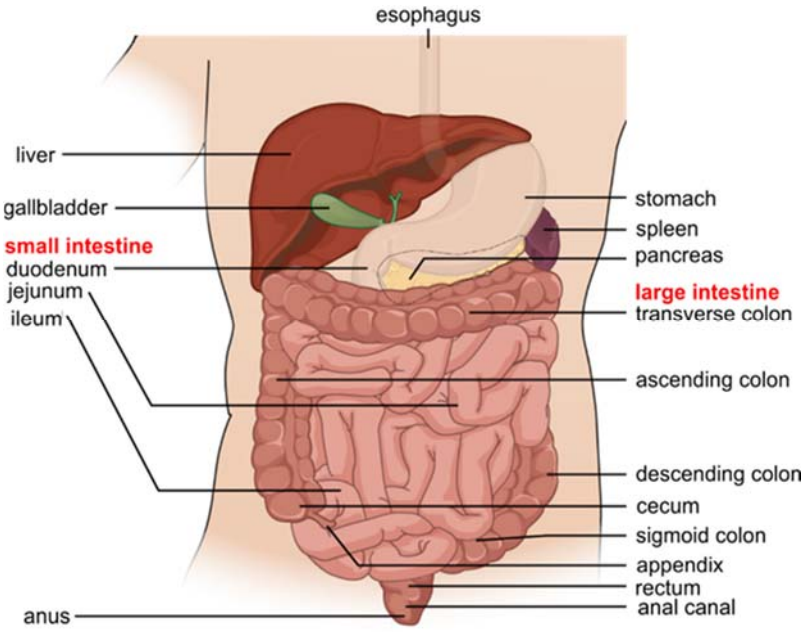

Figure 1.1: Anatomy of the human gastrointestinal tract. Schematic overview depicts the anatomy of the gastrointestinal tract (GI) including the digestive system, the pancreas and the liver. Image modified from [1].

The gastrointestinal (GI) tract is located in the abdomen in close proximity to other organs including the pancreas, the liver and the stomach (Figure 1.1) [1]. It emerges from the embryonic foregut and thus shares its developmental origin with the adjacent GI derivatives pancreas, liver and thyroid [2]. The GI tract fulfils a broad range of functions like food intake, processing and digestion thereby regulating nutrient and energy absorption, where especially the small intestine plays a key role.

Structural and anatomical characteristics of the small intestine are similar between humans and rodents. Anatomically, it can be separated into three major regions: the proximal duodenum, the intermediate jejunum and the distal ileum. Considering its structural organization, the small intestine is built by several tissue layers. The outer layer is called serosa (or *adventitia*) and consists of connective tissue cells. The next layer is formed by an innervated muscle layer, the *muscularis*, characterized by contracting smooth muscle cells to move the chyme through the intestinal tract. Next follows the submucosa connecting *muscularis* and mucosa. The mucosa consists of the *muscularis mucosae*, the *lamina propria* and an epithelial cell layer [3] (Figure 1.2A). The epithelium predominantly contains absorptive enterocytes and is intermingled with hormone-secreting enteroendocrine cells and mucin-producing goblet cells. Mucins are glycosylated proteins clustering in aggregates thus creating a barrier preventing the epithelial layer from mechanical damage and the direct contact with bacteria [4, 5]. The small intestinal mucosa is hallmarked by the formation of villi and crypts (Figure 1.2AB). The microvilli structure on the apical membrane of the enterocytes, also known as brush border, significantly enhances the surface area of the small intestinal epithelium and thereby increases the capacity for energy and nutrient absorption [6, 7]. Underneath the mucosa lies the submucosa that consists of a densely packed structure of connective tissue that is strongly innervated by the so called enteric nervous system [8] and further comprises a network of blood- and lymphatic vessels [3]. Together, this layered organization represents a strong barrier of the organ that maintains its structural integrity and provides several regulatory entities to support the main physiological function of food digestion as well as nutrient and energy absorption [3, 9].

Among all nutrients, carbohydrates, proteins and fats are key components that need to be processed within the small intestine. Proteins are first digested into amino acids that are then absorbed by specialized transporters expressed on enterocytes including the high abundant di/tripeptide transporter 1 (PEPT1) [7, 10]. Within enterocytes, the peptides get hydrolyzed in the cytoplasm and released to the blood via transport across the basolateral membrane [7]. Dietary fat is first digested by the pancreatic enzyme lipase in the upper jejunum followed by absorption in either a transport protein-dependent or -independent manner mediated by enterocytes [11, 12]. Within the enterocytes, the breakdown products of the fat are finally packed into lipoprotein particles, known as chylomicrons and exported via the lymphatic system into the

bloodstream [10, 12]. The solute transport of sugar molecules across the brush border membrane of the mucosa is accomplished by specialized membrane transporter proteins [10]. After the initial break down of starches and disaccharides (lactose, sucrose) by salivary and pancreatic enzymes like amylase, mucosa-derived enzymes control the digest to monosaccharides (glucose, fructose and galactose) which can be transported by their related transport proteins [7, 13]. For the absorption of glucose and galactose, the sodium (Na^+) dependent glucose cotransporter 1 (SGLT1) mediates the uptake of both monosaccharides from the small intestinal lumen into enterocytes [14, 15]. The glucose transporter 5 (GLUT5) enables the absorption of fructose into enterocytes by facilitated diffusion [16]. After uptake, the glucose transporter 2 (GLUT2) is responsible for the basolateral membrane crossing of glucose, galactose and fructose from the cytosol of enterocytes into the blood stream [17].

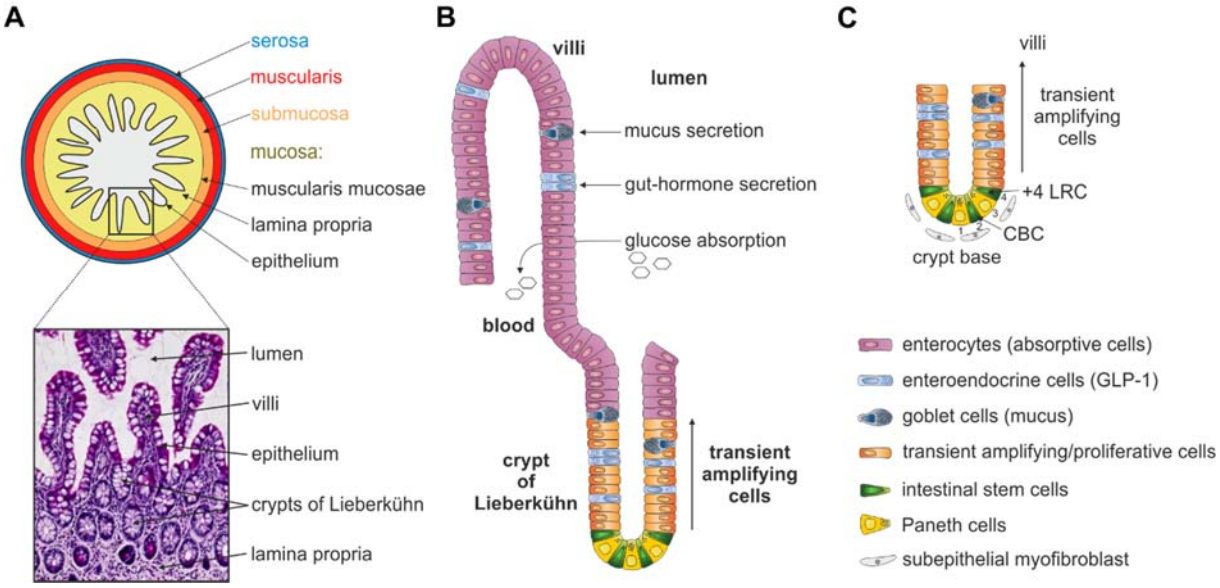

Figure 1.2: Structural and cellular organization of the small intestine. (A) Schematic representation of the small intestine in cross-section. Shown are all cell layers with special focus on the villi-crypt organization of the mucosa that is further notified by a representative image of a H&E-stained section of the human small intestine. (B) Schematic overview of the mucosa-specific cellular composition with indicated functional aspects. (C) Schematic illustration of the intestinal stem cell niche also known as intestinal crypt. Shown are the main intestinal stem cell types ($Lgr5^+$)-CBCs and +4 LRCs surrounded by Paneth cells

1.1.2. Intestinal stem cells - a multipotent stem cell type

Stem cells are defined by their unlimited self-renewal capacity and the potential to differentiate into diverse somatic cell types [18]. Their stem cell-specific differentiation range is described as potency that serves also as classification criteria of diverse stem cell populations [18, 19].

During development, the first type of stem cells arises at the zygote state called totipotent stem cells harboring the ability to develop into embryonic and extra-embryonic tissue thereby giving rise to a complete functional organism [20, 21]. Later at the blastocyst stage, pluripotent stem cells reside in the inner cell mass [22]. When isolated and cultured *in vitro*, these cells are known as embryonic stem cells (ESCs). An artificial pluripotent stem cell type are the so called induced pluripotent stem cells (iPSCs) generated by a transcription factor-driven reprogramming process [19, 23, 24]. Both pluripotent stem cell types are able to continuously self-renew and exhibit the capacity for multilineage differentiation into the three germ layers (meso-, endo- and ectoderm) [25]. With ongoing development, tissue-specific multipotent stem cells differentiate into progenitor cells of the residing tissue before final specification is reached [18, 26]. While during embryogenesis all types of stem cells are present, only multipotent tissue-specific stem cells can be found in the adult.

Multipotent stem cells reside in a defined microenvironment, the so called stem cell niche to maintain their specific properties [27, 28]. In adult mammals, the intestinal epithelium represents a stem cell niche harboring multipotent intestinal stem cells (ISCs) [29, 30] embedded within the submucosal crypts of Lieberkühn that are distributed around the villi structures [31] (Figure 1.2A-C).

ISCs exhibit a high self-renewing rate and differentiation capacity as manifested by a complete regeneration cycle of the intestinal epithelium within 4-5 days [32]. In 1974, the existence of fast-cycling, crypt base columnar (CBC) cells, intermingled within Paneth cells, was demonstrated by Cheng and Leblond [33]. By performing lineage-tracing experiments they could prove that CBCs harbor multipotent stem cell characteristics giving rise to all four differentiated cell types of the intestine [34, 35] comprising the absorptive epithelial lineage (enterocytes), mucin-secreting goblet cells, enteroendocrine cells (e.g. K- and L-cells) and Paneth cells [31, 32, 36-38]. Recently, Barker et al. unmasked the Leucine-rich repeat-containing G-protein coupled

receptor 5 (Lgr5) to be exclusively expressed in high-mitotic CBC cells [39]. By means of transgenic Lgr5 reporter mice it was possible to trace Lgr5$^+$-derived descendants. These experiments showed that symmetrically dividing Lgr5$^+$ CBC cells comprise a high capacity for self-renewal and the ability to derive all four intestinal lineages [39, 40]. In addition to Lgr5, gene profiling analysis revealed further markers specific for Lgr5$^+$-ISCs such as olfactomedin-4 (Olfm4), achaete-scute complex homolog 2 (Ascl2), SPARC related modulator calcium binding 2 (Smoc2) or tumor necrosis factor superfamily member 19 (TNFRSF19) [41]. Recently, Lgr5$^+$-ISCs were demonstrated to be maintained and expanded in a 3D Matrigel® culture system [29, 42].

In addition to the Lgr5$^+$-ISCs, an alternative paradigm identified the +4 LRC cell population as multipotent stem cell type within the intestinal epithelium. The radiation-sensitive +4 label-retaining cells (+4 LRCs) were first described by Potten et al. named after their specific position within the intestinal epithelium relative to the crypt bottom that displays mitotic quiescence [43, 44]. Later, the expression of B lymphoma Mo-MLV insertion region 1 homolog (Bmi1) and mouse telomerase reverse transcriptase (mTert) was specifically attributed to +4 LRCs and lineage tracing experiments revealed stem cell characteristics for these cells [30, 45]. Fate mapping studies demonstrated +4 LRCs as facultative stem cells, differentiating into Paneth and secretory-lineage cells under normal conditions [46]. In addition, they are thought to revert into fast-cycling Lgr5$^+$-ISCs upon depletion or injury of the CBC stem cell population [38, 46, 47].

1.1.3. The intestinal stem cell niche - important factors regulating the multipotency of ISCs

The term stem cell niche describes a micro-environment where stem cells are associated with several other cell types that provide necessary signals to maintain stem cell identity [48]. The intestinal stem cell niche is constituted by close proximity of ISCs with adjacent Paneth cells [35, 49] and cells from the stromal microenvironment [50, 51] (Figure 1.3). The close arrangement with both cell types facilitates the distribution and availability of crucial factors for niche homeostasis and maintenance of ISC stemness or regulation of ISC differentiation.

Wnt signaling is crucial to maintain stemness of ISCs at the crypt base [52, 53]. Mechanistically, Paneth cell-secreted Wnt3 (named after the *Drosophila* segment polarity gene wingless and the homologue from vertebrates integrated or int-1) binds to the Frizzled-LRP5/6 receptor complex and induces the formation of the β-catenin complex that translocates to the nucleus initiating the transcription of proliferation and anti-differentiation associated genes via activation of the transcription factor 4 (Tcf4) [29] (Figure 1.3). Further supportive for ISC stemness is the binding of the Wnt agonist R-spondin1 to the LGR5 receptor thereby disabling the turnover of the Wnt receptor complex and simultaneously enhancing the Wnt-induced phosphorylation of low-density lipoprotein receptor related protein 6 (LRP6) [54, 55], a process that finally results in the amplification of Wnt signaling within Lgr5^{+}-ISCs [49].

Notch signaling is also involved in maintaining intestinal stem cell identity. The Paneth cell-expressed Notch ligands delta-like 1 and 4 (Dll1/4) mediate the release of the Notch intracellular domain (NICD) and activation of recombinant signal binding protein for immunoglobulin J (RBP-J) thereby inhibiting differentiation of ISCs when cells reside at the crypt base [37] (Figure 1.3).

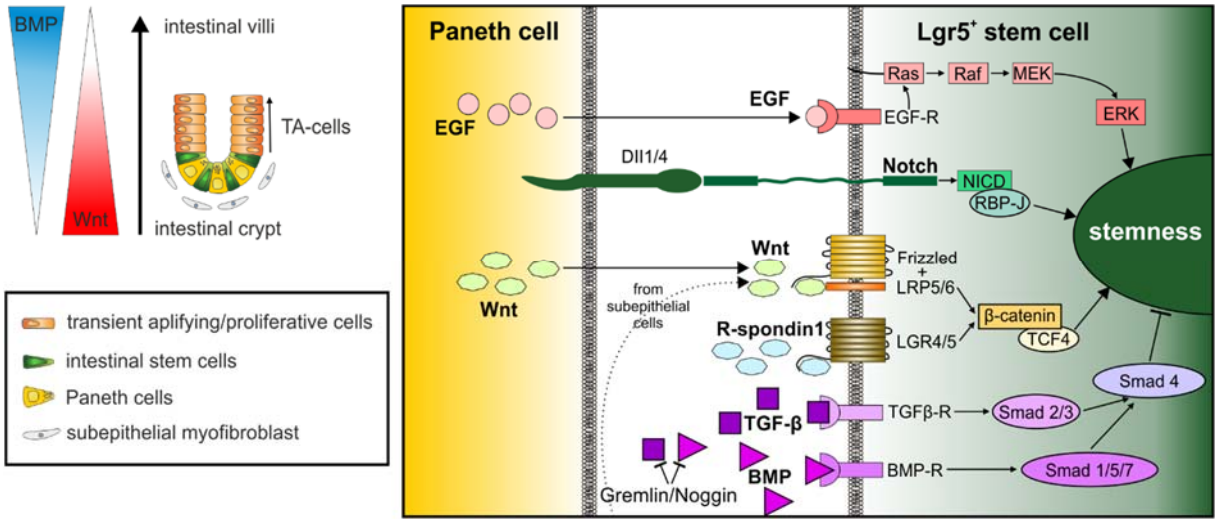

Figure 1.3: Maintenance of the intestinal stem cell pool depends on various niche-derived signals. While active Wnt signaling at the crypt base maintains ISC stemness, activation of BMP signaling within the transit amplifying area drives differentiation and specification of ISC-derived transient amplifying progenitors (TAPs). Scheme shows an overview and the interplay of all important signals within the intestinal niche. BMP = bone morphogenetic protein; Dll = Delta-like ligand; EGF = epithelial growth factor; ERK = extracellular-signal regulated kinase; LGR = leucine-rich repeat-containing G-protein coupled receptor; LRP = low-density lipoprotein receptor related protein; MEK = mitogen activated protein kinase; NICD = Notch intracellular domain; R = receptor; RBP-J = recombinant signal binding protein for immunoglobulin J; Raf = rapid accelerated fibrosarcoma; Ras = G-protein RAS

superfamily; Smad = from SMA protein *C. Elegans* and MAD protein *Drosophila*; TCF4= transcription factor 4; TGF = transforming growth factor; Wnt = wingless Int. Figure modified from [56].

Another important factor that is released by Paneth cells and adjacent fibroblasts is the epidermal growth factor (EGF) that further supports survival and proliferation of $Lgr5^+$-ISCs and epithelial progenitor cells [49, 56, 57]. EGF enhances the mitogenic activity in stem cells by binding to the EGF receptor (EGF-R) [57, 58]. Furthermore, upon receptor activation, the activated tyrosine kinase cascade Ras/Raf/MEK/ERK prevents apoptosis of crypt cells [56, 57].

An additional dominant signaling pathway within the intestinal stem cell niche is the epithelia-derived bone morphogenetic protein (BMP) signaling that dominantly regulates differentiation of $Lgr5^+$-ISCs [59-63]. At the crypt base, active BMP and transforming growth factor beta superfamily (TGF-β) signaling results in activation of Smad protein transcription factors (Smad1, 5 and 7) that repress intestinal stem cell marker genes like Lgr5 [56, 64, 65]. In order to maintain stemness, subepithelial myofibroblasts therefore secrete the potent BMP signaling inhibitors gremlin 1, gremlin 2 and chordin-like 1 that block activation of BMP signaling at the crypt base [50, 62].

Upon initiation of differentiation, ISCs give rise to progenitor cells that migrate upwards in the crypt into the transient amplifying area where BMP signaling regulates differentiation of the ISC-derived transiently amplifying progenitors (TAPs) [59-63] (Figure 1.3). Interestingly and in contrast to their action at the crypt base, Notch signaling also supports terminal differentiation of TAPs into absorptive enterocytes or other secretory cell types [37, 38, 66] when active in the transient amplifying area. The close contact of TAPs with Notch ligand-expressing Paneth cells activates the downstream target hairy and enhancer of split 1 (Hes1), a mediator for the absorptive lineage commitment [37, 66], which acts as repressor of the mouse atonal (ato) homolog 1 (Math1) transcription factor [67], that in turn is necessary for specification along the secretory lineage.

1.2. The Pancreas

1.2.1. An overview on pancreas anatomy and function

In general, the pancreas can be divided into three regions: the head, the body and the tail. It is located in the upper abdomen embedded between the spleen, the stomach and the duodenum (Figure 1.1 and 1.4). Both, the human and the murine pancreas is enclosed by a fibrous layer of mesenteries while connective septa (parenchyma) shape and organize the organ in lobes and lobules [68]. In contrast to human, the murine pancreas is less defined in shape and more distributed within the mesenteries in the duodenal-, the splenic- and the gastric lobe, however, these differences have no impact on organ function [69, 70].

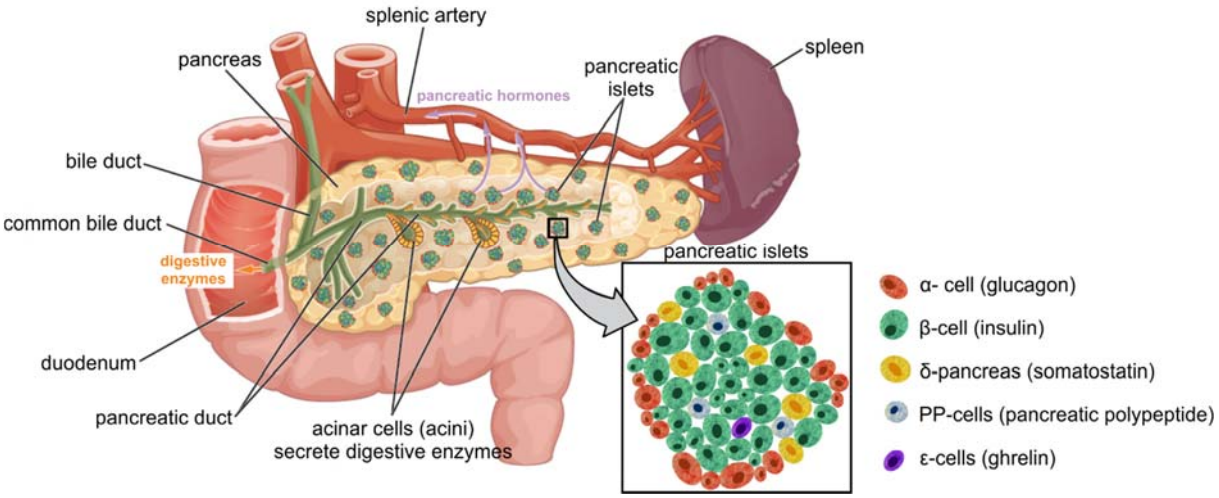

Figure 1.4: Overview of pancreas localization and anatomy. The pancreas is composed of an endo- and exocrine part each fulfilling diverse functions. While the exocrine acinar cells secrete digestive enzymes via the pancreatic duct system into the small intestine, the endocrine islet cluster cells secrete specific hormones into the bloodstream. The image is adapted and modified from an OpenStax College resource [71].

In general, the pancreas is a gland composed of two parts with diverse functions, the exocrine and the endocrine pancreas.

The exocrine pancreas represents up to 99% of total organ mass. It is built by acinar cells arranged in dense clusters called acini that are lined up around small ducts, which assemble into the main pancreatic duct ending up within the small intestine [69] (Figure 1.4). Mechanistically, the exocrine acinar cells secrete enzymes including lipases,

proteases or α-amylase [72] that are transported via the pancreatic duct system to the small intestine, where they fulfill a dominant role in food digestion [73].

The endocrine pancreas is aggregated into so called Islets of Langerhans that are embedded within the exocrine tissue (Figure 1.4). These islet clusters were first discovered in 1969 by their namesake Paul Langerhans [74]. They are typically composed of five main cell types that secrete specific hormones into the bloodstream thereby regulating nutrient metabolism and blood glucose homeostasis [75, 76].

Murine islets comprise around 15-20% glucagon-secreting (GCG) α-cells and 60-80% insulin (INS)-secreting β-cells [77-80]. Insulin is a peptide hormone that lowers blood glucose levels by mediating glucose uptake into cells [81]. The anabolic properties of insulin are manifested by promoting amino acid incorporation into proteins and triggering lipogenesis and glycogenesis [82-85]. Furthermore, insulin comprises mitogenic capacities as manifested by enhancing cell division and growth [86]. The major opponent of insulin is the catabolic hormone glucagon. Glucagon avoids hypoglycemia in fasting periods by initiating gluconeogenesis in the liver. Consequently, glucagon release results in the rise of blood glucose levels [81, 87-90]. The remaining 5-10% of all islet cells are represented by δ-cells secreting somatostatin (STT), ghrelin-secreting ε-cells and PP-cells that secrete pancreatic polypeptide [77-79]. Somatostatin inhibits glucagon, insulin and pancreatic polypeptide (PP) release within the islet [76]. PP is described to be a satiety messenger involved in the regulation of food uptake and digestion [91]. Ghrelin has appetite regulatory abilities and may inhibit insulin, glucagon, somatostatin and PP release [92].

Morphologically, the α-, δ-, ε- and PP-cells reside in the peripheral mantle around the central β-cell core [79, 80]. While total β-cell mass of pancreatic islets vary among species, islet size distribution is relatively similar in healthy individuals [69, 70, 79]. In addition, the detailed cellular composition and overall islet architecture is different between species, as these characteristics are adapted in an evolutionary manner to mediate organism-specific needs in hormone secretion to control blood glucose homeostasis [79, 80]. In this context, human islets do not display the same cytomorphology than murine islets. In humans, the α-cell population is dispersed throughout the complete islet, a morphological alteration that allows the human islet to respond already to low glucose concentrations of around 1 mM, a glucose level where murine islets cannot respond to [78]. Further, there are also differences in islet size

and cytomorphology between diverse species as adaptation to pathologic or changed physiological circumstances including diabetes, obesity or pregnancy [80, 93-95]. Together, this diversity highlights the high plasticity and fast adaptation of pancreatic islets in response to metabolic alterations.

1.2.2. Pancreas development

Similar to the small intestine, the pancreas emerges from the endodermal gut tube epithelium [96]. Murine pancreas development starts at around embryonic day 8 (E8) induced by retinoid acid (RA) that is secreted by the adjacent mesoderm and simultaneous inhibition of sonic hedgehog (SHH) signaling by fibroblast growth factor 2 (FGF2) and Activin β2 released from the notochord [75] (Figure 1.5A). A process called the dorsal aorta fusion results in the local separation of the endodermal tissue and the notochord thereby altering the signaling in the surrounding tissue at E8.5-E9.5. The dorsal aorta releases vascular endothelial growth factor (VEGF) thereby promoting the expression of pancreatic and duodenal homeobox 1 (Pdx1) and Pancreas specific transcription factor 1a (Ptf1a), both known as pioneer transcription factors that determine fate specificity of multipotent pancreatic progenitor (MPP) cells and thus pancreatic commitment [75, 97-99]. Between E9-E9.5, a distinct region of the gut tube gains pancreas specificity and forms a bulge that outgrows in a fibroblast growth factor 10 (FGF10)-driven process within the adjacent mesenchymal tissue. This process is called pancreatic evagination and the corresponding tissue predominantly harbors MPP cells and few short-living endocrine cells [75, 100] (Figure 1.5A). The process of pancreatic evagination together with the massive MPP cell proliferation and the formation of a stratified epithelium is known as primary transition [101, 102] (Figure 5B). From E11 to E12.5, the adjacent mesenchymal tissue condenses around the emerging trunk and facilitates the apical and basal polarization of the outer layers of the budding pancreas. Consequently, the formation of a plexus structure that resembles a cuboidal epithelial cell layer organizes around microlumen structures, which coalesce to a continuous tubular central lumen [103]. The plexus structure starts branching and *de novo* formed secondary trunk descendants appear [75]. From E13.5 on, the pancreatic epithelium undergoes a dramatic morphogenetic transformation by differentiation into ductal, acinar or endocrine cell lineages. This process is known as secondary transition and coincides with a massive plexus reorganization finally

resembling a tree-like structure [75, 98, 101] (Figure 1.5B). The growing trunks comprise a tip with fast proliferative MPP cells that convert into acinar cells over time [99, 104] whereas along the trunk a heterogeneous cell population resides and neurogenin 3 (Ngn3) expression determines cellular fate [105]. Low NGN3-expressing cells (Ngn^-) remain uncommitted and might divide asymmetrically while maintaining their endocrine-biased status [106, 107]. In contrast, high $Ngn3^+$ progenitor cells co-express the transcription factor Snail2, a mediator for cellular survival and regulator for epithelial-to-mesenchymal transition. Snail2 mediates the detachment of $Ngn3^+$ cells from the pancreatic trunk to cluster with other endocrine progenitors to assemble in islet-like structures in which they terminally differentiate into islet cell subtypes [73, 108, 109]. Finally, the tertiary transition defines the stage between E16.5 and birth comprising maturation and organization of characteristic islet architecture [77, 79, 103, 110] (Figure 1.5B).

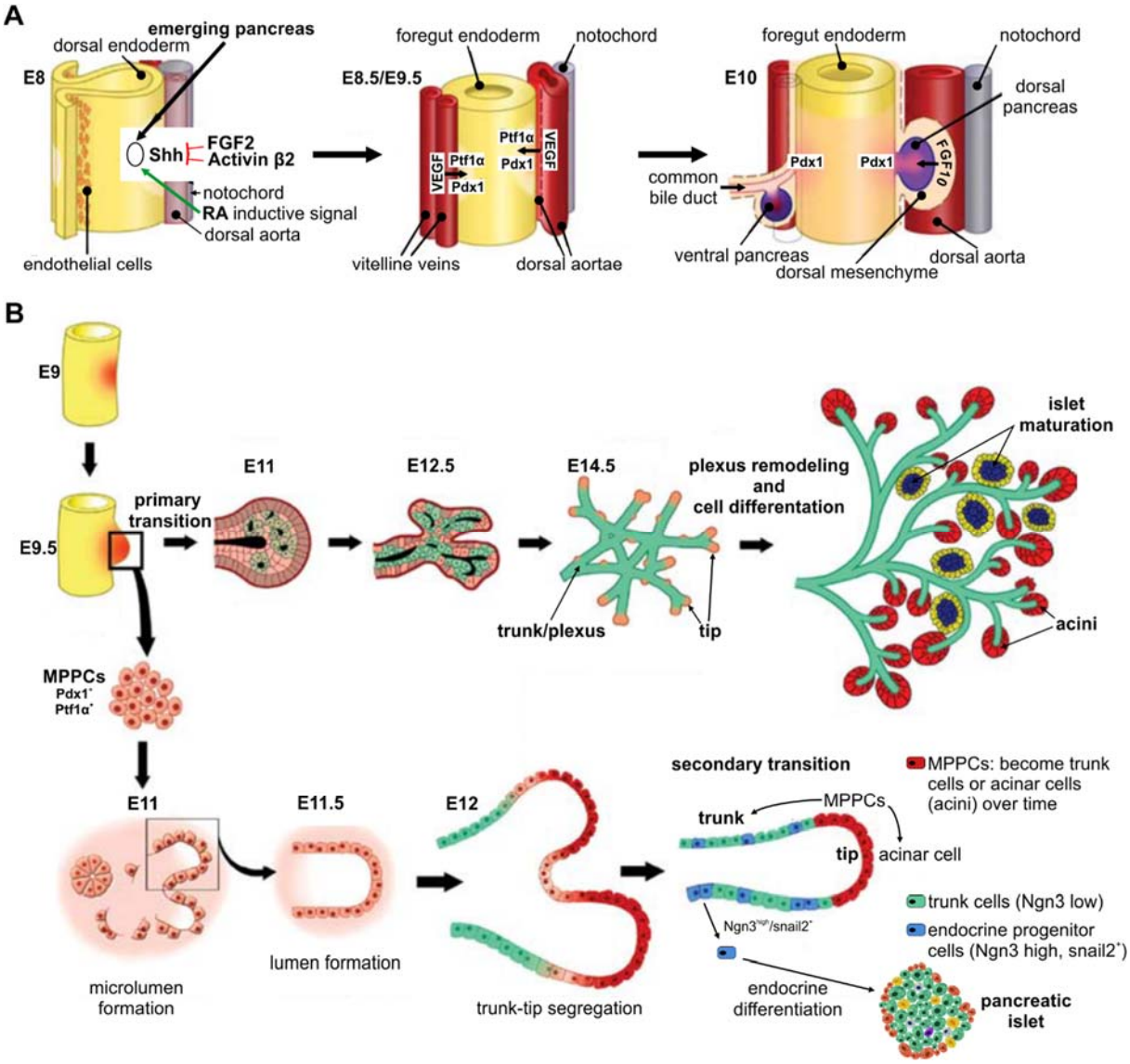

Figure 1.5: Development and organogenesis of the pancreas. (A) Scheme of early embryonic development of the pancreas. Pancreas formation is initiated by retinoic acid (RA) signaling and simultaneous sonic hedgehog (Shh) inhibition by fibroblast growth factor 2 (FGF2) and Activin β2. Pancreatic commitment is determined be the activated transcription factors Pancreatic and duodenal homeobox 1 (Pdx1) and Pancreas specific transcription factor 1a (Ptf1a). (B) Schematic overview of pancreas development including the three transition phases. First transition: formation and expansion of the pancreatic bud. Second transition: differentiation of multipotent pancreatic progenitor cells (MPP cells) in duct, acinar and endocrine lineage cells. Third transition: maturation of pancreatic islets and organization of the functional organ. Images are modified and adapted from [75].

1.2.3. The importance of Ptf1a and Pdx1 during pancreas organogenesis

Transcription factors (TFs) are a class of proteins feasible to bind particular DNA sequences to inhibit or enhance transcription of a target gene [111]. TFs act on multiple levels regulating either their own expression in an auto-regulatory manner or the expression of other targets supported by extrinsic signals from adjacent organs or

tissues that are essential for pancreas development, cell differentiation and maturation [110].

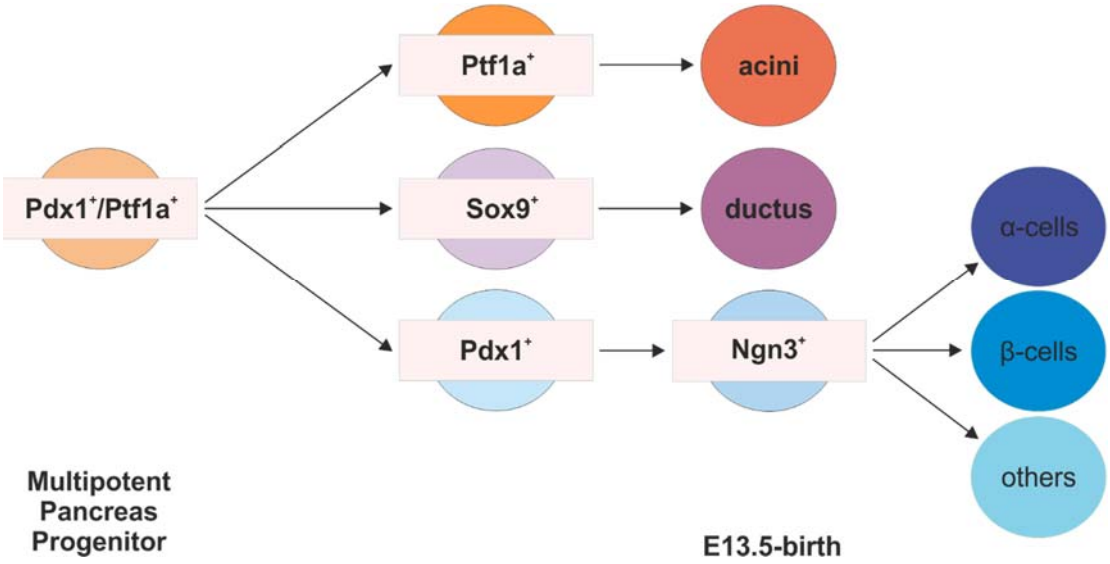

Figure 1.6: Pancreatic lineage differentiation during embryonic mouse development. Scheme shows pancreas lineage differentiation from Ptf1a$^+$/Pdx1$^+$ multipotent pancreatic progenitors (MPPs) to the acinar-, the ductal- and endocrine lineage. Acinar lineage specification is driven by Ptf1a expression (Ptf1a$^+$) and ductal-cell differentiation by Sox9 expression (Sox9$^+$). Endocrine cells share a common Ngn3$^+$ progenitor and differentiate into islet cell subtypes by expressing different transcription factors.

Pancreatic commitment depends on a distinct interplay of several factors. Among them Pdx1 and Ptf1a are the two dominant master regulators for early pancreatic lineage commitment inducing pancreatic bud formation [75, 97, 112, 113]. Further, the importance of motor neuron and pancreas homeobox1 (Mnx1), SRY (Sex Determining Region Y) Box 9 (Sox9), and hepatocyte nuclear factor-1 β (Hnf1b) in pancreatic fate induction is manifested as loss of any of these factors results in pancreatic agenesis with different severity [114-118].

Pdx1 is the first determined transcription factor in MPP cells that reside within the emerging pancreatic buds at around E8.5 in mice [119]. Shortly after Pdx1, Ptf1a is co-expressed within the MPP cell population that gives rise to all pancreatic cell types [97, 115] (Figure 1.6). Both factors are important for early pancreatic development. In addition, each factor characterizes a master regulator for the specification of diverse cell types during ongoing pancreas development.

The importance of Ptf1a expression is shown by loss of function studies demonstrating that pancreatic cells lose their identity and acquire duodenal properties and characteristics after Ptf1a abrogation [115]. Albeit Ptf1a is a transcription factor, its activity strictly depends on the interaction with the so called recombination signal binding protein kappa J (Rbp-j), as only the functional complex of both proteins was shown to maintain proper pancreas development [120, 121]. Ptf1a displays an auto-regulatory capacity supporting its own expression and further comprises binding sites for Pdx1, motor neuron and pancreas homeobox1 (Hb9), hepatocyte nuclear factor 6 (Hnf6) and homeobox protein NK-6 homolog A (Nkx6.1), all of them characterizing important regulators of pancreas development [122-124].

Ptf1a expression is important during early development, however, at later stages, the level of expression determines pancreatic cell fate. While high Ptf1a expression levels regulate the development of MPP cells towards the acinar cell fate, suppression of Ptf1a is necessary for endocrine cell lineage determination [125, 126]. Furthermore, Ptf1a expression is crucial to maintain acinar lineage commitment and thereby the formation of the exocrine pancreas [127]. Similar to Ptf1a, Pdx1 harbors also highly conserved binding sites for several important pancreas-specific transcription factors including muscululoaponeurotic fibrosarcoma oncogene homolog A (MafA), Hnf homeobox A (Hnf1a), Aniridia type II protein (Pax6) and Forkhead Box A2 (FoxA2) [110]. In contrast to Ptf1a, the spatiotemporal expression of Pdx1 is crucial for endocrine development [106, 110]. In summary, pancreas specification and cell lineage differentiation is orchestrated in a complex transcriptional network where the well-defined spatiotemporal expression of the transcription factors Ptf1a and Pdx1 play dominant roles for the specification towards the exocrine or endocrine cell lineage.

1.3. The intestine-pancreas axis - Maintenance of blood glucose homeostasis under healthy and diabetic conditions

1.3.1 Regulation of blood glucose homeostasis under healthy conditions

The ability to maintain blood glucose concentrations at a physiological level of 70-110 mg/dl (human) is referred as blood glucose homeostasis [128]. Glucose is the fuel for all physiological processes within the body and low blood glucose concentrations

(hypoglycemia) result in symptoms like dizziness or reduced concentration ability due to an underrepresentation of glucose in the brain. In contrast, long-term hyperglycemia characterizing too high blood glucose levels can cause severe systemic side effects in the overall organism [129].

A sophisticated interplay between the intestine and the pancreas maintains blood glucose homeostasis (Figure 1.7). In brief, the small intestine absorbs glucose and releases gut hormones (incretins) while the pancreas produces the blood glucose regulating hormones insulin and glucagon. The understanding how intrinsic or extrinsic factors further impact on the interplay between both organs is highly important to understand blood glucose regulation. Furthermore, also the brain (via neurons), the liver, the stomach as well as adipose- and muscle tissue release stimuli including hormones and neuropeptides in order to regulate insulin and glucagon secretion and thereby blood glucose homeostasis [85].

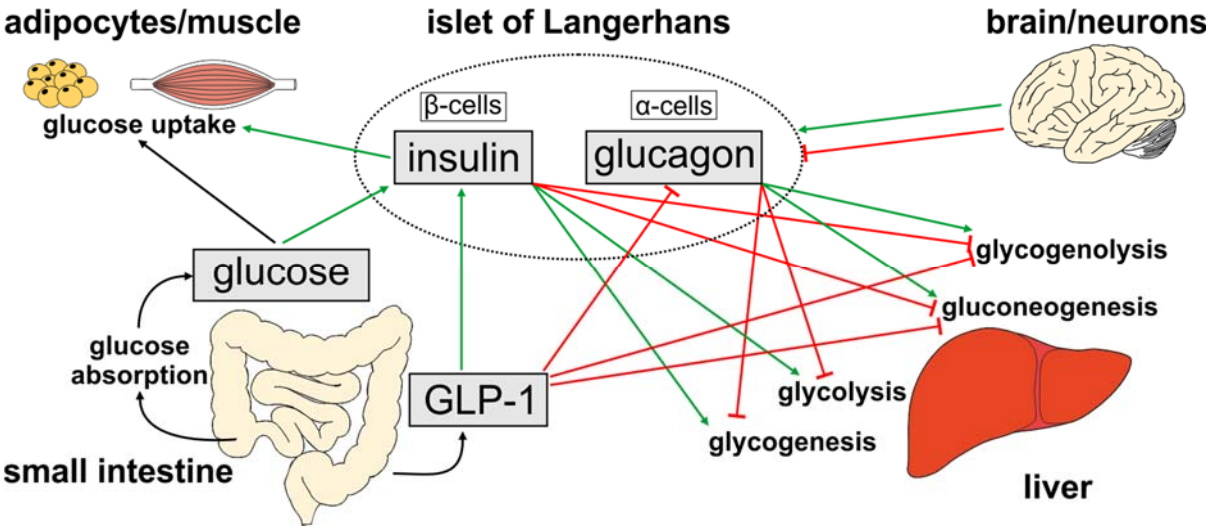

Figure 1.7: The interplay of the small intestine, pancreatic islets and the liver. Schematic overview shows direct insulin and glucagon level regulation. The small intestine absorbs glucose and secrets incretins while the pancreatic β-cells secrete insulin to mediate glucose uptake in body cells (muscle and adipose tissue) to lower blood glucose levels. At low blood glucose concentrations, glucagon is released to trigger endogenous glucose production. The brain directly impacts on pancreatic islets upon intrinsic or extrinsic signals Green arrow = activation/stimulation; red bar = inhibition.

In general, elevated blood glucose levels after meal (postprandial blood glucose) associated with glucose recognition (glucose sensing) in the intestine and pancreas are the main triggers for insulin secretion from pancreatic β-cells [130-133]. In brief,

dietary glucose is absorbed into enterocytes of the small intestine by the sodium and glucose cotransporter SGLT1 [14] from where it is transported by the glucose transporter GLUT2 into the blood stream following the uptake of glucose into pancreatic β-cells also by GLUT2. In the β-cell, glucose undergoes glycolysis and generates adenosine triphosphate (ATP). The increase in ATP results in closure of the ATP-sensitive potassium (K^+) K_{ATP} channels that are normally open to allow equilibration of the resting potential by translocation of K^+ out of the β-cell. Thereby the plasma membrane depolarizes and the voltage-dependent calcium (Ca^{2+}) channels VDCCs grant calcium influx. Elevated intracellular calcium concentrations promote insulin-granules to fuse with the membrane and thus release insulin into the blood stream [85, 134] (Figure 1.8). Insulin decreases blood glucose levels by binding to insulin receptor expressing cells, mainly muscle- and adipose tissue, to recruit the glucose transporter 4 (GLUT4) in order to mediate glucose uptake into these cells [135]. Alternatively, insulin triggers hepatic glucose processing and storage by activating glycolysis and glycogenesis [136, 137] (Figure 7).

In contrast, at low blood glucose levels, ATP-driven channels are inactive on pancreatic α-cells, resulting in a low K_{ATP} channel activity associated with a moderate membrane depolarization. Thereby, specific Na^+ channels become activated and the resulting high action potentials promote the influx of Ca^{2+} and triggers the subsequent release of glucagon granules [138, 139] (Figure 1.8). The secreted glucagon acts on the liver to increase blood glucose levels by promoting gluconeogenesis and glycogenolysis what consequently triggers glucose release into the blood stream [136, 140]. Under high glucose conditions, glucose is absorbed and metabolized from pancreatic α-cells. The increased intracellular ATP to adenosine diphosphate (ADP) ratio blocks the K_{ATP} channels resulting in the depolarization of the cell membrane. The consequences are inactive Na^+ channels and a low action potential height or even a membrane repolarization. Under these conditions, Ca^{2+} channels are inactive and consequently glucagon secretion is blocked [138, 139].

Besides glucose as direct mediator of insulin secretion, dietary fat impacts also on insulin release in an indirect manner. Several studies describe blunted insulin secretion in response to glucose when fed a high-fat diet. However, the exact mechanism remains unknown but possibly fat incorporation in islet-cell membranes or disturbed glucose sensing could be the reason [141-143]. In addition to fat, also circulating

adipose tissue-derived free fatty acids (FFAs) may regulate insulin secretion. This effect is more frequent in obese individuals [144]. Long FFAs bind to the G protein-coupled receptor 40 (GPR40) allowing Ca^{2+} influx and thus insulin secretion while short FFAs inhibit insulin release [145, 146].

Furthermore, a distinct class of gut-derived hormones called incretins are able to potentiate insulin secretion from β-cells (Figure 1.8) [147]. Following the ingestion of glucose [148], fructose [149], amino acids [150] and free fatty acids [151], glucagon-like peptide 1 (GLP-1) is released into the blood stream from intestinal L-cells [147, 152, 153]. The incretin-mediated insulin secretion is dependent on GLP-1 binding to the corresponding GLP-1 receptor (GLP-1R) expressed on pancreatic β-cells [154]. Upon ligand binding, GLP-1R couples with the G-protein complex and releases the $G\alpha_S$ subunit of the receptor complex that triggers membrane-bound adenylyl cyclase to induce cyclic adenosine monophosphate (cAMP) [155]. However, cAMP represents the primary second messenger downstream of GLP-R1 signaling and strictly depends on the availability of ATP produced upon glucose uptake in β-cells [156, 157]. The downstream effectors of cAMP are the protein kinase A (PKA) and the cAMP-regulated guanine nucleotide exchange factor Epac that both block ATP-driven K^+ ion channels [157-159]. Consequently, the GLP-1-mediated and glucose-dependent insulin secretion potentiates the effects of glucose by inhibition of β-cell-specific K^+ ion channels and thereby inducing insulin release (Figure 8). The importance of GLP-R1-mediated insulin secretion was demonstrated in GLP-$R1^{-/-}$ mice that display significantly diminished insulin responses [160]. In addition, GLP-1 does not only affect insulin release, it also promotes gene expression of *Insulin* [161] and increases β-cell proliferation and thus mass [85]. Further, GLP-1 inhibits glucagon secretion from α-cells thereby contributing to the regulation of blood glucose homeostasis [162]. The latter is possibly an indirect effect, as GLP-1 triggers the secretion of glucagon-inhibiting somatostatin from δ-cells [163]. Finally, GLP-1 is also known to fulfill several extra-pancreatic roles like suppression of endogenous glucose production [164] or in general by blunting cellular glucose uptake and disposal [165].

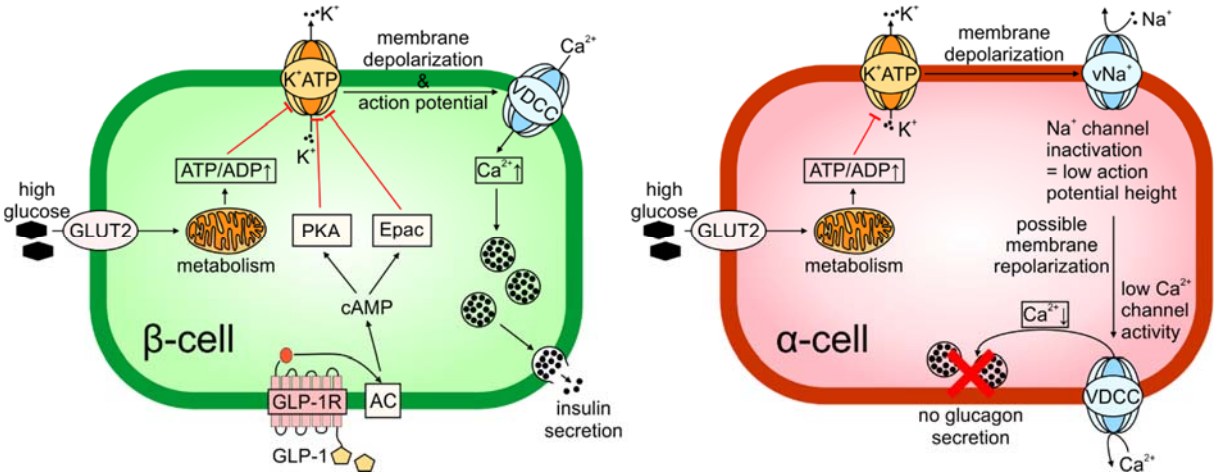

Figure 1.8: Mechanism of insulin secretion from pancreatic β-cells and glucagon release from α-cells. The scheme shows the response of pancreatic β- and α- cells in response to high blood glucose. Insulin secretion is initiated by glucose uptake and promoting action potentials resulting in Ca^{2+} influx and insulin secretion. GLP-1 augments insulin secretion by activation of the GLP-1 receptor and blocking of the K_{ATP} channel via the effector proteins protein kinase A (PKA) and the cAMP-regulated guanine nucleotide exchange factor Epac. High blood glucose concentrations block the release of glucagon by initiating a membrane depolarization and inactivation of the Na^+ channels what hampers Ca^{2+} influx and thereby glucagon release.

1.3.2. The interplay of intestine and pancreas under diabetic conditions

The maintenance of the blood glucose homeostasis is highly important to stay healthy and to maintain essential body functions. Losing the ability to balance blood glucose in a homeostatic range is mainly associated to diabetes and in association with pathologic blood glucose levels, severe complications can emerge over time.

1.3.2.1. Diabetes mellitus - definition, etiology and diagnostics

Diabetes mellitus (DM) depicts a chronic metabolic disorder with an increasing global prevalence. The main symptom is hyperglycemia caused by a disability of the pancreas to produce enough insulin or an acquired insulin resistance. In addition, the ability of glucagon to counteract insulin is lost under diabetic conditions [81, 166] thus hyperinsulinemia and hyperglucagonemia may equally contribute to chronic hyperglycemia [87, 167]. Consequently, the maintenance of blood glucose homeostasis is disturbed. Untreated, the elevated blood glucose level results in severe long-term associated complications like blindness, organ failure or stroke [168, 169]. According to the world health organization (WHO), an estimated number of 422 million

people lived with diabetes mellitus in 2014. An estimated number of 1.6 million people died directly from diabetes in 2015 and another 2.2 million due to high blood glucose levels in 2012. Consequently, diabetes represents an immense social and economic burden resulting in annual expenses of 827 billion US dollar worldwide [170, 171]. So far, diabetes mellitus is an incurable scourge of humanity prevailed in all social classes and regions of the world.

Diabetes mellitus is classified in subtypes, while type 1 and 2 represent the most important representatives [172]. Type 1 diabetes (T1DM) is hallmarked by an autoimmune-mediated destruction of β-cells, associated with an underrepresentation (complete lack) of insulin [173, 174]. However, the vast majority of diabetes patients suffer from type 2 (T2DM) diabetes mellitus characterized by insulin resistance [174]. The emergence of T2DM is closely linked to risk factors including age, ethnicity, obesity, diet habits and life style [175]. Changing and adapting diet behavior and increasing physical activity can reduce obesity and thus decreasing the symptoms of the disease. Hemoglobin A1c (HbA_{1c}; glycated hemoglobin) values are generally used for diagnostics and to monitor the severity of the disease. A value of ≥ 6.5% is associated with diabetes mellitus. In addition, a fasting plasma glucose of <100 mg/dl is normal for a healthy person and ≥126 mg/dl corresponds to T2DM while the range in between marks a prediabetes state [169].

1.3.2.2. Treatment options for diabetes mellitus

Currently, no therapy is available to cure the disease. In any case, the drawbacks and the loss of life quality can be upgraded by drugs, medical devices or surgical interventions depending on the severity and the precise type of DM.

T1DM patients strictly depend on regular insulin administration to amend the low insulin availability and thereby maintaining blood glucose homeostasis [168, 173]. Most emphasizing strategies for T1DM patients comprise the replacement of the lost β-cells by either a whole organ or islet transplantation to restore normoglycemia. However, graft survival is low for clinical intervention [176, 177]. Islets were first transplanted in 1990 in the hepatic portal vein [178], however, most approaches were not efficacy until Shapiro and colleagues established the so called Edmonton islet transplantation protocol [179, 180]. Major drawbacks of islet transplantations are prolonged

immunosuppressive therapies, low donor tissue availability or a too low long-term efficacy [181].

Nowadays, cell replacement strategies using *in vitro* generated bioartificial β-like cells are promising regenerative approaches in the field of translational medicine to stabilize glucose homeostasis, improving life-quality and to cope with the shortage of donor material [182].

Pluripotent human embryonic stem cells (hESCs) or human induced pluripotent stem cells (iPSCs) were recently differentiated and expanded into bioartificial, insulin-producing β-like cells [183-185]. In order to generate functional cells in terms of insulin secretion, the *in vivo* organogenesis is mimicked *in vitro*, however, the final maturation of β-cells occurs only after implantation into a host [186, 187]. In summary, pluripotent stem cells are interesting cell sources to generate bioartificial β-like cells but ethical concerns, tissue rejection and teratoma formation rise concerns regarding the clinical application and the safety for patients [188-192].

Alternative sources to generate insulin-secreting cells were shown by differentiation or conversion of pancreatic ductal- or exocrine cells towards the endocrine lineage [193-196]. However, these cells are difficult to obtain from patients and the available material can only be transplanted as allograft after the generation of hormone-secreting cells. Recent studies further demonstrated that various tissues or especially the adult stem cells of these tissues displayed a great differentiation plasticity upon transient expression of transcription factors. Several publications revealed that simultaneous overexpression of Pdx1, Ngn3 and MafA in liver-, acinar or intestinal cells results in the formation of insulin-secreting cells [197-202]. In summary, these studies demonstrate that various other (adult) stem cell sources display great potential to generate huge numbers of insulin-producing cells *in vitro* and thereby represent interesting approaches for translational therapeutic strategies. For future clinical applications, the derivation of insulin-secreting autografts from adult stem cells is highly promising as the immunological response to such transplants is expected to be low [203].

In contrast to T1DM, T2DM patients are mainly treated by diverse classes of drugs rather than transplantation of functional cells or tissue. The aim of T2DM management is to keep blood glucose in a physiological range and to lower the HbA_{1c} levels in the long term [204]. Metformin is the most prescribed medication and inhibits endogenous

glucose production [205, 206]. Several compounds target pancreatic β-cells directly. Meglitinides and sulfonylureas with K_{ATP} channels to induce β-cell depolarization what enhances Ca^{2+} channel activity and insulin release [207]. The drug-mediated increased insulin quantity was shown to be sufficient in most diabetes patients to overcome insulin resistance [169]. Another class of medication increases the incretin effect by GLP-1 mimetics or inhibition of dipeptidyl peptidase 4 (DPP4) that cleaves GLP-1 within minutes *in vivo* [208, 209]. Thus, DPP4 inhibitors slightly augment insulin secretion, prevent glucagon release and endogenous glucose production [209].

Obesity and hyperglycemia associated to T2DM might be consequences of excessive glucose uptake. In order to minimize the glucose absorption various glucose transporters can be targeted or inhibited. Alpha-glucosidase inhibitors target the small intestine by decelerating carbohydrate splitting and therefore uptake in the blood [210]. The Na^+-D-glucose cotransporter 2 (SGLT2) inhibitors Dapagliflozin, Canagliflozin and Empagliflozin prevent renal glucose absorption [14, 211, 212] and can be combined with other antidiabetic medications, including insulin administration [169]. Intestinal glucose uptake can be blocked by SGLT1 inhibitory compounds like Mizagliflozin or Sotagliflozin [213-216]. Besides reduced and delayed glucose absorption in the small intestine, SGLT1 inhibitors further promote and prolong the release of GLP-1 in the distal gut via free fatty acid receptors 2/3 (FFAR2/3) (Figure 1.9) what improves glycemic control [151, 213, 217, 218].

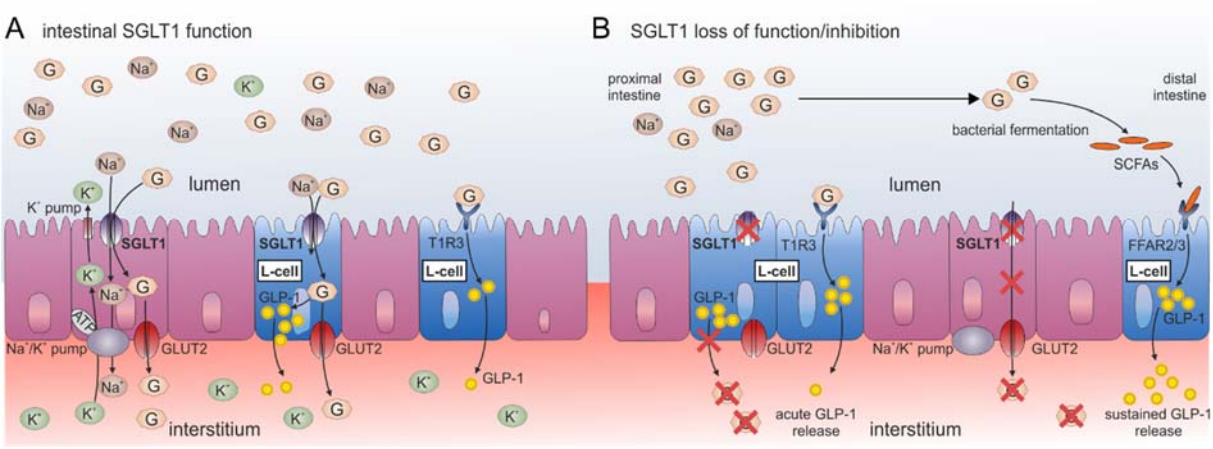

Figure 1.9: Intestinal SGLT1-mediated glucose absorption and GLP-1 release from L-cells. (A) Graph shows the intestinal Na^+/glucose co-absorption mediated by SGLT1 and the simultaneous release of GLP-1 from enteroendocrine L-cells under normal physiological conditions. GLP-1 is released in a SGLT1-dependent- and independent manner (by T1R3). (B) Scheme displays beneficial consequences for T2D patients in the small intestine when SGLT1 function is lost or inhibited: reduced glucose uptake and increased GLP-1 in the distal gut. The sustained GLP-1 release is mediated by gut bacteria that metabolize glucose short chain fatty acids that trigger incretin release from L-cells via FFAR2/3 activation. FFAR2/3 = free fatty acid receptor 2/3; glucose-dependent insulinotropic peptide (GIP); glucagon-like peptide 1 (GLP-1); G = glucose; GLUT2 = glucose transporter type 2 (SLC2A); SCFAs = short chain fatty acids; T1R3 = taste receptor type 1 member 3.

The challenge for successful management of T2DM is defining a monotherapy or combined application of diverse compounds what varies in every individual patient. In the future, higher efficient pharmacological compounds in combination with bariatric surgery [219, 220] could further improve glycemic control and thus ameliorate the life quality of T2DM patients. However, a strict nutrition plan together with a healthy lifestyle will always be essential for successful management of the disease.

1.4. Aim of the thesis

Functional therapeutics for translational approaches in humans strongly depend on a detailed look at the sophisticated interplay of whole organ systems. This thesis focused on the interplay of the small intestine and the pancreas in the context of establishing new therapeutic strategies for Diabetes mellitus, a severe and pandemic disease of our society. In general, this thesis comprises two conceptionally different projects.

- Project 1 focuses on the potential of ISCs as an alternative cell source for the derivation of pancreatic β-like cells to be used in future cell-based replacement strategies for T1DM.
- Project 2 focuses on effects in pancreatic islets after loss of SGLT1 function, a glucose transporter of the small intestine that currently represents an interesting target in new medication-based concepts for T2DM patients.

1.4.1. Establishment of a Ptf1a-based differentiation protocol to derive pancreatic β-like cells from intestinal stem cells

ISCs harbor a high self-renewal capacity and differentiation potential *in vivo*. As the recently developed mini-gut organoid models show [42], ISCs retain these characteristics also *in vitro*. Based on this potential, **ISCs were hypothesized in this work as interesting cell type for the derivation of pancreatic β-like cells**. One of the most important benefits in this context is that intestinal and pancreatic cells share their developmental origin - the endodermal gut tube. Cells of both tissues develop from a common progenitor and therefore exhibit a similar epigenetic memory. In principle, intestinal and pancreatic cells develop from this progenitor due to the activation and suppression of lineage-specific genes. This results in the formation of lineage-specific transcription factors that guide tissue specification. Based on the action of such pioneer transcription factors it is likely to either restore the genetic and epigenetic profile of the common ancestor or directly induce a cell lineage switch towards another cell type, depending on the tissue-specification of the corresponding transcription factors. Supportive for the assumption that ISCs could serve indeed as cell source for the derivation of non-tissue-specific cells are the findings from a recent study demonstrating the transdifferentiation from intestinal to bladder tissue [221].

In the thesis, the Lgr5-eGFP^{+} transgenic mouse line was used in order to precisely isolate single-cell ISCs by FACS due to the Lgr5 promoter-driven eGFP expression. **Differentiation of ISCs towards pancreatic β-like cells should be induced by the ectopic expression of pancreatic transcription factor 1 alpha (Ptf1a)**, which acts as pioneer transcription factor for pancreatic lineage specification during early embryonic development [115]. Later in pancreas organogenesis, Ptf1a determines the acinar cell type [222, 223]. To overexpress Ptf1a in single-cell ISCs, several strategies were applied and compared with each other to determine the best condition that do not only induce Ptf1a expression but also sustains cell survival and proliferation. As ISCs are usually cultured in a 3D microenvironment *in vitro*, there is also the need to establish a monolayer-based cell culture system to achieve high transfection or transduction efficiencies of single cell ISCs. The establishment of a transcription factor-based differentiation protocol always includes the definition of a suitable differentiation-specific medium. Here in this study, a pancreatic differentiation-specific medium formulation, reported in previous publications [224-226], is hypothesized to support pancreatic differentiation of ISCs. Monitoring cellular morphologies and gene expression patterns characteristic for ISCs, pancreatic progenitors, pancreatic islet-specific cell types and pancreatic acinar cells, should reveal differentiation success.

In summary, this part of this thesis should demonstrate the potential of ISCs as alternative stem cell source to derive functional pancreatic cell types *in vitro*.

1.4.2. The role of SGLT1 for pancreatic islet integrity

The most common strategies to target hyperglycemia and improving life quality of T2DM patients is achieved by medical treatments maintaining blood glucose levels in a physiological range. In this context, the dual SGLT1/SGLT2 inhibitor Sotagliflozin is currently of great interest as antidiabetic drug, as it was demonstrated in clinical trials to reduce postprandial glucose excursion, lowering HbA_{1c} values and to enhance GLP-1 secretion [227-233]. While SGLT2 inhibitors are relatively well characterized, few is known about SGLT1 inhibition and risk assessment for application in humans [234]. However, clinical SGLT1 inhibitors were previously considered as safe and only moderate complaints regarding the small intestine were reported so far.

SGLT1 is predominantly expressed on enterocytes of the intestinal brush border membrane and in the proximal nephron of the kidney to mediate intestinal and renal glucose absorption [14, 15, 235]. In addition, SGLT1 expression was confirmed in various other organs including kidney, heart, brain, liver, lung and pancreas [236-240], while the tissue-specific function remains largely unknown. The recent findings of SGLT1 expression in pancreatic α- and intralobular duct cells [236, 238] together with the high relevance of SGLT1 inhibition for clinical applications arose the question if loss or inhibition of SGLT1 function could result in adverse events in other SGLT1 expressing tissues. Consequently, **the aim of this part of the thesis was to investigate if SGLT1 ablation affects pancreatic islet integrity comprising altered pancreatic islet morphology, architecture and function**. To this aim, a global SGLT1 knockout mouse model should provide first insights into this topic [241]. Because SGLT1$^{-/-}$ mice are strictly fed a glucose-deficient, fat-enriched (GDFE) diet to circumvent the glucose-galactose malabsorption syndrome, adequate controls were included in this study to allow the comparison between diet- or knockout-specific effects. By means of immunohistological and FACS analysis, pancreatic islet characteristics including size, cellular composition (cyto-morphology) focusing on α- and β-cells as well as proliferation- and apoptosis rates will be determined. Next, isolated islets stimulated with glucose should reveal functional properties of SGLT1 knockout islets. In addition, to gain insights of the systemic hormone regulation under SGLT1 ablation, mice will be stimulated with glucose and the concentrations of insulin, GLP-1 and glucagon will be analyzed in systemic blood at different time points.

Together, this work will contribute to define the role of pancreatic SGLT1 and will further indicate possible side effects when SGLT1 function is lost.

2. Materials and Methods

2.1. Materials

2.1.1. Chemicals and Reagents

2-Propanol	Carl Roth
Ampligase	Epicenter
Agarose	Biozym Scientific
Bacto-tryptone	AppliChem
BSA	BioFroxx
Calcium chloride	VWR
Cell Recovery Solution	Corning
Citric acid	Sigma Aldrich
CollagenP	Roche
Dipeptidyl peptidase (DPP)-IV inhibitor	Merck Millipore
Dispase	Gibco
DNase I	Roche
Dithizone	Sigma Aldrich
EDTA	Sigma Aldrich
Ethanol	Sigma Aldrich
Ficoll Paque	GE Healthcare
Glucose D (+)	Sigma Aldrich
Lipofectamine™ Ltx	Invitrogen
Lipofectamine™ 2000	Invitrogen
Magnesium chloride	Carl Roth
Magnesium sulfate	Carl Roth
MTT (Thiazolyl blue)	SERVA
Peg 8000	AppliChem
PEI Transfection reagent	Polysciences Inc
Polybrene	Merck Millipore

Poly-L-ornithine	Sigma Aldrich
Potassium chloride	Sigma Aldrich
Potassium dihydrogen phosphate	Merck
RLT buffer	QIAGEN
Roti® Histofix 10%	Carl Roth
Sodium bicarbonate	Carl Roth
Sodium chloride	Sigma Aldrich
Sodium fluoride	FLUKA
Sucrose	Sigma Aldrich
Tissue-Tek® O.C.T.™ Compound	Sakura
Tris Base (Trizma)	Sigma Aldrich
Tri-Sodium-citrate	Sigma Aldrich
Triton-X-100	Sigma Aldrich
Tween 20	Sigma Aldrich
X-FECT Protein transfection reagent	Clontech
Yeast extract	CarlRoth

2.1.2. Commercial kits

AmpliScribe™ T7-Flash™ Transcription Kit	Epicentre
BD Cytofix/cytoperm™ (FACS)	BD
CellTiter-Glo® Luminescent Cell Viability Assay	Promega
DNA Clean&Concentrator™ Kit	Zymo Research
Fluorochrome-labeled Annexin V apoptosis kit	BioLegend
Glucose Colormetric Assay Kit (10009582)	Cayman Chemicals
iScript™ cDNA Synthesis Kit	Biorad
KAPA Mouse genotyping Kit	KAPA
Nucleospin RNA II Kit	Macherey-Nagel
pGEM®-T Easy Vector System Kit	Promega
Plasmid Maxi Kit	QIAGEN

Quant-it dsDNA PicoGreen Kit	Thermo Fisher
RNAeasy Micro Kit	QIAGEN
RNeasy Mini Kit	QIAGEN
ScriptCap™ m7G Capping System	CellScript
ScriptCap™ 2'-O-Methyltransferase Kit	CellScript
SsoFast™ EvaGreen® Supermix	Biorad
SUMO protease cleavage Kit	Invitrogen
Zymoclean™ Gel DNA Recovery Kit	Zymo Research
Zyppy™ Plasma Miniprep Kit	Zymo Research

2.1.3. General solutions and buffer

TAE buffer	40 mM Tris Base
	20 mM Acetate
	1 mM EDTA
	ddH_2O
Krebs buffer (KRB)	137 mM NaCl
	4.7 mM KCl
	1.2 mM KH_2PO_4
	1.2 mM $MgSO_4$-7H20
	2.5 mM $CaCl_2$-2H2O
	25 mM $NaHCO_3$
	ddH_2O
Glucose D (+) Solution	Krebs buffer
	1.65 M Glucose D (+)
	ddH_2O

Citrate buffer pH 4.5	2.5% (w/v) Tri-Sodium-citrate 1.4% (w/v) Citrate 2% (w/v) D (+) Glucose ddH_2O and pH-adjustment
Islet staining solution	10% (w/v) Dithizone 10% (v/v) DMSO Up to 50 ml PBS^+
Islet washing solution A	RPMI 1640 1 × Antibiotic-Antimicotic (v/v) 10 mM Hepes 0.1% (w/v) BSA 10 µg/ml DNase
Islet washing solution B	RPMI 1640 1 × Antibiotic-Antimicotic 10% (v/v) FCS 0.5% (w/v) BSA
TBS-T (Tween)	0.6% (w/v) Tris base 0.9% (w/v) NaCl 0.05% (v/v) Tween 20

2.1.4. Cell culture

2.1.4.1. Cell culture reagents

2-mercaptoethanol	Carl Roth
AA2P	Sigma Aldrich
Advanced DMEM/F12	Gibco

Antibiotic-Antimicotic	Gibco
B-27 (without Vitamin A)	Gibco
B-27 supplement	Gibco
CAAD-cyclopamine	Merck Millipore
CHIR99021	Biomol
Compound-E	Merck Millipore
DMEM/F12	Gibco
DMSO	Sigma Aldrich
D-PBS/PBS^{+}	Gibco
FCS	Lonza
FCS (EScult)	STEMCELL Technologies
FCS (SPOT)	Bio&Cell
FGF10	PeproTech
Gastrin	Sigma Aldrich
Gelatine (48720)	Sigma Aldrich
GlutaMax	Gibco
GMEM	Gibco
HBSS	Gibco
HEPES	Gibco
human R-Spondin	PeproTech
Jagged-1 peptide	AnaSpec Inc.
Matrigel®	Corning
mLIF-ESG1106	Merck Millipore
mouse recombinant EGF	PeproTech
mouse recombinant Noggin	PeproTech
N2 supplement	Gibco
n-Acetylcysteine	Sigma Aldrich
Nicotinamide	Sigma Aldrich
Opti-MEM™ Reduced Serum Medium	Gibco
Penicilin/Streptomicin	Gibco

Retinoic acid (RA)	Sigma Aldrich
Rock inhibitor Y-27632	Tocris
RPMI 1640	Gibco
Sodium pyruvate	Gibco
Trypsin/EDTA	Gibco
Valproic Acid (VA)	Sigma Aldrich

2.1.4.2. Cell culture material

Disposable cell culture pipettes CELLSTAR	Greiner Bio-one
Nunclon™ Delta cell culture material	Thermo Fisher
Standard cell culture material	TPP

2.1.4.3. Cell lines

The HEK293 cell line was generated from human embryonic kidney cells [242]. Cells were used as host for gene expression and obtained from ATCC (ATCC® CRL-1573™). The HEK293T cell line derived from human embryonic kidney cells and harbors the SV40 T-antigen [243]. Cells were obtained from ATCC and used for lentivirus production (ATCC® CRL-3216™). The murine embryonic stem cell line CGR8 (kindly provided by Dr. Francesca Ciccolini, IZN Heidelberg, University of Heidelberg) was generated from the inner cell mass of a 3.5 day old mouse embryo and was used for pancreatic differentiation.

2.1.4.4. Cell culture media

HEK293/HEK293T cell culture medium	DMEM
	10% (v/v) FCS
	1 × Sodium pyruvate (v/v)
	1 × Penicillin/Streptomycin (v/v)

Organoid maintenance medium	Advanced DMEM/F12
(M-medium)	1 × GlutaMax (v/v)
	1 × Penicilin/Streptomicin (v/v)
	10 mM Hepes
	1% (v/v) N2
	0.5% (v/v) B27
	1 µM N-Acetylcysteine
	50 ng/ml EGF
	100 ng/ml Noggin
	500 ng/ml R-spondin1
	10 µM Rock inhibitor Y-27632
Medium YCVJ	(M-medium)
	10 µM Y-27632
	3 µM CHIR99021
	1 mM valproic acid
	1 µM Jagged-1
Murine islet maintenance medium	RPMI 1640
	10% (v/v) FCS
	1 × GlutaMax (v/v)
	1 × Penicilin/Streptomicin (v/v)
	20 mM Hepes
	50 µM 2-Mercaptoethanol
mESC/CGR8 maintenance medium	GMEM
	10% (v/v) ESC approved FCS
	10 µM 2-mercaptoethanol
	1.000 U/ml mLIF

Pancreatic differentiation medium 1	50% DMEM
	50% DMEM/F12
	1 × Glutamax (v/v)
	50 µM 2-mercaptoethanol
	0.5 mM AA2P
	50 ng/ml ActivinA
	200 ng/ml Noggin
	5 µM CHIR 99021
Pancreatic differentiation medium 2	DMEM
	1 × B27 (v/v)
	(A) 250 µM Cyclopamine
	100 ng/ml Noggin
	2 µM RA
	25 µg/ml FGF10
	(B) 50 ng/ml FGF10
	(C) 100 ng/ml Noggin
	(C) 1 µM Compound-E
Pancreatic Organoid Differentiation Medium	Advanced DMEM/F12
(POD-Medium; Adapted from [224]	1 × Penicilin/Streptomicin (v/v)
	0.5% B27 (v/v)
	1.25 µM N-Acetylcysteine
	10 nM gastrin
	50 ng/ml EGF
	100 ng/ml Noggin
	500 ng/ml R-spondin1
	150 ng/ml FGF10
	10 mM Nicotinamide

Cell freezing medium	90% (v/v) FCS 10% (v/v) DMSO

2.1.5. Mouse work

2.1.5.1. Mouse lines

Mouse strain	**Source and Reference**
C57BL6/J (wild type mouse line)	Charles River
B6.129P2-LGR5$^{tm1(cre/ERT2)Cle/J}$ (Lgr5-eGFP mouse line[1])	Jackson Laboratory [39]
B6.Cg-Gt(ROSA)26Sor 5$^{tm9(CAG-Tomato)Hze/J}$ (CAGGS-tdTomato mouse line[2])	Jackson Laboratory [244]
Sglt1$^{-/-}$ (129/OLA/57BL6) (SGLT$^{-/-}$ moue line[3])	Obtained from Prof. Koepsell [241]

[1]Abbreviation of the mouse line in this Thesis. Lgr5-eGFP mice were alternatively described as Lgr5-EGFP-IRES-creERT2 and constitutively expresses the eGFP reporter gene under the control of the murine leucine rich repeat containing G protein coupled receptor 5 (LGR5) promotor

[2]Abbreviation of the mouse line in this Thesis. The line was generated by modifying the Rosa26 locus by inserting a floxed-STOP cassette controlled expression of the fluorescent marker tdTomato driven by the CAGGS promotor.

[3]Abbreviation of the mouse line in this Thesis. The SGLT1$^{-/-}$ mouse misses parts of the SGLT1 promoter and EXON 1. The knocked out elements prevent the translation of the Na (+) –D-glucose cotransporter 1 (SGLT1).

2.1.6. Molecular biology

2.1.6.1. Bacteria strains

Name	Genotype	Application
BL21(DE3)	B F$^-$*ompT gal dcm lon hsdS$_B$*($r_B^-m_B^-$) λ(DE3 (*lacI lacUV5-T7p07 ind1 sam7 nin5*)) (*malB*$^+$)$_{K-12}$(λ^S)	Protein production (Invitrogen)
C3040	F' proA+B+ lacIq Δ(lacZ)M15 zzf::Tn10 (TetR) Δ(ara-leu) 7697 araD139 fhuA ΔlacX74 galK16 galE15 e14-Φ80dlacZΔM15 recA1 relA1 endA1 nupG rpsL (StrR) rph spoT1 Δ(mrr-hsdRMS-mcrBC)	Lentivirus (New England Biolabs)

2.1.6.2. Bacteria culture media

LB

1% (w/v) Bacto-tryptone
0.5% (w/v) Yeast extract
1% (w/v) NaCl

TSS buffer (competent bacteria)

LB Medium
10% (w/v) PEG 8000
3% (v/v) 1M MgCl2
5% (v/v) DMSO

2.1.6.3. Plasmids

Name	Selection marker	Source
pAID1.1-C	KanR/NeoR	CosmoBio
pAID1.1-N	KanR/NeoR	CosmoBio

pReceiver-B-13-Ptf1a	AmpR	Genecopoeia (Mm34576-B13)
pCDH-CMV-MCS-EF1-RFP	AmpR	SystemBiosciences (CD512B-1)
pL-CMV-Ptf1a-EF1α-RFP	AmpR	Generated by Dr. D. Zdzieblo and V. Kryklyva
pL- PGK-Ptf1a-EF1α-RFP	AmpR	Generated by Dr. D. Zdzieblo and V. Kryklyva
pSico PGK puro vector	Puro	Addgene #11586
psPAX2	AmpR	Addgene #12260
pMD2.G	AmpR	Addgene #12259

2.1.7. Polymerase chain reaction (PCR)

2.1.7.1 Materials for PCR and quantitative real-time PCR (qRT-PCR)

100BP DNA ladder plus	Peqlab
Blue DNA Loading dye (6x)	Peqlab
DNA ladder 1kb N3232	New England Biolabs
DNTPs	BIOLINE
GelRed™	GENAXXON
λ-DNA/PstI marker	Fermentas

2.1.7.2. Primer for genotyping by PCR

Primer for genotyping	**Annealing Temperature**	**5' to 3' Sequence**
SGLT1_Primer1_RG22	62°C	GAGCCTGGGCTTCTGGTTCAG
SGLT1_Primer2_RG17	62°C	TCTAGTTGCAGTAGCACACCCC
SGLT1_Primer3_RG24	62°C	GCAGTCTGCAGAGGTGATGAC

LGR5_WT_Forward	60°C	CTGCTCTCTGCTCCCAGTCT
LGR5_WT_Reverse	60°C	ATACCCCATCCCTTTTGAGC
LGR5_Mutant_Reverse	60°C	GAACTTCAGGGTCAGCTTGC

2.1.7.3. Primer for quantitative real-time (qRT-) PCR

Name	5' to 3' Sequence	Source or Reference
Sglt1#	5'-TCTGTAGTGGCAAGGGGAAG-3' 5'-ACAGGGCTTCTGTGTCTTGG-3'	NM_019810.04 # [245]
Rpl15	5'-CTGACCCTGGATGTCTTGGTGC-3' 5'-CCAAGCAGCCACTTCAGTGAACC-3'	NM_025586.3
Rpl6	5'-CGGGAGTACCTGCCAATTCC 5'-GGTGAAAAAGCGCCTGATACA	NM_011290
RPS29	5'-GTCTGATCCGCAAATACGGG 5'-AGCCTATGTCCTTCGCGTACT	NM_009093
*Insulin2**	5'-GCTTCTTCTACACACCCATGTC-3' 5'-AGCACTGATCTACAATGCCAC-3'	NM_001185084.2 *6680463a1
*Glucagon**	5'-TTACTTTGTGGCTGGATTGCTT-3' 5'-AGTGGCGTTTGTCTTCATTCA-3'	NM_008100 *33468853a1
*Somatostatin**	5'-CTGGCTGCGCTCTGCATCGT-3' 5'-GGCCAGTTCCTGTTTCCCGGT-3'	NM_009215.1
*GLP-1R**	5'-ACGGTGTCCCTCTCAGAGAC-3' 5'-ATCAAAGGTCCGGTTGCAGAA-3'	NM_021332 *11024690a1
*Glut2**	5'-TCAGAAGACAAGATCACCGGA-3' 5'-GCTGGTGTGACTGTAAGTGGG-3'	NM_031197 *13654262a1
Sox2	5'-TCTGTGGTCAAGTCCGAGGC-3'	NM_153559

	5’-TTCTCCAGTTCGCAGTCCAG-3’	
Oct4	5’- TCTCCCATGCATTCAAACTG-3’ 5’- GCTCCTGATCAACAGCATCA -3’	NM_001252452
*Nanog**	5’-TCTTCCTGGTCCCCACAGTTT-3’ 5’-GCAAGAATAGTTCTCGGGATGAA-3’	NM_028016 *31338864a1
Sox17	5’-GATGCGGGATACGCCAGTG-3’ 5’-CAACCACCTCGCCTTTCAC-3’	NM_011441
FoxA2	5’-GAACTCCATCCGCCACTCTCT-3’ 5’-AGCCCTTGCCAGGCTTGT-3’	NM_010446.2
Cxcr4	5’-GACTGGCATAGTCGGCAATG-3’ 5’-AGAAGGGGAGTGTGATGACAAA-3’	NM_009911
Nkx6.1	5’-ATGACGGAGAGTCAGGTCAAGGTCT-3’ 5’-CGGCTGCGTGCTTCTTTCTCCA-3’	NM_144955.2
Pdx1	5’-GTTGGGTATAGCCGGAGAGATG-3’ 5’-TTGGAGCCCAGGTTGTCTAAA-3’	NM_008814.3
Ptf1a	5’-AGGCCCAGAAGGTTATCATCTG-3’ 5’-GAAAGAGAGTGCCCTGCAAGA-3’	NM_018809.2
Olfm4	5’-CAGCCACTTTCCAATTTCACTG-3’ 5’-GCTGGACATACTCCTTCACCTTA-3’	NM_001030294
Ascl2	5’-AAGCACACCTTGACTGGTACG-3’ 5’-AAGTGGACGTTTGCACCTTCA-3’	NM_008554
Smoc2	5’-AGTGGAGACATTGGCAAGAAG-3’ 5’-ACACACTTTTTGGGCTTGGATT-3’	NM_022315
Tnfrsf19	5’-CGCTGCCATTCTCTTCCTACT-3’ 5’-CAATCTCCGGCTTCGCAACT-3’	NM_001164155

Lgr5	5'-GGGAAGCGTTCACGGGCCTTC-3' 5'-GGTTGGCATCTAGGCGCAGGG-3'	NM_010195.2
Cdx2	5'-GGAAGCCAAGTGAAAACCAGGACA-3' 5'-TCGGAGAGCCCAAGTGTGGCA-3'	NM_007673.3
Hes1	5'-AAGAAAGATAGCTCCCGGCATTCCA-3' 5'-CCGGCGCGGTATTTCCCCAA-3'	NM_008235.2
Hnf1b	5'-CACCAAGCCGGTTTTCCATAC-3' 5'-GGAGTGTCATAGTCGTCGCC-3'	NM_009330
Sox9	5'-AGTACCCGCATCTGCACAAC-3' 5'-ACGAAGGGTCTCTTCTCGCT-3'	NM_011448
Amylase	5'-TGGCGTCAAATCAGGAACATG-3' 5'-AAAGTGGCTGACAAAGCCCAG-3'	NM_023525
ChymoB1	5'-GCAAGACCAAATACAATGCCC-3' 5'-TGCGCAGATCATCACATCG-3'	NM_025583.2
*Ngn3**	5'-CCAAGAGCGAGTTGGCACT-3' 5'-CGGGCCATAGAAGCTGTGG-3'	NM_009719 *157267375c1
Ki67	5'-CAGAGCTAACTTGCGCTGAC-3' 5'-CGCTTGATGGTGACCAGGTG-3'	NM_001081117.2

2.1.7.4. Oligonucleotides for synthetic RNA generation

Name	Oligonucleotide
5' UTR	5'-TTGGACCCTCGTACAGAAGCTAATACGACTCACTATAGGGAAATAAGAGAGAAAAGAAGAGTAAGAAGAAATATAAGAGCCACCATG-3'
3' UTR	5'-(Phos)GCTGCCTTCTGCGGGGCTTGCCTTCTGGCCATGCCCTTCTTCTCTCCCTTGCACCTGTACCTCTTGGTCTTTGAATAAAGCCTGAGTAGGAAGTGAGGGTCTAGAACTAGTGTCGACGC-3'

5’ Splint	5’-CTGCGGCATGAGGACCTCGTGAACATGGTGGCTCTTATATTTCTTCTT-3’
3’ Splint	5’-CCCGCAGAAGGCAGCTCAGGACACAAACTCAAAGGGTGG-3’

2.1.8. (Immuno-) Histology

2.1.8.1. Material and solution for Histology

Aquatex® Mounting Solution	Merck Millipore
DCS Super Vision 2 HRP Polymer Kit	DCS
Donkey serum	Sigma Aldrich
Entellan	Merck Millipore
Eosin (10177)	Morphisto
Fluoromount-G (with DAPI)	Invitrogen
Glass slides Polysine™	Thermo Fisher
Glass slides SuperFrost® Plus	Langenbrink
Hematoxilin (10231)	Morphisto
Histogel™	VWR
Oil Red O solution	Sigma Aldrich
Saponin	Carl Roth
Xylol	Carl Roth

2.1.8.2. Primary antibodies

Antibody	**Host**	**Dilution**	**Manufacturer**
α-SGLT1	Rabbit	1:100-1:500	From Prof. Koepsell
α-SGLT1	Rabbit	1:100	Merck Millipore (07-1417)
α-Insulin	Mouse	1:1.000	Sigma Aldrich (I2018)
α-Glucagon	Rabbit	1:1.000	Abcam (EP3070)

α-Glucagon	Mouse	1:1.000	Abcam (Ab10988)
α-Ki67	Rabbit	1:100	Abcam (Ab15580)

2.1.8.3. Secondary antibodies

Antibody	**Host**	**Dilution**	**Manufacturer**
α-Mouse-Cy3	Donkey	1:400	Invitrogen (A31570)
α-Mouse-Cy5	Donkey	1:400	Invitrogen (A31571)
α-Rabbit-Cy3	Donkey	1:400	Invitrogen (A31572)
α-Rabbit-Cy5	Donkey	1:400	Invitrogen (A31573)

2.1.9. FACS

2.1.9.1. Material

BD Cytofix/cytoperm™ (FACS)	BD
Fluorochrome-labeled Annexin V apoptosis kit	BioLegend

2.1.10.2. Antibodies

Antibody	**Host/Specification**	**Dilution**	**Manufacturer**
α-OCT3/4-PE	Mouse $IgG1_{Kappa}$	1:100	BD (561556)
α-NANOG-Cy5	Mouse $IgG1_{Kappa}$	1:100	BD (562259)
α-SSEA4-PE	Mouse $IgG3_{Kappa}$	1:100	BD (560128)
α-Mouse-PE (Iso)	α-Mouse $IgG3_{Kappa}$	1:100	BD (559926)
α-Mouse-Cy5 (Iso)	α-Mouse $IgG1_{Kappa}$	1:100	BD (550795)

2.1.10. Software

Bio-Rad CFX Manager 3.1	Biorad
BZ-II Analyzer	Keyence
CorelDRAW Graphics Suite X7	Corel
FIJI ImageJ	NIH (USA)
FlowJo 10.4.1.	FlowJo LLC
Graphpad Prism 6	GraphPad Software Inc.

2.1.11. Microscopes and devices

Amicon® Protein Concentration Cell	Merck Millipore
BD Accuri C6 Cytometer	BD
Cell incubator Heraeus BBD 6220	Thermo Scientific
Centrifuge Heraeus Multifuge X1R	Thermo Scientific
Centrifuge 5417R	Eppendorf
CFX96 Touch™ Real-Time PCR Detection System	Biorad
Confocal microscope TCS SP8	Leica Microsystems
EVOS™ XL Core Imaging System	Thermo Fisher
FACS Calibur BD	BD
Inverse Fluorescence Microscope BZ-7000	Keyence
Leica SM 2010R Microtome	Leica
Leica CM 1850 UV Cryostat	Leica
PCR LabCycler 48	SensoQuest
TECAN Infinite 200 PRO microplate reader	TECAN

2.2. Methods

2.2.1. Mouse work

2.2.1.1. General conditions

All mouse lines were kept and breed at 12h light/dark cycles with water and food *ad libitium.* Handling and housing were conducted in accordance with institutional guidelines and the German animal protection law. All mice were fed with a standard laboratory chow (#1320) obtained from Altromin. Research using the SGLT1 knockout mouse line was approved by the Ethics Committee of the District of Unterfranken, Würzburg, Germany (approval number: 55.2-2531.01-45/14).

2.2.1.2. Dietary conditions for SGLT1 knockout mice

Studies with SGLT1 knockout mice required the feeding with a glucose-deficient, fat-enriched diet (#C-1073, Altromin) to circumvent glucose-galactose malabsorption [241]. For experimental purposes, wild type animals were kept on the same diet to differentiate between SGLT1 knockout- and diet-dependent effects. The dietary composition of both equicaloric diets is represented in Figure 2.1A. The lack of carbohydrates as metabolizable content was substituted by fat and proteins (Figure 2.1B).

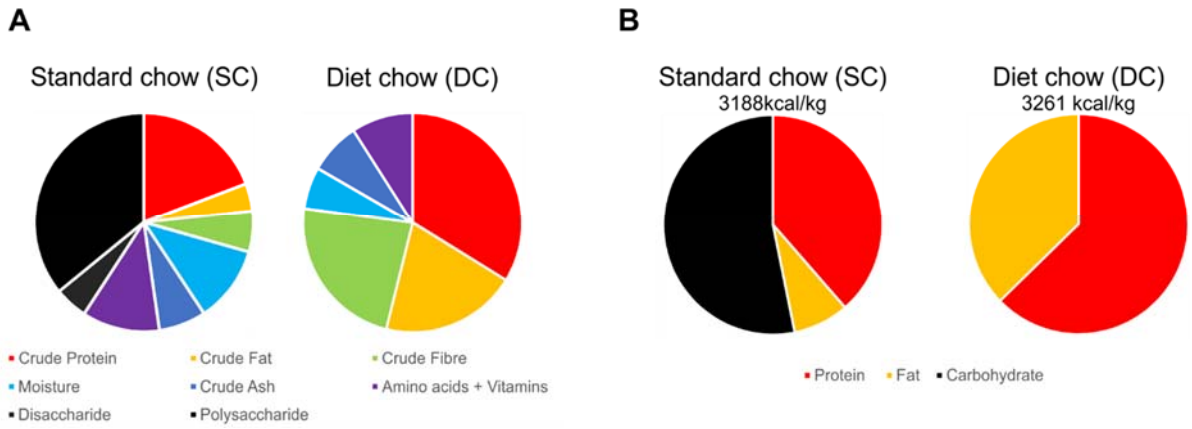

Figure 2.1: Comparison of standard laboratory chow (SC) with the glucose-deficient, fat-enriched (DC) diet for SGLT1 knockout animals. (A) Composition of SC and DC. (B) Energy value and ratio of energy-supplying ingredients of SC and DC diet.

2.2.1.3. Mouse genotyping

Mouse pups were weaned between 21-28 days of age and separated by gender. Mice were numbered consecutively by ear stamps and ear punches were used for genotyping. To this aim, first DNA was isolated using the KAPA Mouse genotyping Kit (KAPA) according to manufacturer's instructions. Briefly, ear punches were placed in 100 µl of KAPA Express Buffer (88 µl ddH_2O, 10 µl of 10 × KAPA Express Extract Buffer and 1U/µl Extract Enzyme) followed by incubation on a PCR LabCycler 48 (SensoQuest) at 75°C for 10 min (tissue lysis) and at 95°C for 5 min (enzyme inactivation). Afterwards, DNA was used for PCR genotyping as described in 2.2.6.7.

2.2.1.4. Oral glucose tolerance test (OGTT)

Before glucose gavage, the mice endured a fasting period of 12h with free water access. The OGTT was performed by bolus-mediated administration of either 6 mg glucose (dissolved in Milli-Q H_2O) per g body weight or PBS as control. After 5 or 60 min the animals were sacrificed and 300 µl blood was directly obtained from the left heart chamber. Immediately, the samples were mixed with 100 µl citrate buffer (pH 4.5) and 100 µmol/L dipeptidyl peptidase (DPP)-IV inhibitor (Merck Millipore) to avoid blood clotting and degradation of GLP-1. Samples were centrifuged for 5 min at 10,000 × g, 4°C. The plasma containing supernatant was stored at -80°C until analysis.

2.2.1.5. Crossing of Lgr5-eGFP- and tdTomato mice to verify RNA or protein uptake in isolated organoids

To generate a test system for RNA or protein uptake verification in murine crypts, the mouse lines B6.129P2-$^{Lgr5tm1(cre/ERT2)Cle/J}$ and B6.Cg-Gt(ROSA)26Sor $5^{tm9(CAG-Tomato)Hze/J}$ were crossed to generate double transgenic Lgr5-eGFP/CAGGStdTomato mice (Figure 2.2A). RNA or protein uptake was tested by using the CRE recombinase protein. Cellular uptake of CRE results in the excision of the floxed STOP-cassette and expression of the red fluorescent tdTOMATO protein in Lgr5-eGFP positive intestinal stem cells (Figure 2.2B).

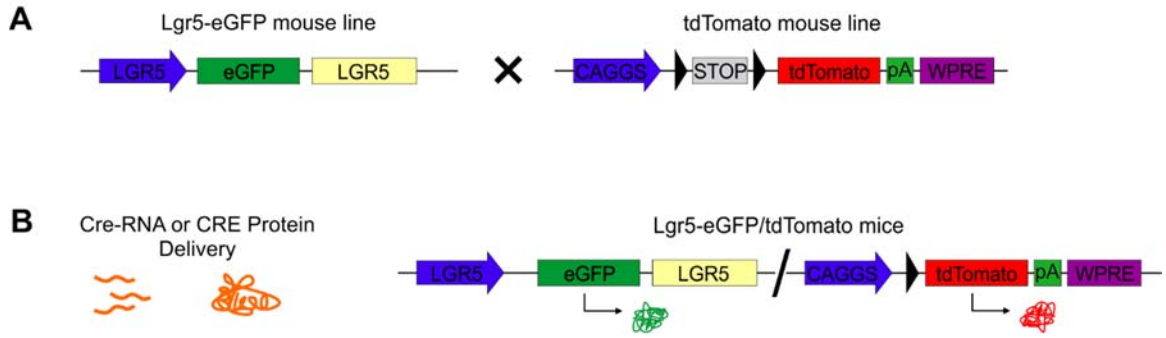

Figure 2.2: Crossing of Lgr5-eGFP/CAGGS-tdTomato mice and mechanism for CRE-mediated tdTOMATO reporter expression. (A) Crossing of Lgr5-eGFP (consecutive eGFP expression under the intestinal stem cell promotor LGR5) × tdTomato mice (expression of tdTOMATO upon CRE delivery under the CAGGS promotor) to generate double transgenic Lgr5-eGFP/tdTomato mice. Offsprings are capable to consecutively express eGFP in ISCs and tdTOMATO in a CRE-mediated manner. (B) Delivery of Cre (RNA or protein) mediates excision of the floxed STOP-cassette and initiation of the red tdTomato expression. This system was used to verify the localization of protein delivery in organoids and to detect co-localization with Lgr5-eGFP$^+$ ISCs.

2.2.1.6. Crypt isolation from Lgr5-eGFP or Lgr5-eGFP/tdTomato mice

Lgr5-eGFP$^+$ or Lgr5-eGFP$^+$/tdTomato$^+$ crypts were obtained from transgenic Lgr5-eGFP or Lgr5-eGFP/tdTomato mice as previously described [39, 42]. In brief, the small intestine was dissected and the villi were scraped away by mechanical force using glass slides. To isolate crypts from the intestinal basal membrane, the tissue was incubated in PBS containing 2 mM EDTA for 30 min at 4°C and rotation at 20 rpm on a rotating shaker. The tissue was transferred into cold HBSS buffer and the crypts were detached from the basal membrane by shaking the samples by hand. The intestinal sample was transferred to a fresh tube and after four rounds of shaking the crypt-containing HBSS was centrifuged for 3 min at 300 × g. Isolated crypts were pooled and used for cell culture or further analysis.

2.2.1.7. Isolation of pancreatic islets

Isolation of murine pancreatic islets was performed as previously described with slight modifications [246, 247]. In brief, animals were opened and a ligation was set close to the major duodenal papilla. A 30G × ½ '' needle was introduced into the cystic duct via the gall bladder until the common bile duct was reached followed by a second ligation around the needle and the common bile duct to avoid backflow to the cystic- and common hepatic ductus. The pancreas was perfused with 2 ml of Collagenase P

solution (Roche; 1 mg/ml CollagenaseP dissolved in RPMI 1640) (Figure 2.3.A-C) followed by dissection and storage in Collagenase P solution on ice. Afterwards, the pancreas was enzymatically digested and dissociated in a 37°C water bath for 10 min. Enzyme activity was stopped in islet washing solution A and islets and cell clumps were settled down for 5 min by gravity on ice. Acinar cell-containing supernatant was aspirated and discarded. This clean-up step was repeated three times. Islets were separated from acinar cells by a Ficoll Paque (GE Healthcare) density gradient centrifugation. Pancreatic islets were harvested from the interphase (Figure 2.3D) and diluted in 15 ml islet washing solution B on 10 cm culture dishes. Islets were handpicked using a 100 µl tip on a common cell culture pipette and transferred to 6-well plates containing islet maintenance medium (Figure 2.3E-F). Pancreatic islets were recovered 1h at 37°C for Glucose stimulated insulin secretion (GSIS). Islets and acinar cells were lysed in RLT buffer for gene expression analysis. For visualization and characterization, pancreatic islets were stained with Dithizone (Sigma Aldrich), a zinc chelating agent specifically binding to zinc ions on β-cells [248]. To this aim, 200 µl of Dithizone solution (10 mg Dithizone in 2 ml DMSO, filtration through 0.45 µm filter and addition of 8 ml DPBS) were applied to 10 ml islet containing media. However, islets used for GSIS were not stained due to deleterious effects on islets regarding insulin secretion [249].

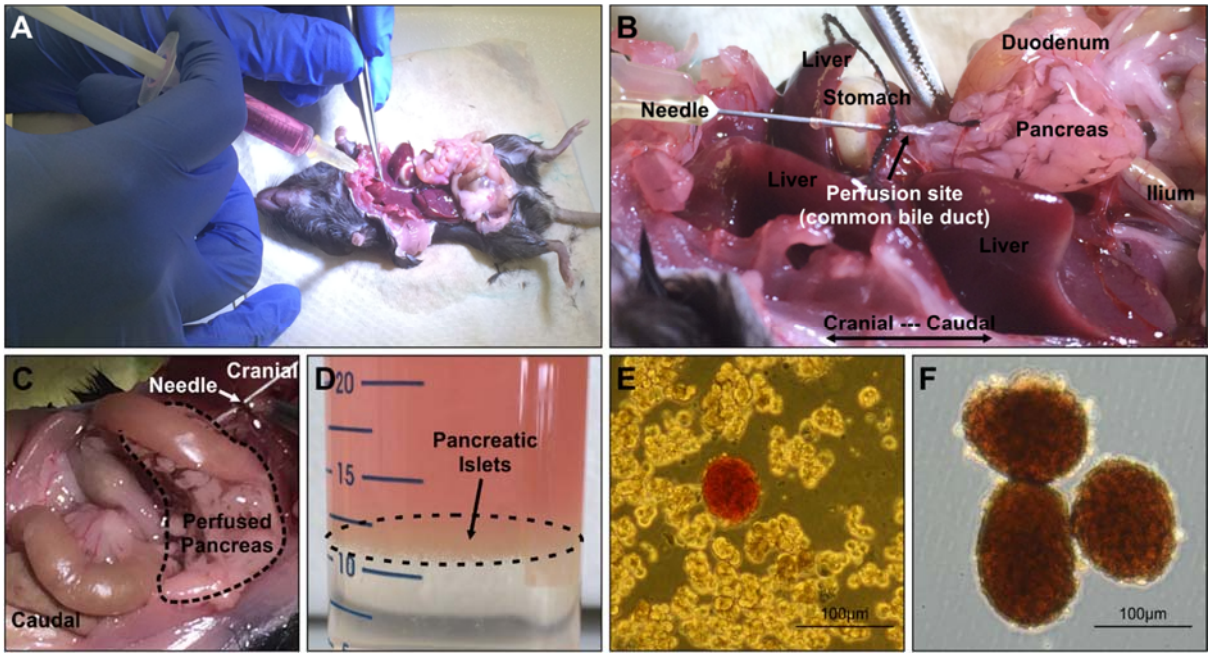

Figure 2.3: Isolation and purification of pancreatic islets. (A-C) Overview of pancreas perfusion via the common bile duct. (D) Pancreatic islets in the interphase after gradient purification centrifugation using Ficoll Paque. (E) Microscope image of a Dithizone-stained pancreatic islet and acinar cells. (F) Image of purified pancreatic islets. Scale bar 100 µm.

2.2.2. Cell culture

2.2.2.1. Cell culture conditions

All cells were cultured at 37°C, 5% CO_2 with saturated humidity.

2.2.2.2. Thawing and freezing of cells

Cryopreserved cells were thawed at 37°C followed by transfer to a falcon tube containing cell type-specific culture media (as described in 2.1.4.4.). Cell suspension was centrifuged at cell type-specific speed and duration (CGR8: 5 min at 90 × g, intestinal crypts/organoids: 3 min at 300 × g, HEK cells: 5 min at 1.200 rpm). The supernatant was removed and the pellet dissolved in cell type-specific growth media for culture (described in 2.1.4.4.) in cell type-specific culture flasks or dishes. Crypt pellets were dissolved in 50 µl/well Matrigel® and seeded in 6 to 12 wells of a 24-well plate. For freezing mCGR8 or HEK cells, confluent cultures were trypsinized using 0.05% Trypsin/EDTA (Gibco; HEK cells) or 0.5% Trypsin/EDTA (CGR8) for 5 min. Cells were counted and 10^6 cells were centrifuged at cell-specific settings followed by dilution in 1 ml cell freezing medium. Intestinal organoids were resolved from Matrigel® using cell recovery solution (Corning) for 30 min on ice and depending on density, the organoids harvested from of 4 to 12 wells were pooled and centrifuged at 300 × g for 3 min. The pellet was dissolved in 1 ml of cell freezing medium. Cells and organoids were stored in Mr. Frosty™ Freezing Containers (Thermo Fisher) at -80°C for 24h before being transferred to liquid nitrogen.

2.2.2.3. HEK293/HEK293T cell culture

Both, HEK293T and HEK293T cells were grown in 10 cm dishes or in T75/T150 flasks. After 2-4 days when cells reached >70% confluence, they were passaged by adding

0.05% Trypsin/EDTA (Gibco) for 5 min followed by cell harvesting and centrifugation at 1,200 rpm for 5 min, RT. Afterwards, cells were passaged at a 1:5-1:20 ratio.

2.2.2.4. CGR8 cell culture

CGR8 cells were maintained on 0.2% gelatin-coated Nunclon™ Delta treated surface 6-well plates. Cell type-specific medium was changed daily and cells were split every second day when they reached ~70% confluence. Passaging of CGR8 cells was performed by detaching cells with 0.5% Trypsin/EDTA (Gibco) followed by harvesting and centrifugation at 90 × g for 5 min, RT before reseeding in ratios of 1:2-1:15.

2.2.2.5. Pancreatic differentiation of CGR8 cells

Pancreatic differentiation was performed according to Mfopou et al. [225] (Figure 2.4). Briefly, 10^5 cells/cm^2 were cultured for 2 days on 0.2% gelatin-coated Nunclon™ Delta treated surfaces. Definitive endoderm (DE) differentiation was initiated by applying differentiation medium 1 for 4 days. Afterwards, cells were cultured in Differentiation medium 2A for 8 days and 4 days in Differentiation medium 2B to differentiate cells from DE stage to pancreatic progenitor stage. From day 18 on, in order to generate islet-like structures of immature endocrine cells, Differentiation medium 2C was applied for 3 days.

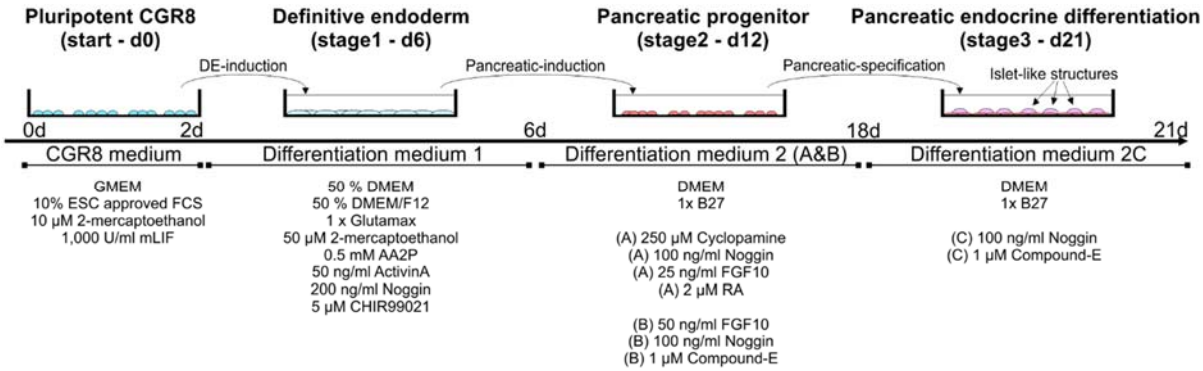

Figure 2.4: Experimental overview of pancreatic differentiation using CGR8 cells. Timeline represents differentiation stages from pluripotent CGR8 cells (start-d0) via definitive endoderm cells (stage1-d6), pancreatic progenitor cells (stage2-d18) towards pancreatic islet-like cell structures (stage3-d21). Stage specific media composition is shown below the timeline.

2.2.2.6. Matrigel®-drop cultures of murine intestinal crypts

Isolated crypts from transgenic mice (see 2.2.1.5.) were centrifuged for 3 min at 300 × g and resuspended in 200-500 µl crypt maintenance medium. 10 µl of crypt suspension were counted to determine crypt numbers. For culture, 500 crypts were embedded in 50 µl Matrigel® (MG) drops on a 24-well plate. After 15 min of MG polymerization at 37°C, 500 µl organoid maintenance medium (M-medium) was added per well. Medium was changed at a daily basis. Once a week, organoids were deprived of Matrigel® by incubation in 500 µl/well cell recovery solution (Corning) for 30 min on ice followed by mechanical dissociation and passaging in a 1:5 ratio. Representative images of eGFP-expressing crypts/organoids comprising weak auto-fluorescence (AF) are shown in Figure 2.5A-B.

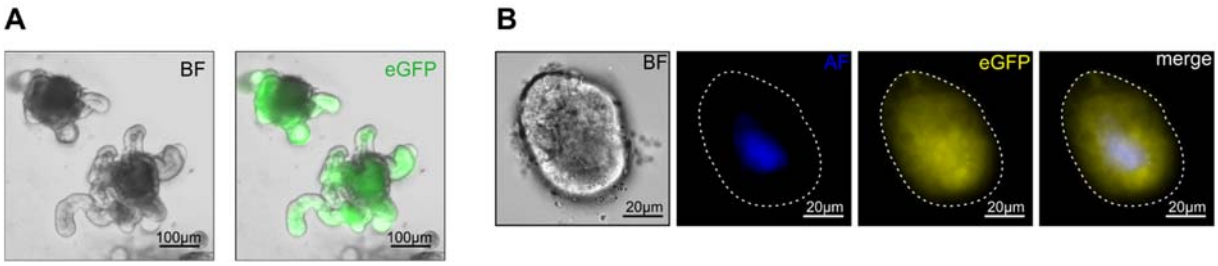

Figure 2.5: Representative image of Lgr5-eGFP$^+$ organoids cultured in Matrigel® (MG) drops. (A) Microscopic images of organoids grown in organoid maintenance medium (M-medium) displaying characteristic morphology (left, bright field image) and intestinal stem cells expressing eGFP throughout the organoid (right, eGFP fluorescence overlay). The images were taken 7 days after passaging. Scale bar represents 100 µm. (B) Lgr5-eGFP$^+$ organoids in MG drops display auto-fluorescence (AF; blue), clearly distinguishable from the LGR5-derived eGFP signal (eGFP; yellow and merge). Scale bars 10 µm.

2.2.2.7. Matrigel®-coating cultures of Lgr5-eGFP$^+$ intestinal stem cells (Lgr5-eGFP$^+$ ISCs)

Matrigel®-coated monolayer cultures of ISCs were prepared from freshly isolated Lgr5-eGFP crypts. As described, crypts were enzymatically digested in 1 mg/ml Dispase (Gibco) and 10 µM DNase (Roche) dissolved in M-medium without supplements followed by mechanical separation by pipet trituration and cell strainers (100 µm to 20 µm). ISCs were separated from single cell suspensions by FACS sorting-based on the LGR5-driven eGFP expression in ISCs. Cell sorting was performed by Christian Linden at the institute of virology (University of Würzburg), using a FACSAria III (BD). 5 × 10^4

Lgr5-eGFP^{+}-ISCs were cultured as monolayers in 24-well plates, pre-coated with 2.5 µl Matrigel® (Corning; 8 mg/ml) and 200 µl culture medium/well.

2.2.2.8. Cell viability determination

To assess qualitative or quantitative cell viability determination, either the tetrazolium dye MTT (SERVA; 3-(4,5-dimethyl-2-thiazolyl)-2,5-diphenyl-2H-tetrazolium bromide) or the CellTiter-Glo® Luminescence Cell Viability Assay (Promega) was used. Qualitative cell viability was carried out by 90 min cell incubation in an MTT staining solution (MTT reagent (3 mg/ml) diluted 1:3 in cell culture medium). The cells were washed with DPBS followed by image documentation. Viable cells are feasible to reduce the MTT reagent to the purple colored and insoluble formazan. For quantitative cell viability determination, 300 µl CellTiter-Glo® reagent was added per well of a 24-well plate and incubated for 1h at 37°C. 100 µl supernatant was transferred to a well of a 96-well plate and the optical density (OD) was measured according to the manufacturer's instructions. All measurements were carried out in triplicates.

2.2.2.9. *Cre*-RNA and CRE-protein transfection of Lgr5-eGFP/tdTomato organoids

Both, the CRE-protein and the *Cre*-RNA were generously provided by Dr. Philipp Wörsdörfer (Prof. Frank Edenhofer, Institute of Anatomy, University of Würzburg) and were tested on Matrigel®-deprived or Matrigel® drop embedded Lgr5-eGFP/tdTomato organoids. For the first approach, organoids were isolated from Matrigel® drop cultures using cell recovery solution (Corning) according to manufacturer's instructions. Transfections were carried out in 24-well plates. Per well, 500 ng *Cre*-RNA was dissolved in 50 µl of Opti-MEM (Gibco). Further, 2.5 µl Lipofectamine Ltx reagent (Invitrogen) was also diluted in 50 µl Opti-MEM followed by 1:1 dilution with the *Cre*-RNA solution and incubation for 5 min at RT. Matrigel® deprived organoids were centrifuged at 300 × g for 3 min and the pellet was resuspended in the 100 µl RNA-lipid mix added to a well. After 4h transfection at 37°C, organoids were transferred to a tube and centrifuged at 300 × g for 3 min and the organoids were washed twice in M-medium. Finally, the organoids were centrifuged at 300 × g for 3 min and the pellet was resuspended in 50 µl/well Matrigel® and reseeded. For Matrigel® embedded

organoid transfection, the culture medium was replaced by 200 µl fresh M-medium and 100 µl of the above mentioned RNA-lipid mix were added dropwise per well. Following 4h incubation, the medium was aspired and Matrigel® embedded crypts were washed three times by rinsing with fresh medium. Transfected organoids were cultured in 500 µl medium and tdTOMATO expression was analyzed 24 to 48h post-transfection.

The CRE-protein transfection was performed in 24-well plates using the Xfect™ Transfection Reagent (Clontech). Per well, 1 µg of CRE protein was dissolved in a final volume of 20 µl Xfect™ Protein Buffer (Clontech). In addition, 3 µl Xfect™ Transfection Reagent was diluted in 17 µl ddH_2O. Both, the CRE protein solution and the Xfect™ Transfection Reagent solution, were mixed with 110 µl crypt maintenance medium and incubated for 30 min at RT. Lgr5-eGFP$^+$/tdTomato$^+$ organoids were deprived from Matrigel® by incubation for 30 min on ice in cell recovery solution (Corning). Organoids were centrifuged at 300 × g for 3 min and the pellet was resuspended in 150 µl Xfect™-Protein complex solution and added to a well for 4h, 37°C. Afterwards, organoids were centrifuged for 3 min at 300 × g and washed twice in crypt maintenance medium. The pellet was resuspended in 50 µl/well Matrigel® and seeded in drops. Organoids were cultured in maintenance medium for 24-48h before analysis.

2.2.2.10. Generation of recombinant PTF1A and transfection of Lgr5-eGFP$^+$-ISCs and organoids

The recombinant PTF1A-protein was produced as shown in Figure 2.6. In brief, BL21 *E.coli* were transformed with the plasmid pReceiver-B13-Ptf1a (GeneCopoeia) containing a His/SUMO-tag. Obtained colonies were grown in LB medium up to an OD_{600} of 0.6 when protein expression was induced by addition of IPTG (1mM final concentration) and bacteria were propagated for further 3h. Bacteria were spun down for 15 min at 2.000 × g, 4°C and lysed in 8M Urea buffer (100 mM NaH_2PO_4, 10 mM Tris and 8M urea; pH = 8). Proteins were loaded to Nickel columns (Invitrogen), immobilized via the His-tag and eluted with elution buffer (100 mM NaH_2PO_4, 10 mM Tris and 8M urea; pH = 5.9). Afterwards, the eluate was dialyzed against PBS and concentrated using the Amicon concentrator cell (Invitrogen). The concentrated protein was cleaved by using SUMO protease (Invitrogen) for 2h at 30°C according to manufacturer's recommendations. Afterwards, SUMO protease was removed by affinity chromatography on a nickel column and washing with the SUMO protease

washing Buffer (Invitrogen). The protein solution was dialyzed against PTF1A buffer (10 mM Tris, 150 mM NaCl and 50 mM L-Arginine; pH = 7.4) and concentrated in an Amicon concentrator using a 10 kDa cut-off molecular weight membrane (Merck Millipore). Afterwards, Sabine Wilhelm (TERM, University of Würzburg) tested protein functionality with an Electrophoretic Mobility Shift Assay (EMSA) as previously described [122]. Active and functional recombinant PTF1A was stored in PTF1A buffer at -80°C.

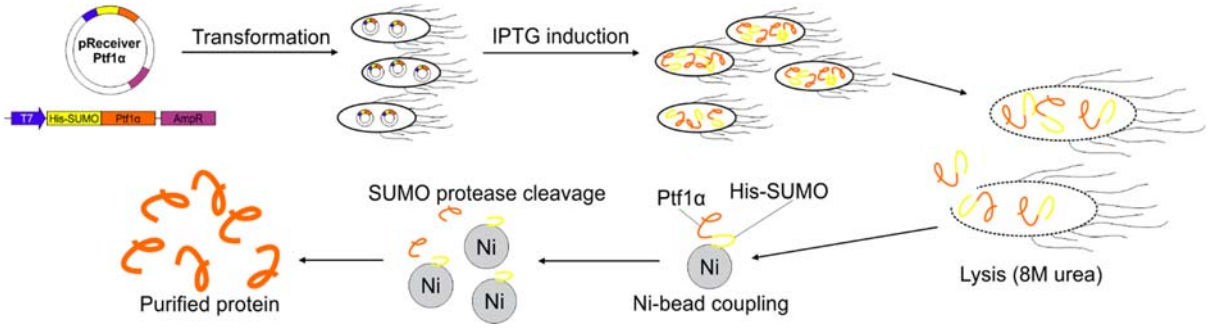

Figure 2.6: Schematic representation of recombinant PTF1A production. The bacteria were transformed and IPTG induced following standard protocols. After lysis, protein was coupled to Ni-beads and SUMO protease cleaved to harvest the protein in almost native configuration. Recombinant PTF1A was concentrated and stored at -80°C.

On one hand, Lgr5-eGFP^{+} organoids from two Matrigel® drops were pooled and Matrigel®-deprived by incubation in cell recovery solution (Corning) for 30 min on ice. Protein transfection was carried out in 24-well plates. Per well, 3 µg of recombinant PTF1A was diluted in 17 µl Xfect™ Protein Buffer (Clonetech). Then, in a separate tube 6 µl Xfect™ Transfection Reagent (Clonetech) were mixed with 14 µl ddH_2O. Both, the 20 µl transfection reagent solution and the 20 µl PTF1A solution were combined and mixed with 110 µl crypt medium in a new tube and incubated for 30 min, RT. Matrigel® recovered organoids were centrifuged for 3 min at 300 × g and the pellet was resuspended in the 150 µl PTF1A-Xfect™ solution and transferred to an empty well. The cell-penetrating peptide Xfect™ mediates PTF1A transport across the cell membrane via endocytosis. Transfection was carried out for 4h, 37°C on a shaker (50 rpm). Organoids were washed in crypt culture medium, centrifuged for 3 min at 300 × g and embedded in Matrigel® drops.

On the other hand, freshly sorted Lgr5-eGFP^{+}-ISCs were seeded at a density of ~ 5 × 10^5 cells/cm^2 on 24-well plates and grown for 48h prior to protein-transfection. The transfection was performed as described above by using 8 µl of the X-Fect™ Transfection Reagent and 3 µg PTF1A per well. The 150 µl CPP-PTF1A solution were incubated for 4h, 37°C. Afterwards, cells were washed twice by rinsing with culture medium and grown for up to 7 days.

2.2.2.11. Liposomal PTF1A delivery in Lgr5-eGFP^{+}-ISCs and organoids

In general, liposomes consist of a phospholipid to cholesterol ration of 2:1. The liposome lipid mixture used in this thesis was generated by Dr. Marco Favretto (Radboud University Nijmegen, Netherlands). The formulation of the liposomes is shown in Figure 2.7.

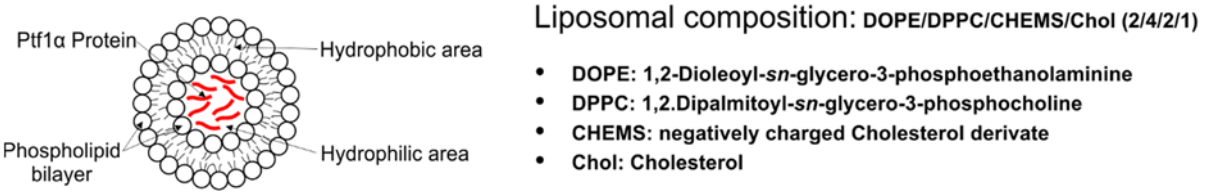

Figure 2.7: Schematic overview of pH-sensitive Liposomes for PTF1A delivery. Liposomes were composed of a phospholipid bilayer surrounding the hydrophilic core where PTF1A was encapsulated. Liposome formulation was DOPE/DPPC/CHEMS/Chol in a ratio of 2:4:2:1. Lipid composition was prepared by Dr. Marco Favretto.

The applied liposomes consisted of 1.000 µg/ml phospholipids harboring 10 µg PTF1A representing a lipid to protein ratio of 1:200. To prepare the liposomes, phospholipids were centrifuged for 3 min at 3.000 rpm and were shock frozen at -80°C for few minutes. Ready-to-use liposomes were generated by repeating this freeze/thaw cycle 3 times. Afterwards, 5 µg PTF1A were added to 500 µl lipid-solution. For protein-encapsulation, the PTF1A-lipid mix was shock-frozen at -80°C and subsequently water bath-sonicated at 37°C for 5 min. The freeze/sonication step was repeated three times. The liposomal delivery reaction was carried out in 24-well plates. Per well, Matrigel® deprived organoids were resuspended in 100 µl M-medium and transferred to an empty well or 100 culture medium was added to ~ 5 × 10^5 Lgr5-eGFP^{+} ISCs/well. Then

100 µl of the freshly prepared liposomes (1 µg PTF1A) were applied dropwise to the organoids or cells and incubated for 4h, 37°C. Afterwards, the organoids were washed three times in culture medium and centrifuged 3 min at 90 × g and seeded in Matrigel® drops and Lgr5-eGFP$^+$ ISCs were rinsed three times with culture medium organoids or cells were analyzed immediately after liposomal PTF1A delivery or 24 to 48h after the experiment. For visualization, PTF1A was coupled on the N-terminus with the positively charged fluorescent dye Tetra Methyl Rhodamine (TMR). To verify possible cytotoxicity of the liposomal compounds, empty liposomes served as control (mock) and were applied and tested as the above described PTF1A liposomes.

2.2.2.12. Lentivirus production and Lgr5-eGFP$^+$ organoid transduction

Lentiviral particles were generated by transfection of HEK293T cells using target gene-specific lentiviral vectors in combination with packing-plasmids encoding components of the viral capsid and the envelope. One day before transfection, 2 × 10^5 HEK293T cells were seeded per well on 6-well plates. Prior to transfection, the culture medium was replaced by fresh medium. Transfection was performed using PEI (Polysciences Inc). In brief, the lentiviral target-gene specific vectors encoding Ptf1a, the packing plasmids psPAX2 (Addgene, 12260) and pMD2 (Addgene, 12259) were mixed in a molecular ratio of 4:2:1 to a final quantity of 3 µg DNA and diluted in 200 µl serum-free DMEM. 9 µg of 1 µg/µl PEI transfection reagent (3:1-PEI µg to total DNA µg) was added to the DNA, vortexed and incubated for 15 min at RT. HEK293T cells were transfected by dropwise addition of the PEI/DNA mix. 9-12h post-transfection, the HEK293T culture medium was replaced by M-medium. 48h later, virus was harvested and filtered through a 0.45 µm filter and supplemented with 8 µg/ml polybrene (Merck Millipore). Virus containing supernatant was added to Matrigel®-deprived organoids in one well of a 6-well plate and centrifuged for 1h at 300 × g followed by 2-3h static incubation at 37°C. After three centrifugation/washing steps using maintenance medium, organoids were embedded in Matrigel® drops to recover for 12-24h. At this stage, pancreatic induction was initiated by applying Pancreatic Organoid Differentiation (POD) Medium [224]. Organoids were cultured for 7 days with daily medium change. Mechanically dissociated organoids were passaged 1:5 and from non-cultured crypts, gene expression was analyzed by qRT-PCR. After 14 days,

organoid morphologies were documented, lysed in RLT buffer or conserved in Histogel™ (VWR) for (immuno-) histological analysis.

2.2.2.13. Glucose stimulated insulin secretion (GSIS) of pancreatic islets

Freshly isolated islets were recovered for 90 min at 37°C in islet maintenance medium. Islets were equilibrated in 3.3 mM D (+) glucose solution for 30 min. Afterwards, 10-15 islets were placed in 500 µl 3.3 mM or 16.7 mM D (+) glucose solution and stimulated for 1h at 37°C. Insulin content of the supernatant was quantified with the ultrasensitive mouse insulin ELISA (ALPCO). After glucose stimulation, islets were collected and DNA content was calculated by means of the Quant-it dsDNA PicoGreen Kit (Thermo Fisher) to normalize the measured insulin values. Insulin secretion capacity of islets is shown as stimulation index. To calculate the stimulation index, the mean of normalized insulin values from 16.3 mM glucose samples was divided by the mean of normalized 3.3 mM glucose samples values. In addition, glucagon concentrations in the supernatant were determined using the Glucagon ELISA (Mercodia; 10-1281-01) according to the manufacturer's protocol.

2.2.3. Histology

2.2.3.1. Sample preparation and conservation

Intestinal crypts/organoids were washed three times in PBS^- prior to fixation in 4% PFA for 1h. Following multiple washing steps in PBS^-, samples were embedded in HistoGel™ before being preserved in paraffin. Dissected organs like pancreas or small intestine were fixed in 4% PFA for 2-3h, RT. Afterwards, probes were preserved in paraffin for histological analysis. For all (immuno-)histological pancreas analyses using paraffin conserved probes, samples were cut according to the scheme in Figure 2.8. and mounted on Polysine™ glass slides (Thermo Fisher).

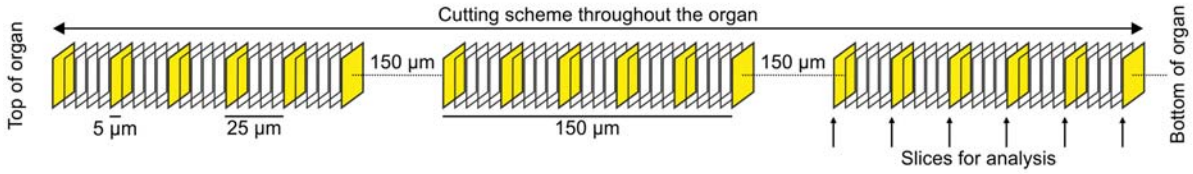

Figure 2.8: Schematic overview of pancreatic serial sectioning. Whole pancreas was cut from top to bottom into 150 µm series with 5 µm thick sections. In between the sections, 150 µm were discarded. Every sixth section of a series was used for H&E or (immune-) histochemical analyses.

Alternatively, for analysis of pancreatic cryosections, the dissected organs were fixed in 10% Roti® Histofix for 2h, washed twice in PBS^- and incubated in 30% sucrose for 12h at 4°C. The pancreata were embedded in Tissue-Tec and later cut in 5 µm thick sections and mounted on SuperFrost® Plus glass slides (Langenbrink). The cryosections were air-dried for 30-60 min at RT prior to Red Oil O stainings (2.2.3.3). Remaining samples were stored at -80°C.

2.2.3.2. H&E staining and quantification

Slides were incubated at 60°C to melt the paraffin before being transferred to Xylen I followed by Xylen II (for 10 min each) to remove remaining paraffin. Samples were rehydrated by dipping three times in the following descending alcohol series: twice 96% EtOH, 70% EtOH, 50% EtOH and stopping in ddH_2O. Nuclei were stained for 6 min in Hematoxylin (Morphisto). After washing in ddH_2O, slides were placed for 5 min in tap water to develop the staining. Cytoplasmatic structures and the extracellular matrix were stained in Eosin (Morphisto) for 6 min. Samples were dehydrated in an ascending alcohol series by dipping twice in 70% EtOH, twice in 96% EtOH, followed by 5 min incubation in Isopropanol I, Isopropanol II, Xylene I and Xylene II. Samples were mounted with Entellan (Merck Millipore) and sealed with a coverslip. For islet size measurements and nuclei counting, the Fiji Image J software was used.

2.2.3.3. Red Oil O staining

Red Oil O solution (Sigma Aldrich) was used to stain triglycerides (fat tissue) of pancreatic cryosections. The staining was performed according to manufacturer's

recommendations. In brief, the Oil Red working solution was prepared 24h before staining by mixing 60% stock solution (0.5 g Red Oil O/ 100 ml isopropanol) with 40% ddH_2O. Prior to use the solution was filtrated. Air-dried pancreas slices (2.2.3.1) were placed in PBS^- and dipped once in ddH_2O followed by a 5 min incubation in 60% isopropanol. Afterwards, slides were incubated for 10 min in Oil Red O working solution followed by another 5 min in 60% isopropanol. The samples were dipped in ddH2O before 15 sec nucleus staining in Hematoxylin and bluing for 1 min in tap water. Finally, slides were washed in ddH_2O before the samples were covered in the aqueous mounting solution Aquatex® (Merck Millipore).

2.2.3.4. Immunohistochemistry

Pancreas sections were deparaffinized and rehydrated as described in 2.2.10.2. A heat-mediated antigen retrieval was performed by boiling samples for 30 min in citrate buffer (pH 6). Sections were permeabilized in 0.2% Triton-X-100 (Sigma Aldrich) and blocking solution (5% w/v BSA in PBS^-) was applied for 30 min to avoid unspecific binding. Slices were stained with primary antibody O/N at 4°C. The next morning, slices were washed three times in TBS-T before incubation with secondary antibodies for 60 min, RT in the dark. Slices were washed three times in TBS-T and mounted in Fluoromount-G supplemented with DAPI (Invitrogen). For any staining using the customized anti-SGLT1 antibody [241] DAB-based immunohistology was performed using the DCS Super Vision 2 HRP-Polymer Kit (DCS) following the manufacturer's guidelines with adaptions published by Sabolic et al. 2006 [250]. Briefly, deparaffinized and rehydrated slices were heated in citrate buffer (pH 6) for 4 × 5 min in a microwave at 800W. The sample was permeabilized for 5 min in 0.5% Triton-X-100, dissolved in PBS^-. Samples were washed 5 × 5 min in PBS^- and endogenous peroxidase activity was blocked for 10 min in 3% H_2O_2 (DCS) dissolved in ddH_2O for 20 min at RT. Unspecific binding sites were blocked for 20 min at RT in 1% (w/v) BSA, dissolved in PBS^-. Primary antibody was diluted 1:500 and incubated o/n at 4°C. Next day, slides were washed 4 × 5 min in PBS^- and incubated for 10 min at RT, in polymer-enhancer solution (DCS). Samples were washed 4 × 5 min in PBS^- and incubated for 20 min at RT in HRP-polymer solution (DCS). Slides were counterstained for 90 sec in Hematoxylin (Morphisto) and bluing was allowed for 90 sec in tap water. Samples were

rehydrated in an ascending series, as described in 2.2.3.2 and mounted with Entellan (Merck Millipore).

2.2.3.5. Image acquisition

Fluorescence labeled samples were analyzed using the Inverse fluorescence microscope BZ-7000 (Keyence) or the confocal microscope TCS SP8 (Leica Microsystems). The EVOS™ XL Core Imaging System (Thermo Fisher) was used for daily image acquisition and cell/organoid morphology documentation.

2.2.4. Fluorescence-activated cell sorting (FACS)

2.2.4.1. Analysis of mouse ES cell pluripotency

CGR8 cells from one well of a 6-well plate were harvested by trypsinization and centrifugation at 90 × g for 5 min. Cells were washed three times in FACS buffer (1% (v/v) FCS, 2 mM EDTA dissolved in PBS^-). Cells were spun at 90 × g for 5 min and the pellet was resuspended in 250 µl BD Fix/Perm™ solution (BD) and incubated for 20 min on ice. Afterwards, cells were washed twice in FACS buffer before they were stained light-protected for 30 min on ice in 50 µl FACS Buffer with fluorescent dye labelled antibodies. After two washes, cells were resuspended in FACS buffer and analyzed with the BD FACS Calibur (BD).

2.2.4.2. Apoptosis assay of pancreatic islet cells

Pancreatic islets were isolated as previously described. A single cells suspension was generated by islet incubation in 0.05% trypsin-EDTA (Gibco) for 5 min at 37°C followed by mechanical dissociation using a pipette and a 20 µm cell strainer. The cells were washed and stained in the dark with 5 µl of AnnexinV-FITC and 5 µl 7-AAD viability staining solution (BioLegend) before analysis with the BD Accuri™ C6 Cytometer (BD). For precise determination of the apoptotic cell population, apoptosis was induced in a positive control by incubation of cells at 60°C for 5 min prior to staining.

2.2.5. ELISA

The samples were measured in duplicates by strictly following the manufacturer's recommendations. The Glucose Colorimetric Assay Kit (Cayman Chemicals; 10009582) was used to determine glucose concentrations. To assess insulin, total GLP-1 and glucagon we used the Insulin Ultrasensitive Mouse ELISA (ALPCO; 80-INSMSU-E01), the Total GLP-1 ELISA (Merck Millipore; EZGLP1T-36K) or the Mercodia Glucagon ELISA (Mercodia; 10-1281-01). Determination of the OD was carried out with the Infinite 200 PRO microplate reader (TECAN).

2.2.6. Molecular Biology

2.2.6.1. Generation of synthetic Ptf1a RNA

The generation of Ptf1a-templates for *in vitro* transcription was performed as previously described [251] (Figure 2.9A) in collaboration with Dr. Philipp Wörsdörfer (Prof. Frank Edenhofer, Institute of Anatomy, University of Würzburg). In brief, using the forward primer (5'-phos-GACGCCGTACTCCTGGAGCACTT-3') and the corresponding reverse primer (5'-TCAGGACACAAACTCAAAGGGTGG-3'), Ptf1a was amplified from the pReceiver-B-13-Ptf1a plasmid (GeneCopoeia). Afterwards, 200 nM of 5' and 3' untranslated regions (UTRs) oligonucleotides, 200 nM Ptf1a amplicon and 100 nM Ptf1a-specific splint-oligonucleotides (Figure 2.9B) were ligated using 1U (1 µl) of thermostable ampligase (Epicenter). The reaction was performed in 5 cycles under the following conditions: 95°C for 10 sec, 45°C for 1 min, 50°C for 1 min; 55°C for 1 min; 60°C for 1 min. The sense 5'UTR primer (5'-TTGGACCCTCGTACAGAAGCTAATA CG-3') and the antisense 3'UTR primer (5'-GCGTCGACACTAGTTCTAGACCCTCA-3') were used to amplify the complete fragment using Q5 polymerase and the following protocol: initial denaturation (98°C for 30 sec), denaturation (98°C for 10 sec), annealing (67°C for 10 sec), elongation (72°C for 30 sec) for 30 cycles and a final extension (72°C for 2 min). The amplicon was subcloned into the pGEM®-T Easy Vector System (Promega) according to manufacturer's recommendations. Constructs were transformed and selected on ampicillin containing LB plates. Constructs were verified by sequencing. The polyA-tail was added by a tail-PCR reaction using the sense 5'UTR primer and the antisense tailing primer (5'-T_{120}CTTCCTACTC AGGCTTTATTCAAAGACCA-3'). The reaction was performed with the Q5 polymerase

(NEB) and the following protocol initial denaturation (98°C for 30 sec), denaturation (98°C for 1 min), annealing (65°C for 30 sec), elongation (72°C for 3 min) for 35 cycles and a final extension (72°C for 10 min). 1 µg linearized polyT-tailed DNA served as template for *in vitro* transcription using the AmpliScribe™ T7-Flash™ Transcription Kit (Epicentre) in a 20 µl reaction mix according to the manufacturers guidelines and subsequent RNase-free DNase treatment to digest template DNA. For the in vitro transcription, modified pseudo-UTP and me-CTP (Trilink) ribonucleotides were added to minimize ssRNA-mediated immunogenic reactions [251]. The generated RNA was purified using the Nucleospin RNA II Kit (Macherey-Nagel), by following the manufacturer's instructions. The 5' capping reaction was performed by the ScriptCap™ m7G Capping System (CellScript) in combination with the ScriptCap™ 2'-O-Methyltransferase Kit (CellScript) according to the provided protocol for simultaneous capping and 2'-O-Methylation.

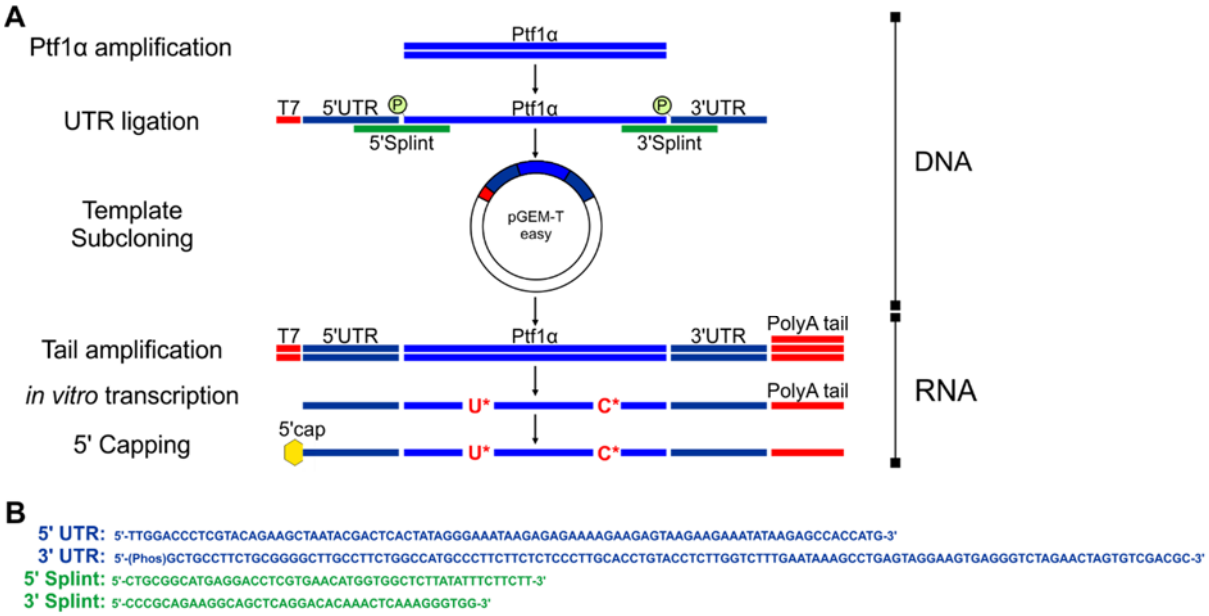

Figure 2.9: Generation of Synthetic modified Ptf1a-RNA. (A) Scheme showing experimental procedure for generation of synthetic Ptf1a-RNA according to Warren et al. 2010. 5' Untranslated region (UTR) and 3'UTR were connected to the Ptf1a coding sequence by specific splint oligonucleotides. Amplicon was cloned into pGEMT-easy vector and verified by sequencing. PolyA-tail was added by Tail-PCR and amplified fragments were used as template for synthetic modified mRNA generation by *in vitro* transcription. 5' cap structure was attached by enzymatic capping. (B) UTR and Splint oligonucleotides are shown in blue and green, respectively.

2.2.6.2. Lentiviral constructs

The Lentiviral plasmid vectors were designed and constructed in our laboratory by Dr. Daniela Zdzieblo & Valentyna Kryklyva. In brief, the lentiviral expression vector pL-CDH-CMV-MCS-EF1α-mRFP-AmpR (pL Mock) served as targeting vector for cloning (Figure 2.10A). The *pL-CDH-PGK-Ptf1a-EF1α-mRFP-AmpR* (pL-PGK-Ptf1a) vector (Figure 2.10B), initially encoded Ptf1a under the CMV promotor and was generated by amplification of the Ptf1a, coding sequence from the pReceiver-B-13-Ptf1a vector and inserted into pL-CDH-CMV-MCS-EF1α-mRFP-AmpR by conventional cloning. Next, the CMV promotor was replaced by the stronger phosphoglycerate kinase (PGK) promotor. To this aim, the PGK coding sequence was amplified from the pSico PGK puro vector (Addgene, 11586) and inserted into pL-CMV-Ptf1a by conventional cloning. In addition, site-directed mutagenesis PCR was used to modify the Kozak consensus sequence, located upstream of the Ptf1a start codon in order to enhance translation efficiency of Ptf1a (Figure 2.10B).

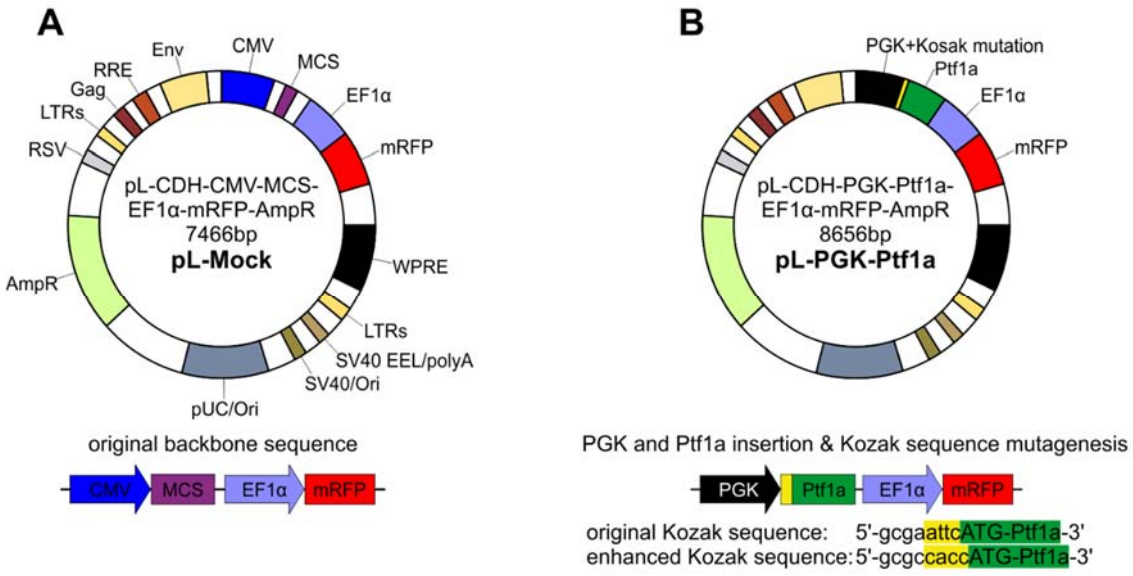

Figure 2.10: Graphical overview of lentiviral plasmid maps with important contents of the constructs. (A) pL-Mock contain a multiple cloning site (MCS) driven by the CMV promotor and mRFP under the EF1α promotor. (B) pL-PGK-Ptf1a encode Ptf1a under the phosphoglycerate kinase PGK promotor and the enhanced Kozak consensus sequence.

2.2.6.3. Transformation and culture of *E. coli*

E.coli were inoculated with 50-100 pg DNA for 30 min on ice. Bacteria were transformed for 30 sec in a 42°C water bath followed by 2 min incubation on ice. Afterwards, 250 ml pre-warmed LB medium (C3040 and BL21) was added and the transformants recovered for 1h at 37°C on an orbital shaker (~ 200 rpm). Bacteria were selected O/N at 37°C on LB-plates, containing 50 µg/ml kanamycin or 100 µg/ml ampicillin.

2.2.6.3. Preparation of competent bacteria

A 5 ml overnight bacteria culture was diluted 1:100 and grown in 100 ml of appropriate culture medium to an OD_{600} of 0.5. The bacteria were harvested and spun down in a precooled centrifuge for 10 min at 3.000 rpm. Then, the supernatant was discarded and the pellet resuspended in 10 ml ice cold TSS buffer. Bacteria were aliquoted in 100 µl/tube and snap frozen in liquid nitrogen. Competent bacteria were kept at -80°C for long-term storage.

2.2.6.4. RNA isolation

To isolate RNA from cells, the sample was lysed in RLT buffer (QIAGEN) complemented with 10 µl/ml 2-mercaptoethanol. For small amounts of cells (2×10^5) or Matrigel®-deprived crypts, the RNeasy micro Kit (QIAGEN) was used, otherwise the RNeasy mini Kit (QIAGEN) was applied. Samples were homogenized through a QIAshredder spin column (QIAGEN) and further processed according to the manufacturer's recommendations including an on-column DNase treatment.

When RNA was isolated from murine organs the explanted tissues were immediately conserved in RNA*later* (QIAGEN). 25 mg tissue was transferred into a 2 ml Eppendorf tube containing a sterile steel bead and 400 µl Qiazol reagent (QIAGEN). Sample was homogenized using the TissueLyser (QIAGEN) for 5 min at 50 hertz. 200 µl Qiazol and 100 µl Chloroform were added to the tube before intense vortex and sample incubation for 15 min on ice. After 15 min centrifugation at 4°C at 12.000 × g, RNA was collected from the aqueous phase and purified on RNeasy mini columns (QIAGEN). RNA

concentrations were measured with the NanoQuant plate in the Infinite 200 PRO microplate reader (TECAN).

2.2.6.5. cDNA synthesis

Previously isolated RNA was reversely transcribed using the iScript cDNA Synthesis Kit (Biorad) according to the following conditions:

5 × iScript reaction mix	*4 µl*
iScript Reverse Transcriptase	*1 µl*
100-1.000 ng RNA template	*× µl*
Nuclease-free water up to 20 µl final volume	*× µl*

The reverse transcription was performed in a 3-step cycler program on the LabCycler48 (SensoQuest) using the following protocol: 5 min at 25°C, 30 min at 42°C and 5 min at 85°C. The cDNA was stored at -20°C.

2.2.6.6. Quantitative real time PCR (qRT-PCR)

To compare mRNA transcription of different tissues or cells, the *reference genes mRPL15*, *mRPL6* and *mRPS29* were used for gene of interest normalization. If sufficient cDNA was available, two reference genes were used to calculate the gene expression by the $2^{-\Delta\Delta Ct}$ method in accordance to the MIQE guidelines [252, 253]. Alternatively, one reference gene was used [254]. The qRT-PCR reactions were conducted in duplicates on the CFX96 Touch™ Real-Time PCR Detection System (Biorad) with the following mixture:

SsoFast EvaGreen Supermix (Biorad)	*10 µl*
Sense primer (400 nM)	*2 µl*
Antisense primer (400 nM)	*2 µl*
cDNA (10-20 ng/well)	*2 µl*
ddH_2O up to 20 µl total volume (Braun)	*4 µl*

The qRT-PCR included an initial denaturation (95°C for 3 min) and 40 cycles of the following 2-step settings: denaturation (95°C for 10 sec) and annealing and extension

(60°C for 30 sec). To assess amplicon specificity, a melt curve analysis was performed and/or PCR products were verified on an agarose gel.

2.2.6.7. Mouse genotyping

Mouse genotyping was carried out using the KAPA Mouse Genotyping Kit as described in 2.2.1.3. The PCR reaction was performed in a LabCycler48 (SensoQuest) and the following conditions:

2 × KAPA2G Fast Genotyping Mix	*12.5 µl*
10 µM primer1	*1.5 µl*
10 µM primer2	*1.5 µl*
10 µM primer3	*1.5 µl*
Template DNA (crude extract)	*2 µl*
ddH_2O up to 25 µl total volume	*6 µl*

The PCR was performed as follows: initial denaturation (95°C for 3 min), 35 cycles of denaturation (95°C for 15 sec), annealing (60°C for the Lgr5-eGFP mouse line or 62°C for SGLT1 knockout mice for 15 sec) and extension (72°C for 15 sec). To determine the genotypes of mice, the amplicons were loaded on a 1% agarose gel and separated for 45 min at 120V. Table below shows characteristic band sizes for determination of wild type, SGLT1 and LGR5 mice.

Genotype	**Band size(s) in base pairs**
SGLT1 wild type (+/+)	216
SGLT1 heterozygous (+/-)	216 & 349
SGLT1 knockout (-/-)	349
Lgr5-eGFP wild type (+/+)	298
Lgr5-eGFP heterozygous (+/-)	298 & 174

2.2.7. Statistics

Statistical significance was calculated by one-way ANOVA with Tukey's multiple comparison test, when values of three or more conditions were compared. If only two datasets were analyzed, the values were determined with an unpaired t-test. Unless otherwise stated all data represent mean values ± standard deviation whereby ANOVA significances were hallmarked with an asterisk (*) and t-test significances with a cross (×), respectively. Values with $P < 0.05$ were considered as significant in any statistical analysis

3. Results

3.1. Establishment of a Ptf1a-based protocol to induce the differentiation of intestinal stem cells (ISCs) towards pancreatic β-like cells

Transplantation of insulin-secreting β-cells currently represents a promising strategy for the treatment of T1DM patients. Due to donor shortage, diverse cell sources are currently under investigation to derive functional, insulin-secreting β-like cells *in vitro*. The aim of this work was to differentiate multipotent intestinal stem cells (ISCs) towards pancreatic β-like cells *in vitro* by the ectopic expression of the pancreas-specific transcription factor Ptf1a. Applying media formulations routinely used for the differentiation of pluripotent stem cells towards β-like cells should further support the differentiation process.

3.1.1. Pancreatic differentiation of murine embryonic stem cells

Prior to the derivation of β-like cells from multipotent ISCs, a previously published embryonic stem cell (ESC)-based pancreatic differentiation protocol [225, 255, 256] was reproduced to establish a gold standard control for the ISC-based experiments. To this aim, the murine ESC line CGR8 was used in this work.

3.1.1.1. The murine embryonic stem cell line CGR8 grows best under EScult-FCS conditions

CGR8 cells were cultured under feeder-free conditions on gelatin-coated tissue culture plastic. To preserve the pluripotent nature of these cells, an appropriate ESC medium formulation is mandatory. Among the media components, an ESC culture approved FCS is of high importance. Therefore, two ESC-specific FCS (EScult-FCS, SPOT-FCS) were compared in this study to define the best culture condition for the CGR8 cell line. No relevant difference in cell morphology was detected when CGR8 cells were cultured with EScult- or SPOT-FCS (Figure 3.1A). In both cultures, mESCs formed characteristic dome-shaped colonies consisting of small cells with a high nucleus-to-

cytoplasm ratio (see magnification Figure 3.1A). Cumulative population doubling analysis was performed over a period of 72h to investigate cellular growth capacity. Figure 3.1B demonstrates better cell growth under EScult- vs. SPOT-FCS conditions. Therefore, EScult-FCS was chosen as medium supplement for all upcoming experiments using CGR8 cells. Finally, EScult-FCS-cultured cells were analyzed by FACS for their expression of characteristic markers (SSEA-4, OCT3/4 and NANOG) to verify their pluripotent cell identity. As shown in Figure 3.1C, 97.3% of all cells were positive for SSEA-4, 97.1% for OCT3/4 and 95.2% for NANOG.

In summary, CGR8 cells grown in EScult-FCS supplemented medium demonstrated ESC-specific characteristics i.e. a stem cell-specific cell morphology, proper growth characteristics of fast proliferating cells and expression of pluripotency markers.

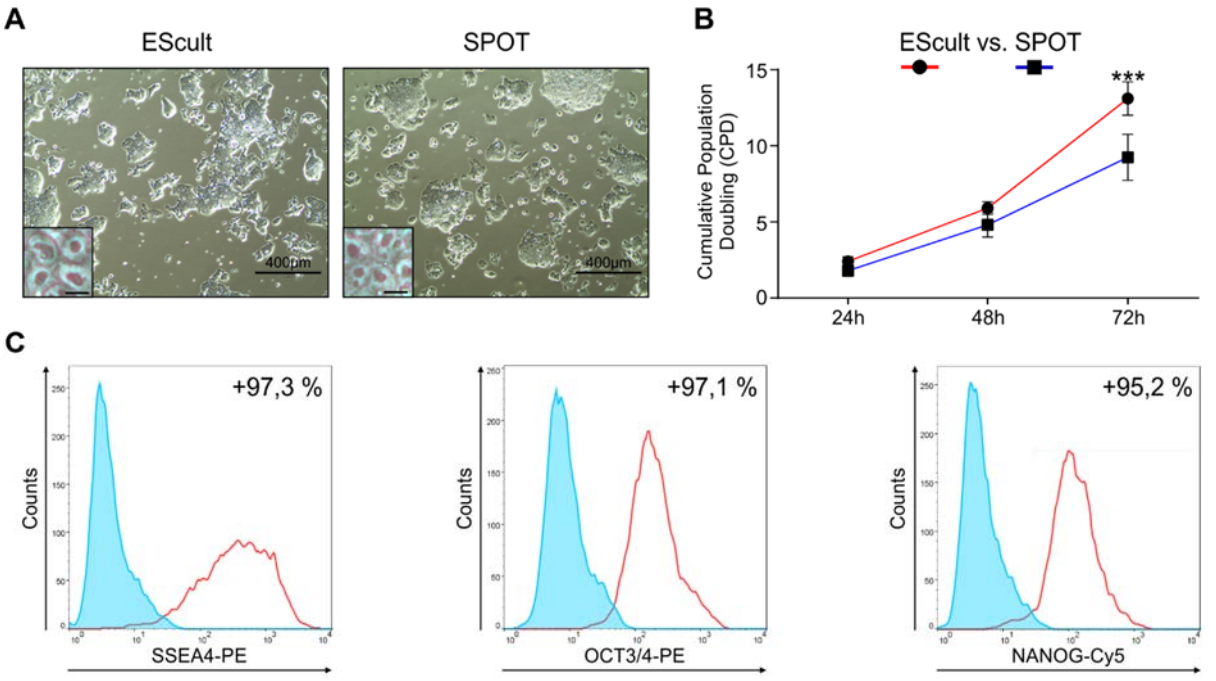

Figure 3.1: Characterization of the murine (m)ESC line CGR8. CGR8 cells were cultured with two different mESC-specific FCS to determine best growth conditions. (A) Representative microscope pictures of CGR8 cells grown in medium supplemented with either EScult- or SPOT-FCS. Scale bars represent 400 µm and 10 µm in the magnification. (B) Graph representing the corresponding cumulative population doubling (CPD) analysis after 24h, 48h and 72h under EScult-FCS (red) or SPOT-FCS (blue) conditions. Significance was calculated by student's t-test. ***$P < 0.001$. $n = 3$. (C) FACS plots of one representative experiment showing SSEA-4, OCT4 and NANOG positive CGR8 cells grown under EScult-FCS conditions.

3.1.1.2. CGR8-derived cells show pancreatic lineage-specific gene expression profiles after induction of pancreatic differentiation

After having established the conditions for CGR8 maintenance culture, pancreatic differentiation was induced according to the protocol published by Mfopou et al. [225]. The progression from pluripotent ESCs (start of differentiation d0; stage 0) via definitive endoderm (DE d6; stage 1) and a pancreatic endocrine progenitor (PEP) stage (d18; stage 2) towards pancreatic endocrine cell (PEC) types like β- or α-cells (d21; stage 3) was monitored by analyzing cell morphology and characteristic gene expression patterns.

After induction of differentiation, CGR8 cells changed their stem cell-specific morphology from dome-shaped round colonies (see Figure 3.2) towards clustered colonies within a dense cobblestone-like monolayer when stage 1 (DE) was reached after 6 days of differentiation (Figure 3.2A). From DE on, ongoing differentiation towards pancreatic endoderm was characterized by massive cell death and the formation of islet-like clusters after 18 days of differentiation at stage 2 containing PEP cells (Figure 3.2A). Finally, during pancreatic specification of PEP cells towards PECs (stage 3; d21), islet-like structures condensed and expanded in size (see images in Figure 3.2A).

Gene expression analysis at d0 for the pluripotency markers *mNanog*, *mOct4* and *mSox2* revealed a significant higher expression level of all markers compared to stage 1, 2 or 3 indicating the loss of pluripotency and induction of differentiation (Figure 3.2B-D). Next, expression of the DE markers *mSox17*, *mFoxA2* and *mCxcr4* was investigated. In comparison to d0, all marker genes were upregulated at stage 1 (*mSox17* - 8.16 fold ± 2.56; *mFoxA2* - 2.65 fold ± 0.04; *mCxcr4* - 19.16 fold ± 6.29) (Figure 3.2E-G). In contrast, all DE markers were significantly downregulated in stage 2 and 3 cells (Figure 3.2E-G) demonstrating ongoing differentiation.

When analyzing gene expression patterns characteristic for PEP cells (stage 2), only *mPtf1a* expression was significantly upregulated (33% ± 10.53%) compared to DE cells, while *mNkx6.1* and *mPdx1* gene expression was only slightly increased (Figure 3.2H-J). However, compared to d0, all markers showed significant induction of gene expression in stage 2 cells (Figure 3.2H-J). Comparing gene expression ratios between stage 2 and stage 3 cells, a significant increase of *mPdx1* expression (47% ±

18.11%) was observed, whereas *mNkx6.1* and *mPtf1a* showed only a moderate increase in expression values (Figure 3.2I-J).

Last, the expression of *mInsulin*, *mGlucagon* and *mSomatostatin* characterizing the three major endocrine cell types α-, β- and δ-cells, respectively, was analyzed at stage 3 (Figure 3.2K-M). Significantly higher levels of *mInsulin* (1527 ± 240 fold), *mGlucagon* (341 ± 13 fold) and *mSomatostatin* (262 ± 96 fold) were detected in stage 3 cells when compared to CGR8 cells (start d0). In comparison to stage 1 cells, elevated gene expression levels for *mInsulin* (4.08 ± 0.76 fold), *mGlucagon* (26.04 ± 13.13) and *mSomatostatin* (2.74 ± 0.24) could be demonstrated (Figure 3.2K-M). Compared to stage 2, only *mInsulin* was significantly elevated by 57% ± 9.07% at stage 3, while *mGlucagon* and *mSomatostatin* were not significantly increased (Figure 3.2K-M).

Together, these findings demonstrate the induction of pancreatic lineage-specific differentiation of CGR8 cells when applying the recently published protocol from Mfopou et al [225]. Of note, special emphasis was on the media formulation of this protocol, as the same composition was also applied in the following differentiation experiments using ISCs.

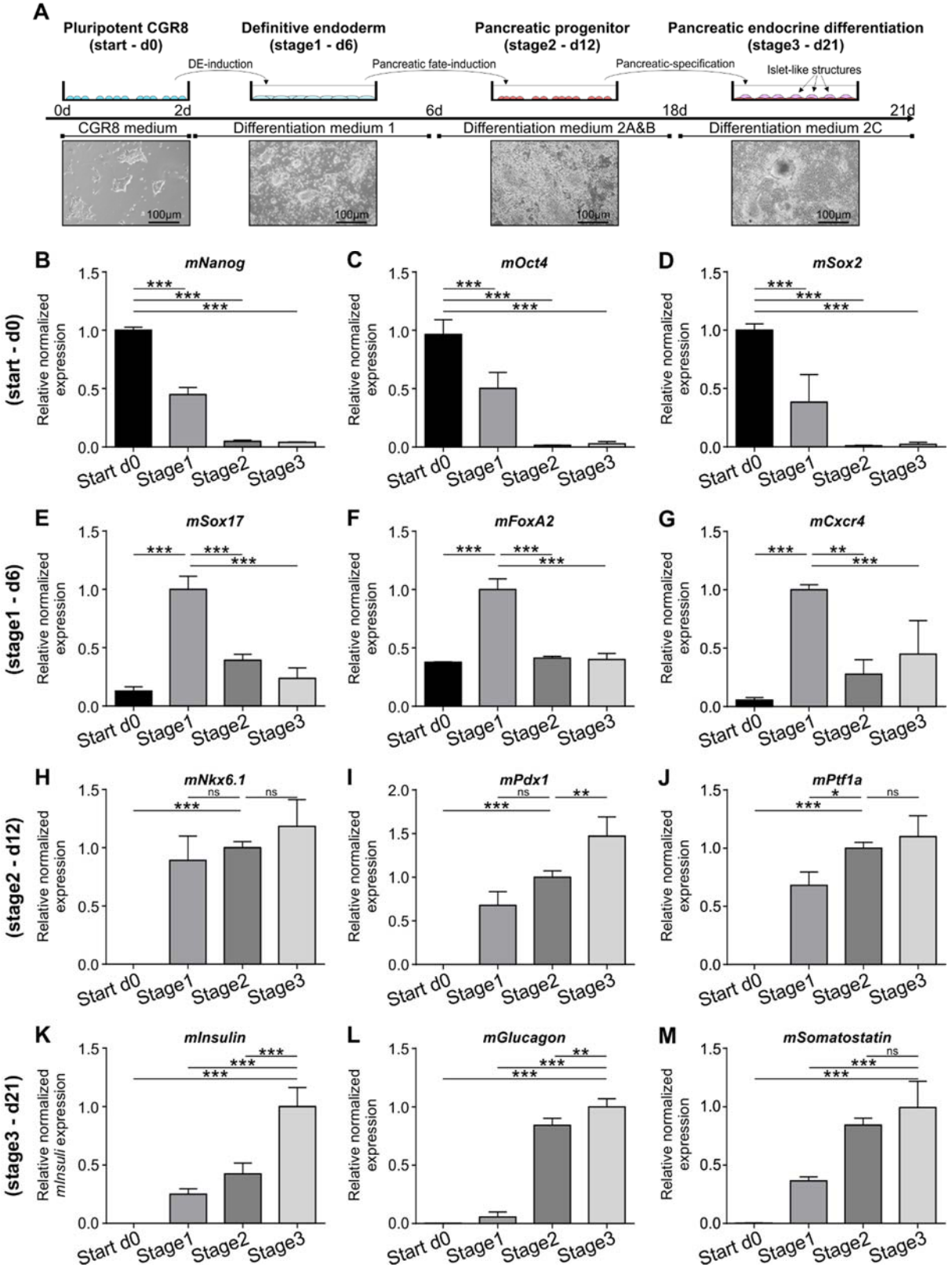

Figure 3.2: Differentiation of CGR8 cells towards pancreatic endocrine cell types. (A) Experimental overview of pancreatic differentiation. Timeline shows differentiation stages from pluripotent CGR8 cells (start; d0) via definitive endoderm cells (stage 1; d6) and pancreatic endocrine progenitors (PEG) (stage 2; d12) towards pancreatic endocrine cell (PEC) types (stage 3; d21). Corresponding stage-specific media and microscope pictures are presented for each stage. Scale bar = 100 µm. (B)-(M): Graphs showing characteristic gene expression patterns determined by qRT-PCR. Shown are relative normalized gene expression values with *mRpl6* and *mRps29* as reference genes. (B-D) Pluripotent cell

state (*mNanog*, *mOct4*, *mSox2).* (E-G) Definitive endoderm state (*mSox17*, *mFoxA2, mCxcr4*). (H-J) Pancreatic progenitor state (*mNkx6.1*, *mPdx1*, *mPtf1a)*. (K-M). Pancreatic endocrine-like cells (*mInsulin*, *mGlucagon, mSomatostatin)*. Expression values in stage-specific cells were set to 1. Statistics were carried out by one-way ANOVA and Dunnett's multiple comparison test. **P < 0.05, **P < 0.01 and ***P < 0.001*. *n = 3.*

3.1.2 Pancreatic differentiation of murine intestinal stem cells

Main aim of this part was to induce pancreatic differentiation of multipotent intestinal stem cells (ISCs). To derive ISCs from the intestine, the Lgr5-eGFP transgenic mouse line was used in this study that allows isolation of ISCs by means of eGFP expression under control of the Lgr5 promotor, an ISC-specific marker [39].

3.1.2.1. Lgr5-eGFP$^+$-ISCs isolated from Lgr5-eGFP transgenic mice express characteristic stem cell markers

ISCs were isolated from transgenic Lgr5-eGFP mice as previously described [42]. Briefly, intestinal crypts were dissociated followed by FACS cell sorting of the eGFP-positive ISC population [39] (Figure 3.3A). While crypt isolation and subsequent FACS analysis revealed 15-20% eGFP-positive events (Figure 3.3B), the total number of Lgr5-eGFP$^+$-ISCs varied from 3×10^5 to 7×10^5 cells per isolation with 4-5 animals used. To assess the quality of the applied isolation protocol, Lgr5-eGFP$^+$-ISCs were analyzed by qRT-PCR for their gene expression profile. Therefore, the characteristic ISC markers *mOlfm4*, *mAscl2*, *mSmoc2*, *mTnfrsf19* and *mLgr5* were analyzed. All genes displayed elevated expression levels in Lgr5-eGFP$^+$-ISCs compared to Lgr5-eGFP negative cells (Figure 3.3C).

Together, the isolated Lgr5-eGFP$^+$-ISCs showed a characteristic gene expression profile as previously reported in 2012 by Munoz et al. [41]. While, the applied isolation strategy derived ISCs expressing characteristic marker genes, the number of available cells turned out to become a bottleneck for a broad experimental set up.

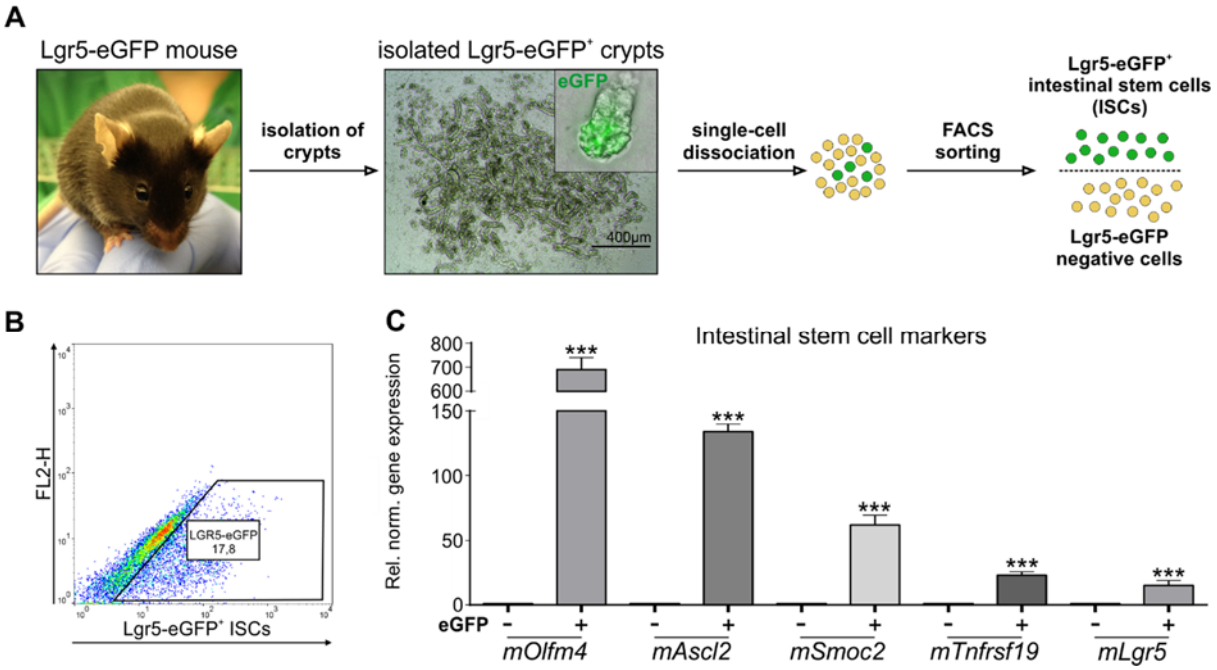

Figure 3.3: Isolation and characterization of Lgr5-eGFP⁺-ISCs. (A) Schematic representation of Lgr5-eGFP⁺-ISC isolation and cell sorting. Scale bar represents 400 µm. (B) Representative FACS dot-plot demonstrating the Lgr5-eGFP⁺-ISC population among all intestinal cell types isolated from Lgr5-eGFP crypts. 15-20% Lgr5-eGFP⁺ ISCs could be obtained per isolation. (C) Gene expression pattern of intestinal cells analyzed by qRT-PCR. *mOlfm4*, *mAscl2*, *mSmoc2*, *mTnfrsf19*, *mLgr5* are characteristic for ISCs. Values are shown as relative normalized gene expression with *mRpl6* and *mRps29* as reference. Significance was calculated by student's t-test. Lgr5-eGFP negative cells were used as control set to 1. ***$P < 0.001$. $n = 3$.

3.1.2.2. Defined conditions for single cell monolayer cultures of Lgr5-eGFP⁺-ISCs

In this work, ectopic expression of the transcription factor *Ptf1a* in single cell ISCs by cell transduction was hypothesized to induce pancreatic differentiation. In general, ISCs are cultured in a 3D environment, embedded in a Matrigel® drop (MG drop culture). When ISCs grow in a MG drop culture system in combination with cell type-specific organoid maintenance medium, they typically form organoids characterized by crypt structures with cellular buds arranged around a central lumen (Figure 3.4B) [42]. Previous studies described Matrigel® drop cultures as hard to transduce [257] and thereby characterize this culture system as disadvantageous for Ptf1a delivery and expression. Therefore, a monolayer-based cell culture system using Matrigel® as coating substrate (MG coating culture) was established to allow transduction of single cell ISCs with higher efficiency. Single cell ISCs grown in MG coating cultures lack a 3D environment mimicking the intestinal niche therefore missing important cell-cell contacts and signals that stimulate ISC growth, survival and differentiation. In addition

to the new established MG coating culture system, also the organoid maintenance medium (M-medium) was modified in this work to support ISC survival and differentiation under this conditions.

Single cell Lgr5-eGFP^{+}-ISCs were grown in MG coating cultures comparing diverse media compositions (Figure 3.4A). Standard MG drop cultures served as controls. Cells grown under standard conditions (MG drop culture combined with unmodified M-medium) showed characteristic organoid formation (Figure 3.4B). No or only few cells were detected in MG coating cultures where the standard M-medium or medium Y (M-medium + 10 µM Rock inhibitor Y27632) were applied for up to 7 days revealing that additional factors are required to sustain ISC survival and differentiation (Figure 3.4C). In contrast, all other tested media compositions supported cell growth (Figure 3.4C). On day 7, medium YC (M-medium + Y27632 and 3 µM GSK3 inhibitor CHIR 99021) and YCV (M-medium + Y27632 and 3 + µM CHIR 99021 and 1 mM of the histone deacetylase inhibitor valproic acid) resulted in spheroid-like clusters of cells (Figure 3.4C). However, most cells were detected in medium YCVJ (M-medium + Y27632 + 3 µM CHIR 99021 + 1 mM valproic acid and 1 µM of the Notch agonist Jagged-1), where cells clustered together and lined up in a thin monolayer resembling an epithelial cell-like layer on the MG surface (Figure 3.4C).

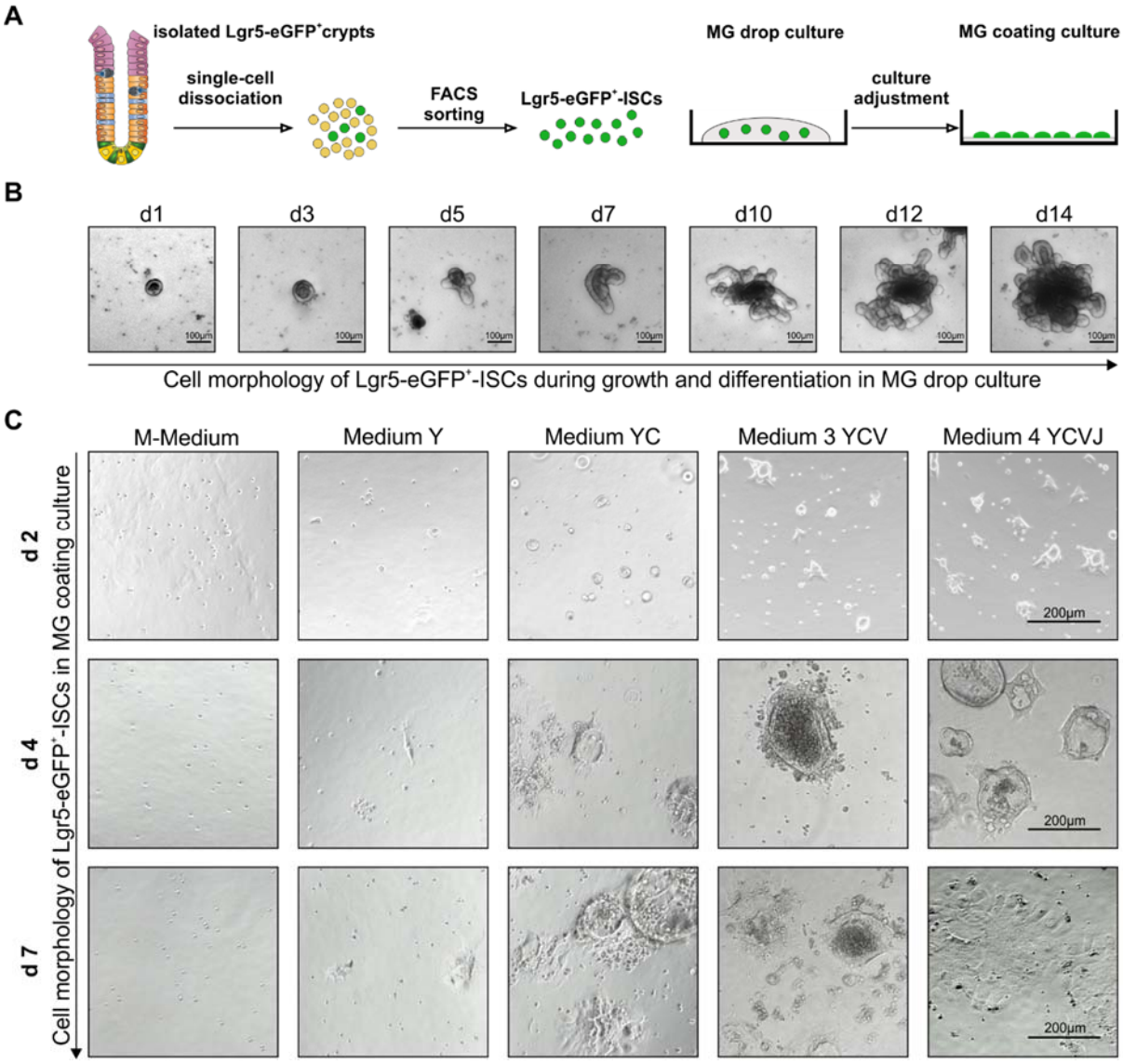

Figure 3.4: Lgr5-eGFP$^+$-ISCs in MG drop- or MG coating-culture using diverse media formulations. (A) Experimental overview of FACS-isolated, single cell Lgr5-eGFP$^+$-ISCs under Matrigel® (MG) drop vs. MG coating culture conditions. Lgr5-eGFP$^+$ crypts were isolated and FACS-sorted for LGR5-eGFP$^+$ single cells followed by seeding in MG drop- or MG coating-culture. (B) Microscope pictures representing characteristic cell morphologies at d1, d3, d5, d7, d10, d12 and d14 of Lgr5-eGFP$^+$ ISCs grown in standard MG drop cultures and M-medium. (C) Characteristic images of LGR5-eGFP$^+$ ISCs seeded as single cells in MG coating cultures after isolation and FACS purification. Different media compositions were compared to M-medium and cell morphology was monitored at d2, d4 and d7. Media formulations were based on M-medium containing R-spondin1, EGF and Noggin supplemented with 10 µM Rock inhibitor Y27632 (Medium Y); supplemented with Y27632 and 3 µM GSK3 inhibitor CHIR 99021 (Medium YC); supplemented with Y27632, 3 µM CHIR 99021 and 1 mM of the histone deacetylase inhibitor valproic acid (Medium YCV) or supplemented with Y27632, 3 µM CHIR 99021, 1 mM valproic acid and 1 µM of the Notch agonist Jagged-1 (Medium YCVJ). Media composition of Medium YCVJ according to [258]. Scale bars represent 100 µm and 200 µm.

In addition to cell morphology, quantitative analysis of emerging colony-like structures indicating cellular proliferation were performed on day 2. As shown in Figure 3.5A, significantly more colonies were detected in medium YCV and YCVJ compared to medium Y and YC, respectively. On day 7, counting of colonies was impossible due to colony coalescence to a continuous cell layer in medium YC and YCV (Figure 3.5D). To verify these findings cell viability was analyzed. Figure 3.5B-D shows increased viability of ISCs cultured in medium YC, YCV and YCVJ whereas medium YCVJ-cultured cells represented highest viability after 2 and 7 days (Figure 3.5B-C) compared to standard M-medium (Figure 3.5B-C).

In conclusion, medium YCVJ formulation was considered as best medium to culture single cell Lgr5-eGFP^{+}-ISCs under MG coating conditions and was therefore applied for further experiments.

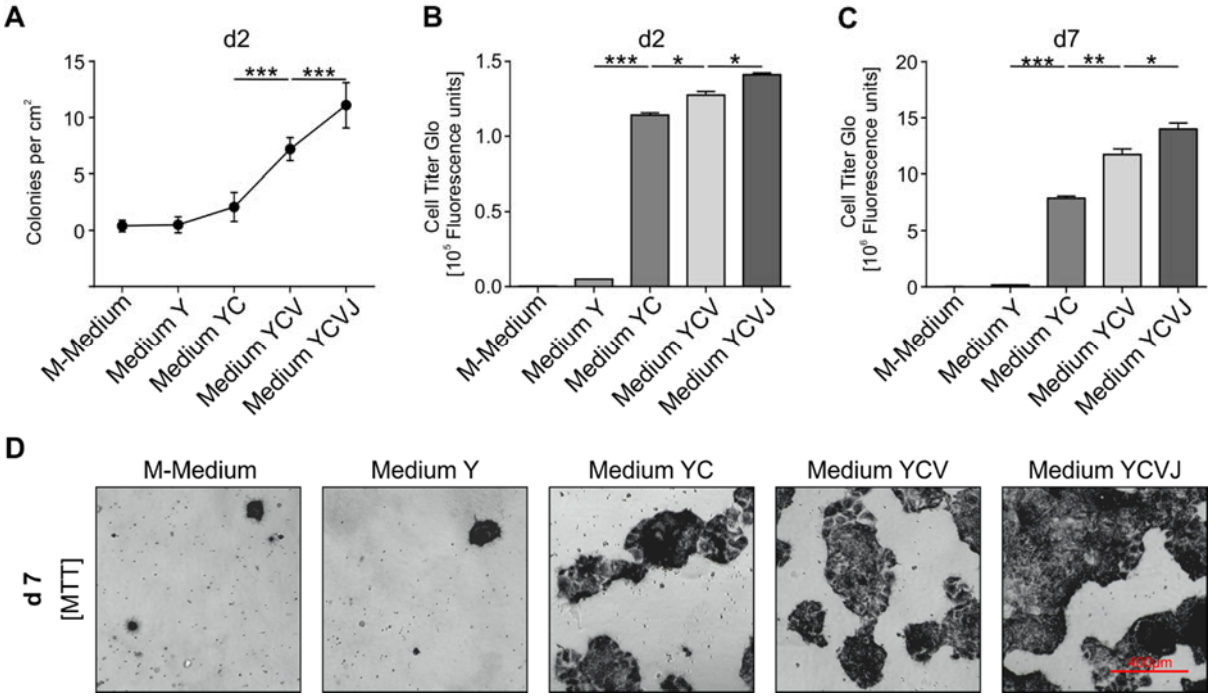

Figure 3.5: Organoid maintenance medium supplemented with Y27632, CHIR 99021, valproic acid and Jagged-1 displays highest cell viability. (A) Graph shows number of colonies per cm^2 after 2 days of culture. Colonies were counted from representative microscopic images. M-medium = organoid maintenance medium. (B-C) Graphs demonstrating cellular viability obtained by performing a Cell Titer Glo assay on day 2 and 7 of MG coating cultures with diverse media compositions. Cellular viability of ISCs grown in M-medium served as control. Significance was calculated by unpaired t-test with Welch's correction. **P < 0.05, **P < 0.01 and ***P < 0.001. n = 3.* (D) Representative microscopic images of MTT-stained Lgr5-eGFP^{+}-ISCs grown for seven days in MG coating cultures with M-medium or media composition Y, YC, YCV, or YCVJ. Scale bar represent 400 µm.

3.1.2.3. Applied technologies for the ectopic expression of *Ptf1a* in single cell ISCs or organoids

After having established the MG coating culture system for maintaining single cell Lgr5-eGFP^{+}-ISCs, the next step was to define the best strategy for ectopic expression of pancreatic transcription factor 1 alpha (Ptf1a) in these cells. As the MG coating culture system and the applied media formulation YCVJ were both conceptually new approaches established for the first time in this work, several techniques were tested and compared with each other to induce transcription factor expression with highest efficiency. An overview of all applied techniques is shown in Figure 3.6.

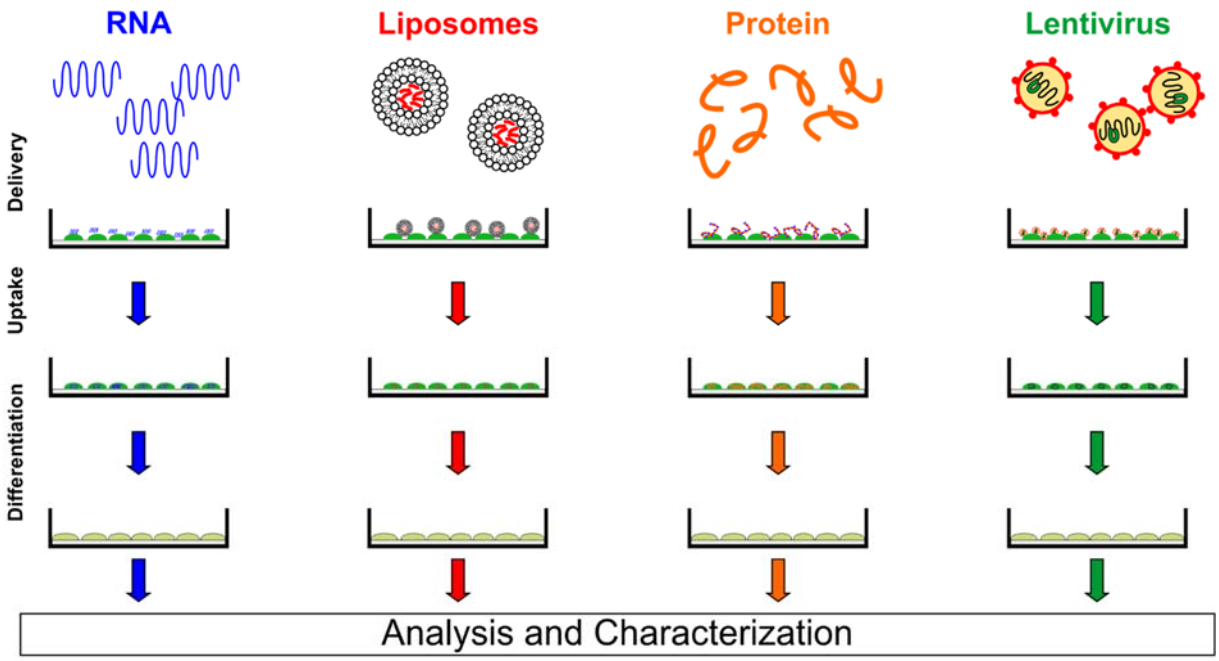

Figure 3.6: Synopsis of applied strategies for ectopic *Ptf1a* expression in Lgr5-eGFP^{+}-ISCs or organoids. Methods to induce ectopic *Ptf1a* expression in Lgr5-eGFP^{+}-ISCs or intestinal organoids grown and differentiated under Matrigel®-based culture conditions include RNA and protein transfection, liposomal delivery of PTF1A protein or lentivirus-mediated consecutive Ptf1a expression.

3.1.2.3.1. *Cre*-RNA transfection of Lgr5-eGFP^{+}/CAGGS-tdTomato^{+} organoids resulted in tdTOMATO expression

RNA transfection is a commonly used method to ectopically express non-cell type-specific molecules. In brief, this method describes the expression of RNA in cells and the subsequent translation via DNA to functional protein. Recent studies demonstrated a high transfection efficiency of difficult-to-transfect human iPSCs by means of

synthetic modified mRNAs [251]. In view of these promising results, RNA transfection was considered as interesting option to ectopically express *Ptf1a* in Lgr5-eGFP$^+$-ISCs. However, before applying this method on the single cell ISCs in MG coating cultures under medium YCVJ conditions, this approach was tested on organoids first. To this aim, crypts were isolated from double transgenic mice expressing eGFP under the Lgr5 promoter and tdTOMATO driven by the CAGGS promoter (Lgr5-eGFP$^+$/td-Tomato$^+$; see methods part 2.2.1.5.) and cultured in MG drop cultures with M-medium for 3-4 days until homogenous organoids structures were detected. Successful transfection of these cells with synthetic RNA for Cre recombinase will result in eGFP$^+$/tdTOMATO$^+$ organoids (Figure 3.7A).

Cre-RNA (kindly provided by Dr. P. Wörsdörfer, University of Würzburg) transfection was performed either on Lgr5-eGFP$^+$/CAGGS-tdTomato$^+$ organoids in MG drop cultures or on Matrigel®-deprived organoids with subsequent re-seeding into MG drop culture and use of M-medium (Figure 3.7B). Delivery of RNA to organoids in MG drop culture might be difficult; however, this strategy was tested to investigate if RNA transfection works under these conditions. In both conditions, *Cre*-RNA was transfected into organoids where the floxed STOP cassette was excised and expression of the red fluorescent reporter (tdTOMATO) was initiated (Figure 3.7C). The Lgr5-eGFP$^+$-ISC-associated eGFP-signal was detected throughout the entire organoid, albeit the stem cells reside in the periphery. While the eGFP signal is quite strong when acquiring images from the entire organoid, it can be clearly distinguished from the typical auto-fluorescence signal derived from MG-drop cultured organoids (Figure 3.7C; see also Figure 2.4 in 2.2.2.6.). In contrast, the tdTOMATO signal was detected in the periphery of transfected organoids, highly concentrated in few clusters but not in all regions (Figure 3.7C). Only few spots were detected with eGFP and tdTOMATO colocalization, while the precise localization of the signal remained elusive.

Together, the results of this experiment do not allow to state which cell type was transfected within the organoid. However, the obtained results indicate successful RNA delivery into organoids, regardless if organoids were transfected under Matrigel®-deprived or under MG drop culture conditions using M-medium. The generation of a synthetic modified mRNA specific for Ptf1a failed in this work due to unknown complications during cloning. Therefore, no further experiments were performed on

single cell ISCs grown on MG coating cultures using RNA transfection and YCVJ medium conditions.

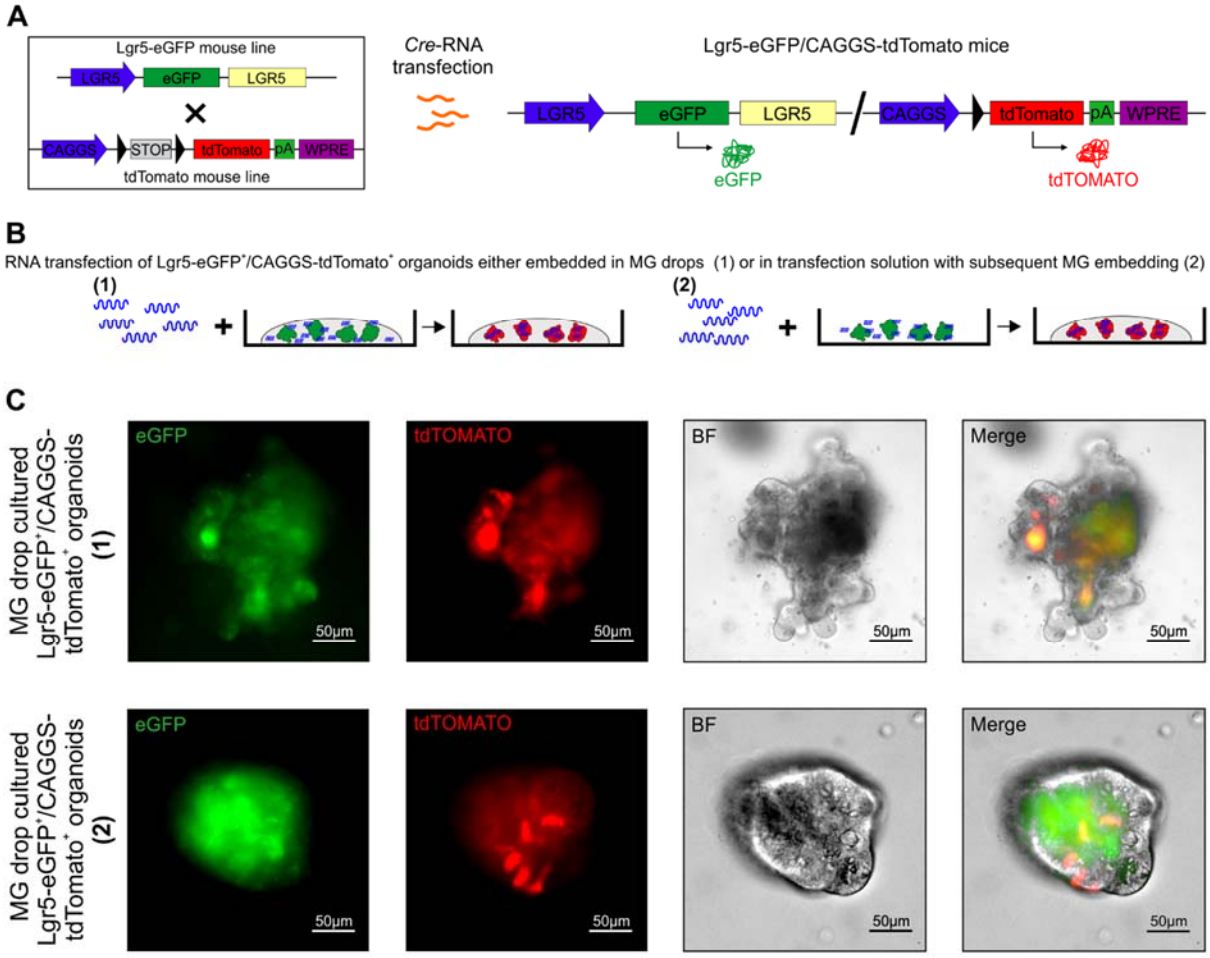

Figure 3.7: *Cre*-RNA transfected Lgr5-eGFP⁺/CAGGS-tdTomato⁺ organoids. (A) Scheme showing experimental strategy for *Cre*-RNA transfection in MG drop embedded organoids (1) or in MG-deprived organoids prior to embedding in MG drop culture (2). (B) Representative microscope images of Lgr5-eGFP⁺/CAGGS-tdTomato⁺ crypts in MG drop culture 24h post *Cre*-RNA transfection. Organoids in the upper panel (1) were transfected while being embedded in Matrigel® and in the lower panel (2) organoids were embedded in MG drops after transfection. Green indicates expression of eGFP (from Lgr5-eGFP⁺ISCs) and red represents tdTOMATO expressed in *Cre*-transfected cells. BF = Bright field. Scale bars represent 50 µm. *n* = 2.

3.1.2.3.2. Liposomal-mediated protein delivery into single cell Lgr5-eGFP+-ISCs is associated with cytotoxicity

Liposomes refer to a class of spherical vesicles consisting of at least one phospholipid bilayer used for the administration of drugs, compounds or molecules. The pH-sensitive liposomes used in this experiment were formulated by Dr. Marco Favretto

(University of Nijmegen, RIMLS, the Netherlands) as described in methods part 2.2.2.11. Mechanistically, these liposomes are stable at a physiological pH and become destabilized after cellular ingestion in the rather acidic intracellular environment [259] thereby releasing their hydrophilic protein cargo [260], recombinant bioactive PTF1A in the current study. The PTF1A containing liposomes were applied to Lgr5-eGFP$^+$-ISCs cultured on MG coated surfaces in the presence of medium YCVJ. In addition, PTF1A-specific liposomes were applied to MG-deprived Lgr5-eGFP$^+$ organoids followed by culture as MG drop cultures with organoid maintenance medium (Figure 3.8A). To visualize successful PTF1A protein delivery in target cells, recombinant PTF1A was tagged with the fluorescent dye tetra-methylrhodamine (TMR).

In a first step, PTF1A-loaded liposomes and empty liposomes (mock) were exposed to Lgr5-eGFP$^+$-ISCs growing on MG coated surfaces and compared to non-treated control cells (Figure 3.8A). The next day, PTF1A-TMR localization was analyzed using a confocal microscope. The signal in TMR$^+$ cells was exclusively detected in the cytosol but not within the nucleus (Figure 3.8B). PTF1a delivery worked for Lgr5-eGFP$^+$-ISCs, however, after being exposed to liposomes all cells and organoids underwent apoptosis after a period of 24 to 36h. This cytotoxic effect made it impossible to proceed with liposomes as carrier to express PTF1A in Lgr5-eGFP$^+$-ISCs. To verify if liposomes are also toxic to organoids, the PTF1A uptake was monitored 4h post-liposome exposure, before Matrigel® embedding for MG drop culture (Figure 3.8C). The TMR signal was detected in all organoids in the central lumen but was absent in the periphery where Lgr5-eGFP$^+$ cells are situated (Figure 3.8C). Furthermore, MG drop cultured organoids died after a period of 48h after Matrigel® embedding.

In summary, both, liposome-treated organoids and single cell ISCs displayed high cytotoxicity suggesting that the used liposome formulation is an inappropriate delivery technique for PTF1A.

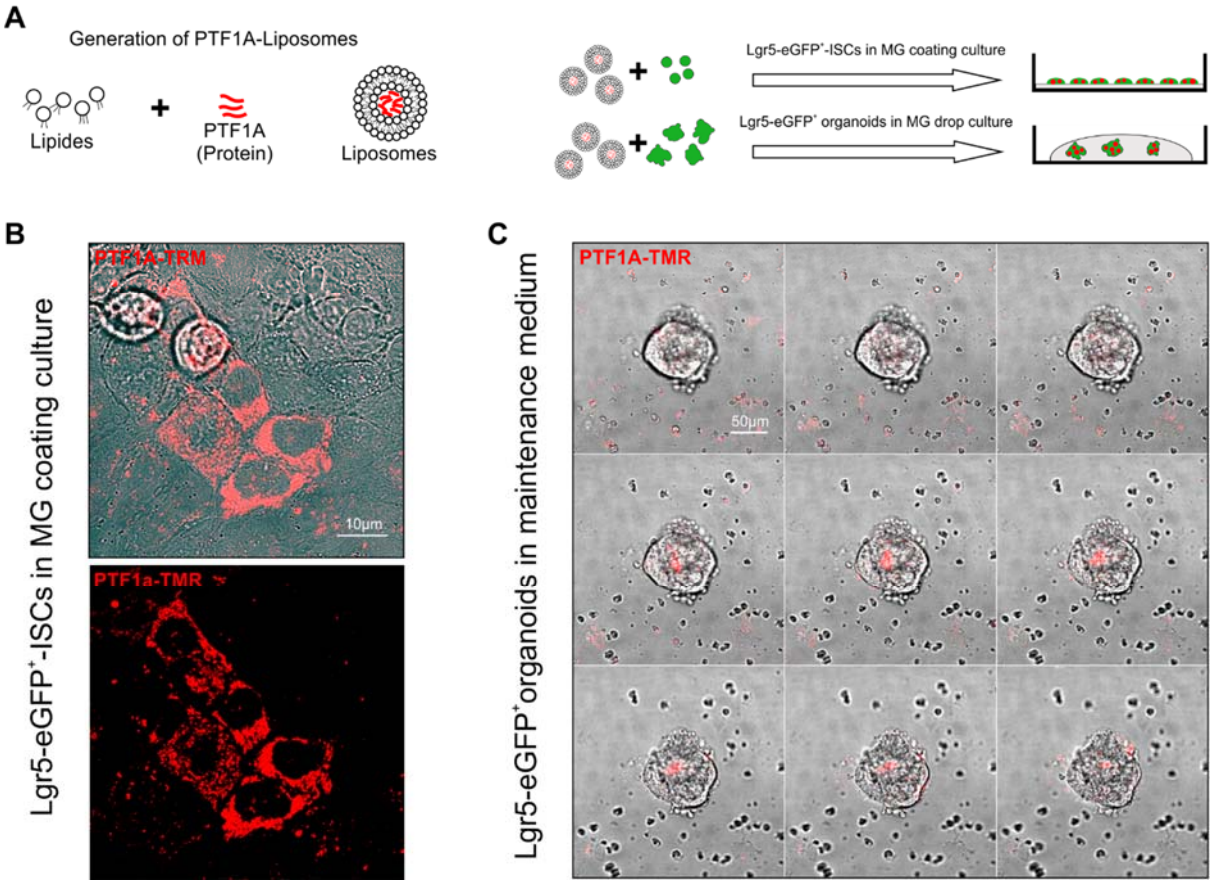

Figure 3.8: Liposomal-mediated PTF1A delivery into Lgr5-eGFP⁺-ISCs and Lgr5-eGFP⁺ organoids. (A) Overview of liposome generation and experimental outline for liposomal-mediated PTF1A delivery into target cells. (B) Representative images from single Lgr5-eGFP⁺-ISCs grown under MG coating conditions 16h after liposome treatment. PTF1A was coupled to tetra-methylrhodamine (TMR) for visualization. (C) Confocal images showing an Lgr5-eGFP⁺ organoid in maintenance medium, 4h after liposomal PTF1a delivery, scanned from top (image top panel left side) to bottom (lower panel right). Scale bars represent 10 µm and 50 µm. *n = 2.*

3.1.2.3.3. Cell penetrating peptide-functionalized protein is ingested in organoids

As alternative to cytotoxic PTF1A-liposomes, recombinant PTF1A can also be transfected using cell-penetrating peptides (CPP) to mediate cellular uptake. To this aim, CPPs from Xfect (Clonetech) were linked to PTF1A and applied to Lgr5-eGFP⁺-ISCs. CPPs are short peptides comprised of polycationic or amphipathic segments ranging from 6 to about 30 amino acids in total and are capable to chemically interact with a cargo to mediate cellular incorporation via endocytosis [261]. To validate CPP-mediated protein transfection, first CRE protein was CPP-functionalized prior to transfection of Matrigel®-deprived Lgr5-eGFP⁺/CAGGS-tdTomato⁺ organoids (Figure 3.9A-B and methods part 2.2.1.5.). Cellular CRE protein uptake was successful as indicated by the expression of tdTOMATO in this organoids that in addition displayed

LGR5-driven eGFP expression (Figure 3.9B). These data indicate functionality of the technique using organoids that are cultured under MG drop conditions with organoid maintenance medium. Therefore, in the next step functionalized TMR-labeled PTF1A was transfected into Lgr5-eGFP^{+} organoids. The TMR-PTF1a signal was detected in the mantle of the organoids where it colocalized with the ISC-specific eGFP signal (Figure 3.9C). In both approaches, the protein signal (red) was not detected in the core of the organoids (Figure 3.9B).

Together, these findings underline the functionality of CPP-mediated protein transfection in all peripheral regions of murine organoids. Nevertheless, the efficacy and the definition which cell type within the organoid structure was transfected remains unanswered but the positive preliminary results proposed this application to be tested on sorted Lgr5-eGFP^{+}-ISCs.

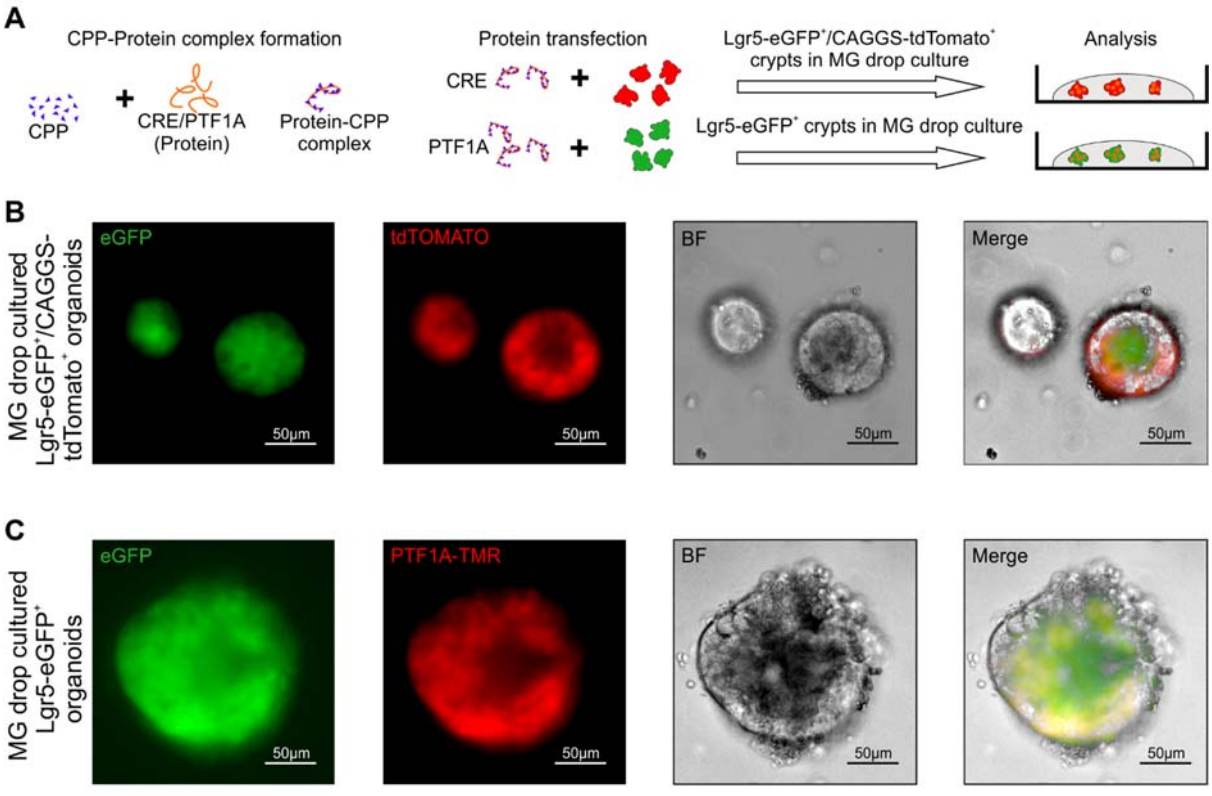

Figure 3.9: Cell-penetrating peptides (CPP) -mediated protein transfection of intestinal organoids. (A) Experimental overview showing schematic CPP-protein complex formation and transfection strategy for functionalized protein delivery into organoids. (B-C) Microscopic images of CRE protein transfected Lgr5-eGFP^{+}/tdTomato^{+} organoids (B) and TMR-PTF1a protein transfected Lgr5-eGFP organoids (C). Green indicates expression of eGFP (from Lgr5-eGFP^{+}ISCs) and red represents tdTOMATO expressed in CRE-transfected cells or PTF1a linked to a TMR dye. BF = Bright field. Scale bars represent 50 µm. *n = 2.*

3.1.2.3.4. PTF1A protein transfection of Lgr5-eGFP^{+}-ISCs results in short-term upregulation of pancreas-specific genes

The preceding results demonstrated that CPP-functionalization was the best possibility to transfect intestinal organoids with PTF1A protein. Therefore, CPP-functionalized PTF1A was expressed in the next step in single cell ISCs grown as monolayer in MG coating culture using medium YCVJ. The main aim of this work was to derive β-like cells from PTF1A transfected ISCs. In a first step, the pancreatic lineage-specific genes *mPtf1a*, *mPdx1*, *mNkx6.1* and *mHes1* indicating a general lineage switch of ISCs towards a pancreatic fate were analyzed after 2 and 7 days post-transfection by qRT-PCR. The ISC-specific marker *mLgr5* and the intestinal marker *mCdx 2* were analyzed to monitor loss of intestinal- and ISC identity.

Single cell Lgr5-eGFP^{+}-ISCs were isolated as previously described and cultured under MG coating conditions in medium YCVJ for 48h. PTF1A protein was CPP-functionalized and transfected using X-fect followed by culture in MG coating cultures applying organoid maintenance medium (M-medium; control) or medium YCVJ for 2 or 7 days prior to analysis (Figure 3.10A). Transfected cells were compared to untransfected controls. Cell morphology analysis 2 days post-transfection revealed no surviving cells when organoid maintenance medium was used and only few viable cells assembling in spheroid-like clusters when medium YCVJ was applied to transfected cells (Figure 3.10B). After 7 days, the spheroid-like cell clusters increased in size but shared a similar morphology between PTF1A-transfected and untransfected conditions (Figure 3.10E).

Gene expression analysis performed at day 2 post-transfection comparing transfected and untransfected cells grown in medium YCVJ resulted in a significant upregulation of the intestinal-associated genes *mLgr5* and *mCdx2* and the pancreas-specific genes *mPtf1a*, *mPdx1* and *mNkx6.1* (Figure 3.10C-D). However, the gene expression profiles at day 7 showed no differences between transfected and untransfected cells for all genes analyzed when cultured in medium YCVJ (Figure 3.10F-G).

In summary, these data manifest the necessity to maintain single cell ISCs in MG coating conditions using medium YCVJ. Furthermore, while PTF1A-transfected cells displayed elevated gene expression levels for pancreatic markers in the short term, expression was not stable to be detected at day 7 post transfection.

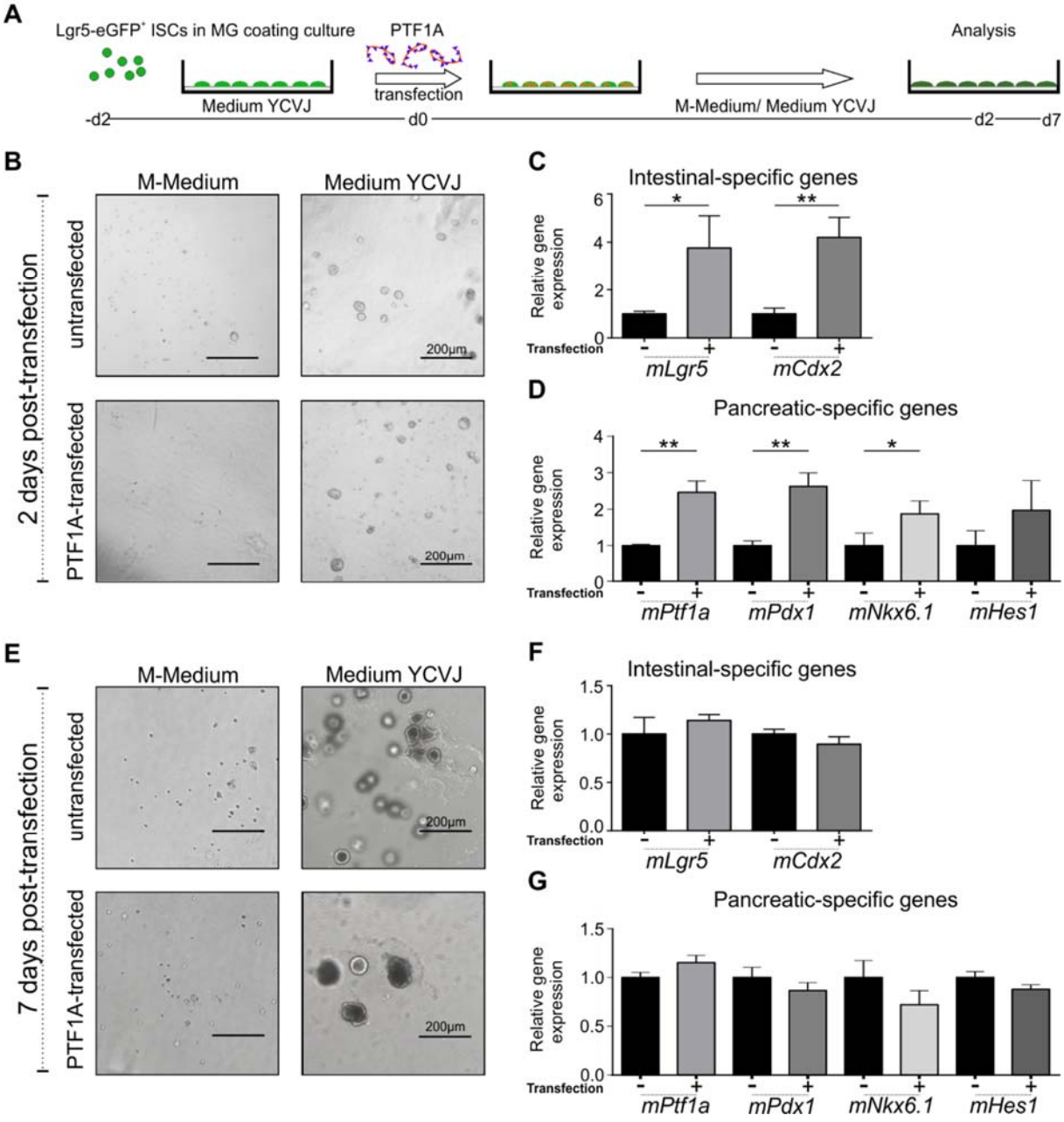

Figure 3.10: Gene expression profiles in Lgr5-eGFP$^+$-ISCs after PTF1A transfection. (A) Experimental overview for PTF1A transfection of Lgr5-eGFP$^+$-ISCs maintained in MG coating culture and medium YCVJ for 2 days prior to transfection. Cells were grown in M-medium (control) or medium YCVJ and analyzed for cell morphology and gene expression pattern after 2 and 7 days. (B) Representative microscope images showing the morphology of Lgr5-eGFP$^+$-ISCs cultured on MG coating 2 days post-transfection, comparing organoid maintenance medium and medium YCVJ. Scale bars represent 200 µm. (C-D) Graphs demonstrating characteristic intestinal- (*mLgr5 and mCdx2*) and pancreas-specific (*mPtf1a, mPdx1, m Nkx6.1 and mHes1*) gene expression patterns obtained by qRT-PCR analysis, 2 days post-transfection. (E) Images as described in B, 7 days post-transfection. (F-G) Graphs as described for C and D, 7 days post transfection. Statistics were carried out by one-way ANOVA and Tukey's multiple comparison test comparing transfected vs. untransfected cells. **P < 0.05, **P < 0.01 and ***P < 0.001*. *mRpl6* and *mRps29* served as reference genes. *n = 3.*

4.1.2.3.5. PTF1A transfection of single cell ISC cultures combined with the application of a pancreas-specific differentiation medium induced the expression of pancreatic marker genes defining acinar cell identity

As transfection of CPP-functionalized PTF1A protein was shown to induce the expression of pancreas-specific genes like *mPtf1a*, *mPdx1*, *mNkx6.1* in the short term, the next step was to achieve similar results in the long-term. In general, differentiation of stem cells is guided by the application of cell lineage-specific culture media containing important signaling molecules mimicking the *in vivo* development [185, 186, 225, 226]. To this aim, the next step was to verify if the application of a pancreas-specific differentiation medium (250 µm Cyclopamine, 100 ng/ml Noggin, 25 ng/ml FGF10 and 2 µM RA), usually used to induce pancreatic progenitors from definitive endoderm cells [225], could support the upregulation of pancreas-specific genes in PTF1A-transfected single cell ISCs (Figure 3.11A). ISCs were cultured as described and maintained in medium YCVJ prior to PTF1A transfection (Figure 3.11A). After protein transfection, the pancreatic differentiation medium was applied for up to 7 days. Cell morphology and gene expression pattern were analyzed after 2 and 7 days in culture.

As Figure 3.11B shows, untransfected and transfected ISCs cultured in pancreatic differentiation medium displayed similar morphologies. At day 2, cells grew as round-shaped, spheroid-like colonies with protuberances. While untransfected control cells displayed the same morphology on day 3, PTF1A-transfected cells started to attach to the Matrigel® coating as indicated by the more flattened appearance of their colonies. These cell aggregates increased in size during the next days and around day 7, the clusters started to fall apart (at a critical size of about 150-200 µm) as shown by losing their boundaries and shape. At this time point, single cells appeared around the colony-like structures and started to grow as monolayer. At day 7, similar observations were made for untransfected colonies, however, the emerging monolayer formation was observed in a decimated extent compared to PTF1A-transfected cells (Figure 3.11B).

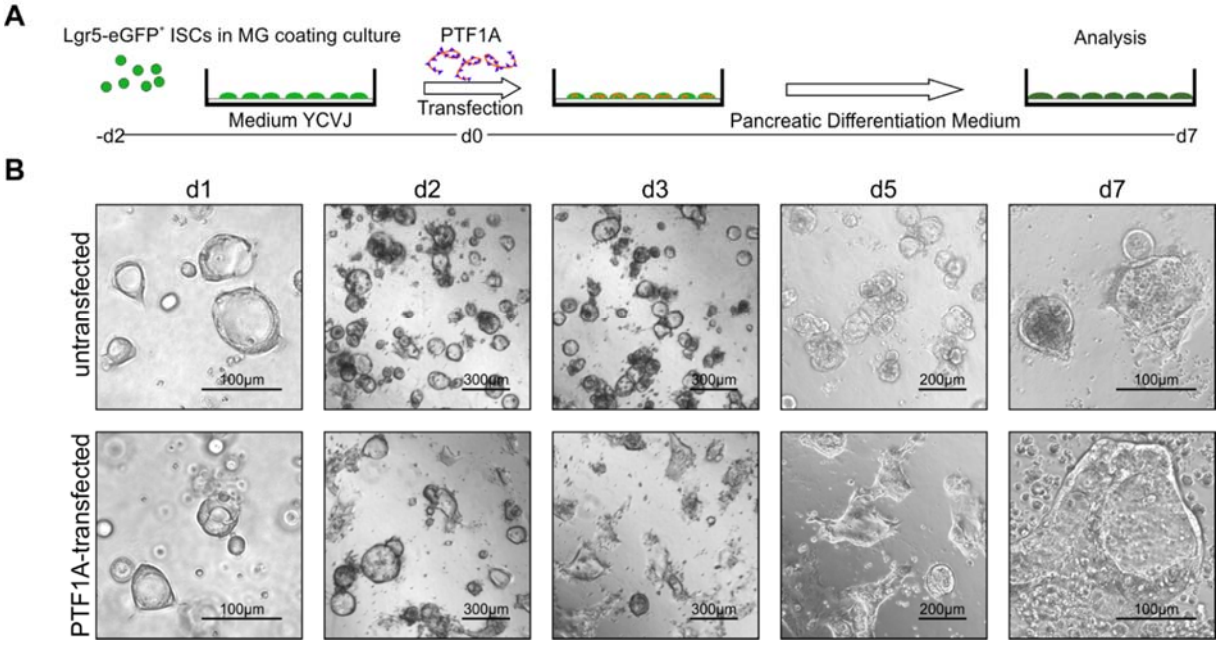

Figure 3.11: Cell morphology of PTF1A-transfected ISCs. (A) Experimental overview for PTF1A transfection of Lgr5-eGFP^{+}-ISCs. After isolation, ISCs were cultured in medium YCVJ under MG coating-culture conditions for 2 days prior to transfection. After transfection, cells were grown in pancreatic differentiation medium for up to 7 days in total. Analyses were performed after 2 and 7 days. (B) Representative microscopic images of PTF1A-transfected and untransfected ISCs cultured in pancreatic differentiation medium. Pictures indicate cellular morphologies at d1, d2, d4 and d7 post transection. Scale bars represent 100 µm, 200 µm or 300 µm. *n = 3.*

Gene expression analysis was performed with markers specific for the pancreatic lineage (*mHnf1b*, *mSox9*), for PEPs (*mPdx1*) and for PECs characterizing the three main endocrine islet cell types α-, β- and δ-cells (*mInsulin*, *mGlucagon* and *mSomatostatin*). As Ptf1a is known to be a master regulator of the acinar cell fate in late developmental stages, also the acinar cell-specific markers *mAmylase* and *mChymoB1* were analyzed (Figure 3.12A-J).

First, the importance of the application of the pancreatic differentiation medium was analyzed by comparing untransfected cells grown in medium YCVJ (control) and untransfected cells grown in the pancreatic differentiation medium (d7 no Ptf1A). Statistical analysis revealed a highly significant upregulation of pancreatic-specific gene expression of all genes analyzed, ranging from 5.9 fold for *mInsulin* as lowest to 100 fold for *mAmylase* as highest expression range, when grown in pancreatic differentiation medium (Figure 3.12B-J). In addition, cells grown in pancreatic differentiation medium had an 11,866 fold decreased *mOlfm4* expression, indicating loss of intestinal stem cell identity of untransfected cells after being exposed to

pancreatic differentiation medium (Figure 3.12K). Focusing on the impact of PTF1A-transfection, only significant increased gene expression values for the acinar cell markers *mAmylase* (181.6% ± 12.8%) and *mChymoB1* (60.1% ± 11.8%) were detected when comparing transfected and untransfected ISCs grown in pancreatic differentiation medium (Figure 3.12H-I). Of note, all other analyzed genes showed similar expression values in both groups (Figure 3.12C-G,K).

In conclusion, application of the pancreatic differentiation medium alone was sufficient to induce pancreas-specific gene expression patterns in ISCs, albeit the hypothesized specification into β-like cells was not observed. PTF1A transfection was rather shown to result in elevated gene expression levels specific for the acinar cell lineage.

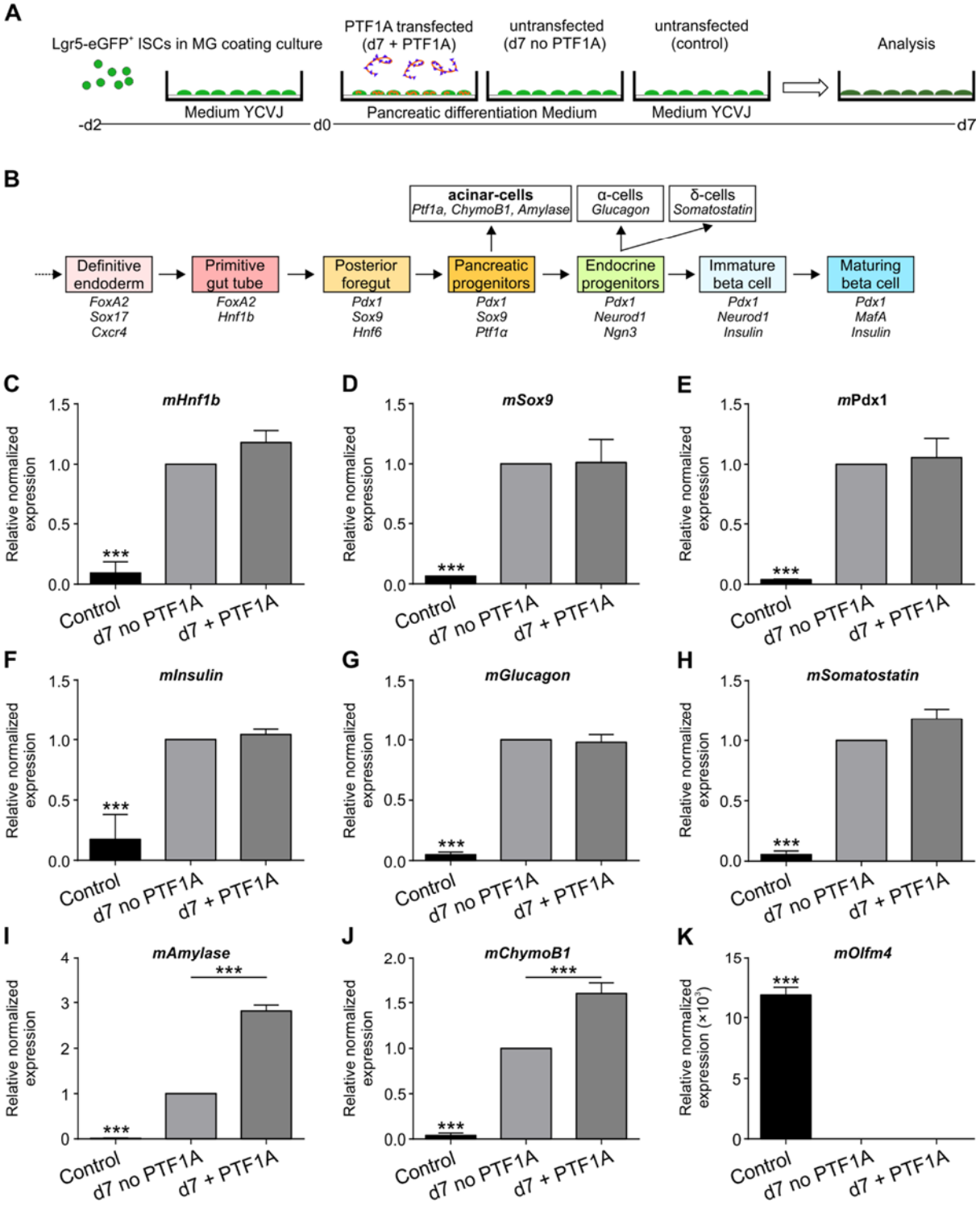

Figure 3.12: PTF1A transfection of Lgr5-eGFP⁺-ISCs grown in pancreatic differentiation medium results in the upregulation of genes specific for acinar cells. (A) Schematic overview of the experimental strategy. At day 7, gene expression of PTF1A transfected ISCs (d7 + PTF1a) grown in pancreatic differentiation medium was compared to untransfected ISCs grown in pancreatic differentiation medium (d7 no PTF1a) or in medium YCVJ (control). (B) Scheme represents a timeline of differentiation stages and stage- or lineage-specific genes during pancreatic differentiation. (B-K) Graphs represent characteristic stage-specific gene expression analyses carried out by qRT-PCR. (C-E) Pancreatic precursor stages were represented by primitive gut tube (*mHnf1b*), posterior foregut (*mSox9, mPdx1*) and PEP (*mSox9* and *mPdx1*) specific genes. (F-H) PEC-specific genes (*mInsulin*, *mGlucagon* and *mSomatostatin*). (I-J) Acinar lineage-specific genes (*mAmylase* and *mChymoB1*). (K)

The intestinal stem cell-specific marker *mOlfm4*. Values of the untransfected cells grown in pancreatic differentiation medium were set to 1. Statistics were carried out by student's t-test. Significance of controls to d7 + PTF1A and d7 no PTF1A is indicated by asterisks on the (control) bar. **P < 0.05, **P < 0.01 and ***P < 0.001*. *mRpl6* and *mRps29* served as reference genes. *n = 3.*

4.1.2.3.6. Upregulation of acinar-specific gene expression patterns in Lgr5-eGFP$^+$ organoids transduced with Ptf1a-encoding lentiviral vectors

PTF1A protein transfection was shown to induce rather an acinar lineage-specific gene expression pattern in ISCs than a β-cell-specific gene expression program. However, the effect was marginal, conceivably due to low transfection efficiency. As an alternative, lentiviral transduction was hypothesized to increase the efficiency of Ptf1a expression in ISCs what possibly also stimulates the upregulation of β-cell-like genes.

In another project of our laboratory (Masterproject Valentyna Kryklyva), it was demonstrated that lentivirus-promoted Ptf1a transduction of single cell ISCs resulted in cell death soon after transduction. However, an intestinal cell line (K8) comprising intestinal stem cell characteristics was successfully transduced as indicated by the induction of an acinar lineage-specific gene expression program without significant upregulation of β-cell-specific genes when pancreatic differentiation medium was applied [262]. Of note, the effect of the pancreatic differentiation medium exceeded the effect of Ptf1a transduction in terms of acinar cell lineage specific gene expression. Recently, it was proposed that a 3D culture environment for pancreatic progenitors may enhance their differentiation capacity [263]. Even if it was not the main goal of this work, the next step of this study was therefore to investigate if a 3D, Matrigel®-based environment could positively support the conversion of Ptf1a-transduced ISCs towards a β-like cell phenotype. To this aim, Lgr5-eGFP$^+$ organoids were used for ectopic expression of Ptf1a applying lentiviral transduction (Figure 3.13A).

First, it was assessed if lentiviral transduction is suitable for whole organoid structures. Therefore, Lgr5-eGFP$^+$ organoids were incubated in lentiviral supernatants containing pL-PGK-Ptf1a (see also 2.2.6.2. in materials and methods) a construct where *Ptf1a* expression is driven under the phosphoglycerate kinase (PGK) promotor previously shown to be efficient in murine embryonic stem cells [264]. To verify transduction success of Lgr5-eGFP$^+$ organoids, red fluorescent protein (RFP) was expressed under the elongation factor 1 alpha (EF1α) promotor independently from *Ptf1a* expression (Figure 3.13B and 2.2.6.2.). Subsequently after transduction, the organoids were

embedded in MG drops and cultured in organoid maintenance medium (2.1.4.4.) for 24h, followed by the application of pancreatic organoid differentiation (POD) medium, based on intestinal organoid medium supplemented with fibroblast growth factor 10 (FGF10) and nicotinamide [224, 263]. The POD medium differs from the pancreatic differentiation medium used before but was previously described to promote pancreatic progenitor expansion and differentiation towards endocrine linages, however, the final maturation of pancreatic organoids cultured in this medium were achieved *in vivo* only [224]. In the current study, a modified pancreatic organoid medium (also see 2.1.4.4.) was applied, containing increased nicotinamide and FGF10 concentrations that were hypothesized to further promote pancreatic differentiation [225, 226]. In the first step, the results showed that *Ptf1a* expression was achieved under the phosphoglycerate kinase (PGK) promotor what resulted in a red signal throughout the organoids while the signal strongly colocalized with the ISC-derived eGFP signal (Figure 3.13B).

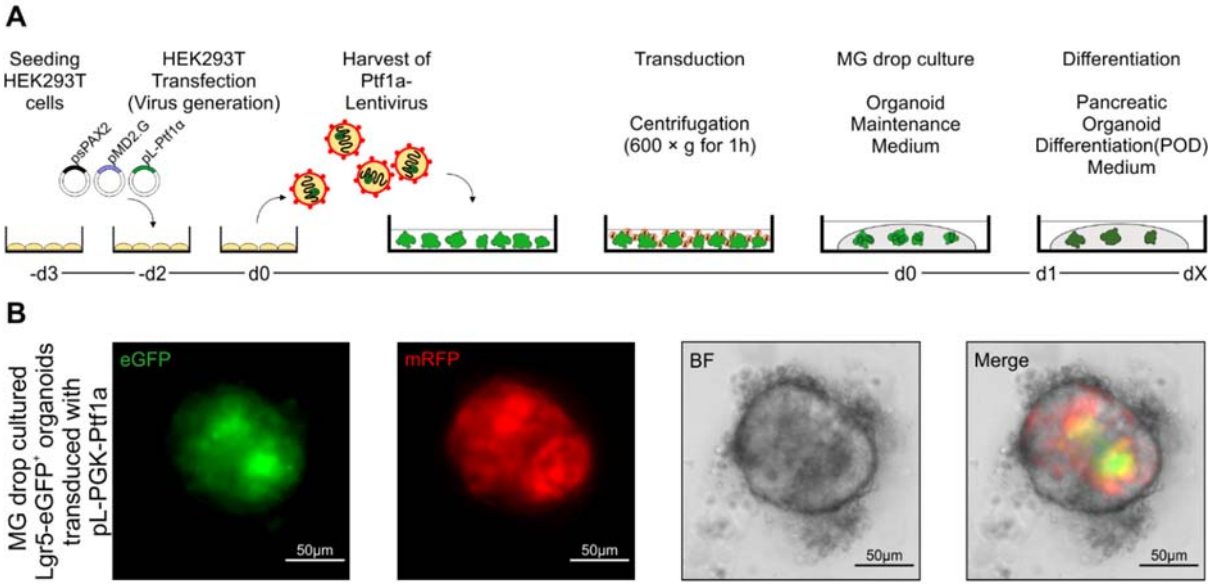

Figure 3.13: Lentiviral *Ptf1a*-expression in Lgr5-eGFP⁺ organoids. (A) Experimental overview of lentiviral production in HEK293T cells two days before viral transduction of Matrigel®-deprived Lgr5-eGFP⁺ organoids. MG drop embedded organoids were cultured with organoid maintenance medium for 1 day before pancreatic organoid differentiation (POD) medium was applied. (B) Representative images of an Lgr5-eGFP⁺ organoid 24h post pL-PGK-Ptf1a transduction cultured in MG drop culture. Green signal represents eGFP (from ISCs) and red signal RFP (red fluorescent protein from lentivirus). BF = Bright field. Scale bars represent 50 µm. *n = 3.*

To analyze if the applied lentiviral transduction protocol results in upregulation of pancreas-specific gene expression patterns, PEP- (*mNgn3, mPdx1 and mPtf1a*), β-cell- (*mInsulin*) or acinar- (*mAmylase, mChymoB1*) cell associated marker genes were investigated by qRT-PCR after 7 or 14 days (Figure 3.14A-G).

In pL-PGK-Ptf1a transduced organoids, the PEP marker *mNgn3* expression was unaltered after 7 days whereas after 14 days in culture the expression was significantly increased. While *mPdx1* was unaltered at both time points analyzed, *mPtf1a* was strongly upregulated in Ptf1a-transduced organoids after 7 (+ 329 fold) and 14 days (+ 499 fold) (Figure 3.14C-D). Next, *mInsulin* was analyzed to verify if Ptf1a transduction induced β-like cell expression, however, no upregulation of mRNA levels were detected in mock- or Ptf1a-transduced organoids (Figure 3.14E). In contrast, when analyzing the acinar cell-specific expression of *mAmylase* after 7 days in culture, mock- and Ptf1a-transduced organoids revealed a 3 fold upregulation (Figure 3.14F). However, after 14 days in culture only pL-PGK-Ptf1a transduced organoids displayed a 10-fold increased gene expression of *mAmylase* (Figure 3.14F). The second analyzed acinar cell-specific gene *mChymoB1* was significantly upregulated after 7 days (2.49×10^4) and 14 days (1.75×10^4) while mock-transduced conditions showed no upregulation (Figure 3.14G).

Together, these data indicate that Ptf1a transduction promoted an acinar lineage-specific gene expression pattern (*mAmylase* and *mChymoB1)* when cultured under pancreatic organoid differentiation medium.

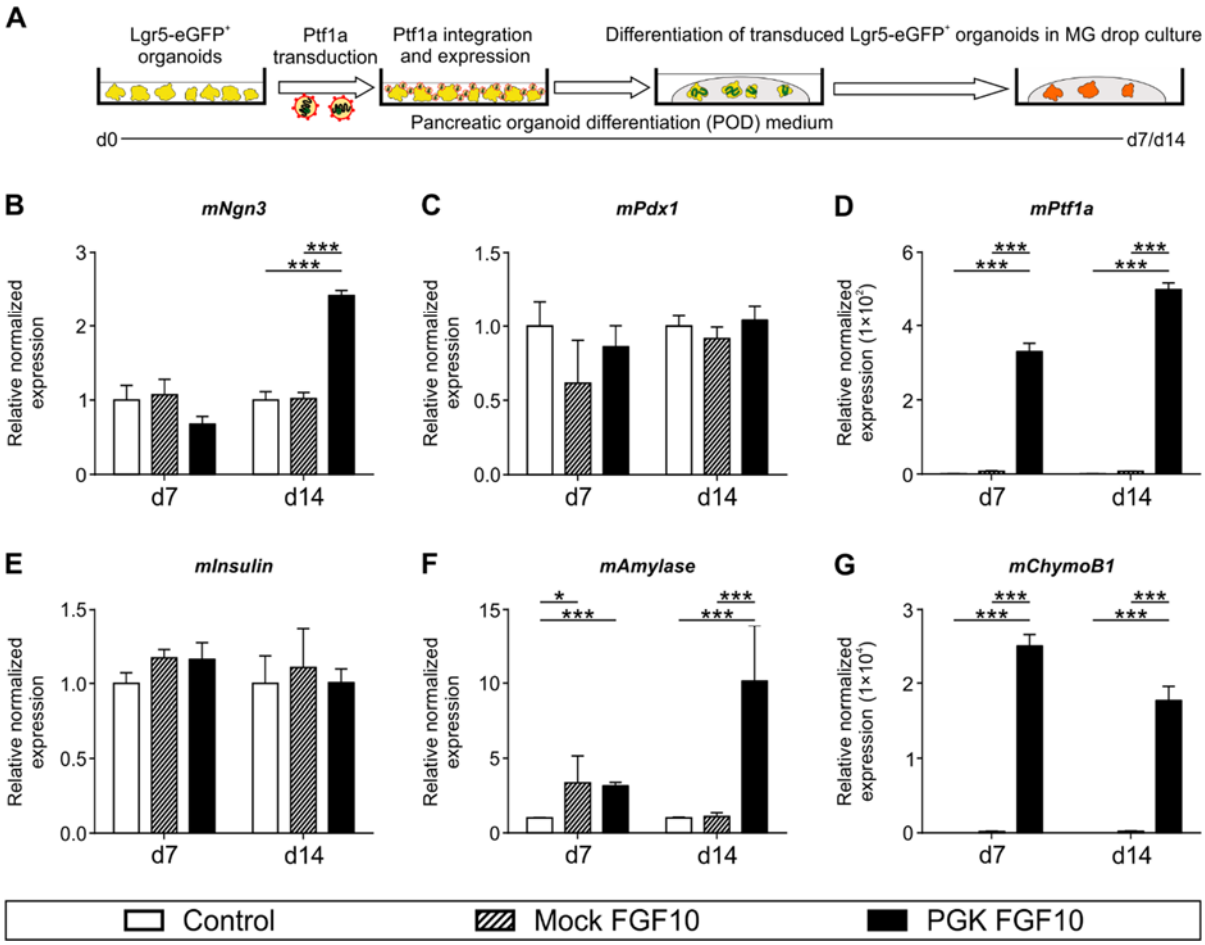

Figure 3.14: Ptf1a transduction in Lgr5-eGFP⁺ organoids revealed an acinar cell-like transcriptional signature. The differentiation of Lgr5-eGFP⁺ organoids was performed in pancreatic organoid differentiation medium following pL-PGK- Ptf1a transduction in organoid maintenance medium and subsequent embedding and culture in MG drops. (A) Schematic overview and timeline of the lentiviral strategy under MG drop culture conditions. (B-G) Graphs displays *mNgn3* (B), *mPdx1* (C), *mPtf1a* (D), *mInsulin* (E), *mAmylase* (F) and *mChymoB1* (G) gene expression carried out by qRT-PCR using *mRpl15* as reference gene. Controls represent untransduced organoids grown in pancreatic organoid differentiation (POD) medium set to 1. Statistics were carried out by student's t-test. *$P < 0.05$ and ***$P < 0.001$. $n = 3$.

3.2. Impact of Na^+-D-glucose cotransporter 1 (SGLT1) ablation on pancreatic islets

The second aim of this thesis was to investigate impacts on pancreatic islets due to loss of SGLT1 function by using a previously established SGLT1 knockout ($SGLT1^{-/-}$) mouse model [241]. $SGLT1^{-/-}$ animals ($SGLT1^{-/-}$DC) thrived normal when fed a glucose-deficient, fat-enriched diet chow (DC) whereas feeding standard chow (SC) results in the development of the lethal Glucose-Galactose Malabsorption syndrome [218, 241]. To determine SGLT1 knockout specific effects, $SGLT1^{-/-}$DC mice were compared to wild type mice fed with the same glucose-deficient, fat-enriched diet (WTDC). In addition, to verify diet-dependent effects, wild type mice fed a standard chow (WTSC) were compared with WTDC animals. All experiments were conducted with 12-14 week old animals (equal to 38-47 human years), an age where murine development is ceased and age-related diseases are not yet advanced [265].

3.2.1. Wild type and SGLT1 knockout mice fed by a glucose-diminished, fat-enriched diet display reduced intestinal glucose absorption and lower body weight

As SGLT1 is pivotal for intestinal glucose absorption, first the capacity for intestinal glucose uptake was determined for each mouse line. This is of high importance, as glucose is a main regulator of cellular phenotype and functionality in pancreatic islets [85].

For blood glucose determination, mice were deprived of food for 12h followed by the oral administration of D-glucose or PBS as control (Figure 3.15A-B). Fasting blood glucose concentrations were similar in WTSC, WTDC and $SGLT1^{-/-}$DC mice demonstrating similar glucose conditions at the basal level (Figure 3.15A). The absorbed glucose after bolus was determined by normalizing the blood glucose concentrations measured 5 min after glucose gavage to the corresponding blood glucose levels measured after PBS gavage. An increase in relative normalized glucose levels within the blood was detected in WTSC (+ 3.19 mmol/L) and WTDC (+ 1.40 mmol/L) mice. However, WTDC mice showed lower levels than WTSC animals

indicating an attenuated function of SGLT1 in diet fed mice. Further, no glucose was absorbed in SGLT1$^{-/-}$DC mice 5 min after oral glucose administration (Figure 3.15B).

In view of the diminished capacity of diet fed wild type or SGLT1 knockout mice for glucose uptake, the body weight of these mice was analyzed next. To this aim, the body weight of all mouse groups was juxtaposed and significantly decreased weights were found in WTDC (23.46 ± 0.9 g) and SGLT1$^{-/-}$DC (22.43 ± 1.4 g) mice when compared to WTSC controls (26.43 ± 1.5 g) (Figure 3.15C).

A laparotomy was performed to investigate if the glucose-deficient, fat-enriched diet impacts macroscopically on abdominal characteristics (Figure 3.15D-F) like the incorporation of fat or overall organ appearance. While the characteristics of abdominal organs were similar between WTSC and WTDC animals, SGLT1$^{-/-}$DC mice displayed a distended intestinal tract in contrast to WTDC and WTSC littermates (Figure 3.15D-F). Of note, the liver in SGLT1$^{-/-}$DC animals seems to be enlarged displaying a more pale color compared to both wildtype controls, however, the underlying reason remains unknown so far (Figure 3.15D-F). The yellowish-bright appearance of the stomach and the small- and large intestine was only detected in animals fed a glucose-deficient, fat-enriched diet and thus represent a possible explanation for the altered coloration of these organs (Figure 3.15D-F). Fat was incorporated in all animals and optically no significant differences were detected (Figure 3.15D-F).

As the focus in this work was on pancreatic islets, pancreata were dissected and analyzed in more detail. Macroscopic analysis of dissected pancreata from all groups revealed no obvious differences (Figure 3.15D-F).

In summary, loss of SGLT1 function and feeding a glucose-deficient, fat-enriched diet to wild type mice hampered intestinal glucose absorption associated with reduced body weight in mice. Macroscopically, diet fed mice showed a distinct color of the stomach and the intestine, while SGLT1$^{-/-}$DC mice displayed also an enlarged liver.

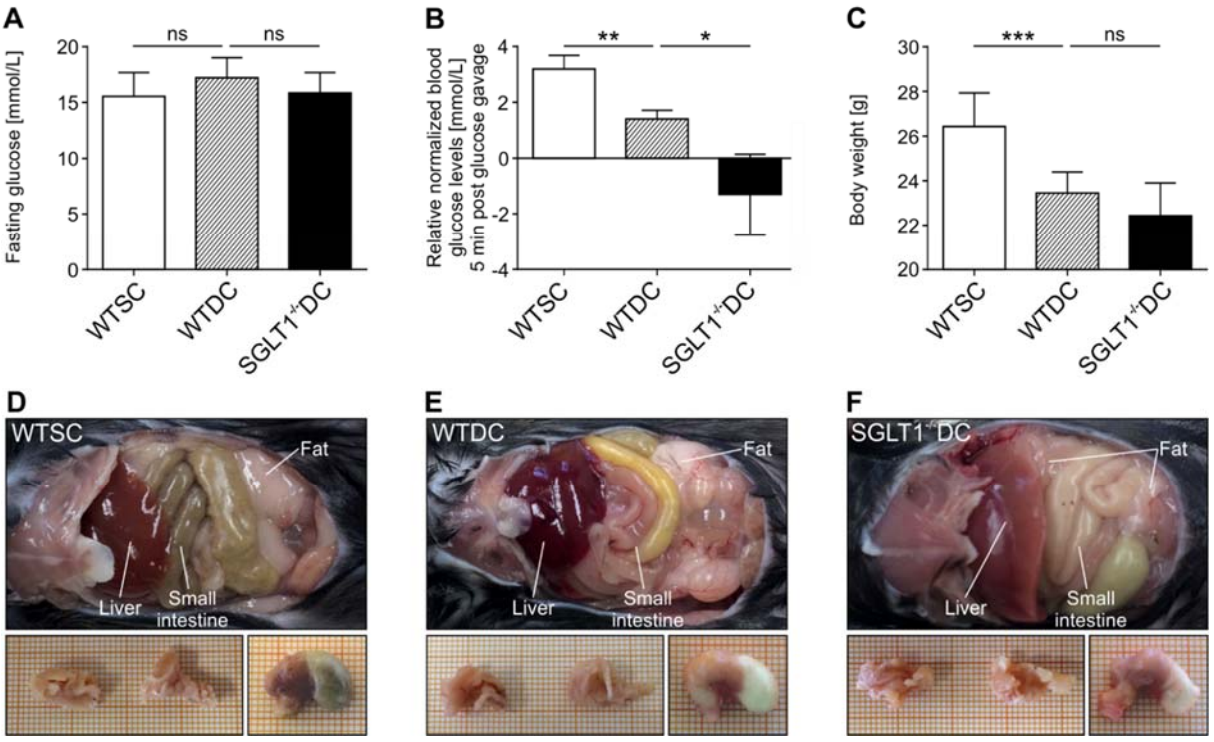

Figure 3.15: Glucose administration, body weight and abdominal characteristics in WTSC, WTDC and SGLT1$^{-/-}$DC mice. (A) Fasting blood glucose levels. Animals were fasted for 12h prior to experimentation. Graph demonstrates blood glucose values 5 min after oral administration of PBS (*n = 4*). (B) SGLT1 transporter functionality assessed by determination of blood glucose levels after glucose stimulation. Blood glucose values were determined 5 min after PBS or glucose gavage. Graph displays the relative blood glucose levels normalized to the blood glucose levels measured in corresponding PBS samples (*n = 3-4* (C) Graph displays the body weight of 12-14 week old WTSC, WTDC and SGLT1$^{-/-}$DC animals (*n = 11-12*). Statistics were carried out by one-way ANOVA and Tukey's multi comparison test. **P < 0.05, **P < 0.01 and ***P < 0.001*. (D-F) Representative images of abdomen from WTSC, WTDC and SGLT1$^{-/-}$DC mice. Magnifications display pancreata (left) or the stomach (right). Parts of the figure were modified from [266].

3.2.2. Small intestinal but not pancreatic *Slc5a1* expression is regulated when feeding a glucose-deficient, fat- enriched diet to mice

SGLT1 is encoded by the *Slc5a1* gene predominantly expressed in the small intestine and to a lower extent in the kidney [14, 267]. In both organs, the main function is either small intestinal or renal glucose absorption [14, 234, 235]. Nevertheless, SGLT1 expression was demonstrated in a broad range of other tissues [14, 237-240, 268] including pancreatic islets [236] and in the membrane of intralobular ducts of the pancreatic exocrine tissue [238]. In line with these previous findings, *mSglt1* expression was detected in the small intestine and at lower abundance in the kidney, whereas only minor expression levels were demonstrated for lung, brain, heart, liver,

spleen and also the pancreas of WTSC mice (Figure 3.16A). Pancreatic *mSglt1* expression was only 0.17% in pancreatic islets and 0.24% in the pancreatic exocrine tissue, respectively, when compared to small intestinal *Sglt1* mRNA expression (Figure 3.16A).

To further verify possible nutrient-dependent or tissue-specific regulatory effects, small intestinal and pancreatic *Sglt1* mRNA expression was compared between WTSC, WTDC and SGLT1$^{-/-}$DC mice. A 6.3-fold downregulation of small intestinal *mSlc5a1* expression was detected in WTDC mice in comparison to animals fed on standard chow (WTSC) (Figure 3.16B). In contrast, no diet-dependent differences were observed in pancreatic islets or pancreatic exocrine tissue (Figure 3.16C-D). Consistent with previous studies, the current observations confirmed that *mSlc5a1* is either regulated in an organ-specific manner [14, 238] or by dietary components like glucose [13, 269, 270].

Furthermore, in none of the experiments significant levels of *Sglt1* mRNA expression were detected in SGLT1$^{-/-}$ mice (Figure 3.16B-D). The global knockout of the used animal model was verified by PCR on intestinal and pancreatic DNA samples using wild type and knockout-specific primers (Figure 3.16E-G; see also 2.1.7.2.). The SGLT1$^{-/-}$ specific DNA band appeared at 349 base pairs (bp) on an agarose gel revealing the missing SGLT1 promoter and the exon1 fragment in SGLT1$^{-/-}$DC mice while samples derived from wild type animals displayed a 216 bp band (Figure 3.16E-G).

In conclusion, these results provide evidence for *Sglt1* mRNA expression in various WTSC or WTDC derived tissues and organs, including pancreatic islets and pancreatic exocrine tissue. In contrast, in SGLT1$^{-/-}$DC mice, no *Sglt1* mRNA was detected in the small intestine or the pancreas confirming the global knockout in these animals. While small intestinal SGLT1 is regulated in a diet-dependent manner in wildtype animals, there were no indications for similar regulatory mechanisms in context of pancreatic *Sglt1* mRNA expression.

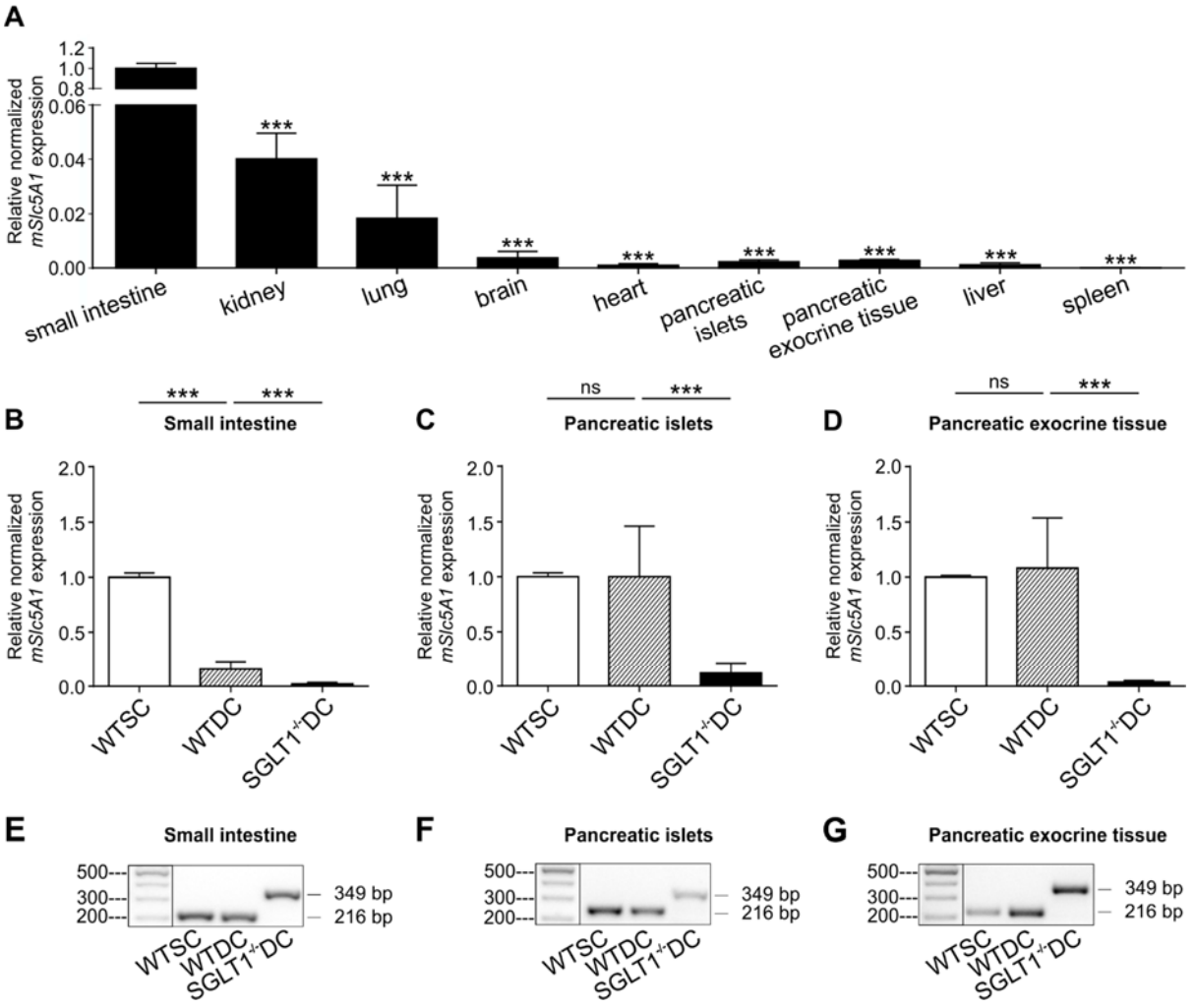

Figure 3.16: Small intestinal but not pancreatic *Slc5a1* expression is regulated by glucose-deficient, fat-enriched diet. (A-D) Graphs represent *mSglt1* gene expression analyzed by qRT-PCR. (A) Gene expression was determined in small intestine (S.I.) and compared to kidney, lung, brain, heart, pancreatic islets (P.I.), pancreatic exocrine tissue (EXT), liver and spleen. All organs were obtained from female WTSC mice (*n = 5*). (B-D) Gene expression of S.I., P.I. and EXT was compared between female wild type mice fed with standard (WTSC) chow or diet chow (WTDC) and SGLT1 knockout mice (SGLT1$^{-/-}$DC). (*n = 4-7)*. Significance was calculated by one-way ANOVA and a Dunnett's (A) or a Tukey's (B-D) posthoc test using *mRPL15* as reference gene. *ns = not significant*, **P < 0.05, **P < 0.01 and ***P < 0.001.* (E-G) Representative gel electrophoresis pictures showing SGLT1$^{-/-}$ verification in S.I, P.I and EXT of WTSC, WTDC and SGLT1$^{-/-}$DC mice. Wild type-specific band at 216 base pairs (bp) and Sglt1 knockout-specific band at 349 bp. Primers are shown in 2.1.7.2. (*n = 3*). Parts of the figure adapted from [266].

3.2.3. SGLT1 is predominantly expressed in wild type small intestine and absent in SGLT1 knockout mice

As *Sglt1* mRNA expression was confirmed in small intestine and pancreas, the next aim was to perform immunohistological analysis to verify protein localization. Using a

customized antibody against SGLT1 [241] and a commercially available SGLT1 antibody (Millipore), expression was validated on the apical brush border of the small intestine in wild type animals but not in SGLT1$^{-/-}$DC mice (Figure 3.17A). However, the intensity of the corresponding fluorescence signal in WTDC mice appeared weaker than in WTSC controls (Figure 3.17A). Staining of the pancreas revealed no specific staining in pancreatic islets for both antibodies, however, the customized antibody [241] colocalized with blood vessels and the pancreatic duct system in a highly unspecific manner as signals were detected in all groups, including SGLT1$^{-/-}$DC animals (Figure 3.17B).

Together, a SGLT1-specific antibody staining in pancreatic intralobular ducts, as recently shown by Madunic et al. [238], was not reproducible in this work. Intestine-specific staining patterns for SGLT1 were in line with previous reports [238, 241, 271].

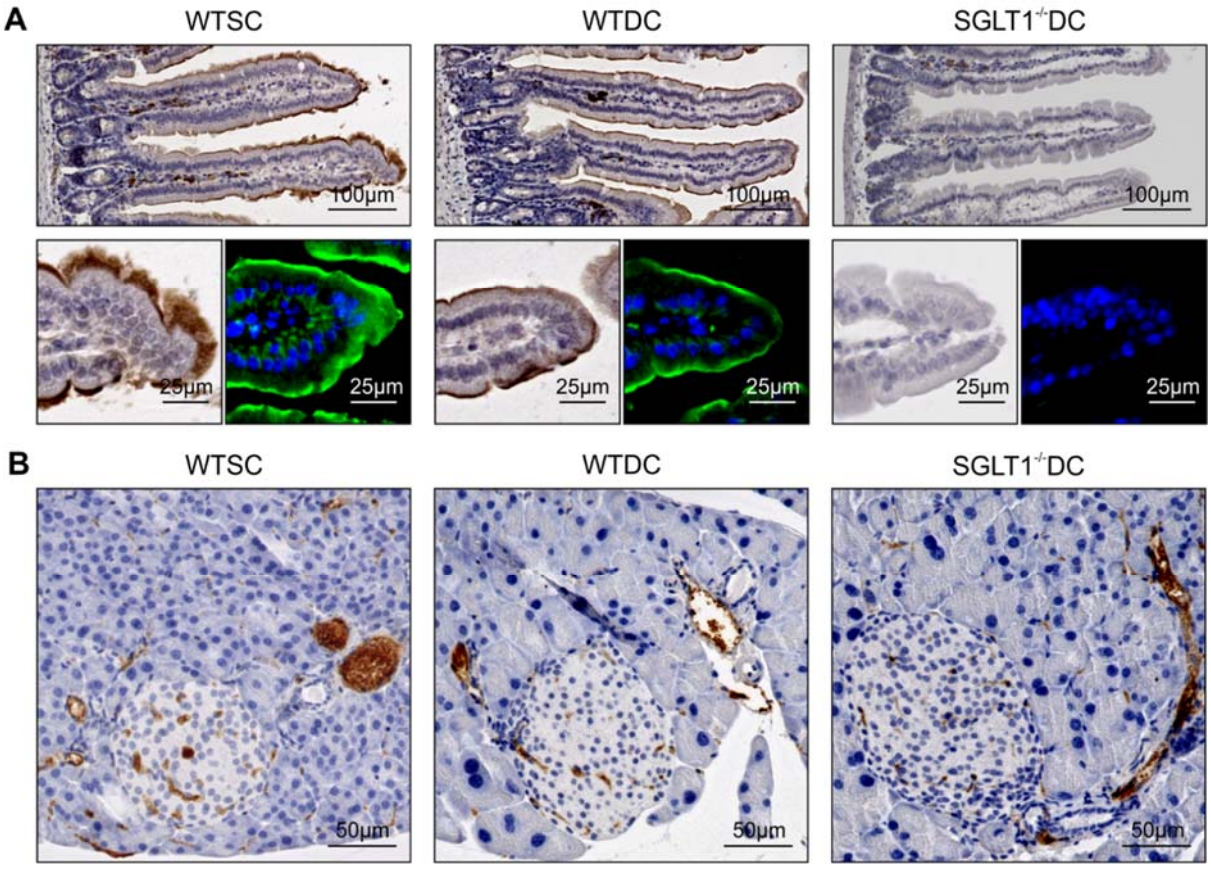

Figure 3.17: SGLT1 is predominantly expressed in wild type small intestine and not detectable in SGLT1 knockout mice. (A-B) Representative SGLT1 staining of small intestine (A) and pancreata (B) dissected from WTSC, WTDC and SGLT1$^{-/-}$DC. DAB staining was performed with a customized SGLT1 antibody (provided by Prof. Koepsell) and immunohistochemistry by a commercial SGLT1

antibody (Millipore). Scale bars represent 25 µm, 50 µm and 100 µm. Histology was performed with male animals (*n = 3*).

3.2.4. Pancreatic islets derived from SGLT1$^{-/-}$DC animals are enlarged and reveal reduced numbers of proliferative and apoptotic cells

The main issue of this study was to investigate if SGLT1 ablation affects pancreatic islets. Therefore, the first analytical approach was to characterize pancreatic islet sizes in WTSC, WTDC and SGLT1$^{-/-}$DC mice (Figure 3.18A-B; analysis according to 2.2.3.1.). No significant differences were observed between standard chow or diet fed wild type mice, however, WTDC animals displayed a tendency for an increase in compiled islet area (WTSC: 7852.90 µm^2 ± 883.75; WTDC: 9578.69 µm^2 ± 2441.49). Furthermore, SGLT1$^{-/-}$DC islets displayed a significantly increased compiled islet area (14182.5 µm^2 ± 4413.2) compared to WTDC islets (Figure 3.18A-B). The increased compiled islet area served as basis for the next analysis to verify if SGLT1$^{-/-}$DC animals display a disturbed frequency of islet size distribution.

Under normal and healthy conditions, islet sizes vary from small to large in well described ranges while islet size distribution is known to adapt in response to altered physiological conditions such as pregnancy, aging, obesity, or metabolic disorders [94, 272, 273]. To determine islet size distribution, all islets were classified either as small islets encompassing an area of < 12 × 10^3 µm^2 or large islets covering an area of > 12 × 10^3 µm^2 (Figure 3.18C). The proportion of small and large pancreatic islets differed significantly between all groups. In total, SGLT1$^{-/-}$DC animals comprised 39% large islets, WTDC 29% and WTSC 19% (Figure 3.18C). The next goal was to analyze if the increased islet size in SGLT1$^{-/-}$DC results from altered cellular density. To this aim, the total nuclei numbers were analyzed and displayed as nuclei per 100 µm^2 islet area, regardless of islet size. These analyses revealed similar results for all three animal groups (WTSC: 1.003 ± 0.21 nuclei / 100 µm^2; WTDC: 0.933 ± 0.06 / 100 µm^2; SGLT1$^{-/-}$DC: 0.937 ± 0.16 / 100 µm^2) (Figure 3.18D). Given that WTSC, WTDC and SGLT1$^{-/-}$DC derived islets harbor diverse endocrine cell types with equal sizes, cellular density within islets was displayed as total nuclei numbers per islet. In total, 60% more cells were detected in SGLT1$^{-/-}$DC islets compared to islets of WTDC mice, while both wild type groups showed similar numbers, what is consistent with the above described compiled islet area observations (Figure 3.18E, A).

In summary, these data provide evidence that WTSC, WTDC and SGLT1$^{-/-}$DC islet cells are equal in size but SGLT1$^{-/-}$ islets are significantly enlarged and harbor more cells than islets from wild type littermates.

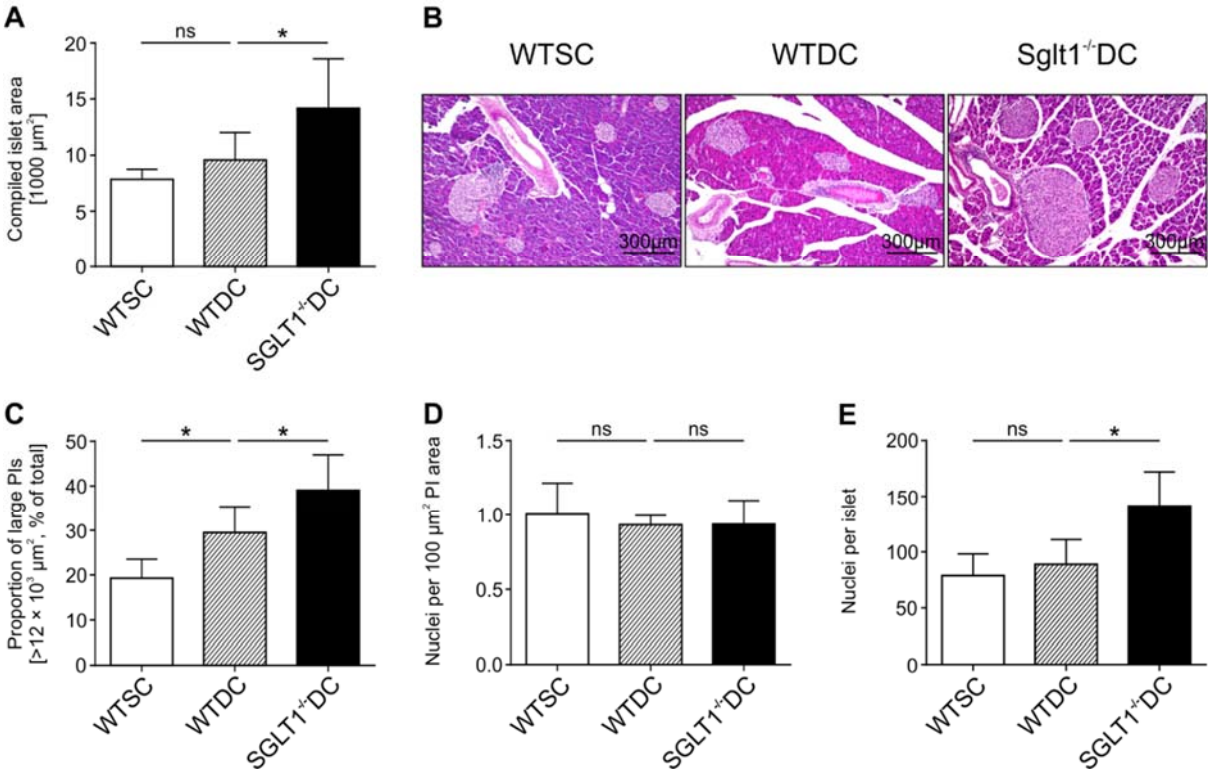

Figure 3.18: Pancreatic islets from SGLT1$^{-/-}$DC animals are enlarged and contain an increased proportion of large islets compared to controls. (A) Compiled islet areas were determined by measuring the islet areas per animal on 4-6 H&E-stained sections representing the whole organ as described in 2.2.3.1. The compiled islet area is shown as mean ± SD from 6 animals per group. (B) Representative images of H&E-stained pancreas sections from all animal groups. Scale bars = 300 µm (C) Graph shows the percentage of large pancreatic islets (> 12 × 10^3 µm^2) from all islets measured in A. (D) Figure represents the number of nuclei per 100 µm^2 islet area, as determined from the H&E-stained sections measured in A. (E) Graph represents the average number of total nuclei per islet and was counted from the sections described in A. Statistical significance was carried out by one-way ANOVA and Tukey's multiple comparison test. *ns = not significant, *P < 0.05, **P < 0.01*. The experiments were performed with male mice. *(n = 6)*. Figure modified from [266].

Another reason for the enlarged islets sizes in SGLT1$^{-/-}$DC animals could be due to increased islet cell proliferation and/or simultaneous suppression of apoptosis. Therefore, pancreas slices were stained for the proliferation marker KI67 to determine the number of proliferative cells (Figure 3.19A-B) [274]. Per islet 1.64 ± 0.42 KI67$^+$ cells were detected in WTSC, 1.14 ± 0.29 in WTDC and 0.47 ± 0.15 SGLT1$^{-/-}$DC mice (Figure 3.19A-B). These findings demonstrated a trend in diet-dependent reduction of

KI67^{+} cells while the decrease of proliferative cells reached significance when SGLT1 function was completely lost (Figure 3.19B). In addition and consistent with KI67 protein expression, a tendency for diet- and SGLT1 knockout-dependent down regulation of *Ki67* mRNA levels in pancreatic islets of WTDC and SGLT1$^{-/-}$DC compared to WTSC was demonstrated (Figure 3.19C).

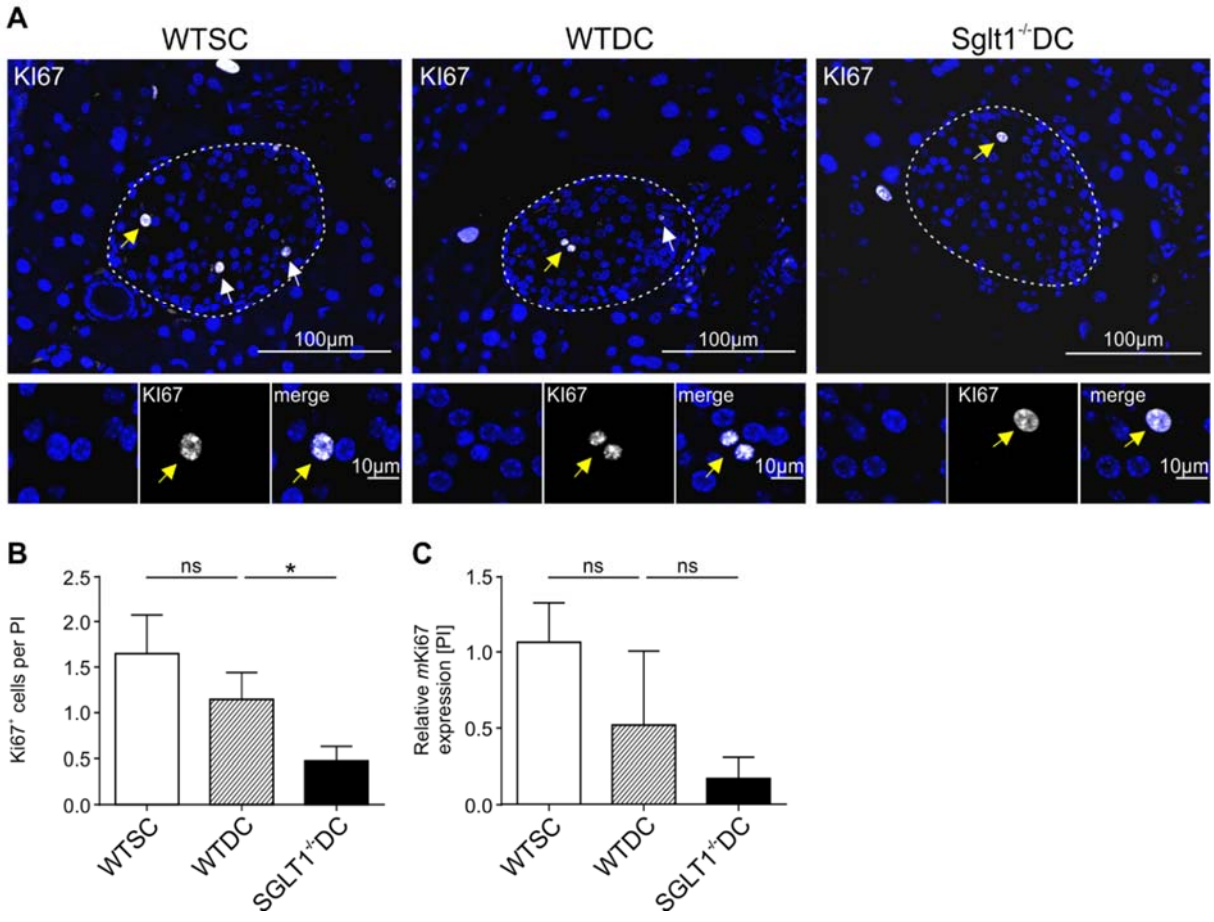

Figure 3.19: SGLT1$^{-/-}$DC islets display less proliferative cells compared to wild type islets. (A) Representative images from consecutively sliced pancreas sections (2.2.3.1) stained for the proliferation marker KI67 (white, highlighted with arrows, yellow arrow corresponds to KI67^{+} cell in magnification). DNA was stained using DAPI (blue). Scale bars represent 100 µm or 10 µm in the magnification. (B) Graph shows the mean number of KI67^{+} cells in pancreatic islets of WTSC, WTDC and SGLT1$^{-/-}$DC. Histology was performed with organs dissected from male mice (*n = 5*). (C) Graph represents *mKi67* gene expression analyzed by qRT-PCR using *mRPL15* as reference gene. Significance was determined by one-way ANOVA and Tukey's posthoc test. *ns = not significant*, **P < 0.05.* Gene expression experiment was performed with islets obtained from female mice *(n = 5).* Figure adapted from [266].

To determine the frequency of apoptotic cells in pancreatic islets, freshly isolated islets were dissociated and analyzed by FACS (Figure 3.20A-G). There was no difference between WTSC and WTDC mice detectable, however, SGLT1$^{-/-}$DC islets exhibited 66% less apoptotic cells compared to WTDC.

In summary, these data demonstrate increased SGLT1$^{-/-}$DC islets associated with reduced proliferative and apoptotic cell numbers.

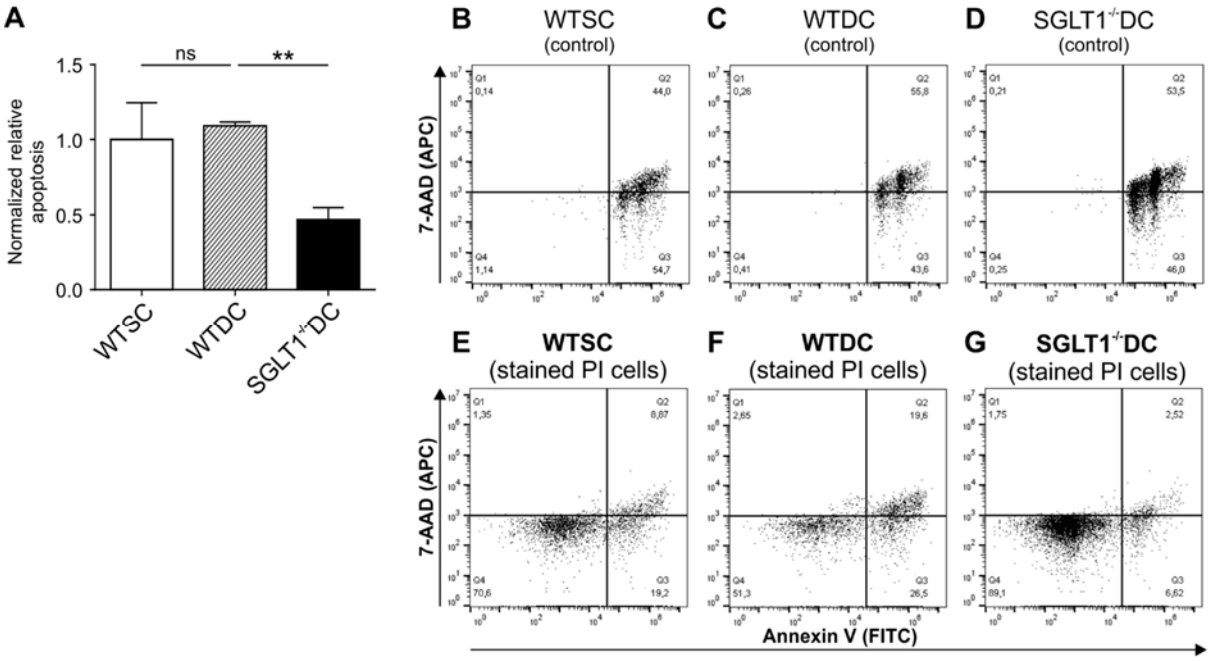

Figure 3.20: Pancreatic islets derived from SGLT1$^{-/-}$DC animals harbor less apoptotic cells in comparison to wild type islets. (A) The graph represents the number of apoptotic cells per pancreas shown as normalized relative value. WTSC value was set to 1 for calculation. Statistical significance was calculated with one-way ANOVA and Tukey's posthoc test. ***P < 0.01, ns = not significant*. (B-G) Dot plots representing apoptotic cells from isolated PIs stained with the Annexin V-FITC/7AAD-PE apoptosis detection kit. Control cells from all animals were incubated for 5 min at 60°C to induce apoptosis. The islets for apoptosis analysis were isolated from male mice *(n = 3)*. Figure adapted from [266].

3.2.5. SGLT1 plays a major role in maintaining pancreatic islet cytomorphology

Based on the observation that SGLT1$^{-/-}$DC islets are enlarged, the next aim was to verify which endocrine cell type is responsible for the increased size and if the typical islet architecture is maintained by the loss of SGLT1 function. Typical murine islets harbor a β-cell core composed of 60-80% of total cells whereas the second most frequent endocrine cell population, the α-cells (15-20%), reside at a peripheral layer intermingled with less frequent δ-, ε- and PP-cells [77, 79, 80]. To investigate pancreatic islet cytomorphology, double IHC staining using antibodies against insulin (INS) and glucagon (GCG) were performed. Beside the typical islet phenotype, an atypical islet phenotype was determined, being composed of less than 60% β-cells (INS^{+}) in the core and an increased α-cell (GCG^{+}) frequency (> 20%) in the periphery in all three investigated animal groups (Figure 3.21A). Nevertheless, the frequency of atypical islet phenotypes diverged significantly between the animal groups. In total, 22.4 ± 12.1% atypical islets were detected in WTSC, 40.6 ± 12% in WTDC and 72.2 ± 12.2% in SGLT1$^{-/-}$DC mice (Figure 3.21B).

Next, the numbers of β- and α-cells of all islets analyzed were counted, regardless of size or phenotype. This analysis revealed a substantial SGLT1 knockout-dependent decrease of α-cells, possibly at the expense of β-cells, while the glucose-deficient, fat-enriched diet contributed to a similar phenotype without reaching significance (Figure 3.21C-D). In addition, mRNA abundancy for *mInsulin* and *mGlucagon* in isolated islets was determined by qRT-PCR. Expression of both genes was comparable in WTDC and SGLT1$^{-/-}$DC mice, while significantly altered gene expression levels were observed between WTSC and WTDC (Figure 3.21E-F).

Together, SGLT1 removal results in atypical α- and β-cell proportions and a disturbed cytomorphology of pancreatic islets, while feeding a glucose-deficient, fat-enriched diet impacts on transcriptional regulation of insulin and glucagon.

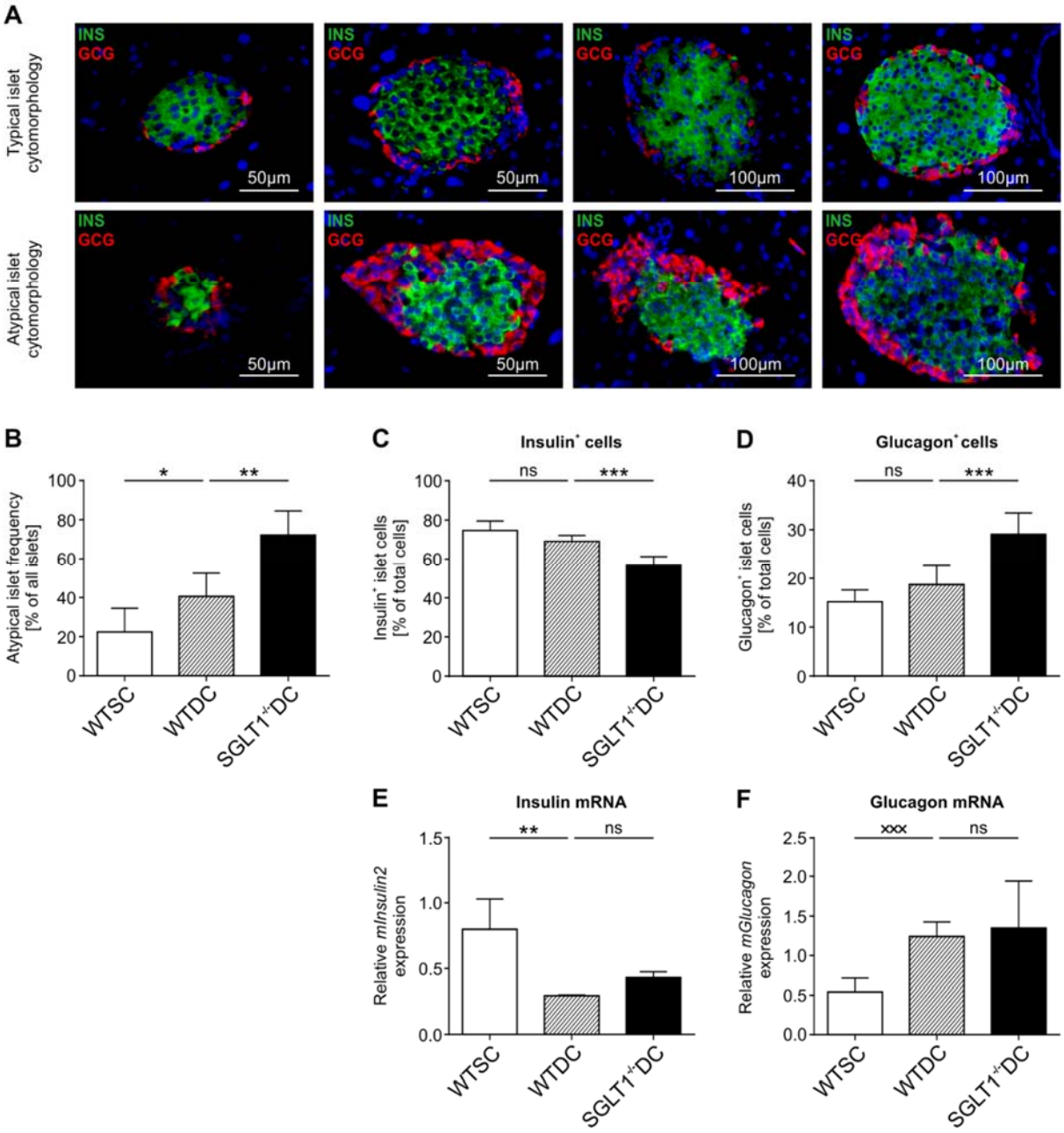

Figure 3.21: SGLT1 plays a major role in maintaining pancreatic islet cytomorphology. (A) Characteristic microscope images of pancreatic islets showing a typical (top panel, < 80% INS^+ cells in green or < 20% GCG^+ cells shown in red) or atypical (lower panel, > 80% INS^+ or > 20% GCG^+ cells) cytomorphology. (B) Graph represents the proportion of pancreatic islets with atypical cytomorphology from all islets analyzed. From all mice, 4-6 stained sections from different stacks were analyzed as described in 2.2.3.1. Scale bars represent 50 µm or 100 µm (*n = 6)*. Only male animals were used for analysis. (C-D) From all analyzed islets, the percentage of INS^+ β-cells (C) or GCG^+ α-cells (D) are shown as described in B. (E-F) Graph represents gene expression analysis of *mInsulin* (E) and *mGlucagon* (F) from isolated islets of female WTNC, WTDC and SGLT1$^{-/-}$DC animals analyzed by qRT-PCR with *mRPL15* as reference. One-way ANOVA (*) or unpaired t-test (×) revealed significance: **P < 0.05, **P < 0.01, ***P < 0.001, ns = not significant* and *×××P < 0.001. n = 6-7* per group.

3.2.6. Impaired insulin secretion capacity, abnormal glucagon levels and reduced expression levels for GLP1-R and GLUT2 under glucose-deficient, fat-enriched diet conditions that do not associate with increased fat incorporation

Wondering if the observed aberrant α- and β-cell proportions or the diet-dependent transcriptional regulation of *Insulin* and *Glucagon* further impact on islet functionality, next the capacity of pancreatic islets for insulin or glucagon secretion in response to glucose was investigated *in vitro* (Figure 3.22A-D). To this aim, WTSC-, WTDC- and SGLT1$^{-/-}$DC-derived islets were cultured in 3.3 mM glucose following by exposure to either 3.3 mM or 16.7 mM glucose for 60 min. Secreted insulin and glucagon was measured in the supernatant. Values were normalized to the islet DNA content. In case of insulin, data are represented as stimulation index (S.I.), a value characterizing the ability of pancreatic islets to secrete insulin in response to glucose. The S.I. was calculated by dividing the insulin/DNA ratio obtained under 16.7 mM glucose conditions by the insulin/DNA ratio under 3.3 mM glucose concentration. While the S.I. of 2.5 obtained for WTSC islets is in the normal range of 2 to 4, WTDC- or SGLT1$^{-/-}$DC-derived islets displayed significantly reduced values of 1.2 or 0.9, respectively. This indicates a diminished capacity for insulin release of islets derived from these animals in the presence of high glucose (Figure 3.22A-B).

As insulin and glucagon interfere in an antagonistic manner to orchestrate glucose homeostasis [90, 275], the disturbed insulin secretion capacity could also affect the release of glucagon in these islets. As shown in Figure 3.22, similar values for secreted glucagon were observed within all groups, regardless of exposure to 3.3 mM or 16.7 mM glucose (Figure 3.22C-D). This indicates that albeit glucagon levels in WTDC and SGLT1$^{-/-}$DC animals reached similar levels as those observed for WTSC islets, glucagon is not responsible for the reduced insulin content. In addition, these data points also to higher glucagon values in WTDC and SGLT1$^{-/-}$DC mice without insulin-stimulation.

Given that glucagon was not affecting insulin secretion capacities *in vitro*, further possible mechanisms that might affect aberrant insulin responses were investigated in WTDC and SGLT1$^{-/-}$DC islets. Alternative pathways to induce insulin secretion comprise GLP-1 receptor (GLP-1R) activation and downstream signaling mediated by

GLP-1 binding [156, 276]. Indeed, analyzing *GLP-1R* mRNA expression demonstrated a 2-fold downregulation of WTDC compared to WTSC, whereas similar expression levels were shown for WTDC and SGLT1$^{-/-}$DC (Figure 3.22F). Of note, removal of SGLT1 had no significant effect on insulin secretion and thus substantiates that feeding the glucose-deficient, fat-enriched diet contributes to the disturbed insulin secretion pattern observed in WTDC and SGLT1$^{-/-}$DC mice (Figure 3.22A-B), possibly by disturbing β-cell glucose sensing.

Glucokinase-mediated glucose sensing strictly depends on β-cell glucose uptake by Glucose transporter 2 (GLUT2) and therefore a failure or downregulation of GLUT2 could result in dysfunctional insulin secretion [130]. Comparing *GLUT2* mRNA levels in WTSC-, WTDC- and SGLT1$^{-/-}$DC-derived islets revealed no significant alterations along the groups (Figure 3.22E).

A third possible explanation could be fat incorporation, which was recently shown to result in diminished glucose stimulated insulin secretion [141-143]. As the missing glucose and therefore metabolizable energy was substituted by fat in the applied diet of WTDC or SGLT1$^{-/-}$DC animals, a possible incorporation of fat/triglycerides within the pancreas and in particular in pancreatic islets was analyzed by Oil Red O staining (Figure 3.22G). In contrast to fat tissue, only non-relevant fat/triglyceride depositions were detected within pancreatic islets or the exocrine pancreas of WTSC, WTDC or SGLT1$^{-/-}$DC mice (Figure 3.22G). Of note, these observations are in line with the above described body weight data (Figure 3.15C), indicating that no additional fat is incorporated in 12-14 week old WTDC or SGLT1$^{-/-}$DC animals as their body weights are significantly lower compared to WTSC (Figure 3.22C).

In conclusion, previous observations were confirmed showing that feeding a glucose-deficient, fat-enriched diet contributes to diminished glucose-mediated insulin secretion and aberrant glucagon values *in vitro*.

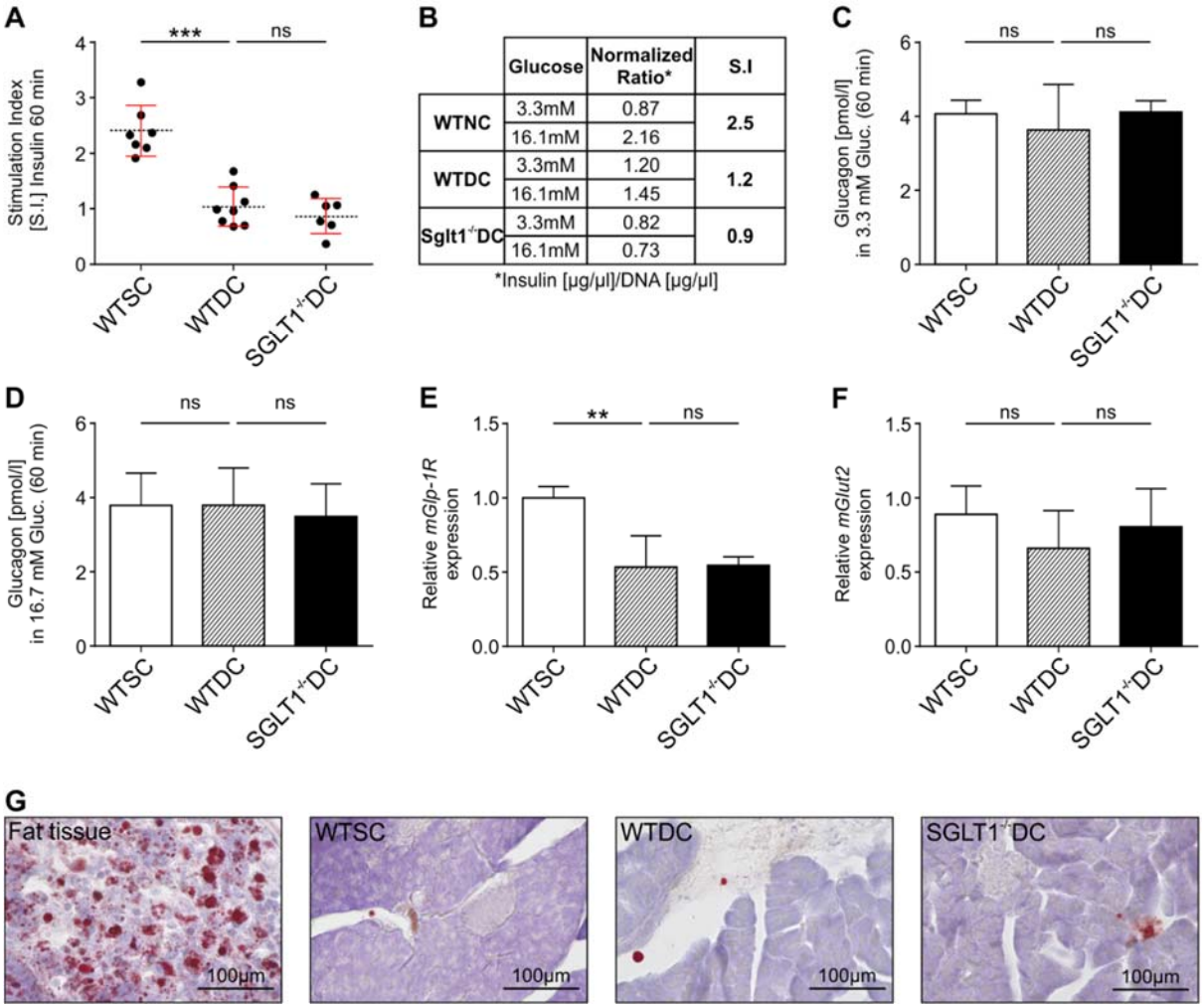

Figure 3.22: Impaired glucose-stimulated insulin secretion as effect of glucose-deficient, fat-enriched diet. (A) Graph shows the stimulation index (S.I.) revealing the capacity of islets to secrete insulin in response to glucose stimulation. Isolated islets were stimulated by 3.3 mM or 16.7 mM glucose for 60 min. Insulin content was normalized to islet DNA (insulin/DNA ratio). S.I. index was calculated by dividing the insulin to DNA ratio from 16.7 mM by the ratio from 3.3 mM glucose stimulation. Individual values are shown as mean ± SD (B). (C-D) Graphs represent absolute glucagon secretion values normalized to DNA in 3.3 mM (C) or 16.7 mM (D) for 60 min. Experiments were performed with islets isolated from male mice (insulin: *n = 6 – 9*; glucagon: *n =4-6*). (E-F) Gene expression levels of *mGLP-1R* and *mGLUT2* were analyzed by qRT-PCR with *mRPL15* as reference gene. Experiments were performed with isolated islets from female mice (*n = 4*). (E-F) Islets were obtained and stimulated as in (A). Secreted glucagon value are shown as mean normalized to DNA ± SD in 3.3 mM (E) or 16.7 mM glucose (F) Significances were calculated by one-way ANOVA with posthoc Tukey's test. ***P < 0.01, ***P < 0.001, ns = not significant*. Gene expression experiments were performed with female mice (*n = 4*). (G) Representative images of an Oil Red O staining (fat/triglycerides) from WTSC, WTDC and SGLT1$^{-/-}$DC pancreata and WTSC fat tissue (*n = 2*). Scale bars represent 100 µm. Parts of the figure were modified from [266].

3.2.7. SGLT1 ablation in combination with glucose-deficient, fat-enriched diet results in abnormal blood insulin, GLP-1 and glucagon concentrations

With the intention to compare the *in vitro* insulin and glucagon secretion with the *in vivo* situation an oral glucose tolerance test (OGTT) was performed. Besides insulin and glucagon, also the role of intestinal GLP-1 release and its possible impact on pancreatic hormone regulation was accounted in these experiments. Previous studies working with SGLT1 knockout mice demonstrated disturbed insulin and GLP-1 secretion following OGTT. However, these studies compared SGLT1$^{-/-}$DC with WTSC [241] or with wild type animals fed for only one week prior to experimentation with the glucose-deficient, fat-enriched diet [271]. The first study omitted the effect of the diet at all, while the results of the second study might be misinterpreted due to the short diet application. In the current study prolonged glucose-deficient, fat-enriched diet application was included with the relevant control groups and insulin, GLP-1 and glucagon concentrations within the blood were analyzed 5 and 60 min after OGTT. 5 minutes after glucose gavage, blood insulin levels were increased by 380% compared to the PBS control, whereas no insulin secretion was detected neither in WTDC nor in SGLT1$^{-/-}$DC animals (Figure 3.23A). After 60 min, the insulin levels of WTSC and SGLT1$^{-/-}$DC were assimilated to the fasting levels while the insulin content was slightly increased (34%) in WTDC mice (Figure 3.23B). In SGLT1$^{-/-}$DC animals no insulin response was detected at any of the measurement time points (Figure 3.23A-B).

A major trigger for insulin secretion is GLP-1 [147, 152, 277]. Therefore, the next aim was to investigate if the disturbed insulin responses were associated with an altered GLP-1 release. 5 min after OGTT, the increase of total GLP-1 in systemic blood was compared to PBS controls and an increase of 80 ± 29 pMol and 58 ± 20 pMol was found in WTSC and WTDC mice, respectively. Between both wild types (WTSC and WTDC), the extent of the GLP-1 increase was comparable, while in SGLT1$^{-/-}$DC animals no GLP-1 secretion was detected 5 min after OGTT (Figure 3.23C). Analyzing total GLP-1 levels after 60 min glucose gavage revealed no elevated levels in WTSC (Figure 3.23D). Moreover, in WTDC mice GLP-1 concentrations were increased by 52 ± 20 pMol and by 126 ± 62 pMol in SGLT1$^{-/-}$DC mice. In this case, the increase in SGLT1$^{-/-}$DC animals was significantly higher compared to the increase in WTDC mice (Figure 3.23D). The current data support the previously reported sustained GLP-1 release when SGLT1 function is lost or inhibited [151, 217, 234, 278].

PBS-gavaged mice were expected to contain similar GLP-1 levels in all groups to serve as controls and references. Nonetheless, after 5 min WTSC PBS-control mice harbored more systemic total GLP-1 than PBS-treated WTDC or SGLT1$^{-/-}$DC mice (Figure 3.23C). In contrast, after 60 min WTDC PBS-gavaged animals displayed increased GLP-1 concentrations in the blood compared to WTSC and SGLT1$^{-/-}$DC PBS-controls (Figure 3.23C-D).

Next, the increase of systemic blood glucagon normalized to PBS controls was compared 5 min after OGTT. A significant increase for glucagon was revealed in WTSC (+ 3.25 ± 0.25 pmol/L) and WTDC (+ 3.75 ± 0.70 pmol/L) mice, whereas in SGLT1$^{-/-}$DC a marginal but non-significant blood glucagon elevation was observed (Figure 3.23E). In addition, the observed blood glucagon level in WTDC was significantly higher compared to SGLT1$^{-/-}$DC animals (Figure 3.23E). After 60 min, in WTSC mice no glucagon secretion and in WTDC animals only a tendency for elevated glucagon levels was observed (Figure 3.23F). In contrast, a 215% increased blood glucagon concentration compared to the PBS control was detected in SGLT1$^{-/-}$DC animals (Figure 3.23F).

Taken together, insulin, GLP-1 and glucagon secretion is affected by loss of SGLT1 function and by the application of a glucose-deficient, fat-enriched diet.

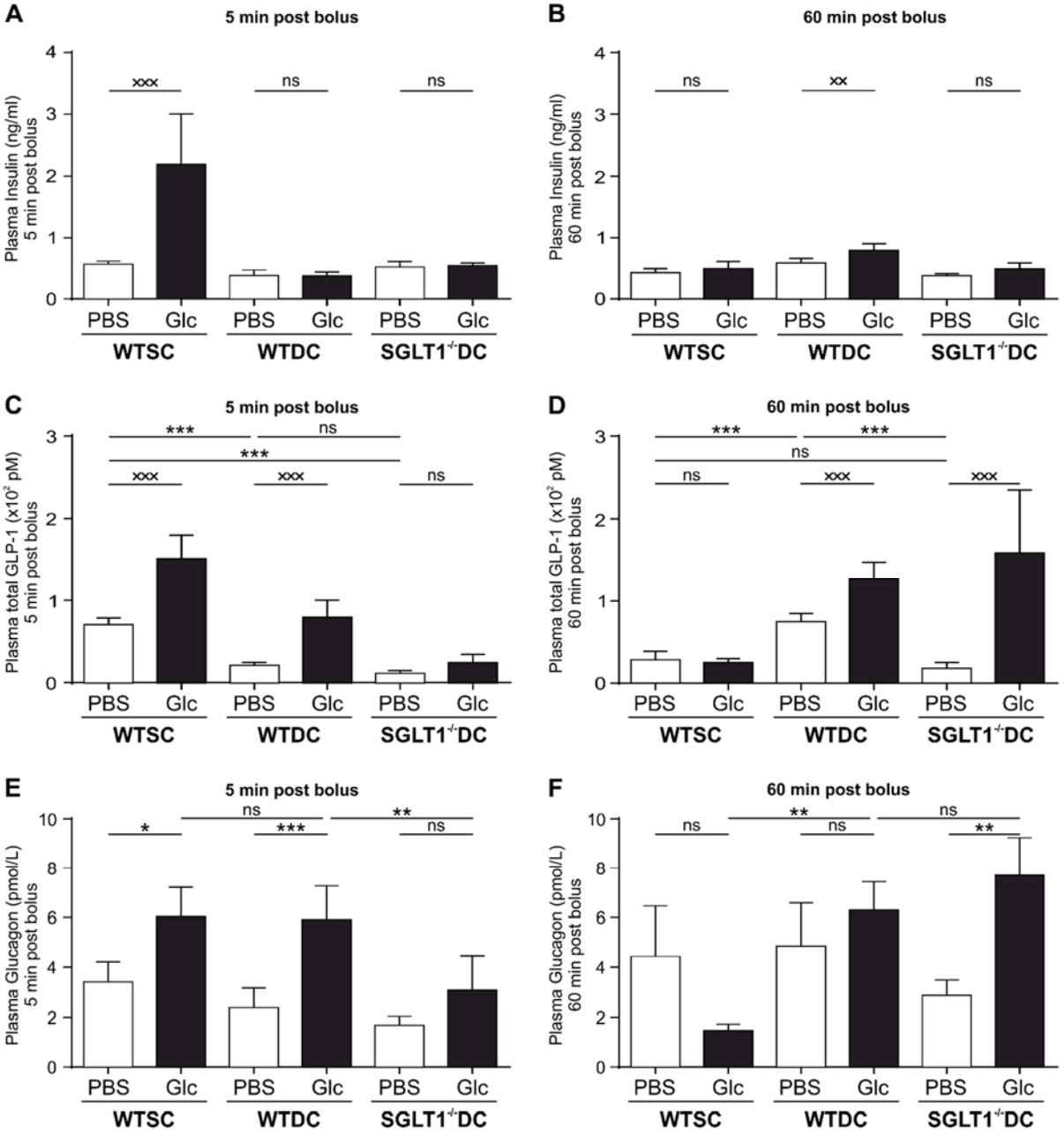

Figure 3.23: SGLT1 ablation in combination with a glucose-deficient, fat enriched diet results in abnormal blood insulin, GLP-1 and glucagon concentrations. (A-F) Graphs represent insulin and total GLP-1 concentrations in systemic blood obtained 5 or 60 min after an oral glucose tolerance test (OGTT). Male WTSC, WTDC or SGLT1$^{-/-}$DC mice were gavaged with glucose or PBS as control. Insulin, total GLP-1 and glucagon concentrations were determined by ELISA and statistically analyzed using a one-way ANOVA with Tukey's multi comparison test (*$*P < 0.05$, $**P < 0.01$, $***P < 0.001$, ns = not significant*) or by a student's t-test, when two groups were compared ($^{\times\times}P < 0.01$ and $^{\times\times\times}P < 0.001$). *n = 4-7* male animals per group and time point.

4. Discussion

4.1. The ectopic expression of Ptf1a alone is not capable to initiate the differentiation of ISCs to β-like cells

One main goal of this thesis was to establish a differentiation protocol to generate β-like cells from Lgr5-eGFP^{+}-ISCs by ectopic expression of the transcription factor Ptf1a. The results demonstrated morphological changes after Ptf1a expression and culture under MG coating conditions in the presence of media formulations that were recently described as specific for the induction of pancreatic fate from pluripotent stem cells [225, 226, 256]. Further, under these conditions, cells showed an upregulation of genes associated to the pancreatic acinar cell state but not β-cell-specific markers. Together, this indicates that the transient expression of Ptf1a under the applied cell culture conditions is not sufficient to induce a distinct cell lineage switch towards β-like cells. However, it demonstrates the potential of multipotent ISCs as possible stem cell source for the derivation of pancreatic cell types that might be used in future cell-based regenerative approaches for diabetic patients, albeit proof of concept has to be shown in detail using human ISCs in future studies.

4.1.1. Multipotent ISCs as source for the derivation of bioartificial β-like cells

Type 1 diabetes is hallmarked by an autoimmune-dependent destruction of β-cells resulting in acute insulin deficiency and chronic hyperglycemia [279, 280]. Currently, no permanent cure for type 1 diabetes is available and lifelong application of insulin is inevitable to avoid severe complications such as diabetic ketoacidosis [168, 281]. However, stable insulin analogues and hormone regulating drugs together with medical devices such as implanted insulin pumps are available to improve patient's life quality [282-285]. In the past, great advances were made to derive bioartificial endocrine progenitors or insulin-secreting β-cells from pluripotent ESCs [184-186]. Of note, transplantation of ESC-derived cell types comprise several drawbacks including graft rejection, teratoma formation and ethical concerns [188-192].

The aim of the current study was to assess the potential of multipotent intestinal stem cells (ISCs) as alternative cell source to pluripotent stem cell types. In the intestine, highly proliferative multipotent stem cells generate all four intestinal cell lineages and thereby maintain the constant renewal and regeneration of the intestinal epithelium [36]. Recently, ISCs were supposed to transdifferentiate into functional urothelial cells upon injury [221]. The differentiation was accompanied by a changed molecular profile of the cells from intestinal towards an urothelial pattern [221], what further underlines the potential of ISCs to give rise to non-intestinal lineage cell types.

For the current study, it was assumed that ectopic expression of the transcription factor Ptf1a is sufficient to induce a pancreas-specific gene expression pattern in ISCs by modulating the transcriptional program and thereby promoting the switch from intestinal- to pancreatic fate. In order to mediate direct cell reprogramming, transcription factors must not only comprise the ability to access defined genetic loci but also regulate differentiation by coordinating either the activation or repression of genes that are differently expressed in the cell of origin and the required cell type [286]. The efficacy and potential of a transcription factor-based cellular conversion within the same germ layer was emphasized by several publications [287, 288]. After having started the Ptf1a project, Chen et al. demonstrated that ectopic expression of the transcription factors Pdx1, Ngn3 and MafA could convert intestinal crypts to β-like cells [200]. In summary, the studies from Popov et al. and Chen et al. underline the huge potential of ISCs to differentiate into non-intestinal cell lineages within the endoderm germ layer [200, 221].

Of great interest in the context of most (trans-)differentiation approaches is the epigenetic memory of the initial and differentiated cell type [289]. Similar or an equal epigenetic memory could be an advantage for differentiation of ISCs to the pancreatic lineage, as both share a common ancestry [290]. The overall epigenetic pattern within a cell type massively affects gene expression regulation concerning the activation or repression of lineage-specific programs [291]. In line with this, a recent study revealed that iPSCs generated from β-cells comprise an unique DNA-methylation pattern and an open chromatin structure at β-cell-specific genes compared to other iPSCs possibly resulting in an increased capacity to differentiate into insulin-secreting cells [291].

Currently, the ISC-differentiation protocol was established in a murine model. For future translational applications in human, the ISC-isolation and purification has to be

modified as in mice the stem cells were harvested and sorted by FACS-based on their Lgr5-driven eGFP expression what is not possible for patient-derived ISCs. In addition, the Ptf1a-mediated differentiation protocol to generate pancreatic cell types eventually needs further adaptations as the process might last longer in humans and the differentiation media require additional supplementation. Importantly, ISCs can be obtained by endoscopic biopsies or isolated from surgically resected tissues with intestinal origin and cultured *in vitro* [292, 293]. *Ex vivo* expansion and differentiation of ISCs allows the generation of almost unlimited quantities of patient-specific donor material. Using these cells for an autologous transplantation would further minimize a possible immunological rejection of the graft [203].

In general, stem cells have high potential in regenerative medicine and β-cell replacement strategies. However, adult intestinal stem cells harbor not the same differentiation plasticity as pluripotent stem cells what might lower the success rate in generating artificial pancreatic cells but the similar developmental origin of ISCs, the huge number of cells available, the relatively simple accessibility and the well-established *in vitro* expansion could be beneficial regarding the differentiation towards β-like cells.

4.1.2. ISCs can be cultured as single-cell monolayers on Matrigel® coatings with an ISC-specific maintenance medium

As mentioned before, ISCs could represent an interesting cell source for the generation of pancreatic cells. The main challenges included the establishment of a suitable platform where single-cell ISCs can be cultured, expanded and where the transcription factor Ptf1a can be delivered into the cells to induce pancreatic gene expression programs and thus a pancreatic fate.

Properties of multipotent Lgr5-eGFP$^+$-ISCs include their capacity for self-renewal and proliferation but also their potential for differentiation along the intestinal axis. In general, ISCs are grown in a 3D-Matrigel®-based environment with maintenance medium providing essential growth factors for generating multi-cellular crypt organoid structures [42]. However, genetic manipulation of Matrigel®-embedded cells/organoids remain inefficient [257, 294]. To this aim, a new protocol for the culture of Lgr5-eGFP$^+$-ISCs on a 2D-Matrigel® coated surface was established. This method allows the

accessibility of ISCs in order to facilitate single or multiple rounds of Ptf1a delivery. This is important as the efficacy of delivery correlates with the expression rate of Ptf1a what was further hypothesized to increase their differentiation capacity towards pancreatic cells. Nevertheless, as this culture condition was a conceptionally new approach, also the best possible media composition was evaluated to improve growth and proliferation of Lgr5-eGFP^{+}-ISCs.

The stemness of intestinal stem cells strictly depends on the extrinsic signals that are provided in the culture medium by growth factors and small molecules to mimic the intestinal stem cell niche. The standard protocols provide a coordinated stimulation of various factors including Wnt signaling by R-spondin1, inhibition of BMP by noggin and addition of EGF to support proliferation [42, 58]. The combination of these factors in the medium mimic the *in vivo* situation and allows maintenance and expansion of ISCs *in vitro* [49, 56, 58] The successful growth of single Lgr5-eGFP^{+}-ISCs strictly depends on the addition of the Rho kinase inhibitor Y-27632, as otherwise dissociated single-cells die immediately after cell sorting [42]. Y-27632 is an inhibitor of p160-Rho associated coiled-coil kinase (ROCK) and thereby prevents apoptosis of dissociated stem cells [295]. However, addition of Y-27632 alone was not sufficient to allow growth of Lgr5-eGFP^{+}-ISCs on a 2D Matrigel® coated surface and therefore additional factors were tested. Crucial for the expansion of Lgr5-eGFP^{+}-ISCs is the small molecule CHIR99021 that stimulates the canonical Wnt pathway and valproic acid, an inhibitor of histone deacetylases and activator of the Notch signaling [258]. Both factors were previously described to promote self-renewal and their addition to the culture medium increases the number of Lgr5-eGFP^{+} cells in intestinal organoid cultures in MG drops [258]. The best single-cell ISC maintenance medium (described as medium YCVJ) further comprised the Notch agonist Jagged-1 [296]. The higher number of surviving and growing Lgr5-eGFP^{+}-ISCs upon Jagged-1 supplementation could be explained by mimicking the composition of important intestinal niche factors in a more *in vivo*-like manner [29, 42, 56]. The data shown in this study could show for the first time that Lgr5-eGFP^{+}-ISCs can be cultured on a MG-coated 2D environment. In addition, the ISCs are accessible for genetic manipulation and revealed best growth capacities when cultured in medium YCVJ.

4.1.3. Pros and cons of the applied strategies to ectopically express regulatory factors like PTF1a or CRE protein in single-cell ISCs

Differentiation of ISCs can be induced by ectopically expressing regulatory proteins like transcription factors [200, 226]. In this context, high efficiency of factor delivery into target cells is one of the most critical steps in developing new differentiation protocols. In this work, four different strategies were tested and compared with each other to ectopically express Ptf1a in single-cell ISCs or intestinal organoids. These strategies included RNA and protein transfection, liposomal delivery of active PTF1A protein or lentiviral transduction.

The successful uptake and ectopic expression of Ptf1a was determined by microscopy. To this aim, a reporter-based system was used (Cre recombinase/RFP expressing lentivirus) or the recombinant PTF1A protein was linked to a fluorescent tetra methyl rhodamine (TMR) dye. In single-cell Lgr5-eGFP^{+}-ISCs these methods were feasible, however, the signal was faint and faded rapidly. In organoids the detection of Ptf1a was difficult due to several problems. Matrigel®-embedded organoids display a typical auto-fluorescence [297] that is weaker and not congruent with the LGR5-driven eGFP signal but impeded the detection or localization of Ptf1a (see Figure 2.4 in Material and Methods). Nevertheless, analyzing living organoids resulted in a strong eGFP signal throughout the structure and single cell ISCs were impossible to detect with the microscopes available. In contrast, the eGFP signal was quenched in PFA-fixed organoids and staining with an anti-eGFP antibody resulted in unspecific staining within the crypt structures. In summary, microscopic analysis revealed that Ptf1a was successfully delivered and expressed in organoids. However, if or how many Lgr5-eGFP^{+} stem cells within organoids were successfully transfected or transduced remains elusive.

The first strategy that was tested for ectopic *Ptf1a* expression was synthetic mRNA transfection. Synthetic mRNAs were previously shown to transfect target cells with high efficacy and were therefore used in cell reprogramming [251]. Additionally and in contrast to genome integrating virus-mediated gene transfer, the transfected mRNAs are stable for 2-3 days and cause no oncogenic adverse events when used in human applications [298]. Furthermore, modifying the synthetic mRNA by adding a 7-methylguanosine cap was previously shown to dramatically increases the RNA half-life and to enhance the translation [299]. In mammalian cells, exogenous single strand

RNA (ssRNA) are immediately cleared by interferon-mediated immune responses [300, 301]. To circumvent this problem, eukaryotic mRNA becomes modified *in vivo* to reduce immunological recognition [302, 303]. By the incorporation of artificial nucleotides including 5-methylcytidine in place of cytidine the same effect could be achieved in synthetic mRNAs [251].

Control experiments in Lgr5-eGFP^{+}/CAGGS-tdTomato^{+} organoids using *Cre*-mRNA showed tdTOMATO expression in clusters in the organoid-periphery where ISCs reside. The results indicate that the transfection worked while only subsets of cells were transfected and the reason for the clustered tdTOMATO signal remains elusive. *Cre*-mRNA was not tested anymore because the generation of synthetic Ptf1a-RNA failed. In collaboration with Dr. Philipp Wörsdörfer, no Ptf1a-specific mRNA could be generated while the RNAs that were used for his own research could be produced without problems. Technically, the limiting step was that the ligation of the amplified Ptf1a template into the cloning vector *pGEM-T Easy* failed. Possible reasons remain unknown and other approaches to circumvent the problem were also not working. Therefore, the synthetic mRNA strategy was not further considered.

The next method included the delivery of recombinant PTF1A protein in Lgr5-eGFP^{+}-ISCs or organoids by means of liposomes that were formulated by Dr. Marco Favretto (Radbout University Nijmegen, the Netherlands). Liposomes gained high importance in the context of drug delivery, as the cargo can be provided and released in a highly controlled manner due to the adjustable lipid composition of the liposomal structures [304]. Albeit, PTF1A could be delivered with high efficiency into target cells using liposomes, this application resulted in high cytotoxicity 24-48 after delivery. Possible reasons for this could be either the lipid composition or the size of the used lipids. Altered lipid composition and adaptation or reducing the liposome size could improve delivery efficacy with a reduction in cell toxicity [305]. The procedure of liposome generation can strongly impact on the vesicle size and possibly smaller liposomes could have improved the cellular uptake and/or could have prevented cytotoxicity. However, there was a shortage of time and therefore no further liposome compositions and formulations were tested and thus no more experiments were conducted using liposomes.

In a next step, PTF1A delivery was achieved by using CPP-mediated protein transfection of single cell ISCs. The obtained results show that all protein-based

approaches displayed unfavorable drawbacks like too less efficiency of protein delivery, cellular survival or only few impact on gene expression profiles. The recombinant PTF1A protein was already prepared at the chair for Tissue Engineering and Regenerative Medicine (TERM) before the beginning of this project and was tested for functionality by performing an electrophoretic mobility shift assay (EMSA) [122, 306, 307]. Briefly, this method reveals the ability of trimeric transcription factor complex that comprises of the recombinant Ptf1A together with the commercially available subunits PTF1-J, RBPJ and PTF1-L RBPJL to interact with a sequence-specific oligonucleotide probe mimicking the *in vivo* binding site (TC box) for this complex. If the complex interacts with the oligonucleotides, the migration of PTF1A on a non-denaturating polyacrylamide gel is decelerated resulting in a shifted band compared to the unbound control [122]. The EMSA analysis revealed an expected band shift and therefore protein activity was verified. However, the outcome of the experiments presented in this thesis indicated that the recombinant PTF1A possibly comprised a reduced efficiency or only a part of the generated PTF1A protein was functional. A possible explanation for this could be that the heterologous overexpression of the protein in the bacterial cytoplasm resulted in the formation of inclusion bodies in the course of protein generation. While insoluble inclusion bodies are known to facilitate the harvest of large protein quantities, they also coincide with diminished refolding capacities and thus a reduced biological activity of the protein [308]. Nevertheless, PTF1A transfection mediated by cell penetrating peptide (CPP) functionalization revealed an induction of acinar cell-specific markers associated with a high rate of cell death during the differentiation process. It was hypothesized that possibly due to low PTF1A functionality or transfection efficacy, the transcription factor-mediated boost was not strong enough to induce expression of characteristic β-cell-specific genes. In addition, a stronger Ptf1a expression was assumed to even trigger transcription of characteristic β-like cell markers.

Based on these findings, a lentiviral expression system was used as alternative. In detail, a vector system was used to consecutively express Ptf1a under the control of the phosphoglycerate kinase (PGK) promotor with a modified Kozak sequence for maximal gene transcription. In general, lentiviral systems display a broad-range of cell transduction and are highly efficient for transgene expression [309, 310]. In contrast to PTF1A delivery, the lentiviral approach resulted in less cell death and the efficacy in terms of increased gene expression pattern was significantly increased.

The aim of this project was to establish a differentiation protocol to derive β-like cells from murine ISCs that should be translated to human ISCs at a later stage. In this thesis it was shown that lentivirus-mediated protein expression is a promising strategy to ectopically express a transcription factor to promote a cell conversion in ISCs. For a better translational application for future cell-replacement strategies in human, the use of non-host integrating system like adenovirus comprises several advantages over lentiviral strategies [311, 312]. The transgene delivery and expression is increased compared to lentivirus and no immune reaction against the virus capsid was described so far. In addition, the dosing and the clinical application options are well established in a versatile and customized manner [311].

4.1.4. Role of the transcription factor Ptf1a for the differentiation of multipotent ISCs towards cells displaying pancreas-specific gene expression patterns

The biological meaning of transdifferentiation describes the conversion of a differentiated somatic cell into another somatic cell [313]. The multipotent intestinal stem cells are capable to differentiate into all intestinal cell types and in the current study the aim was to convert ISCs to pancreatic progenitors with subsequent differentiation in β-like cells. However, as ISCs are not terminally differentiated cells, this transformation describes rather a differentiation than a transdifferentiation process. In this context, master regulatory genes like transcription factors (TFs) represent a central aspect [314]. TFs specifically bind to regulatory DNA sequences and thereby regulate gene expression [111, 315]. In terms of cellular conversion or differentiation to a somatic cell type, TFs must switch on genes that are silenced (inactive) in the original cell or vice versa. An inactive gene is characterized by being engaged in a closed chromatin state called heterochromatin. For the activation of a silenced gene, a TF needs to bind to a regulatory domain within a gene that activates the gene or make other binding sites available by inducing chromatin remodeling to make the DNA interaction sites accessible for other factors [286, 315]. A distinct class of TFs, so called pioneer factors are master regulators for cell fate determination [315]. Pioneer factors are able to bind to DNA in nucleosomes or in condensed chromatin structures and recruit other non-pioneer factors including chromatin modifiers, and other TFs that bind

to now accessible nucleosomal DNA to implement new transcriptional programs that drive cellular fate [286, 316]. In other words, the possibility for a successful cell conversion largely depends on the level of chromatin density or factors that remodel the chromatin structure to make the nucleosomal DNA accessible for gene activation or repression. This fact explains the huge potency of stem cells in terms of differentiation plasticity as they comprise a high content of open chromatin (euchromatin) and consequently DNA binding sites are more permissive for TFs to promote differentiation [317]. Further, it was hypothesized that a possibility for low efficient transdifferentiation or cell conversion depends on the failure to the initial genetic program of the original cell prior to induce new lineage specific transcriptional pattern [318].

In the actual work, the transcription factor Ptf1a was hypothesized to induce pancreas-specific differentiation of multipotent Lgr5-eGFP^{+}-ISCs. Ptf1a is a master regulator transcription factor crucial for pancreas development and lineage commitment [75, 97, 112, 115, 126, 319-321]. The murine pancreas emerges from embryonic day E9.5 by developing a bud-like evagination from the dorsal foregut in the adjacent mesenchyme [75, 102]. At this stage, a temporary Ptf1a^{+} population of multipotent progenitor cells (MPCs) appears in the dorsal and the ventral pancreatic buds, capable to give rise to the endocrine, the exocrine and the ductal cell lineage in the developing pancreas [99, 106, 115]. Depletion of Ptf1a results in loss of pancreatic fate, as was shown by nascent pancreatic progenitor cells conversion and differentiation into non-pancreatic tissue [97, 115, 127, 321]. In addition, Ptf1a was demonstrated to convert duodenum, stomach and liver into pancreas and subsequent development of endo- and exocrine cell lineage [319].

The results of this project provided evidence that ectopic expression of Ptf1a alone was not enough to induce transcriptional programs characteristic for β-like cells derived from Lgr5-eGFP^{+}-ISCs. In contrast, the obtained results revealed an acinar-lineage specific mRNA fingerprint, manifested by upregulation of the acinar marker genes *mAmylase* and *mChymoB1* [322, 323]. However, in this thesis only gene expression was investigated, but no protein expression, FACS or functional assays have to be performed in future studies to prove pancreatic exocrine identity and function.

In general, it is known from the literature that Ptf1a expression is an early developmental trigger for pancreas commitment but only active in a short time frame

whereas prolonged expression results in the formation of exocrine/acinar pancreas formation [115]. As lentiviral Ptf1a was demonstrated to be the most efficient Ptf1a expression strategy in target cells, Ptf1a should be expressed in a tightly controlled time-frame to induce the endoderm lineage and subsequently inhibited to avoid acinar lineage induction. A strategy to circumvent this problem could be the application of an inducible (e.g. tetracycline-based) system to gain temporal control of gene expression [324, 325] or the combination with other TFs like Pdx1 or Ngn3 (see later in the discussion) [222].

Finally, Lgr5-eGFP$^+$ organoids were transduced with Ptf1a-lentivirus, embedded in MG drops and grown with pancreas organoid differentiation (POD) medium. The reason for this approach was that the 3D microenvironment and the alignment of progenitor cells were shown to improve the expansion and differentiation efficacy towards the endocrine lineages [263, 326, 327]. In transduced Lgr5-eGFP$^+$ organoids the highest mRNA levels of *mPtf1a*, *mAmylase* and *mChymoB1* were observed when Ptf1a expression was consecutively driven under the PGK promotor. This observation was interesting, because Ptf1a is a key acinar cell marker that further maintains the formation of the heterotrimeric transcription factor 1 (PTF1) complex [120, 328, 329], responsible for transcriptional regulation of secretory enzymes of the acinar tissue [330-332], which is in line with the observed upregulation of *mAmylase* and *mChymoB1* in this study. Albeit a significant induction of the endocrine progenitor *mNgn3* was detected when the organoids were cultured in POD-medium, no specific endocrine lineage gene expression was observed.

In this thesis, evident was provided that transient Ptf1a expression alone was not sufficient to induce β-like cell gene expression programs but instead acinar-like cell mRNA profiles. Consequently, pioneer-like abilities able to induce a pancreatic fate were demonstrated for Ptf1a. The chromatin remodeling, the recruitment of additional factors as well as the DNA accessibility was sufficient to induce acinar lineage-specific gene expression, however, for the upregulation of β-cell-specific genes other factors are required. In contrast, ISCs were previously shown to have the epigenetic profile and chromatin constitution as well as the potency to be converted into insulin-secreting β-like cells upon ectopic expression of the transcription factors Pdx1, Ngn3 and MafA [200]. The results presented in this thesis demonstrated that besides the impact of transcription factors also the differentiation media composition plays a pivotal role in

pancreatic differentiation processes, especially in single-cell Lgr5-eGFP^{+}-ISCs applications.

4.1.5. The differentiation medium composition and its effect on pancreatic differentiation efficacy

Developmental processes are often guided by external signals that induce intracellular signaling pathways. Gene regulation highlights the end of signaling cascades and is mainly executed by transcription factors that actually govern the differentiation status of a cell [111, 333]. This intracellular signal transduction pathways can be regulated by external factors including small molecules and growth factors [334, 335] that can be supplemented into the differentiation medium. For this reason the medium composition of a particular differentiation medium is of high relevance and has to be adapted to the actual differentiation stage of the cells.

The choice of the most suitable pancreatic differentiation medium was difficult in this project as no background knowledge was available at which differentiation stage the Ptf1a-expressing ISCs could be. An early developmental stage within the pancreatic lineage was assumed and it was hypothesized that an adequate differentiation medium could induce differentiation into β-like cells (see 2.1.4.4. in material and methods) [255]. The BMP agonist noggin and the sonic hedgehog inhibitor cyclopamine with ubiquitous retinoid acid signaling (RA) were shown to stimulate PDX1 expression and inhibition of hepatic differentiation at the same time [336-339]. In addition, FGF10 supplementation favors proliferation of late stage pancreatic progenitor cells to functional endocrine cells [340, 341]. Furthermore, lentivirus-mediated Ptf1a expression in single-cell ISCs resulted in apoptosis, however, the intestinal cell line K8 revealed an upregulation of the acinar marker *mAmylase* when cultured in differentiation medium supplemented with retinoic acid (RA) and nicotinamide [204, 226, 262]. In mESCs, nicotinamide and RA were previously described to stimulate insulin secretion after pancreatic induction by Ptf1a expression and concurrently favored the generation of endocrine-like cells at the expense of acinar cells [226]. The outcome of this study was not congruent with the results of this work as only acinar gene expression was elevated. The application of differentiation medium alone [225, 255] resulted in significant upregulation of characteristic pancreatic progenitor mRNA

levels in Lgr5-eGFP$^+$-ISCs (*mHnf1b*, *mSox9* and *Pdx1*) and downregulation of the ISCs marker Olfm4 [41] independent of transient Ptf1a expression what further underlines the importance of the differentiation medium.

When pancreatic differentiation was investigated in Lgr5-eGFP$^+$ organoids, the POD media composition was based on pancreatic organoid medium [224] and extended by higher concentrations of FGF10 that was shown to be essential for pancreas progenitor proliferation and to derive the endocrine lineage [225, 255, 340]. Nicotinamide was also included to support the induction of endocrine progenitors [342] and indeed only in the transduced organoids elevated *mNgn3* mRNA levels were observed. Furthermore, FGF10 was demonstrated to maintain and increase the expression of Ptf1a in early pancreatic development and thereby could promote the cellular conversion from intestinal- to pancreatic fate [343].

In summary, the data of this thesis revealed that ectopic Ptf1a expression in combination with appropriate differentiation media compositions could not induce β-like cell gene expression in Lgr5-eGFP$^+$-ISCs. However, the application of pancreatic differentiation medium alone was shown to induce differentiation and loss of intestinal stem cell identity. In ESC and K8 cell, the application of the differentiation medium alone had a stronger impact on acinar-like cell gene expression than ectopic Ptf1a expression.

4.1.6. Alternative transcription factor-based approaches for the generation of β-like cells from Lgr5-eGFP$^+$-ISCs

Transient Ptf1a expression was shown to induce the expression of acinar-specific genes but not β-like cell expression as previously shown when Pdx1, Ngn3 and MafA were expressed to act in concert to convert various cell types into insulin-secreting cells [197-202, 344]. In contrast to Ptf1a, the combination of Pdx1, Ngn3 and MafA works in synergism and potentiates the effect of each other. Pdx1 is the first active pancreatic transcription factor that mediates pancreatic fate induction, triggers β-cell differentiation and remains expressed in mature β-cells [198, 201, 344-346]. Furthermore, Neurogenin3 (Ngn3) induces the proliferation of Ngn3$^+$ cells that represent the most important endocrine progenitor stage [106, 347] and strictly depend

on the presence of Pdx1 [97]. In addition, MafA acts at this stage and drives the conversion from Ngn3$^+$ towards endocrine cells and mediates the differentiation into functional β-cells mainly by enhancing the effect of Pdx1 [344, 348].

For further applications, a combined ectopic expression of Pdx1 and Ptf1a could be beneficial to transduce Lgr5-eGFP$^+$-ISCs as previous studies revealed that Pdx1 and Ptf1a are sufficient to convert endodermal cells into pancreatic precursor cells [112]. Due to time reasons the lentiviral constructs were not generated and thus this approach not yet tested. Ptf1a and Pdx1 are the earliest expressed genes in pancreatic development and play crucial roles for the determination of a common pancreatic progenitor stage from where the endocrine or acinar lineage derives [97, 124, 222]. Nevertheless, Ptf1a is restricted to be expressed in a short time frame to induce pancreatic fate and from then on, Ptf1a expression should be inhibited to avoid acinar lineage differentiation [75, 115, 122, 223, 320]. To circumvent this problem, an inducible on/off expression system or an inhibition of Ptf1a at a given time point by using si/shRNA could be a possibility. For the differentiation towards β-like cells, the initial boost of Ptf1a could be important as previous studies reported that Pdx1 was transactivated by Ptf1a [349]. However, Pdx1 mRNA levels were not upregulated following ectopic *Ptf1a* expression neither in organoids nor in Lgr5-eGFP$^+$-ISCs, indicating that this activator effect was not functional in our system.

As mentioned above, the common precursor for β-cell differentiation are Ngn3$^+$ cells [106, 347]. From this developmental stage, Pax4, Nkx6.1 and Pdx1 are the most important factors to induce the generation of functional β-cells [350-353]. Of note, Ptf1a inhibition is also important at this stage as the Nkx6.1 function is antagonized by Ptf1a [123]. The importance of *Pax4* expression was demonstrated in murine knockout studies where upon Pax4 depletion no β-cells were observed [354]. Pdx1 hallmarks a key β-cell marker and its expression is inevitable to give rise to insulin-secreting β-cells [113, 344, 345, 353]. Consequently, stimulation and induction of Pdx1 improves the differentiation of the β-cell lineage. A prominent inducer for Pdx1 expression is the transforming growth factor beta (TGF-β) family member Activin B [355] or the small molecule BRD7552 harboring a potent Pdx1 expression inducing capacity in pancreatic islet- and ductal cells [355] that both could be added to the differentiation medium. In detail, once PDX1$^+$ cells emerged from Lgr5-eGFP$^+$-ISCs due to Activin B application, BRD7552 stimulation or transient *Pdx1* expression, the endocrine

progenitor cells could be further expanded with the supplementation of the β-like cell inducing small molecules AT7867, BRD7389 or GW8510. AT7867 was proved to stimulate the proliferation of PDX1 expressing pancreatic progenitors as was demonstrated by highly elevated $KI67^+$ cell numbers after application [356]. So far, low availability of pancreatic progenitors is a major drawback in cell replacement strategies for T1DM, AT7867 driven proliferation could represent a valid solution for this obstacle [356]. In addition, the compounds BRD7389 or GW8510 were used to induce insulin gene expression in pancreatic α-cells and could represent interesting approaches to convert progenitor cells towards β-like cells [357, 358]. In this context, another interesting compound is the epidermal growth factor betacellulin (BTC). Recently, BTC alone or in combination with Activin A was demonstrated to promote the differentiation and proliferation, of pancreatic islets or fetal pancreatic cells towards β-cells [359-361]. Therefore, BTC in combination with ectopic expression of pancreas-specific transcription factors Ptf1a and/or Pdx1 represents a powerful tool to trigger pancreatic progenitors or closely related cells towards insulin-secreting β-like cells. Even more important is the ability of betacellulin to convert various cells, including acinar-, α-, intestinal- and mesenchymal stem cells into insulin-secreting cells [303, 362-365]. Albeit the mentioned effects are beneficial for β-cell differentiation assays, there are doubts due to missing knowledge of the mechanism and concerns remain if the derived cells remain functional in the long term [366]. In summary, the combined expression of Ptf1a and Pdx1 could improve the induction of pancreatic fate.

4.2. The Na^+-D- glucose cotransporter SGLT1 plays an important role for pancreatic islet identity

SGLT1 represents the primary transporter within the brush border of the small intestine for active glucose transport thereby playing a dominant role for the regulation of blood glucose concentration. Recently, evidence was reported that SGLT1 is not exclusively expressed in the small intestine. Instead, several studies showed SGLT1 expression also in various other organs like kidney, brain, heart and pancreas [235-239, 245, 268, 367].

Currently new agents regulating blood glucose concentrations of diabetic patients are of high importance. In this context, the dual SGLT1/2 inhibitor Sotaglifozin (LX4211) is of great interest and actually under investigation in phase III clinical trials [227, 229, 368]. While a positive impact on postprandial blood glucose concentrations and reduced HbA_{1C} levels were shown, only few knowledge about potential side effects is available so far [228, 230-233].

In view of the potential of pharmacological SGLT1 inhibition together with the need to investigate possible adverse events, especially in other SGLT1 expressing tissues, the aim of this work was to verify if loss of SGLT1 function affects morphological and functional properties of murine pancreatic islets. For this purpose, a global SGLT1 knockout mouse line was used that was fed a glucose-deficient, fat-enriched diet (GDFE) to circumvent the glucose-galactose malabsorption syndrome [241]. C57BL6/J wildtype mice on standard chow (SC) or GDFE diet served as control groups to determine diet- or knockout-dependent effects. In summary, the observed data of this work revealed a nutrient-dependent regulation of intestinal SGLT1 expression associated with an impaired SGLT1 function for glucose transport. Both, the impairment of intestinal SGLT1 and the global loss of SGLT1 function, resulted in functional, structural and (cyto-)morphological alterations of pancreatic islets in mice.

4.2.1. SGLT1-expression pattern and nutrient-dependent regulation

In line with previous studies, the obtained data of this work confirmed SGLT1 mRNA expression in several murine organs [235, 236, 238, 268] with highest expression levels in the small intestine. In contrast, only marginal expression levels were obtained

for all other analyzed organs including pancreatic islets or pancreatic exocrine tissue. Given that SGLT1 is only expressed in cellular subsets of the pancreas such as islet-specific α-cells or intralobular duct cells located within the exocrine tissue, the low abundance of pancreatic Sglt1 mRNA obtained in this study is not surprising and in line with previously published data [236, 238].

In addition to the differences in expression strength in individual organs indicating a tissue-specific regulation of SGLT1, this work demonstrates also a nutrient-dependent control specifically for small intestinal SGLT1 expression and function. Feeding the GDFE diet to C57BL6/J wildtype mice resulted in downregulation of small intestinal SGLT1 at the transcriptional level as shown by qRT-PCR. The nutrient-dependent regulation of small intestinal *Sglt1* expression was already shown before and both key players of the GDFE diet, glucose and dietary fat, play prominent roles in this context [267, 270, 369, 370]. While this work demonstrates a negative impact on *Sglt1* expression in absence of glucose, high glucose concentrations were shown to stimulate the upregulation of Sglt1 mRNA levels in mammals [270, 371, 372]. Contributing to the downregulation of SGLT1 is the enriched fat content within the GDFE diet, which is in line with recently published data that also demonstrate a fat-mediated effect [370]. In contrast to the influence of a high-fat content, low-fat conditions in combination with a high-starch component of the diet results in the upregulation of rodent SGLT1 [373]. Underlying mechanisms for both, either the glucose- or fat-dependent regulation of SGLT1, remains elusive so far. However, different dietary components were recently shown to impact on epigenetic marks that are associated with transcriptional activation such as the trimethylation of lysine 4 at histone 3 (H3K4) [374]. In this context, rats on a low-fat diet in combination with a high amount of starch showed elevated levels of mono-, di- and trimethylation of the H3K4 mark at promoter, enhancer and also transcribed regions of the *Slc5A1* gene possibly accounting for the increased SGLT1 expression levels in this animals [374]. Together, these data indicate that different dietary components could affect specific epigenetic patterns that regulate SGLT1 expression and functionality. In line with this, also reduced blood glucose concentrations were observed after OGTT in GDFE fed mice along with the decreased Sglt1 mRNA expression.

SGLT1 was characterized as high-affinity but low-capacity glucose transporter [375, 376]. These SGLT1-specific kinetics underline that the quantity of the SGLT1 transporter molecules available within the brush border membrane defines the capacity of intestinal glucose absorption. Further, protein abundancy strongly depends on the amount of glucose present within the small intestine stimulating the release of SGLT1 protein-loaded vesicles from the trans-Golgi apparatus, a fast-induced process regulated by a specific domain of the RS1 (RSC1A1) protein RS1-Reg [377]. Together, these characteristics of SGLT1 protein abundancy and function can explain the reduced blood glucose levels 5 min after OGTT in animals fed GDFE (WTDC) in comparison to WTSC mice.

4.2.2. Global loss of SGLT1 results in structural and cellular rearrangements of pancreatic islet clusters

The recently published α-cell-specific expression of SGLT1 [236, 367] together with the increasing interest in SGLT1 inhibitors as anti-hyperglycemic agents let to the investigation of possible alterations of pancreatic endocrine cell populations when SGLT1 function is lost or impaired. Consequently, the central aspect of this work was the comparison of pancreatic islets from WTSC, WTDC and SGLT1$^{-/-}$DC mice to highlight effects on islet size or cytomorphology associated to SGLT1 ablation or impairment due to GDFE diet feeding.

For all analytical purposes focusing on islet architecture, the stereological method [94, 378] was applied in this work describing the examination of whole pancreata by dissecting the organ followed by cutting into serial sections (see material and methods 2.2.3.1.) and subsequent immunohistological analysis. This method does not only represent a randomized analysis tool but also allows the identification of small and large islets. This is of great importance as the islet size represents a critical aspect regarding the physiological function of the islet. In contrast to large islets, small islets were shown to secrete more insulin in response to glucose and to have a higher oxygen consumption [379, 380]. Further, small islets reveal higher survival rates compared to large islets as shown in transplantation studies [381]. Therefore, it is highly important to include small islets when investigating islet morphology in correlation with functional aspects.

By applying stereological analysis, a huge number of islets were analyzed in this work (size: 2135 islets in total; cytomorphology: 1125 islets in total) demonstrating several SGLT1 knockout-specific effects on pancreatic islets. One of the main findings was that SGLT1$^{-/-}$ islets displayed an increased mean islet area associated with a reduction of apoptotic cell numbers. In addition, also the proliferation rate was significantly decreased in SGLT1 knockout islets. Underlying mechanisms for these findings have to be determined in follow-up studies but the missing of glucose accounts as a main reason. Besides an indirect effect due to the abrogated glucose transport within the small intestine, a direct effect within the pancreatic islet is conceivable. Recently, SGLT1 was described to be expressed on pancreatic α-cells [236, 367], a finding that suggests the involvement of SGLT1 in intra-islet-specific glucose sensing. As glucose is known to affect β-cell proliferation and survival in an age- and concentration-dependent manner [382, 383], a disturbed glucose sensing could possibly account for the diminished proliferation observed for the SGLT1 knockout islet. In this context, low glucose availability was associated with reduced β-cell proliferation and survival [382]. In addition, increased glucose concentrations were shown to stimulate apoptosis within pancreatic islets [384-386]. Recently, Madunic et al. provided evidence for SGLT1 localization in intralobular ducts of the pancreatic exocrine tissue [238]. On this basis, SGLT1-mediated glucose transport and distribution within pancreatic compartments could be another important regulator for intra-pancreatic glucose availability and thus sensing. Together, the loss of SGLT1 could result in a local hypoglycemia-like condition where the low glucose availability causes reduced islet cell proliferation and apoptosis as observed in SGLT1$^{-/-}$DC animals.

Another key finding of this work is the elevated proportion of islets displaying an atypical cytomorphology when SGLT1 is abrogated. The atypical islet cytomorphology was manifested by a significantly increased proportion of glucagon-producing α-cells and a reduced number of insulin-secreting β-cells. Together with the findings of an increased mean islet size, these data indicate a specific function of SGLT1 for maintaining typical islet structure and cytomorphology. An underlying reason for this observation is missing but the loss of α-cell-specific SGLT1 and therefore lack of glucose availability and/or sensing within the islet could provoke the observed increase of α-cells to circumvent the underrepresentation of glucose by an α-cell-mediated glucagon release and subsequent activation of endogenous glucose production (EGP)

in the liver. Furthermore, besides the reduction in apoptosis in pancreatic islets, the increased α-cell number possibly contributes to larger islet sizes in SGLT1$^{-/-}$DC mice.

Pancreatic islets were recently shown to possess a high morphogenetic plasticity to cope with changing physiological circumstances [95, 333] possibly explaining the increased α-cell proportions observed under the given physiological conditions. One option is an intra-islet-specific transdifferentiation process towards the α-cell type at the expense of other endocrine cell subtypes including β-cells [387-389]. Mechanistically, β- to α-cell conversions associate with the upregulation of specific transcription factors like the Aristaless related homeobox (ARX) that trigger and guide the cell type switch by affecting important gene expression programs [387, 389]. Of note, converted α-like cells do not only secrete glucagon but rather express also the β-cell-specific markers Pdx1 and/or Nkx6.1 [389]. To what extent possible conversions towards α-like cells might occur under SGLT1 knockout conditions remains unknown. However an ongoing study by Dr. Daniela Zdzieblo revealed first indications that an increased number of transdifferentiation events take place in SGLT1$^{-/-}$DC islets. Alternatively, also an exo-to-endocrine conversion followed by migration and later integration into the islet structure could possibly explain the atypical islet phenotype harboring increased α-cell proportions [201, 390, 391]. The latter would also explain increased islet sizes and concomitantly decreased proliferation rates in SGLT1$^{-/-}$DC islets. Due to a shortage in time, the origin of the increased α-cell numbers will be investigated in ongoing studies. Furthermore, also pancreatic duct cells comprise the ability to evolve towards the endocrine lineage during development [194, 392-394]. This finding is of special interest as SGLT1 expression was previously described in the luminal domain of intralobular and interlobular ducts [238]. Therefore, loss of SGLT1 could alter interstitial glucose availability thereby affecting islet architecture and endocrine α- or β-cell frequencies at early developmental stages. Previous studies support this assumption where the role of glucose in the developing pancreas was investigated in E13.5 rat pancreata revealing that in the presence of glucose the number of insulin^{+} cells was 20-fold higher and *mInsulin2* expression was significantly upregulated in a dose-dependent manner [395]. Further studies are needed to analyze the longitudinal effects of SGLT1 knockout on islet architecture and cytomorphology to determine if the observed alterations emerge already during early development and how they evolve during ageing.

Interestingly, feeding the GDFE diet altered the mean islet size as well as α- and β-cell proportions in a similar direction as global abrogation of SGLT1, however, the effect strength was only moderate and not significant. A possible explanation for the pronounced differences between WTDC and SGLT1$^{-/-}$DC animals might be the remaining SGLT1 expression in WTDC mice. These observations support a dominant function of small intestinal SGLT1 in context of the observed findings in this work. Nevertheless, the highly significant differences between GDFE fed wildtype mice and SGLT1 knockout mice indicate that pancreatic SGLT1 contributes to the maintenance of proper islet identity and therefore adds an additional role besides glucose transport to the portfolio of SGLT1 regulated processes.

4.2.3. Disturbed insulin responses when SGLT1 function is lost or impaired

The main physiological function of SGLT1 is glucose absorption following a meal. The first response to rising postprandial blood glucose concentrations is β-cell-mediated insulin secretion to lower blood glucose to a homeostatic level. However, the β-cell-driven decrease in blood glucose concentration is impaired under diabetic conditions. For that reason, great hopes are pinned on pharmacological inhibition of SGLT1 that was demonstrated in phase III clinical trials to decrease postprandial glucose excursion and thereby contributing to glycemic control in diabetic patients. The findings of this work showed that global SGLT1 abrogation or a GDFE diet-dependent impairment of intestinal SGLT1 function associates with an altered capacity of pancreatic islets for insulin secretion as indicated by the missing insulin responses after an oral glucose tolerance test (OGTT) in the short- and long-term. The obtained findings 5 min after OGTT are overall in line with previous observations [241]. In contrast, the absence of any insulin response 60 min after OGTT is new and indicates an inability of SGLT1 knockout islets to properly respond to a glucose challenge in the long-term. Interestingly, previously published studies showed diminished responses when SGLT1$^{-/-}$DC mice were analyzed 10-15 min after OGTT [241, 271], a time frame that was not considered in the experiments presented in this thesis. Together, these observations demonstrate that loss or the impairment of SGLT1 function result in a delayed and strongly attenuated insulin response of pancreatic β-cells. As these findings were obtained for SGLT1$^{-/-}$DC and WTDC mice, they argue for a dominant role

of small intestinal SGLT1 in context of insulin secretion from pancreatic β-cells rather than the newly detected pancreatic SGLT1. In line with this is, that adequate blood glucose concentrations indeed signify the main trigger for proper insulin secretion [133, 276]. The impairment or inability for glucose absorption within the small intestine could therefore explain the aberrant insulin responses in WTDC and SGLT1$^{-/-}$DC mice.

Arguing against an exclusive role only for small intestinal SGLT1 are the data obtained from the glucose stimulation experiments performed *in vitro*. Glucose stimulated islets isolated from WTDC or SGLT1$^{-/-}$DC mice showed no insulin response indicating a functional impairment of the β-cell itself, however, the reason for this remains unknown.

Besides the combination of a failure in small intestinal SGLT1 function together with a functional impairment of islet-specific β-cells, also the fat component of the applied GDFE diet could contribute to the missing insulin responses [130, 141-143]. In this context, a fat-enriched diet was described to alter the lipid composition within islet cell membranes and thereby prevent adequate glucose sensing and possibly glucose transportation [142] culminating in a negative impact on insulin secretion. As the data presented in this work could not reveal fat deposition within or the proximity of pancreatic islets, the fat component within the GDFE diet seems to play only a secondary role in this context. The most conceivable hypothesis to explain the disturbed glucose-stimulated insulin release is therefore the diet-dependent chronic underrepresentation of glucose itself and the inability to absorb glucose in the intestine due to SGLT1 abrogation or impairment. In addition, also the observed glucose insensitivity of β-cells plays a role, however, to what extent remains elusive.

Underlying reasons evoking a β-cell impairment are of great interest. First investigations in this context were made in this study by focusing on two important mechanisms involved in insulin secretion. Glucose is the key player for initiation of insulin secretion. The role of blood glucose was already discussed, however, at the β-cell level also the availability of the corresponding glucose transporter proteins is necessary to allow intracellular glucose sensing and to promote insulin secretion. In mice, the appropriate transporter is Glucose transporter type 2 (GLUT2) [396]. Interestingly, *GLUT2* mRNA expression was unchanged within all animal groups in this

study arguing against an involvement of GLUT2 in context of β-cell impairment and associated disturbed insulin responses.

The incretin Glucagon-like peptide 1 (GLP-1) is known to potentiate glucose-stimulated insulin secretion from β-cells and could therefore trigger an insulin response in the absence of glucose by binding to its corresponding receptor (GLP-1R) that is expressed on pancreatic β-cells [152, 157, 208] (Figure 1.9). Mechanistically, GLP-1 is released within the small intestine in association to SGLT1-mediated cotransport of Na^+ and glucose resulting in membrane depolarization provoking Ca^{2+} influx and GLP-1 secretion from L-cells [397-399]. A second SGLT1-independent mechanism is the α-gustducin-coupled T1R3 receptor-mediated release of GLP-1 from L-cells [400, 401]. In this work, no acute GLP-1 release was detected in $SGLT1^{-/-}$DC animals 5 min after glucose bolus while increasing levels were observed in WTDC and WTSC animals. The observations made for $SGLT1^{-/-}$DC mice are consistent with previous publications and further emphasize the importance of SGLT1 for the acute release of GLP-1 [148, 241, 268]. Interestingly, WTDC mice demonstrated GLP-1 secretion at lower levels than WTSC animals. This could be explained by findings from Bauer et al. published in 2018. The authors demonstrated that a 40% downregulation of SGLT1 was sufficient to block GLP-1 secretion in the proximal intestine [402]. In this work, a 85% downregulation for *Sglt1* mRNA was shown in WTDC compared to WTSC mice what possibly explains the 50% lower levels of acute GLP-1 release in these mice. While GDFE-fed mice showed an acute release of GLP-1, there were no insulin responses. Interestingly, this finding supports the hypothesis of a cellular dysfunctionality of pancreatic β-cells when SGLT1 is impaired or lost. The attenuated mRNA expression levels observed for diet fed wild type or SGLT1 knockout mice could therefore indeed contribute to a weaker GLP-1-mediated insulin secretion. Arguing against this mechanistic explanation is that *GLP-1R* mRNA levels are not directly regulated by low glucose availability [403] while at high glucose levels the *GLP-1R* mRNA was significantly downregulated in isolated islets [403, 404]. However, the deregulated *GLP-1R* mRNA expression levels possibly evoke as a secondary effect due to the missing of proper SGLT1 function.

In addition to the acute release of GLP-1, also a sustained GLP-1 release was reported in this work. However, only for WTDC mice and not the standard chow fed control

animals. In contrast to the acute GLP-1 release, also SGLT1$^{-/-}$DC mice showed increased GLP-1 levels 60 min after glucose gavage. This observation is in line with other studies where a delayed GLP-1 release was reported when SGLT1 function was lost [151, 217, 234] (Figure 1.9B). Of note, the findings of this work showed for the first time that also the impairment of SGLT1 function could result in the sustained release of GLP-1. Mechanistically, a similar explanation is hypothesized as in case of total SGLT1 loss. It is known that SGLT1$^{-/-}$DC mice are incapable to absorb glucose in the proximal small intestine. Consequently, an increased quantity of glucose is delivered to distal gut, where a high number of L-cells reside comprising alternative nutrient sensing mechanisms [153, 218, 278]. The distal glucose load promotes microbial fermentation and the generation of short-chain-fatty-acids (SCFAs) that are recognized by G-protein coupled free fatty receptor 2/3 (FFAR2/3) localized on distal enteroendocrine L-cells that are responsible for the sustained GLP-1 secretion [151] (Figure 1.9B).

4.2.4. Aberrant glucagon secretion in SGLT1$^{-/-}$DC animals

Glucose homeostasis is a highly complex regulated mechanism in which insulin and glucagon are playing the leading role [405]. Glucagon is released under hypoglycemic conditions in order to mediate an increase in blood glucose [87, 406]. In line with this classical function are the observation 5 min after OGTT, demonstrating elevated glucagon concentrations in WTSC mice as response to the rise in insulin secretion and thereby physiological processing of blood glucose. The fact that at this time point both, insulin and glucagon, showed elevated concentrations is controversial but could result from two possibilities. First, it could be a technical issue that the analysis time point chosen in this study was not adequate to exactly display the fine-tuned regulation of rising insulin concentrations followed by a temporally delayed increase in blood glucagon. Second, it could result from the amount of applied glucose during OGTT performance. While application of 2 mg glucose per g body weight results in increased insulin levels only, higher glucose applications as used in this study (6 mg/g body weight) could induce simultaneous glucagon and insulin release as was shown in isolated islets *in vitro* [406].

Besides low glucose availability, other possibilities like effector molecule-based mechanisms are conceivable to regulate glucagon secretion. Among these regulatory elements, somatostatin [407], Zn^{2+} [408] or γ-aminobutyric acid [409] represent the most important ones. A crucial role in this context seems to depend on glucose sensing. Beside the β-cells, also glucagon-secreting α-cells comprise a glucose sensing machinery [410], while several other tissues including the intestine, the hepatoportal vain and various brain regions were shown to comprise glucose sensing neurons [411]. In addition, a glucose-dependent neuronal activation of the observed glucagon release is also possible [409, 412-414]. This assumption is underlined by obtained results of the *in vitro* islet stimulation experiments where similar glucagon levels were observed in islets derived from WTSC, WTDC and SGLT1$^{-/-}$DC mice in islets.

The highly upregulated blood glucagon levels analyzed after 60 min following OGTT are also controversial because of two reasons. First, blood GLP-1 concentrations were increased in the same time frame, however, GLP-1 is known to block glucagon release from α-cells [162, 204]. Together with the increase in α-cell mass, this indicates that also α-cell functionality or behavior displays irregularities under loss or impairment of SGLT1. Second, as SGLT1 ablation hinders glucose absorption, low glucose availability and hypoglycemic conditions are known to drive glucagon secretion from pancreatic α-cells [415, 416]. Consequently, the secreted and elevated blood glucagon levels might activate EGP [88, 89, 417], however, blood glucose levels were reduced under loss or impairment of SGLT1. This in addition indicates irregular α-cell functionality differing from its classical function under normal physiological conditions.

Over decades, disturbed β-cell function was claimed to be the key contributor to the pathophysiology of T2DM that is hallmarked by obesity, chronic hyperglycemia and defects in insulin secretion coupled with aberrant glucagon levels and thereby elevated EGP [204, 418]. Conversely, elevated EGP correlates with hyperglycemia and further progression of the Type 2 diabetes phenotype [419]. Currently, SGLT2 inhibitors represent promising strategies in Type 2 diabetes management with moderate side effects [420]. Mechanistically, inhibition of SGLT2 was demonstrated to be linked to increased blood glucagon levels and simultaneous elevation of EGP [236, 421, 422]. Data regarding SGLT1 inhibition and the consequences on glucagon secretion are not available. The data of this thesis provide first evidence that also SGLT1 dysfunction is

linked to elevated blood glucagon levels. Mice displaying an impaired or abrogated SGLT1 function (WTDC and SGLT1$^{-/-}$DC), showed significantly elevated levels of blood glucagon after OGTT in the long-term and further increased mRNA levels specific for islet expressed glucagon. The latter observation is in line with previous findings from studies in obese (ob/ob) mice displaying decreased *Sglt1* and *Sglt2* gene expression levels at an advanced age, after substantial weight gain and acquisition of hyperglycemia along with elevated *Glucagon* mRNA expression [236]. Together, these data point toward a dominant role for glucagon and the involvement of α-cells in T2DM, which was so far for a long time underestimated. In terms of clinical applications and the management of diabetes mellitus, the inhibition or suppression of glucagon secretion could therefore benefit over most insulin-associated treatment options [417].

4.2.5. Importance of theSGLT1 knockout mice-specific data generated in this study for the application of pharmacological SGLT1 inhibitors tested in human clinical trials

The main goal of this study was to investigate the effect of SGLT1 ablation on pancreatic islets. To draw firm conclusions of the observed data to the clinical application of pharmacological SGLT1 inhibitors in humans, it is important to consider some differences and similarities between rodent and human islet architecture. In general, the total β-cell number varies between human (50-60%) and rodent (80-75%) islets [79, 80]. In addition, islet architecture is different between both species, too. Murine islets consist of an α-cell mantle and a β-cell core containing all other endocrine subtypes whereas in human islets all different endocrine cell types are intermingled and lined up along blood vessels [77-80]. In view of a possible transdifferentiation process, which seems to account for the increase of the α-cell population at the expense of β-cells within SGLT1 knockout islets, it is of great interest, if loss or impairment of SGLT1 function affects human islets in a similar way. However, one has to consider that genetic abrogation of SGLT1 and pharmacological SGLT1 inhibition are not the same and therefore could result in different outcomes, especially in view of different cytomorphological situations.

The proportion and arrangement of pancreatic islet cell types vary among species to cope with physiological conditions and the species-specific architecture was

manifested in an evolutionary process [80]. In this context, human and murine islets comprise a high plasticity to adopt to changing metabolic or pathological conditions including altered cytomorphology and endocrine proportions [79, 80, 95]. Similar to the observed findings for SGLT1 knockout islets, human and murine islets display a reduced β-cell and increased α-cell proportion under diabetic conditions [79, 423, 424]. Considering similar effects in human islets after impairment of SGLT1, this suggested therapeutic strategy could even worsen the already aberrant cytomorphological characteristics in diabetic islets.

Islet architecture is proposed to affect functional properties. Murine β-cells are arranged in clusters with many cell-cell interactions resulting in a coordinated insulin release [78]. In contrast, human β-cells are interspersed throughout the islet what results in a heterogeneous response to glucose [78]. Further, while murine islets harbor a higher threshold for glucose concentrations in order to secrete insulin, human β-cells display a higher sensitivity for even very low blood glucose concentrations [78, 425]. In view of this high sensitivity of human islets, it is therefore of great importance to develop pharmacological agents that inhibit the function of SGLT1 in a highly specific manner to reach a fine-tuned level of inhibition and therefore diminished concentration of postprandial blood glucose.

Recently, the dual SGLT1/SGLT2 inhibitory agent Sotagliflozin was demonstrated to suppress postprandial glucose excursion thereby improving glycemic control under diabetic conditions as displayed by lower HbA_{1C} (glycated hemoglobin) values [230-232]. Further, Sotagliflozin in combination with insulin administration was shown to be a promising medication for type 1 diabetes patients [229]. However, only short-term SGLT1-inhibition studies were performed so far and few knowledge about adverse events in other SGLT1-expressing organs is not available. Albeit Sotagliflozin can be detected in the plasma within 15 min and reaches its pharmacokinetic half-life 29h after administration (according to manufacturer), the half maximal inhibitory concentration (IC_{50}) of 36 nmol/l should theoretically not inhibit SGLT1 in other organs [216, 231], a hypothesis that still needs to be proven. In addition, given that long-term SGLT1 inhibition in humans possibly results in a similar effect as revealed for the mice in this study; the increase in SGLT1 expressing α-cells would draw even more pronounced physiological consequences in men. Nevertheless, till now there are no reliable data how loss of SGLT1 function could affect α-cell properties and functionality in humans.

In this context, the role of SGLT1 expressing α-cells and glucagon is of high interest as possibly increased EGP acts counterproductive on the sought improvement in diabetes management [417].

The Na^+-D-glucose cotransporter SGLT1 plays the leading role for intestinal glucose transport thereby impacting on postprandial blood glucose concentrations, a function that characterizes this transporter as highly interesting therapeutic target for diabetic patients. Together with already published findings, the data of this study provided evidence for a tissue-specific and nutrient-dependent regulation of murine SGLT1 with special emphasis on the marginal expression of SGLT1 within pancreatic components and an impaired SGLT1 function when a glucose-diminished, fat-enriched diet is applied over several weeks. In view of blood glucose regulation under diabetic conditions, this data indicate that the prescription of special diets needs to be reconsidered especially when applied in combination with diabetes-related drugs.

The main finding of this work demonstrated that loss of SGLT1 function effects on pancreatic islet integrity comprising increased islet sizes associated with altered proliferation and apoptosis rates, aberrant α- and β-cell proportions as well as an atypical hormone secretion behavior of α- and β-cells. The involvement of SGLT1 in this context could result from three possible scenarios. First, global loss of SGLT1 affects also pancreatic SGLT1 expression and thus directly affects islet cytomorphology and function due to a disturbed intra-islet-specific glucose transport and/or sensing. Second, intestinal SGLT1 ablation may indirectly influence pancreatic islet morphology and function by attenuated intestinal glucose absorption and disturbed enteroendocrine hormone secretion. Third, an interplay of both. The combination of intestinal and pancreatic SGLT1 is the most conceivable hypothesis; however, further studies are necessary to prove this. Together with the obtained findings of this work, the current interest in SGLT1 inhibition as potential medical intervention for diabetic patients, underlines the importance of long-term SGLT1 inhibition studies to reveal adverse events in other SGLT1 expressing tissues and organs. SGLT1 inhibition as medical treatment for diabetes should not only be beneficial in terms of glycemic control but mainly safe for diabetes patients.

4.3. Conclusion

Central aspect of this thesis that combines both individual projects was to demonstrate the importance of a biological relationship as well as the systemic interaction between the small intestine and the pancreas. In terms of regenerative cell-based replacement strategies for T1DM, the common ancestry and thus a similar genetic background of intestinal and pancreatic cell types was shown to positively influence the differentiation of ISCs towards pancreatic cells. The importance of a sophisticated interaction between several organs is highlighted when applying medications regulating blood glucose homeostasis. While glucose is absorbed in the intestine, pancreatic hormones are secreted in response to elevated blood glucose levels. When blocking the intestinal glucose transporter SGLT1, this interplay is disturbed and the data presented in this thesis revealed severe adverse events under this condition. Therefore, a global view on systemic multi-organ interactions is of high importance when developing new medication-based strategies for T2DM patients.

Bibliography

[1] OpenStax Microbiology. Microbiology, Chapter 24.1 Anatomy and Normal Microbiota of the Digestive System, Figure 1 2018 [updated 29. Mai 2018]. Available from: http://cnx.org/contents/e42bd376-624b-4c0f-972f-e0c57998e765@5.3.

[2] Faure S., de Santa Barbara P., 2011. Molecular embryology of the foregut. Journal of pediatric gastroenterology and nutrition. 52 Suppl 1:S2-3.

[3] Blaker P.A., Irving P. Physiology and function of the small intestine. In: Lomer M, editor. Advanced Nutrition and Dietetics in Gastroenterology: John Wiley & Sons, Ltd. Published; 2014.

[4] Birchenough G.M., Johansson M.E., Gustafsson J.K., Bergstrom J.H., Hansson G.C., 2015. New developments in goblet cell mucus secretion and function. Mucosal immunology. 8(4):712-9.

[5] Turner J.R., 2009. Intestinal mucosal barrier function in health and disease. Nature reviews Immunology. 9(11):799-809.

[6] Helander H.F., Fandriks L., 2014. Surface area of the digestive tract - revisited. Scandinavian journal of gastroenterology. 49(6):681-9.

[7] Kiela P.R., Ghishan F.K., 2016. Physiology of Intestinal Absorption and Secretion. Best Pract Res Cl Ga. 30(2):145-59.

[8] Furness J.B., 2012. The enteric nervous system and neurogastroenterology. Nature reviews Gastroenterology & hepatology. 9(5):286-94.

[9] Sancho E., Batlle E., Clevers H., 2003. Live and let die in the intestinal epithelium. Current opinion in cell biology. 15(6):763-70.

[10] Goodman B.E., 2010. Insights into digestion and absorption of major nutrients in humans. Advances in physiology education. 34(2):44-53.

[11] Abumrad N.A., 2005. CD36 may determine our desire for dietary fats. The Journal of clinical investigation. 115(11):2965-7.

[12] Iqbal J., Hussain M.M., 2009. Intestinal lipid absorption. American journal of physiology Endocrinology and metabolism. 296(6):E1183-94.

[13] Drozdowski L.A., Thomson A.B., 2006. Intestinal sugar transport. World journal of gastroenterology. 12(11):1657-70.

[14] Wright E.M., Loo D.D., Hirayama B.A., 2011. Biology of human sodium glucose transporters. Physiological reviews. 91(2):733-94.

[15] Turk E., Martin M.G., Wright E.M., 1994. Structure of the human Na++/glucose cotransporter gene SGLT1. The Journal of biological chemistry. 269(21):15204-9.

[16] Burant C.F., Takeda J., Brot-Laroche E., Bell G.I., Davidson N.O., 1992. Fructose transporter in human spermatozoa and small intestine is GLUT5. The Journal of biological chemistry. 267(21):14523-6.

[17] Thorens B., 2015. GLUT2, glucose sensing and glucose homeostasis. Diabetologia. 58(2):221-32.

[18] Wagers A.J., Weissman I.L., 2004. Plasticity of adult stem cells. Cell. 116(5):639-48.

[19] De Los Angeles A., Ferrari F., Xi R., Fujiwara Y., Benvenisty N., Deng H., et al., 2016. Corrigendum: Hallmarks of pluripotency. Nature. 531(7594):400.

[20] Baker C.L., Pera M.F., 2018. Capturing Totipotent Stem Cells. Cell stem cell. 22(1):25-34.

[21] Seydoux G., Braun R.E., 2006. Pathway to totipotency: lessons from germ cells. Cell. 127(5):891-904.

[22] Nichols J., Smith A., 2012. Pluripotency in the embryo and in culture. Cold Spring Harbor perspectives in biology. 4(8):a008128.

[23] Takahashi K., Tanabe K., Ohnuki M., Narita M., Ichisaka T., Tomoda K., et al., 2007. Induction of pluripotent stem cells from adult human fibroblasts by defined factors. Cell. 131(5):861-72.

[24] Takahashi K., Yamanaka S., 2006. Induction of pluripotent stem cells from mouse embryonic and adult fibroblast cultures by defined factors. Cell. 126(4):663-76.

[25] Puri M.C., Nagy A., 2012. Concise Review: Embryonic Stem Cells Versus Induced Pluripotent Stem Cells: The Game Is On. Stem cells. 30(1):10-4.

[26] Merrell A.J., Stanger B.Z., 2016. Adult cell plasticity in vivo: de-differentiation and transdifferentiation are back in style. Nature reviews Molecular cell biology. 17(7):413-25.

[27] Clevers H., Watt F.M., 2018. Defining Adult Stem Cells by Function, Not by Phenotype. Annual review of biochemistry.

[28] Rezza A., Sennett R., Rendl M., 2014. Adult stem cell niches: cellular and molecular components. Current topics in developmental biology. 107:333-72.

[29] Date S., Sato T., 2015. Mini-gut organoids: reconstitution of the stem cell niche. Annual review of cell and developmental biology. 31:269-89.

[30] Barker N., van Oudenaarden A., Clevers H., 2012. Identifying the stem cell of the intestinal crypt: strategies and pitfalls. Cell stem cell. 11(4):452-60.

[31] Barker N., van de Wetering M., Clevers H., 2008. The intestinal stem cell. Genes Dev. 22(14):1856-64.

[32] van der Flier L.G., Clevers H., 2009. Stem cells, self-renewal, and differentiation in the intestinal epithelium. Annual review of physiology. 71:241-60.

[33] Cheng H., Leblond C.P., 1974. Origin, differentiation and renewal of the four main epithelial cell types in the mouse small intestine. I. Columnar cell. The American journal of anatomy. 141(4):461-79.

[34] Cheng H., Leblond C.P., 1974. Origin, differentiation and renewal of the four main epithelial cell types in the mouse small intestine. V. Unitarian Theory of the origin of the four epithelial cell types. The American journal of anatomy. 141(4):537-61.

[35] Clevers H., 2013. The intestinal crypt, a prototype stem cell compartment. Cell. 154(2):274-84.

[36] Barker N., 2014. Adult intestinal stem cells: critical drivers of epithelial homeostasis and regeneration. Nature reviews Molecular cell biology. 15(1):19-33.

[37] Pellegrinet L., Rodilla V., Liu Z., Chen S., Koch U., Espinosa L., et al., 2011. Dll1- and dll4-mediated notch signaling are required for homeostasis of intestinal stem cells. Gastroenterology. 140(4):1230-40 e1-7.

[38] van Es J.H., Sato T., van de Wetering M., Lyubimova A., Yee Nee A.N., Gregorieff A., et al., 2012. Dll1+ secretory progenitor cells revert to stem cells upon crypt damage. Nat Cell Biol. 14(10):1099-104.

[39] Barker N., van Es J.H., Kuipers J., Kujala P., van den Born M., Cozijnsen M., et al., 2007. Identification of stem cells in small intestine and colon by marker gene Lgr5. Nature. 449(7165):1003-7.

[40] Snippert H.J., van der Flier L.G., Sato T., van Es J.H., van den Born M., Kroon-Veenboer C., et al., 2010. Intestinal crypt homeostasis results from neutral competition between symmetrically dividing Lgr5 stem cells. Cell. 143(1):134-44.

[41] Munoz J., Stange D.E., Schepers A.G., van de Wetering M., Koo B.K., Itzkovitz S., et al., 2012. The Lgr5 intestinal stem cell signature: robust expression of proposed quiescent '+4' cell markers. The EMBO journal. 31(14):3079-91.

[42] Sato T., Vries R.G., Snippert H.J., van de Wetering M., Barker N., Stange D.E., et al., 2009. Single Lgr5 stem cells build crypt-villus structures in vitro without a mesenchymal niche. Nature. 459(7244):262-5.

[43] Potten C.S., Hume W.J., Reid P., Cairns J., 1978. The segregation of DNA in epithelial stem cells. Cell. 15(3):899-906.

[44] Potten C.S., 1977. Extreme sensitivity of some intestinal crypt cells to X and gamma irradiation. Nature. 269(5628):518-21.

[45] Montgomery R.K., Carlone D.L., Richmond C.A., Farilla L., Kranendonk M.E., Henderson D.E., et al., 2011. Mouse telomerase reverse transcriptase (mTert) expression marks slowly cycling intestinal stem cells. Proc Natl Acad Sci U S A. 108(1):179-84.

[46] Buczacki S.J., Zecchini H.I., Nicholson A.M., Russell R., Vermeulen L., Kemp R., et al., 2013. Intestinal label-retaining cells are secretory precursors expressing Lgr5. Nature. 495(7439):65-9.

[47] Tian H., Biehs B., Warming S., Leong K.G., Rangell L., Klein O.D., et al., 2011. A reserve stem cell population in small intestine renders Lgr5-positive cells dispensable. Nature. 478(7368):255-9.

[48] Schofield R., 1978. The relationship between the spleen colony-forming cell and the haemopoietic stem cell. Blood cells. 4(1-2):7-25.

[49] Sato T., van Es J.H., Snippert H.J., Stange D.E., Vries R.G., van den Born M., et al., 2011. Paneth cells constitute the niche for Lgr5 stem cells in intestinal crypts. Nature. 469(7330):415-8.

[50] Kosinski C., Li V.S., Chan A.S., Zhang J., Ho C., Tsui W.Y., et al., 2007. Gene expression patterns of human colon tops and basal crypts and BMP antagonists as intestinal stem cell niche factors. Proc Natl Acad Sci U S A. 104(39):15418-23.

[51] Powell D.W., Pinchuk I.V., Saada J.I., Chen X., Mifflin R.C., 2011. Mesenchymal cells of the intestinal lamina propria. Annual review of physiology. 73:213-37.

[52] Kuhnert F., Davis C.R., Wang H.T., Chu P., Lee M., Yuan J., et al., 2004. Essential requirement for Wnt signaling in proliferation of adult small intestine and colon revealed by adenoviral expression of Dickkopf-1. Proc Natl Acad Sci U S A. 101(1):266-71.

[53] Reya T., Clevers H., 2005. Wnt signalling in stem cells and cancer. Nature. 434(7035):843-50.

[54] Carmon K.S., Gong X., Lin Q., Thomas A., Liu Q., 2011. R-spondins function as ligands of the orphan receptors LGR4 and LGR5 to regulate Wnt/beta-catenin signaling. Proc Natl Acad Sci U S A. 108(28):11452-7.

[55] de Lau W., Barker N., Low T.Y., Koo B.K., Li V.S., Teunissen H., et al., 2011. Lgr5 homologues associate with Wnt receptors and mediate R-spondin signalling. Nature. 476(7360):293-7.

[56] Sato T., Clevers H., 2013. Growing self-organizing mini-guts from a single intestinal stem cell: mechanism and applications. Science. 340(6137):1190-4.

[57] Suzuki A., Sekiya S., Gunshima E., Fujii S., Taniguchi H., 2010. EGF signaling activates proliferation and blocks apoptosis of mouse and human intestinal stem/progenitor cells in long-term monolayer cell culture. Laboratory investigation; a journal of technical methods and pathology. 90(10):1425-36.

[58] Holmberg F.E., Seidelin J.B., Yin X., Mead B.E., Tong Z., Li Y., et al., 2017. Culturing human intestinal stem cells for regenerative applications in the treatment of inflammatory bowel disease. EMBO molecular medicine. 9(5):558-70.

[59] Fevr T., Robine S., Louvard D., Huelsken J., 2007. Wnt/beta-catenin is essential for intestinal homeostasis and maintenance of intestinal stem cells. Molecular and cellular biology. 27(21):7551-9.

[60] Batts L.E., Polk D.B., Dubois R.N., Kulessa H., 2006. Bmp signaling is required for intestinal growth and morphogenesis. Developmental dynamics : an official publication of the American Association of Anatomists. 235(6):1563-70.

[61] Auclair B.A., Benoit Y.D., Rivard N., Mishina Y., Perreault N., 2007. Bone morphogenetic protein signaling is essential for terminal differentiation of the intestinal secretory cell lineage. Gastroenterology. 133(3):887-96.

[62] He X.C., Zhang J., Tong W.G., Tawfik O., Ross J., Scoville D.H., et al., 2004. BMP signaling inhibits intestinal stem cell self-renewal through suppression of Wnt-beta-catenin signaling. Nature genetics. 36(10):1117-21.

[63] Maloum F., Allaire J.M., Gagne-Sansfacon J., Roy E., Belleville K., Sarret P., et al., 2011. Epithelial BMP signaling is required for proper specification of epithelial cell lineages and gastric endocrine cells. American journal of physiology Gastrointestinal and liver physiology. 300(6):G1065-79.

[64] Haramis A.P., Begthel H., van den Born M., van Es J., Jonkheer S., Offerhaus G.J., et al., 2004. De novo crypt formation and juvenile polyposis on BMP inhibition in mouse intestine. Science. 303(5664):1684-6.

[65] Qi Z., Li Y., Zhao B., Xu C., Liu Y., Li H., et al., 2017. BMP restricts stemness of intestinal Lgr5(+) stem cells by directly suppressing their signature genes. Nature communications. 8:13824.

[66] Krausova M., Korinek V., 2014. Wnt signaling in adult intestinal stem cells and cancer. Cellular signalling. 26(3):570-9.

[67] Jensen J., Pedersen E.E., Galante P., Hald J., Heller R.S., Ishibashi M., et al., 2000. Control of endodermal endocrine development by Hes-1. Nature genetics. 24(1):36-44.

[68] Dolensek J., Pohorec V., Rupnik M., Stozer A. Pancreas Physiology, Challenges in Pancreatic Pathology. 2017. In: Pancreas Physiology, Challenges in Pancreatic Pathology [Internet]. IntechOpen. Available from: https://www.intechopen.com/books/challenges-in-pancreatic-pathology/pancreas-physiology.

[69] Dolensek J., Rupnik M.S., Stozer A., 2015. Structural similarities and differences between the human and the mouse pancreas. Islets. 7(1).

[70] Liu X.Y., Xue L., Zheng X., Yan S., Zheng S.S., 2010. Pancreas transplantation in the mouse. Hepatobiliary & pancreatic diseases international : HBPD INT. 9(3):254-8.

[71] OpenStax College. Anatomy & Physiology, Chapter 17.9 The Endocrine Pancreas, Figure 1 2016 [17.9 The Endocrine Pancreas]. Available from: https://legacy.cnx.org/content/col11496/1.8/.

[72] Whitcomb D.C., Lowe M.E., 2007. Human pancreatic digestive enzymes. Digest Dis Sci. 52(1):1-17.

[73] Slack J.M., 1995. Developmental biology of the pancreas. Development. 121(6):1569-80.

[74] Ramirez-Dominguez M., 2016. Historical Background of Pancreatic Islet Isolation. Advances in experimental medicine and biology. 938:1-9.

[75] Pan F.C., Wright C., 2011. Pancreas organogenesis: from bud to plexus to gland. Developmental dynamics : an official publication of the American Association of Anatomists. 240(3):530-65.

[76] Da Silva Xavier G., 2018. The Cells of the Islets of Langerhans. Journal of clinical medicine. 7(3).

[77] Brissova M., Fowler M.J., Nicholson W.E., Chu A., Hirshberg B., Harlan D.M., et al., 2005. Assessment of human pancreatic islet architecture and composition by laser scanning confocal microscopy. Journal of Histochemistry & Cytochemistry. 53(9):1087-97.

[78] Cabrera O., Berman D.M., Kenyon N.S., Ricordi C., Berggren P.O., Caicedo A., 2006. The unique cytoarchitecture of human pancreatic islets has implications for islet cell function. Proc Natl Acad Sci U S A. 103(7):2334-9.

[79] Kim A., Miller K., Jo J., Kilimnik G., Wojcik P., Hara M., 2009. Islet architecture A comparative study. Islets. 1(2):129-36.

[80] Steiner D.J., Kim A., Miller K., Hara M., 2010. Pancreatic islet plasticity: interspecies comparison of islet architecture and composition. Islets. 2(3):135-45.

[81] Goke B., 2008. Islet cell function: alpha and beta cells--partners towards normoglycaemia. International journal of clinical practice Supplement. (159):2-7.

[82] Biolo G., Declan Fleming R.Y., Wolfe R.R., 1995. Physiologic hyperinsulinemia stimulates protein synthesis and enhances transport of selected amino acids in human skeletal muscle. The Journal of clinical investigation. 95(2):811-9.

[83] McTernan P.G., Harte A.L., Anderson L.A., Green A., Smith S.A., Holder J.C., et al., 2002. Insulin and rosiglitazone regulation of lipolysis and lipogenesis in human adipose tissue in vitro. Diabetes. 51(5):1493-8.

[84] Miller T.B., Jr., Larner J., 1973. Mechanism of control of hepatic glycogenesis by insulin. The Journal of biological chemistry. 248(10):3483-8.

[85] Roder P.V., Wu B., Liu Y., Han W., 2016. Pancreatic regulation of glucose homeostasis. Exp Mol Med. 48:e219.

[86] Wilcox G., 2005. Insulin and insulin resistance. The Clinical biochemist Reviews. 26(2):19-39.

[87] Cryer P.E., 2012. Minireview: Glucagon in the pathogenesis of hypoglycemia and hyperglycemia in diabetes. Endocrinology. 153(3):1039-48.

[88] Ramnanan C.J., Edgerton D.S., Kraft G., Cherrington A.D., 2011. Physiologic action of glucagon on liver glucose metabolism. Diabetes, obesity & metabolism. 13 Suppl 1:118-25.

[89] Sharabi K., Tavares C.D., Rines A.K., Puigserver P., 2015. Molecular pathophysiology of hepatic glucose production. Molecular aspects of medicine. 46:21-33.

[90] Unger R.H., 1971. Glucagon physiology and pathophysiology. The New England journal of medicine. 285(8):443-9.

[91] Katsuura G., Asakawa A., Inui A., 2002. Roles of pancreatic polypeptide in regulation of food intake. Peptides. 23(2):323-9.

[92] Muller T.D., Nogueiras R., Andermann M.L., Andrews Z.B., Anker S.D., Argente J., et al., 2015. Ghrelin. Molecular metabolism. 4(6):437-60.

[93] Brereton M.F., Iberl M., Shimomura K., Zhang Q., Adriaenssens A.E., Proks P., et al., 2014. Reversible changes in pancreatic islet structure and function produced by elevated blood glucose. Nature communications. 5:4639.

[94] Jo J., Hara M., Ahlgren U., Sorenson R., Periwal V., 2012. Mathematical models of pancreatic islet size distributions. Islets. 4(1):10-9.

[95] Jamal A.M., Lipsett M., Sladek R., Laganiere S., Hanley S., Rosenberg L., 2005. Morphogenetic plasticity of adult human pancreatic islets of Langerhans. Cell death and differentiation. 12(7):702-12.

[96] Zorn A.M., Wells J.M., 2009. Vertebrate endoderm development and organ formation. Annual review of cell and developmental biology. 25:221-51.

[97] Burlison J.S., Long Q., Fujitani Y., Wright C.V., Magnuson M.A., 2008. Pdx-1 and Ptf1a concurrently determine fate specification of pancreatic multipotent progenitor cells. Developmental biology. 316(1):74-86.

[98] Pan F.C., Brissova M., 2014. Pancreas development in humans. Current opinion in endocrinology, diabetes, and obesity. 21(2):77-82.

[99] Zhou Q., Law A.C., Rajagopal J., Anderson W.J., Gray P.A., Melton D.A., 2007. A multipotent progenitor domain guides pancreatic organogenesis. Developmental cell. 13(1):103-14.

[100] Herrera P.L., 2000. Adult insulin- and glucagon-producing cells differentiate from two independent cell lineages. Development. 127(11):2317-22.

[101] Benitez C.M., Goodyer W.R., Kim S.K., 2012. Deconstructing pancreas developmental biology. Cold Spring Harbor perspectives in biology. 4(6).

[102] Jorgensen M.C., Ahnfelt-Ronne J., Hald J., Madsen O.D., Serup P., Hecksher-Sorensen J., 2007. An illustrated review of early pancreas development in the mouse. Endocrine reviews. 28(6):685-705.

[103] Villasenor A., Chong D.C., Henkemeyer M., Cleaver O., 2010. Epithelial dynamics of pancreatic branching morphogenesis. Development. 137(24):4295-305.

[104] Rieck S., Bankaitis E.D., Wright C.V., 2012. Lineage determinants in early endocrine development. Seminars in cell & developmental biology. 23(6):673-84.

[105] Magenheim J., Klein A.M., Stanger B.Z., Ashery-Padan R., Sosa-Pineda B., Gu G., et al., 2011. Ngn3(+) endocrine progenitor cells control the fate and morphogenesis of pancreatic ductal epithelium. Developmental biology. 359(1):26-36.

[106] Gu G., Dubauskaite J., Melton D.A., 2002. Direct evidence for the pancreatic lineage: NGN3+ cells are islet progenitors and are distinct from duct progenitors. Development. 129(10):2447-57.

[107] Miyatsuka T., Kosaka Y., Kim H., German M.S., 2011. Neurogenin3 inhibits proliferation in endocrine progenitors by inducing Cdkn1a. Proc Natl Acad Sci U S A. 108(1):185-90.

[108] Gouzi M., Kim Y.H., Katsumoto K., Johansson K., Grapin-Botton A., 2011. Neurogenin3 initiates stepwise delamination of differentiating endocrine cells during pancreas development. Developmental dynamics : an official publication of the American Association of Anatomists. 240(3):589-604.

[109] Rukstalis J.M., Habener J.F., 2007. Snail2, a mediator of epithelial-mesenchymal transitions, expressed in progenitor cells of the developing endocrine pancreas. Gene expression patterns : GEP. 7(4):471-9.

[110] Dassaye R., Naidoo S., Cerf M.E., 2016. Transcription factor regulation of pancreatic organogenesis, differentiation and maturation. Islets. 8(1):13-34.

[111] Spitz F., Furlong E.E., 2012. Transcription factors: from enhancer binding to developmental control. Nature reviews Genetics. 13(9):613-26.

[112] Afelik S., Chen Y., Pieler T., 2006. Combined ectopic expression of Pdx1 and Ptf1a/p48 results in the stable conversion of posterior endoderm into endocrine and exocrine pancreatic tissue. Genes Dev. 20(11):1441-6.

[113] Murtaugh L.C., 2007. Pancreas and beta-cell development: from the actual to the possible. Development. 134(3):427-38.

[114] Haumaitre C., Barbacci E., Jenny M., Ott M.O., Gradwohl G., Cereghini S., 2005. Lack of TCF2/vHNF1 in mice leads to pancreas agenesis. P Natl Acad Sci USA. 102(5):1490-5.

[115] Kawaguchi Y., Cooper B., Gannon M., Ray M., MacDonald R.J., Wright C.V., 2002. The role of the transcriptional regulator Ptf1a in converting intestinal to pancreatic progenitors. Nature genetics. 32(1):128-34.

[116] Li H., Arber S., Jessell T.M., Edlund H., 1999. Selective agenesis of the dorsal pancreas in mice lacking homeobox gene Hlxb9. Nature genetics. 23(1):67-70.

[117] Seymour P.A., Freude K.K., Tran M.N., Mayes E.E., Jensen J., Kist R., et al., 2007. SOX9 is required for maintenance of the pancreatic progenitor cell pool. P Natl Acad Sci USA. 104(6):1865-70.

[118] Stoffers D.A., Zinkin N.T., Stanojevic V., Clarke W.L., Habener J.F., 1997. Pancreatic agenesis attributable to a single nucleotide deletion in the human IPF1 gene coding sequence. Nature genetics. 15(1):106-10.

[119] Ohlsson H., Karlsson K., Edlund T., 1993. IPF1, a homeodomain-containing transactivator of the insulin gene. The EMBO journal. 12(11):4251-9.

[120] Beres T.M., Masui T., Swift G.H., Shi L., Henke R.M., MacDonald R.J., 2006. PTF1 is an organ-specific and Notch-independent basic helix-loop-helix complex containing the mammalian Suppressor of Hairless (RBP-J) or its paralogue, RBP-L. Molecular and cellular biology. 26(1):117-30.

[121] Masui T., Long Q., Beres T.M., Magnuson M.A., MacDonald R.J., 2007. Early pancreatic development requires the vertebrate Suppressor of Hairless (RBPJ) in the PTF1 bHLH complex. Genes Dev. 21(20):2629-43.

[122] Masui T., Swift G.H., Hale M.A., Meredith D.M., Johnson J.E., Macdonald R.J., 2008. Transcriptional autoregulation controls pancreatic Ptf1a expression during development and adulthood. Molecular and cellular biology. 28(17):5458-68.

[123] Schaffer A.E., Freude K.K., Nelson S.B., Sander M., 2010. Nkx6 transcription factors and Ptf1a function as antagonistic lineage determinants in multipotent pancreatic progenitors. Developmental cell. 18(6):1022-9.

[124] Thompson N., Gesina E., Scheinert P., Bucher P., Grapin-Botton A., 2012. RNA profiling and chromatin immunoprecipitation-sequencing reveal that PTF1a stabilizes pancreas progenitor identity via the control of MNX1/HLXB9 and a network of other transcription factors. Molecular and cellular biology. 32(6):1189-99.

[125] Dong P.D., Provost E., Leach S.D., Stainier D.Y., 2008. Graded levels of Ptf1a differentially regulate endocrine and exocrine fates in the developing pancreas. Genes Dev. 22(11):1445-50.

[126] Fukuda A., Kawaguchi Y., Furuyama K., Kodama S., Horiguchi M., Kuhara T., et al., 2008. Reduction of Ptf1a gene dosage causes pancreatic hypoplasia and diabetes in mice. Diabetes. 57(9):2421-31.

[127] Krapp A., Knofler M., Ledermann B., Burki K., Berney C., Zoerkler N., et al., 1998. The bHLH protein PTF1-p48 is essential for the formation of the exocrine and the correct spatial organization of the endocrine pancreas. Gene Dev. 12(23):3752-63.

[128] Cryer P.E., 2007. Hypoglycemia, functional brain failure, and brain death. The Journal of clinical investigation. 117(4):868-70.

[129] Brealey D., Singer M., 2009. Hyperglycemia in critical illness: a review. Journal of diabetes science and technology. 3(6):1250-60.

[130] Cerf M.E., 2007. High fat diet modulation of glucose sensing in the beta-cell. Medical science monitor : international medical journal of experimental and clinical research. 13(1):RA12-7.

[131] Im S.S., Kang S.Y., Kim S.Y., Kim H.I., Kim J.W., Kim K.S., et al., 2005. Glucose-stimulated upregulation of GLUT2 gene is mediated by sterol response element-binding protein-1c in the hepatocytes. Diabetes. 54(6):1684-91.

[132] Rorsman P., Renstrom E., 2003. Insulin granule dynamics in pancreatic beta cells. Diabetologia. 46(8):1029-45.

[133] Komatsu M., Takei M., Ishii H., Sato Y., 2013. Glucose-stimulated insulin secretion: A newer perspective. J Diabetes Invest. 4(6):511-6.

[134] Henquin J.C., 2000. Triggering and amplifying pathways of regulation of insulin secretion by glucose. Diabetes. 49(11):1751-60.

[135] Leney S.E., Tavare J.M., 2009. The molecular basis of insulin-stimulated glucose uptake: signalling, trafficking and potential drug targets. The Journal of endocrinology. 203(1):1-18.

[136] Rui L., 2014. Energy metabolism in the liver. Comprehensive Physiology. 4(1):177-97.

[137] Noguchi R., Kubota H., Yugi K., Toyoshima Y., Komori Y., Soga T., et al., 2013. The selective control of glycolysis, gluconeogenesis and glycogenesis by temporal insulin patterns. Molecular systems biology. 9:664.

[138] Quesada I., Tuduri E., Ripoll C., Nadal A., 2008. Physiology of the pancreatic alpha-cell and glucagon secretion: role in glucose homeostasis and diabetes. The Journal of endocrinology. 199(1):5-19.

[139] Zhang Q., Ramracheya R., Lahmann C., Tarasov A., Bengtsson M., Braha O., et al., 2013. Role of KATP channels in glucose-regulated glucagon secretion and impaired counterregulation in type 2 diabetes. Cell metabolism. 18(6):871-82.

[140] Exton J.H., Friedmann N., Wong E.H., Brineaux J.P., Corbin J.D., Park C.R., 1972. Interaction of glucocorticoids with glucagon and epinephrine in the control of gluconeogenesis and glycogenolysis in liver and of lipolysis in adipose tissue. The Journal of biological chemistry. 247(11):3579-88.

[141] Ahren B., Gudbjartsson T., Al-Amin A.N., Martensson H., Myrsen-Axcrona U., Karlsson S., et al., 1999. Islet perturbations in rats fed a high-fat diet. Pancreas. 18(1):75-83.

[142] Lichtenstein A.H., Schwab U.S., 2000. Relationship of dietary fat to glucose metabolism. Atherosclerosis. 150(2):227-43.

[143] Wang Y., Miura Y., Kaneko T., Li J., Qin L.Q., Wang P.Y., et al., 2002. Glucose intolerance induced by a high-fat/low-carbohydrate diet in rats effects of nonesterified fatty acids. Endocrine. 17(3):185-91.

[144] Boden G., 2008. Obesity and free fatty acids. Endocrinology and metabolism clinics of North America. 37(3):635-46, viii-ix.

[145] Itoh Y., Kawamata Y., Harada M., Kobayashi M., Fujii R., Fukusumi S., et al., 2003. Free fatty acids regulate insulin secretion from pancreatic beta cells through GPR40. Nature. 422(6928):173-6.

[146] Ximenes H.M., Hirata A.E., Rocha M.S., Curi R., Carpinelli A.R., 2007. Propionate inhibits glucose-induced insulin secretion in isolated rat pancreatic islets. Cell biochemistry and function. 25(2):173-8.

[147] Nauck M.A., Meier J.J., 2016. The incretin effect in healthy individuals and those with type 2 diabetes: physiology, pathophysiology, and response to therapeutic interventions. The lancet Diabetes & endocrinology. 4(6):525-36.

[148] Reimann F., Habib A.M., Tolhurst G., Parker H.E., Rogers G.J., Gribble F.M., 2008. Glucose sensing in L cells: a primary cell study. Cell metabolism. 8(6):532-9.

[149] Kuhre R.E., Gribble F.M., Hartmann B., Reimann F., Windelov J.A., Rehfeld J.F., et al., 2014. Fructose stimulates GLP-1 but not GIP secretion in mice, rats, and humans. American journal of physiology Gastrointestinal and liver physiology. 306(7):G622-30.

[150] Reimann F., Williams L., da Silva Xavier G., Rutter G.A., Gribble F.M., 2004. Glutamine potently stimulates glucagon-like peptide-1 secretion from GLUTag cells. Diabetologia. 47(9):1592-601.

[151] Tolhurst G., Heffron H., Lam Y.S., Parker H.E., Habib A.M., Diakogiannaki E., et al., 2012. Short-Chain Fatty Acids Stimulate Glucagon-Like Peptide-1 Secretion via the G-Protein-Coupled Receptor FFAR2. Diabetes. 61(2):364-71.

[152] Baggio L.L., Drucker D.J., 2007. Biology of incretins: GLP-1 and GIP. Gastroenterology. 132(6):2131-57.

[153] Ezcurra M., Reimann F., Gribble F.M., Emery E., 2013. Molecular mechanisms of incretin hormone secretion. Curr Opin Pharmacol. 13(6):922-7.

[154] Moens K., Heimberg H., Flamez D., Huypens P., Quartier E., Ling Z., et al., 1996. Expression and functional activity of glucagon, glucagon-like peptide I, and glucose-dependent insulinotropic peptide receptors in rat pancreatic islet cells. Diabetes. 45(2):257-61.

[155] Doyle M.E., Egan J.M., 2007. Mechanisms of action of glucagon-like peptide 1 in the pancreas. Pharmacology & therapeutics. 113(3):546-93.

[156] MacDonald P.E., El-Kholy W., Riedel M.J., Salapatek A.M., Light P.E., Wheeler M.B., 2002. The multiple actions of GLP-1 on the process of glucose-stimulated insulin secretion. Diabetes. 51 Suppl 3:S434-42.

[157] Meloni A.R., DeYoung M.B., Lowe C., Parkes D.G., 2013. GLP-1 receptor activated insulin secretion from pancreatic beta-cells: mechanism and glucose dependence. Diabetes, obesity & metabolism. 15(1):15-27.

[158] Leech C.A., Dzhura I., Chepurny O.G., Kang G., Schwede F., Genieser H.G., et al., 2011. Molecular physiology of glucagon-like peptide-1 insulin secretagogue action in pancreatic beta cells. Progress in biophysics and molecular biology. 107(2):236-47.

[159] Light P.E., Manning Fox J.E., Riedel M.J., Wheeler M.B., 2002. Glucagon-like peptide-1 inhibits pancreatic ATP-sensitive potassium channels via a protein kinase A- and ADP-dependent mechanism. Molecular endocrinology. 16(9):2135-44.

[160] Scrocchi L.A., Brown T.J., MaClusky N., Brubaker P.L., Auerbach A.B., Joyner A.L., et al., 1996. Glucose intolerance but normal satiety in mice with a null mutation in the glucagon-like peptide 1 receptor gene. Nature medicine. 2(11):1254-8.

[161] Drucker D.J., Philippe J., Mojsov S., Chick W.L., Habener J.F., 1987. Glucagon-like peptide I stimulates insulin gene expression and increases cyclic AMP levels in a rat islet cell line. Proc Natl Acad Sci U S A. 84(10):3434-8.

[162] De Marinis Y.Z., Salehi A., Ward C.E., Zhang Q., Abdulkader F., Bengtsson M., et al., 2010. GLP-1 inhibits and adrenaline stimulates glucagon release by differential modulation of N- and L-type Ca2+ channel-dependent exocytosis. Cell metabolism. 11(6):543-53.

[163] de Heer J., Rasmussen C., Coy D.H., Holst J.J., 2008. Glucagon-like peptide-1, but not glucose-dependent insulinotropic peptide, inhibits glucagon secretion via somatostatin (receptor subtype 2) in the perfused rat pancreas. Diabetologia. 51(12):2263-70.

[164] Prigeon R.L., Quddusi S., Paty B., D'Alessio D.A., 2003. Suppression of glucose production by GLP-1 independent of islet hormones: a novel extrapancreatic effect. American journal of physiology Endocrinology and metabolism. 285(4):E701-7.

[165] Egan J.M., Meneilly G.S., Habener J.F., Elahi D., 2002. Glucagon-like peptide-1 augments insulin-mediated glucose uptake in the obese state. The Journal of clinical endocrinology and metabolism. 87(8):3768-73.

[166] Gerich J.E., Campbell P.J., 1988. Overview of counterregulation and its abnormalities in diabetes mellitus and other conditions. Diabetes/metabolism reviews. 4(2):93-111.

[167] Unger R.H., Orci L., 1975. The essential role of glucagon in the pathogenesis of diabetes mellitus. Lancet. 1(7897):14-6.

[168] Atkinson M.A., Eisenbarth G.S., Michels A.W., 2014. Type 1 diabetes. Lancet. 383(9911):69-82.

[169] DeFronzo R.A., Ferrannini E., Groop L., Henry R.R., Herman W.H., Holst J.J., et al., 2015. Type 2 diabetes mellitus. Nature reviews Disease primers. 1:15019.

[170] World Health Organization. Global Report on Diabetes 20162016.

[171] World Health Organization. Fact Sheet Diabetes 2017 [updated 15. November 2017]. Available from: http://www.who.int/news-room/fact-sheets/detail/diabetes.

[172] American Diabetes Association. 2014. Diagnosis and classification of diabetes mellitus. Diabetes care. 37 Suppl 1:S81-90.

[173] Daneman D., 2006. Type 1 diabetes. Lancet. 367(9513):847-58.

[174] Kharroubi A.T., Darwish H.M., 2015. Diabetes mellitus: The epidemic of the century. World journal of diabetes. 6(6):850-67.

[175] Jaacks L.M., Siegel K.R., Gujral U.P., Narayan K.M., 2016. Type 2 diabetes: A 21st century epidemic. Best practice & research Clinical endocrinology & metabolism. 30(3):331-43.

[176] Frank A., Deng S., Huang X., Velidedeoglu E., Bae Y.S., Liu C., et al., 2004. Transplantation for type I diabetes: comparison of vascularized whole-organ pancreas with isolated pancreatic islets. Annals of surgery. 240(4):631-40; discussion 40-3.

[177] Gruessner R.W., Gruessner A.C., 2013. The current state of pancreas transplantation. Nature reviews Endocrinology. 9(9):555-62.

[178] Scharp D.W., Lacy P.E., Santiago J.V., McCullough C.S., Weide L.G., Falqui L., et al., 1990. Insulin independence after islet transplantation into type I diabetic patient. Diabetes. 39(4):515-8.

[179] Shapiro A.M., Lakey J.R., Ryan E.A., Korbutt G.S., Toth E., Warnock G.L., et al., 2000. Islet transplantation in seven patients with type 1 diabetes mellitus using a glucocorticoid-free immunosuppressive regimen. The New England journal of medicine. 343(4):230-8.

[180] Shapiro A.M., Ricordi C., Hering B.J., Auchincloss H., Lindblad R., Robertson R.P., et al., 2006. International trial of the Edmonton protocol for islet transplantation. The New England journal of medicine. 355(13):1318-30.

[181] Cogger K., Nostro M.C., 2015. Recent advances in cell replacement therapies for the treatment of type 1 diabetes. Endocrinology. 156(1):8-15.

[182] Dominguez-Bendala J., Lanzoni G., Klein D., Alvarez-Cubela S., Pastori R.L., 2016. The Human Endocrine Pancreas: New Insights on Replacement and Regeneration. Trends in endocrinology and metabolism: TEM. 27(3):153-62.

[183] Pagliuca F.W., Millman J.R., Gurtler M., Segel M., Van Dervort A., Ryu J.H., et al., 2014. Generation of functional human pancreatic beta cells in vitro. Cell. 159(2):428-39.

[184] Kroon E., Martinson L.A., Kadoya K., Bang A.G., Kelly O.G., Eliazer S., et al., 2008. Pancreatic endoderm derived from human embryonic stem cells generates glucose-responsive insulin-secreting cells in vivo. Nature biotechnology. 26(4):443-52.

[185] D'Amour K.A., Bang A.G., Eliazer S., Kelly O.G., Agulnick A.D., Smart N.G., et al., 2006. Production of pancreatic hormone-expressing endocrine cells from human embryonic stem cells. Nature biotechnology. 24(11):1392-401.

[186] Rezania A., Bruin J.E., Riedel M.J., Mojibian M., Asadi A., Xu J., et al., 2012. Maturation of human embryonic stem cell-derived pancreatic progenitors into functional islets capable of treating pre-existing diabetes in mice. Diabetes. 61(8):2016-29.

[187] Bruin J.E., Rezania A., Xu J., Narayan K., Fox J.K., O'Neil J.J., et al., 2013. Maturation and function of human embryonic stem cell-derived pancreatic progenitors in macroencapsulation devices following transplant into mice. Diabetologia. 56(9):1987-98.

[188] de Almeida P.E., Ransohoff J.D., Nahid A., Wu J.C., 2013. Immunogenicity of pluripotent stem cells and their derivatives. Circulation research. 112(3):549-61.

[189] Herberts C.A., Kwa M.S., Hermsen H.P., 2011. Risk factors in the development of stem cell therapy. Journal of translational medicine. 9:29.

[190] Yamada Y., Haga H., Yamada Y., 2014. Concise review: dedifferentiation meets cancer development: proof of concept for epigenetic cancer. Stem cells translational medicine. 3(10):1182-7.

[191] Zhao T., Zhang Z.N., Rong Z., Xu Y., 2011. Immunogenicity of induced pluripotent stem cells. Nature. 474(7350):212-5.

[192] Zheng Y.L., 2016. Some Ethical Concerns About Human Induced Pluripotent Stem Cells. Sci Eng Ethics. 22(5):1277-84.

[193] Bonner-Weir S., Guo L., Li W.C., Ouziel-Yahalom L., Lysy P.A., Weir G.C., et al., 2012. Islet neogenesis: a possible pathway for beta-cell replenishment. The review of diabetic studies : RDS. 9(4):407-16.

[194] Bonner-Weir S., Inada A., Yatoh S., Li W.C., Aye T., Toschi E., et al., 2008. Transdifferentiation of pancreatic ductal cells to endocrine beta-cells. Biochemical Society transactions. 36(Pt 3):353-6.

[195] Bonner-Weir S., Taneja M., Weir G.C., Tatarkiewicz K., Song K.H., Sharma A., et al., 2000. In vitro cultivation of human islets from expanded ductal tissue. Proc Natl Acad Sci U S A. 97(14):7999-8004.

[196] Klein D., Alvarez-Cubela S., Lanzoni G., Vargas N., Prabakar K.R., Boulina M., et al., 2015. BMP-7 Induces Adult Human Pancreatic Exocrine-to-Endocrine Conversion. Diabetes. 64(12):4123-34.

[197] Akinci E., Banga A., Greder L.V., Dutton J.R., Slack J.M., 2012. Reprogramming of pancreatic exocrine cells towards a beta (beta) cell character using Pdx1, Ngn3 and MafA. The Biochemical journal. 442(3):539-50.

[198] Akinci E., Banga A., Tungatt K., Segal J., Eberhard D., Dutton J.R., et al., 2013. Reprogramming of various cell types to a beta-like state by Pdx1, Ngn3 and MafA. PLoS One. 8(11):e82424.

[199] Banga A., Akinci E., Greder L.V., Dutton J.R., Slack J.M., 2012. In vivo reprogramming of Sox9+ cells in the liver to insulin-secreting ducts. Proc Natl Acad Sci U S A. 109(38):15336-41.

[200] Chen Y.J., Finkbeiner S.R., Weinblatt D., Emmett M.J., Tameire F., Yousefi M., et al., 2014. De novo formation of insulin-producing "neo-beta cell islets" from intestinal crypts. Cell reports. 6(6):1046-58.

[201] Li W.D., Nakanishi M., Zumsteg A., Shear M., Wright C., Melton D.A., et al., 2014. In vivo reprogramming of pancreatic acinar cells to three islet endocrine subtypes. eLife. 3.

[202] Zhou Q., Brown J., Kanarek A., Rajagopal J., Melton D.A., 2008. In vivo reprogramming of adult pancreatic exocrine cells to beta-cells. Nature. 455(7213):627-32.

[203] Morizane A., Doi D., Kikuchi T., Okita K., Hotta A., Kawasaki T., et al., 2013. Direct comparison of autologous and allogeneic transplantation of iPSC-derived neural cells in the brain of a non-human primate. Stem cell reports. 1(4):283-92.

[204] Kahn S.E., Cooper M.E., Del Prato S., 2014. Pathophysiology and treatment of type 2 diabetes: perspectives on the past, present, and future. Lancet. 383(9922):1068-83.

[205] Cusi K., Consoli A., DeFronzo R.A., 1996. Metabolic effects of metformin on glucose and lactate metabolism in noninsulin-dependent diabetes mellitus. The Journal of clinical endocrinology and metabolism. 81(11):4059-67.

[206] Turner R.C., Cull C.A., Frighi V., Holman R.R., 1999. Glycemic control with diet, sulfonylurea, metformin, or insulin in patients with type 2 diabetes mellitus: progressive requirement for multiple therapies (UKPDS 49). UK Prospective Diabetes Study (UKPDS) Group. Jama. 281(21):2005-12.

[207] Panten U., Burgfeld J., Goerke F., Rennicke M., Schwanstecher M., Wallasch A., et al., 1989. Control of insulin secretion by sulfonylureas, meglitinide and diazoxide in relation to their binding to the sulfonylurea receptor in pancreatic islets. Biochemical pharmacology. 38(8):1217-29.

[208] Drucker D.J., 2013. Incretin action in the pancreas: potential promise, possible perils, and pathological pitfalls. Diabetes. 62(10):3316-23.

[209] Drucker D.J., Nauck M.A., 2006. The incretin system: glucagon-like peptide-1 receptor agonists and dipeptidyl peptidase-4 inhibitors in type 2 diabetes. Lancet. 368(9548):1696-705.

[210] van de Laar F.A., Lucassen P.L., Akkermans R.P., van de Lisdonk E.H., Rutten G.E., van Weel C., 2005. Alpha-glucosidase inhibitors for patients with type 2 diabetes: results from a Cochrane systematic review and meta-analysis. Diabetes care. 28(1):154-63.

[211] Abdul-Ghani M.A., Norton L., Defronzo R.A., 2011. Role of sodium-glucose cotransporter 2 (SGLT 2) inhibitors in the treatment of type 2 diabetes. Endocrine reviews. 32(4):515-31.

[212] Merovci A., Solis-Herrera C., Daniele G., Eldor R., Fiorentino T.V., Tripathy D., et al., 2014. Dapagliflozin improves muscle insulin sensitivity but enhances endogenous glucose production. The Journal of clinical investigation. 124(2):509-14.

[213] Dobbins R.L., Greenway F.L., Chen L., Liu Y., Breed S.L., Andrews S.M., et al., 2015. Selective sodium-dependent glucose transporter 1 inhibitors block glucose absorption and impair glucose-dependent insulinotropic peptide release. American journal of physiology Gastrointestinal and liver physiology. 308(11):G946-54.

[214] Shibazaki T., Tomae M., Ishikawa-Takemura Y., Fushimi N., Itoh F., Yamada M., et al., 2012. KGA-2727, a novel selective inhibitor of a high-affinity sodium glucose cotransporter (SGLT1), exhibits antidiabetic efficacy in rodent models. J Pharmacol Exp Ther. 342(2):288-96.

[215] Inoue T., Takemura M., Fushimi N., Fujimori Y., Onozato T., Kurooka T., et al., 2017. Mizagliflozin, a novel selective SGLT1 inhibitor, exhibits potential in the amelioration of chronic constipation. Eur J Pharmacol. 806:25-31.

[216] Lapuerta P., Zambrowicz B., Strumph P., Sands A., 2015. Development of sotagliflozin, a dual sodium-dependent glucose transporter 1/2 inhibitor. Diabetes & vascular disease research. 12(2):101-10.

[217] Oguma T., Nakayama K., Kuriyama C., Matsushita Y., Yoshida K., Hikida K., et al., 2015. Intestinal Sodium Glucose Cotransporter 1 Inhibition Enhances Glucagon-Like Peptide-1 Secretion in Normal and Diabetic Rodents. J Pharmacol Exp Ther. 354(3):279-89.

[218] Powell D.R., DaCosta C.M., Gay J., Ding Z.M., Smith M., Greer J., et al., 2013. Improved glycemic control in mice lacking Sglt1 and Sglt2. American journal of physiology Endocrinology and metabolism. 304(2):E117-30.

[219] Shomali M., 2012. Diabetes treatment in 2025: can scientific advances keep pace with prevalence? Therapeutic advances in endocrinology and metabolism. 3(5):163-73.

[220] Pattou F., Daoudi M., Baud G., 2016. Roux-en-Y Gastric Bypass and Intestinal Glucose Handling: A Salty Sweet Operation. Gastroenterology. 151(1):210.

[221] Popov B.V., Zaichik A.M., Budko M.B., Zlobina O.V., Tolkunova E.N., Zhidkova O.V., et al., 2011. Epithelial cells transdifferentiation into bladder urothelium in experiments in vivo. Cell and Tissue Biology. 5(4):358.

[222] Arda H.E., Benitez C.M., Kim S.K., 2013. Gene regulatory networks governing pancreas development. Developmental cell. 25(1):5-13.

[223] Hoang C.Q., Hale M.A., Azevedo-Pouly A.C., Elsasser H.P., Deering T.G., Willet S.G., et al., 2016. Transcriptional Maintenance of Pancreatic Acinar Identity, Differentiation, and Homeostasis by PTF1A. Molecular and cellular biology. 36(24):3033-47.

[224] Huch M., Bonfanti P., Boj S.F., Sato T., Loomans C.J., van de Wetering M., et al., 2013. Unlimited in vitro expansion of adult bi-potent pancreas progenitors through the Lgr5/R-spondin axis. The EMBO journal. 32(20):2708-21.

[225] Mfopou J.K., Geeraerts M., Dejene R., Van Langenhoven S., Aberkane A., Van Grunsven L.A., et al., 2014. Efficient definitive endoderm induction from mouse embryonic stem cell adherent cultures: a rapid screening model for differentiation studies. Stem cell research. 12(1):166-77.

[226] Nair G.G., Vincent R.K., Odorico J.S., 2014. Ectopic Ptf1a expression in murine ESCs potentiates endocrine differentiation and models pancreas development in vitro. Stem cells. 32(5):1195-207.

[227] Buse J.B., Garg S.K., Rosenstock J., Banks P., Sawhney S., Strumph P., et al., 2017. Twenty-Four-Week Efficacy and Safety of Sotagliflozin, a Dual SGLT1 and SGLT2 Inhibitor, as Adjunct Therapy to Insulin in Type 1 Diabetes (inTandem1). Diabetes. 66:A18-A.

[228] Cariou B., Charbonnel B., 2015. Sotagliflozin as a potential treatment for type 2 diabetes mellitus. Expert opinion on investigational drugs. 24(12):1647-56.

[229] Garg S.K., Henry R.R., Banks P., Buse J.B., Davies M.J., Fulcher G.R., et al., 2017. Effects of Sotagliflozin Added to Insulin in Patients with Type 1 Diabetes. The New England journal of medicine.

[230] Sands A.T., Zambrowicz B.P., Rosenstock J., Lapuerta P., Bode B.W., Garg S.K., et al., 2015. Sotagliflozin, a Dual SGLT1 and SGLT2 Inhibitor, as Adjunct Therapy to Insulin in Type 1 Diabetes. Diabetes care. 38(7):1181-8.

[231] Zambrowicz B., Freiman J., Brown P.M., Frazier K.S., Turnage A., Bronner J., et al., 2012. LX4211, a dual SGLT1/SGLT2 inhibitor, improved glycemic control in patients with type 2 diabetes in a randomized, placebo-controlled trial. Clinical pharmacology and therapeutics. 92(2):158-69.

[232] Zambrowicz B., Lapuerta P., Strumph P., Banks P., Wilson A., Ogbaa I., et al., 2015. LX4211 therapy reduces postprandial glucose levels in patients with type 2 diabetes mellitus and renal impairment despite low urinary glucose excretion. Clinical therapeutics. 37(1):71-82 e12.

[233] Rendell M.S., 2018. Efficacy and safety of sotagliflozin in treating diabetes type 1. Expert opinion on pharmacotherapy. 19(3):307-15.

[234] Song P., Onishi A., Koepsell H., Vallon V., 2016. Sodium glucose cotransporter SGLT1 as a therapeutic target in diabetes mellitus. Expert Opin Ther Targets. 20(9):1109-25.

[235] Koepsell H., 2017. The Na+-D-glucose cotransporters SGLT1 and SGLT2 are targets for the treatment of diabetes and cancer. Pharmacology & therapeutics. 170:148-65.

[236] Bonner C., Kerr-Conte J., Gmyr V., Queniat G., Moerman E., Thevenet J., et al., 2015. Inhibition of the glucose transporter SGLT2 with dapagliflozin in pancreatic alpha cells triggers glucagon secretion. Nature medicine. 21(5):512-7.

[237] Elfeber K., Kohler A., Lutzenburg M., Osswald C., Galla H.J., Witte O.W., et al., 2004. Localization of the Na+-D-glucose cotransporter SGLT1 in the blood-brain barrier. Histochemistry and cell biology. 121(3):201-7.

[238] Madunic I.V., Breljak D., Karaica D., Koepsell H., Sabolic I., 2017. Expression profiling and immunolocalization of Na+-D-glucose-cotransporter 1 in mice employing knockout mice as specificity control indicate novel locations and differences between mice and rats. Pflugers Archiv : European journal of physiology.

[239] Salker M.S., Singh Y., Zeng N., Chen H., Zhang S., Umbach A.T., et al., 2017. Loss of Endometrial Sodium Glucose Cotransporter SGLT1 is Detrimental to Embryo Survival and Fetal Growth in Pregnancy. Scientific reports. 7(1):12612.

[240] Zhou L., Cryan E.V., D'Andrea M.R., Belkowski S., Conway B.R., Demarest K.T., 2003. Human cardiomyocytes express high level of Na+/glucose cotransporter 1 (SGLT1). J Cell Biochem. 90(2):339-46.

[241] Gorboulev V., Schurmann A., Vallon V., Kipp H., Jaschke A., Klessen D., et al., 2012. Na(+)-D-glucose cotransporter SGLT1 is pivotal for intestinal glucose absorption and glucose-dependent incretin secretion. Diabetes. 61(1):187-96.

[242] Graham F.L., Smiley J., Russell W.C., Nairn R., 1977. Characteristics of a human cell line transformed by DNA from human adenovirus type 5. The Journal of general virology. 36(1):59-74.

[243] DuBridge R.B., Tang P., Hsia H.C., Leong P.M., Miller J.H., Calos M.P., 1987. Analysis of mutation in human cells by using an Epstein-Barr virus shuttle system. Molecular and cellular biology. 7(1):379-87.

[244] Madisen L., Zwingman T.A., Sunkin S.M., Oh S.W., Zariwala H.A., Gu H., et al., 2010. A robust and high-throughput Cre reporting and characterization system for the whole mouse brain. Nature neuroscience. 13(1):133-40.

[245] Banerjee S.K., McGaffin K.R., Pastor-Soler N.M., Ahmad F., 2009. SGLT1 is a novel cardiac glucose transporter that is perturbed in disease states. Cardiovasc Res. 84(1):111-8.

[246] Li D.S., Yuan Y.H., Tu H.J., Liang Q.L., Dai L.J., 2009. A protocol for islet isolation from mouse pancreas. Nature protocols. 4(11):1649-52.

[247] Zmuda E.J., Powell C.A., Hai T., 2011. A method for murine islet isolation and subcapsular kidney transplantation. Journal of visualized experiments : JoVE. (50).

[248] Hansen W.A., Christie M.R., Kahn R., Norgaard A., Abel I., Petersen A.M., et al., 1989. Supravital dithizone staining in the isolation of human and rat pancreatic islets. Diabetes research. 10(2):53-7.

[249] Conget J.I., Sarri Y., Gonzalez-Clemente J.M., Casamitjana R., Vives M., Gomis R., 1994. Deleterious effect of dithizone-DMSO staining on insulin secretion in rat and human pancreatic islets. Pancreas. 9(2):157-60.

[250] Sabolic I., Skarica M., Gorboulev V., Ljubojevic M., Balen D., Herak-Kramberger C.M., et al., 2006. Rat renal glucose transporter SGLT1 exhibits zonal distribution and androgen-dependent gender differences. American journal of physiology Renal physiology. 290(4):F913-26.

[251] Warren L., Manos P.D., Ahfeldt T., Loh Y.H., Li H., Lau F., et al., 2010. Highly efficient reprogramming to pluripotency and directed differentiation of human cells with synthetic modified mRNA. Cell stem cell. 7(5):618-30.

[252] Bustin S.A., Benes V., Garson J.A., Hellemans J., Huggett J., Kubista M., et al., 2009. The MIQE guidelines: minimum information for publication of quantitative real-time PCR experiments. Clinical chemistry. 55(4):611-22.

[253] Vandesompele J., De Preter K., Pattyn F., Poppe B., Van Roy N., De Paepe A., et al., 2002. Accurate normalization of real-time quantitative RT-PCR data by geometric averaging of multiple internal control genes. Genome biology. 3(7):RESEARCH0034.

[254] Livak K.J., Schmittgen T.D., 2001. Analysis of relative gene expression data using real-time quantitative PCR and the 2(-Delta Delta C(T)) Method. Methods. 25(4):402-8.

[255] Mfopou J.K., Chen B., Mateizel I., Sermon K., Bouwens L., 2010. Noggin, retinoids, and fibroblast growth factor regulate hepatic or pancreatic fate of human embryonic stem cells. Gastroenterology. 138(7):2233-45, 45 e1-14.

[256] Mfopou J.K., Chen B., Sui L., Sermon K., Bouwens L., 2010. Recent advances and prospects in the differentiation of pancreatic cells from human embryonic stem cells. Diabetes. 59(9):2094-101.

[257] Onuma K., Ochiai M., Orihashi K., Takahashi M., Imai T., Nakagama H., et al., 2013. Genetic reconstitution of tumorigenesis in primary intestinal cells. P Natl Acad Sci USA. 110(27):11127-32.

[258] Yin X., Farin H.F., van Es J.H., Clevers H., Langer R., Karp J.M., 2014. Niche-independent high-purity cultures of Lgr5+ intestinal stem cells and their progeny. Nature methods. 11(1):106-12.

[259] Casey J.R., Grinstein S., Orlowski J., 2010. Sensors and regulators of intracellular pH. Nature reviews Molecular cell biology. 11(1):50-61.

[260] Karanth H., Murthy R.S., 2007. pH-sensitive liposomes--principle and application in cancer therapy. The Journal of pharmacy and pharmacology. 59(4):469-83.

[261] Guidotti G., Brambilla L., Rossi D., 2017. Cell-Penetrating Peptides: From Basic Research to Clinics. Trends in pharmacological sciences. 38(4):406-24.

[262] Kryklyva V. The potential of transcription factor Ptf1a to induce pancreatic cell fate in mESCs, mISCs and K8 cells: University of Würzburg; 2017.

[263] Loomans C.J.M., Williams Giuliani N., Balak J., Ringnalda F., van Gurp L., Huch M., et al., 2018. Expansion of Adult Human Pancreatic Tissue Yields Organoids Harboring Progenitor Cells with Endocrine Differentiation Potential. Stem cell reports. 10(3):712-24.

[264] Wang R., Liang J., Jiang H., Qin L.J., Yang H.T., 2008. Promoter-dependent EGFP expression during embryonic stem cell propagation and differentiation. Stem cells and development. 17(2):279-89.

[265] Jackson S.J., Andrews N., Ball D., Bellantuono I., Gray J., Hachoumi L., et al., 2017. Does age matter? The impact of rodent age on study outcomes. Laboratory animals. 51(2):160-9.

[266] Mühlemann M., Zdzieblo D., Friedrich A., Berger C., Otto C., Walles H., et al., 2018. Altered pancreatic islet morphology and function in SGLT1 knockout mice on a glucose-deficient, fat-enriched diet. Molecular metabolism.

[267] Poulsen S.B., Fenton R.A., Rieg T., 2015. Sodium-glucose cotransport. Curr Opin Nephrol Hypertens. 24(5):463-9.

[268] Vrhovac I., Balen Eror D., Klessen D., Burger C., Breljak D., Kraus O., et al., 2015. Localizations of Na(+)-D-glucose cotransporters SGLT1 and SGLT2 in human kidney and of SGLT1 in human small intestine, liver, lung, and heart. Pflugers Archiv : European journal of physiology. 467(9):1881-98.

[269] Ferraris R.P., 2001. Dietary and developmental regulation of intestinal sugar transport. The Biochemical journal. 360(Pt 2):265-76.

[270] Shirazi-Beechey S.P., Hirayama B.A., Wang Y., Scott D., Smith M.W., Wright E.M., 1991. Ontogenic development of lamb intestinal sodium-glucose co-transporter is regulated by diet. The Journal of physiology. 437:699-708.

[271] Roder P.V., Geillinger K.E., Zietek T.S., Thorens B., Koepsell H., Daniel H., 2014. The role of SGLT1 and GLUT2 in intestinal glucose transport and sensing. PLoS One. 9(2):e89977.

[272] Alanentalo T., Hornblad A., Mayans S., Karin Nilsson A., Sharpe J., Larefalk A., et al., 2010. Quantification and three-dimensional imaging of the insulitis-induced destruction of beta-cells in murine type 1 diabetes. Diabetes. 59(7):1756-64.

[273] Roat R., Rao V., Doliba N.M., Matschinsky F.M., Tobias J.W., Garcia E., et al., 2014. Alterations of pancreatic islet structure, metabolism and gene expression in diet-induced obese C57BL/6J mice. PLoS One. 9(2):e86815.

[274] Scholzen T., Gerdes J., 2000. The Ki-67 protein: from the known and the unknown. J Cell Physiol. 182(3):311-22.

[275] Jiang G., Zhang B.B., 2003. Glucagon and regulation of glucose metabolism. American journal of physiology Endocrinology and metabolism. 284(4):E671-8.

[276] Fu Z., Gilbert E.R., Liu D., 2013. Regulation of insulin synthesis and secretion and pancreatic Beta-cell dysfunction in diabetes. Curr Diabetes Rev. 9(1):25-53.

[277] Holst J.J., 2007. The physiology of glucagon-like peptide 1. Physiological reviews. 87(4):1409-39.

[278] Powell D.R., Smith M., Greer J., Harris A., Zhao S., DaCosta C., et al., 2013. LX4211 increases serum glucagon-like peptide 1 and peptide YY levels by reducing sodium/glucose cotransporter 1 (SGLT1)-mediated absorption of intestinal glucose. J Pharmacol Exp Ther. 345(2):250-9.

[279] Atkinson M.A., 2012. The pathogenesis and natural history of type 1 diabetes. Cold Spring Harbor perspectives in medicine. 2(11).

[280] Katsarou A., Gudbjornsdottir S., Rawshani A., Dabelea D., Bonifacio E., Anderson B.J., et al., 2017. Type 1 diabetes mellitus. Nature reviews Disease primers. 3:17016.

[281] Ashcroft F.M., Rorsman P., 2012. Diabetes mellitus and the beta cell: the last ten years. Cell. 148(6):1160-71.

[282] Heller S., Buse J., Fisher M., Garg S., Marre M., Merker L., et al., 2012. Insulin degludec, an ultra-longacting basal insulin, versus insulin glargine in basal-bolus treatment with mealtime insulin aspart in type 1 diabetes (BEGIN Basal-Bolus Type 1): a phase 3, randomised, open-label, treat-to-target non-inferiority trial. Lancet. 379(9825):1489-97.

[283] Kielgast U., Holst J.J., Madsbad S., 2011. Antidiabetic actions of endogenous and exogenous GLP-1 in type 1 diabetic patients with and without residual beta-cell function. Diabetes. 60(5):1599-607.

[284] Oral E.A., 2012. Leptin for type 1 diabetes: coming onto stage to be (or not?). Pediatric diabetes. 13(1):68-73.

[285] Ryan G., Briscoe T.A., Jobe L., 2009. Review of pramlintide as adjunctive therapy in treatment of type 1 and type 2 diabetes. Drug design, development and therapy. 2:203-14.

[286] Iwafuchi-Doi M., Zaret K.S., 2014. Pioneer transcription factors in cell reprogramming. Genes Dev. 28(24):2679-92.

[287] Feng R., Desbordes S.C., Xie H., Tillo E.S., Pixley F., Stanley E.R., et al., 2008. PU.1 and C/EBPalpha/beta convert fibroblasts into macrophage-like cells. Proc Natl Acad Sci U S A. 105(16):6057-62.

[288] Ieda M., Fu J.D., Delgado-Olguin P., Vedantham V., Hayashi Y., Bruneau B.G., et al., 2010. Direct reprogramming of fibroblasts into functional cardiomyocytes by defined factors. Cell. 142(3):375-86.

[289] Kim K., Doi A., Wen B., Ng K., Zhao R., Cahan P., et al., 2010. Epigenetic memory in induced pluripotent stem cells. Nature. 467(7313):285-90.

[290] Gittes G.K., 2009. Developmental biology of the pancreas: a comprehensive review. Developmental biology. 326(1):4-35.

[291] Bar-Nur O., Russ H.A., Efrat S., Benvenisty N., 2011. Epigenetic memory and preferential lineage-specific differentiation in induced pluripotent stem cells derived from human pancreatic islet beta cells. Cell stem cell. 9(1):17-23.

[292] Jung P., Sato T., Merlos-Suarez A., Barriga F.M., Iglesias M., Rossell D., et al., 2011. Isolation and in vitro expansion of human colonic stem cells. Nature medicine. 17(10):1225-7.

[293] Sato T., Stange D.E., Ferrante M., Vries R.G., Van Es J.H., Van den Brink S., et al., 2011. Long-term expansion of epithelial organoids from human colon, adenoma, adenocarcinoma, and Barrett's epithelium. Gastroenterology. 141(5):1762-72.

[294] Maru Y., Orihashi K., Hippo Y., 2016. Lentivirus-Based Stable Gene Delivery into Intestinal Organoids. Methods in molecular biology. 1422:13-21.

[295] Watanabe K., Ueno M., Kamiya D., Nishiyama A., Matsumura M., Wataya T., et al., 2007. A ROCK inhibitor permits survival of dissociated human embryonic stem cells. Nature biotechnology. 25(6):681-6.

[296] Li L., Milner L.A., Deng Y., Iwata M., Banta A., Graf L., et al., 1998. The human homolog of rat Jagged1 expressed by marrow stroma inhibits differentiation of 32D cells through interaction with Notch1. Immunity. 8(1):43-55.

[297] Koo B.K., Stange D.E., Sato T., Karthaus W., Farin H.F., Huch M., et al., 2011. Controlled gene expression in primary Lgr5 organoid cultures. Nature methods. 9(1):81-3.

[298] Steinle H., Behring A., Schlensak C., Wendel H.P., Avci-Adali M., 2017. Concise Review: Application of In Vitro Transcribed Messenger RNA for Cellular Engineering and Reprogramming: Progress and Challenges. Stem cells. 35(1):68-79.

[299] Yisraeli J.K., Melton D.A., 1989. Synthesis of long, capped transcripts in vitro by SP6 and T7 RNA polymerases. Methods in enzymology. 180:42-50.

[300] Diebold S.S., Kaisho T., Hemmi H., Akira S., Reis e Sousa C., 2004. Innate antiviral responses by means of TLR7-mediated recognition of single-stranded RNA. Science. 303(5663):1529-31.

[301] Hornung V., Ellegast J., Kim S., Brzozka K., Jung A., Kato H., et al., 2006. 5'-Triphosphate RNA is the ligand for RIG-I. Science. 314(5801):994-7.

[302] Kariko K., Weissman D., 2007. Naturally occurring nucleoside modifications suppress the immunostimulatory activity of RNA: implication for therapeutic RNA development. Current opinion in drug discovery & development. 10(5):523-32.

[303] Nallagatla S.R., Toroney R., Bevilacqua P.C., 2008. A brilliant disguise for self RNA: 5'-end and internal modifications of primary transcripts suppress elements of innate immunity. RNA biology. 5(3):140-4.

[304] Allen T.M., Cullis P.R., 2013. Liposomal drug delivery systems: from concept to clinical applications. Advanced drug delivery reviews. 65(1):36-48.

[305] Szoka F.C., Jr., Milholland D., Barza M., 1987. Effect of lipid composition and liposome size on toxicity and in vitro fungicidal activity of liposome-intercalated amphotericin B. Antimicrobial agents and chemotherapy. 31(3):421-9.

[306] Fried M., Crothers D.M., 1981. Equilibria and kinetics of lac repressor-operator interactions by polyacrylamide gel electrophoresis. Nucleic acids research. 9(23):6505-25.

[307] Garner M.M., Revzin A., 1981. A gel electrophoresis method for quantifying the binding of proteins to specific DNA regions: application to components of the Escherichia coli lactose operon regulatory system. Nucleic acids research. 9(13):3047-60.

[308] Baneyx F., 1999. Recombinant protein expression in Escherichia coli. Current opinion in biotechnology. 10(5):411-21.

[309] Lois C., Hong E.J., Pease S., Brown E.J., Baltimore D., 2002. Germline transmission and tissue-specific expression of transgenes delivered by lentiviral vectors. Science. 295(5556):868-72.

[310] Naldini L., Blomer U., Gallay P., Ory D., Mulligan R., Gage F.H., et al., 1996. In vivo gene delivery and stable transduction of nondividing cells by a lentiviral vector. Science. 272(5259):263-7.

[311] Crystal R.G., 2014. Adenovirus: the first effective in vivo gene delivery vector. Human gene therapy. 25(1):3-11.

[312] Lee C.S., Bishop E.S., Zhang R., Yu X., Farina E.M., Yan S., et al., 2017. Adenovirus-Mediated Gene Delivery: Potential Applications for Gene and Cell-Based Therapies in the New Era of Personalized Medicine. Genes & diseases. 4(2):43-63.

[313] Graf T., Enver T., 2009. Forcing cells to change lineages. Nature. 462(7273):587-94.

[314] Tosh D., Slack J.M., 2002. How cells change their phenotype. Nature reviews Molecular cell biology. 3(3):187-94.

[315] Zaret K.S., Carroll J.S., 2011. Pioneer transcription factors: establishing competence for gene expression. Genes Dev. 25(21):2227-41.

[316] Iwafuchi-Doi M., Zaret K.S., 2016. Cell fate control by pioneer transcription factors. Development. 143(11):1833-7.

[317] Gaspar-Maia A., Alajem A., Polesso F., Sridharan R., Mason M.J., Heidersbach A., et al., 2009. Chd1 regulates open chromatin and pluripotency of embryonic stem cells. Nature. 460(7257):863-8.

[318] Cahan P., Li H., Morris S.A., Lummertz da Rocha E., Daley G.Q., Collins J.J., 2014. CellNet: network biology applied to stem cell engineering. Cell. 158(4):903-15.

[319] Jarikji Z.H., Vanamala S., Beck C.W., Wright C.V., Leach S.D., Horb M.E., 2007. Differential ability of Ptf1a and Ptf1a-VP16 to convert stomach, duodenum and liver to pancreas. Developmental biology. 304(2):786-99.

[320] Pan F.C., Bankaitis E.D., Boyer D., Xu X., Van de Casteele M., Magnuson M.A., et al., 2013. Spatiotemporal patterns of multipotentiality in Ptf1a-expressing cells during pancreas organogenesis and injury-induced facultative restoration. Development. 140(4):751-64.

[321] Wang Y.J., Park J.T., Parsons M.J., Leach S.D., 2015. Fate mapping of ptf1a-expressing cells during pancreatic organogenesis and regeneration in zebrafish. Developmental dynamics : an official publication of the American Association of Anatomists. 244(6):724-35.

[322] Mfopou J.K., Houbracken I., Wauters E., Mathijs I., Song I., Himpe E., et al., 2016. Acinar phenotype is preserved in human exocrine pancreas cells cultured at low temperature: implications for lineage-tracing of beta-cell neogenesis. Bioscience reports. 36(3).

[323] Delaspre F., Massumi M., Salido M., Soria B., Ravassard P., Savatier P., et al., 2013. Directed pancreatic acinar differentiation of mouse embryonic stem cells via embryonic signalling molecules and exocrine transcription factors. PLoS One. 8(1):e54243.

[324] Barde I., Zanta-Boussif M.A., Paisant S., Leboeuf M., Rameau P., Delenda C., et al., 2006. Efficient control of gene expression in the hematopoietic system using a single Tet-on inducible lentiviral vector. Molecular therapy : the journal of the American Society of Gene Therapy. 13(2):382-90.

[325] Gossen M., Bujard H., 1992. Tight control of gene expression in mammalian cells by tetracycline-responsive promoters. Proc Natl Acad Sci U S A. 89(12):5547-51.

[326] Cortijo C., Gouzi M., Tissir F., Grapin-Botton A., 2012. Planar cell polarity controls pancreatic beta cell differentiation and glucose homeostasis. Cell reports. 2(6):1593-606.

[327] Greggio C., De Franceschi F., Figueiredo-Larsen M., Gobaa S., Ranga A., Semb H., et al., 2013. Artificial three-dimensional niches deconstruct pancreas development in vitro. Development. 140(21):4452-62.

[328] Rose S.D., Kruse F., Swift G.H., MacDonald R.J., Hammer R.E., 1994. A single element of the elastase I enhancer is sufficient to direct transcription selectively to the pancreas and gut. Molecular and cellular biology. 14(3):2048-57.

[329] Obata J., Yano M., Mimura H., Goto T., Nakayama R., Mibu Y., et al., 2001. p48 subunit of mouse PTF1 binds to RBP-Jkappa/CBF-1, the intracellular mediator of Notch signalling, and is expressed in the neural tube of early stage embryos. Genes to cells : devoted to molecular & cellular mechanisms. 6(4):345-60.

[330] Bonner-Weir S., 2001. beta-cell turnover: its assessment and implications. Diabetes. 50 Suppl 1:S20-4.

[331] Cockell M., Stevenson B.J., Strubin M., Hagenbuchle O., Wellauer P.K., 1989. Identification of a cell-specific DNA-binding activity that interacts with a transcriptional activator of genes expressed in the acinar pancreas. Molecular and cellular biology. 9(6):2464-76.

[332] Harding J.D., MacDonald R.J., Przybyla A.E., Chirgwin J.M., Pictet R.L., Rutter W.J., 1977. Changes in the frequency of specific transcripts during development of the pancreas. The Journal of biological chemistry. 252(20):7391-7.

[333] van der Meulen T., Huising M.O., 2015. Role of transcription factors in the transdifferentiation of pancreatic islet cells. Journal of molecular endocrinology. 54(2):R103-17.

[334] Zaret K.S., 2009. Using small molecules to great effect in stem cell differentiation. Cell stem cell. 4(5):373-4.

[335] Discher D.E., Mooney D.J., Zandstra P.W., 2009. Growth factors, matrices, and forces combine and control stem cells. Science. 324(5935):1673-7.

[336] Johannesson M., Stahlberg A., Ameri J., Sand F.W., Norrman K., Semb H., 2009. FGF4 and retinoic acid direct differentiation of hESCs into PDX1-expressing foregut endoderm in a time- and concentration-dependent manner. PLoS One. 4(3):e4794.

[337] Micallef S.J., Janes M.E., Knezevic K., Davis R.P., Elefanty A.G., Stanley E.G., 2005. Retinoic acid induces Pdx1-positive endoderm in differentiating mouse embryonic stem cells. Diabetes. 54(2):301-5.

[338] Shim J.H., Kim S.E., Woo D.H., Kim S.K., Oh C.H., McKay R., et al., 2007. Directed differentiation of human embryonic stem cells towards a pancreatic cell fate. Diabetologia. 50(6):1228-38.

[339] Yelon D., Stainier D.Y., 2002. Pattern formation: swimming in retinoic acid. Current biology : CB. 12(20):R707-9.

[340] Bhushan A., Itoh N., Kato S., Thiery J.P., Czernichow P., Bellusci S., et al., 2001. Fgf10 is essential for maintaining the proliferative capacity of epithelial progenitor cells during early pancreatic organogenesis. Development. 128(24):5109-17.

[341] Ye F., Duvillie B., Scharfmann R., 2005. Fibroblast growth factors 7 and 10 are expressed in the human embryonic pancreatic mesenchyme and promote the proliferation of embryonic pancreatic epithelial cells. Diabetologia. 48(2):277-81.

[342] Otonkoski T., Beattie G.M., Mally M.I., Ricordi C., Hayek A., 1993. Nicotinamide is a potent inducer of endocrine differentiation in cultured human fetal pancreatic cells. The Journal of clinical investigation. 92(3):1459-66.

[343] Jacquemin P., Yoshitomi H., Kashima Y., Rousseau G.G., Lemaigre F.P., Zaret K.S., 2006. An endothelial-mesenchymal relay pathway regulates early phases of pancreas development. Developmental biology. 290(1):189-99.

[344] Matsuoka T.A., Kawashima S., Miyatsuka T., Sasaki S., Shimo N., Katakami N., et al., 2017. Mafa Enables Pdx1 to Effectively Convert Pancreatic Islet Progenitors and Committed Islet alpha-Cells Into beta-Cells In Vivo. Diabetes. 66(5):1293-300.

[345] Gao T., McKenna B., Li C., Reichert M., Nguyen J., Singh T., et al., 2014. Pdx1 maintains beta cell identity and function by repressing an alpha cell program. Cell metabolism. 19(2):259-71.

[346] Zhu Y., Liu Q., Zhou Z., Ikeda Y., 2017. PDX1, Neurogenin-3, and MAFA: critical transcription regulators for beta cell development and regeneration. Stem cell research & therapy. 8(1):240.

[347] Gradwohl G., Dierich A., LeMeur M., Guillemot F., 2000. neurogenin3 is required for the development of the four endocrine cell lineages of the pancreas. Proc Natl Acad Sci U S A. 97(4):1607-11.

[348] Kaneto H., Miyatsuka T., Kawamori D., Yamamoto K., Kato K., Shiraiwa T., et al., 2008. PDX-1 and MafA play a crucial role in pancreatic beta-cell differentiation and maintenance of mature beta-cell function. Endocrine journal. 55(2):235-52.

[349] Miyatsuka T., Matsuoka T.A., Shiraiwa T., Yamamoto T., Kojima I., Kaneto H., 2007. Ptf1a and RBP-J cooperate in activating Pdx1 gene expression through binding to Area III. Biochemical and biophysical research communications. 362(4):905-9.

[350] Collombat P., Xu X., Ravassard P., Sosa-Pineda B., Dussaud S., Billestrup N., et al., 2009. The ectopic expression of Pax4 in the mouse pancreas converts progenitor cells into alpha and subsequently beta cells. Cell. 138(3):449-62.

[351] Nelson S.B., Schaffer A.E., Sander M., 2007. The transcription factors Nkx6.1 and Nkx6.2 possess equivalent activities in promoting beta-cell fate specification in Pdx1+ pancreatic progenitor cells. Development. 134(13):2491-500.

[352] Schaffer A.E., Taylor B.L., Benthuysen J.R., Liu J., Thorel F., Yuan W., et al., 2013. Nkx6.1 controls a gene regulatory network required for establishing and maintaining pancreatic Beta cell identity. PLoS genetics. 9(1):e1003274.

[353] Yang Y.P., Thorel F., Boyer D.F., Herrera P.L., Wright C.V., 2011. Context-specific alpha- to-beta-cell reprogramming by forced Pdx1 expression. Genes Dev. 25(16):1680-5.

[354] Sosa-Pineda B., Chowdhury K., Torres M., Oliver G., Gruss P., 1997. The Pax4 gene is essential for differentiation of insulin-producing beta cells in the mammalian pancreas. Nature. 386(6623):399-402.

[355] Frandsen U., Porneki A.D., Floridon C., Abdallah B.M., Kassem M., 2007. Activin B mediated induction of Pdx1 in human embryonic stem cell derived embryoid bodies. Biochemical and biophysical research communications. 362(3):568-74.

[356] Kimura A., Toyoda T., Nishi Y., Nasu M., Ohta A., Osafune K., 2017. Small molecule AT7867 proliferates PDX1-expressing pancreatic progenitor cells derived from human pluripotent stem cells. Stem cell research. 24:61-8.

[357] Fomina-Yadlin D., Kubicek S., Vetere A., He K.H., Schreiber S.L., Wagner B.K., 2012. GW8510 increases insulin expression in pancreatic alpha cells through activation of p53 transcriptional activity. PLoS One. 7(1):e28808.

[358] Fomina-Yadlin D., Kubicek S., Walpita D., Dancik V., Hecksher-Sorensen J., Bittker J.A., et al., 2010. Small-molecule inducers of insulin expression in pancreatic alpha-cells. Proc Natl Acad Sci U S A. 107(34):15099-104.

[359] Demeterco C., Beattie G.M., Dib S.A., Lopez A.D., Hayek A., 2000. A role for activin A and betacellulin in human fetal pancreatic cell differentiation and growth. The Journal of clinical endocrinology and metabolism. 85(10):3892-7.

[360] Oh Y.S., Shin S., Lee Y.J., Kim E.H., Jun H.S., 2011. Betacellulin-induced beta cell proliferation and regeneration is mediated by activation of ErbB-1 and ErbB-2 receptors. PLoS One. 6(8):e23894.

[361] Brun T., Franklin I., St-Onge L., Biason-Lauber A., Schoenle E.J., Wollheim C.B., et al., 2004. The diabetes-linked transcription factor PAX4 promotes {beta}-cell proliferation and survival in rat and human islets. The Journal of cell biology. 167(6):1123-35.

[362] Li W.C., Horb M.E., Tosh D., Slack J.M., 2005. In vitro transdifferentiation of hepatoma cells into functional pancreatic cells. Mechanisms of development. 122(6):835-47.

[363] Paz A.H., Salton G.D., Ayala-Lugo A., Gomes C., Terraciano P., Scalco R., et al., 2011. Betacellulin overexpression in mesenchymal stem cells induces insulin secretion in vitro and ameliorates streptozotocin-induced hyperglycemia in rats. Stem cells and development. 20(2):223-32.

[364] Watada H., Kajimoto Y., Miyagawa J., Hanafusa T., Hamaguchi K., Matsuoka T., et al., 1996. PDX-1 induces insulin and glucokinase gene expressions in alphaTC1 clone 6 cells in the presence of betacellulin. Diabetes. 45(12):1826-31.

[365] Yoshida S., Kajimoto Y., Yasuda T., Watada H., Fujitani Y., Kosaka H., et al., 2002. PDX-1 induces differentiation of intestinal epithelioid IEC-6 into insulin-producing cells. Diabetes. 51(8):2505-13.

[366] Dahlhoff M., Wolf E., Schneider M.R., 2014. The ABC of BTC: structural properties and biological roles of betacellulin. Seminars in cell & developmental biology. 28:42-8.

[367] Segerstolpe A., Palasantza A., Eliasson P., Andersson E.M., Andreasson A.C., Sun X., et al., 2016. Single-Cell Transcriptome Profiling of Human Pancreatic Islets in Health and Type 2 Diabetes. Cell metabolism. 24(4):593-607.

[368] Danne T., Cariou B., Banks P., Sawhney S., Strumph P., Writing S.I., 2017. 24-week efficacy and safety of sotagliflozin, a dual SGLT1 and SGLT2 inhibitor, as adjunct therapy to insulin in type 1 diabetes (inTandem2). Diabetologia. 60:S87-S.

[369] Hornby P.J., Du F., Hinke S., Wallace N., Cavanaugh C., Bender C., et al., 2017. SGLT1 Inhibition has Modest Gastrointestinal Consequences in Mice and Rats. The FASEB Journal. 31(1_supplement):673.7-.7.

[370] Richards P., Pais R., Habib A.M., Brighton C.A., Yeo G.S., Reimann F., et al., 2016. High fat diet impairs the function of glucagon-like peptide-1 producing L-cells. Peptides. 77:21-7.

[371] Dyer J., Hosie K.B., Shirazi-Beechey S.P., 1997. Nutrient regulation of human intestinal sugar transporter (SGLT1) expression. Gut. 41(1):56-9.

[372] Ferraris R.P., Diamond J., 1997. Regulation of intestinal sugar transport. Physiological reviews. 77(1):257-302.

[373] Inoue S., Mochizuki K., Goda T., 2011. Jejunal induction of SI and SGLT1 genes in rats by high-starch/low-fat diet is associated with histone acetylation and binding of GCN5 on the genes. Journal of nutritional science and vitaminology. 57(2):162-9.

[374] Inoue S., Honma K., Mochizuki K., Goda T., 2015. Induction of histone H3K4 methylation at the promoter, enhancer, and transcribed regions of the Si and Sglt1 genes in rat jejunum in response to a high-starch/low-fat diet. Nutrition. 31(2):366-72.

[375] Lehmann A., Hornby P.J., 2016. Intestinal SGLT1 in metabolic health and disease. American journal of physiology Gastrointestinal and liver physiology. 310(11):G887-98.

[376] Wright E.M., Loo D.D., Hirayama B.A., Turk E., 2004. Surprising versatility of Na+-glucose cotransporters: SLC5. Physiology. 19:370-6.

[377] Chintalapati C., Keller T., Mueller T.D., Gorboulev V., Schafer N., Zilkowski I., et al., 2016. Protein RS1 (RSC1A1) Downregulates the Exocytotic Pathway of Glucose Transporter SGLT1 at Low Intracellular Glucose via Inhibition of Ornithine Decarboxylase. Molecular pharmacology. 90(5):508-21.

[378] Jo J., Choi M.Y., Koh D.S., 2007. Size distribution of mouse Langerhans islets. Biophys J. 93(8):2655-66.

[379] MacGregor R.R., Williams S.J., Tong P.Y., Kover K., Moore W.V., Stehno-Bittel L., 2006. Small rat islets are superior to large islets in in vitro function and in transplantation outcomes. American journal of physiology Endocrinology and metabolism. 290(5):E771-9.

[380] Papas K.K., Long R.C., Jr., Constantinidis I., Sambanis A., 1996. Effects of oxygen on metabolic and secretory activities of beta TC3 cells. Biochim Biophys Acta. 1291(2):163-6.

[381] Lehmann R., Zuellig R.A., Kugelmeier P., Baenninger P.B., Moritz W., Perren A., et al., 2007. Superiority of small islets in human islet transplantation. Diabetes. 56(3):594-603.

[382] Assefa Z., Lavens A., Steyaert C., Stange G., Martens G.A., Ling Z., et al., 2014. Glucose regulates rat beta cell number through age-dependent effects on beta cell survival and proliferation. PLoS One. 9(1):e85174.

[383] Stamateris R.E., Sharma R.B., Kong Y., Ebrahimpour P., Panday D., Ranganath P., et al., 2016. Glucose Induces Mouse beta-Cell Proliferation via IRS2, MTOR, and Cyclin D2 but Not the Insulin Receptor. Diabetes. 65(4):981-95.

[384] Cerf M.E., 2013. Beta cell dysfunction and insulin resistance. Front Endocrinol (Lausanne). 4:37.

[385] Kim W.H., Lee J.W., Suh Y.H., Hong S.H., Choi J.S., Lim J.H., et al., 2005. Exposure to chronic high glucose induces beta-cell apoptosis through decreased interaction of glucokinase with mitochondria: downregulation of glucokinase in pancreatic beta-cells. Diabetes. 54(9):2602-11.

[386] Maedler K., Spinas G.A., Lehmann R., Sergeev P., Weber M., Fontana A., et al., 2001. Glucose induces beta-cell apoptosis via upregulation of the Fas receptor in human islets. Diabetes. 50(8):1683-90.

[387] Chakravarthy H., Gu X., Enge M., Dai X., Wang Y., Damond N., et al., 2017. Converting Adult Pancreatic Islet alpha Cells into beta Cells by Targeting Both Dnmt1 and Arx. Cell metabolism. 25(3):622-34.

[388] Thorel F., Nepote V., Avril I., Kohno K., Desgraz R., Chera S., et al., 2010. Conversion of adult pancreatic alpha-cells to beta-cells after extreme beta-cell loss. Nature. 464(7292):1149-54.

[389] Spijker H.S., Ravelli R.B., Mommaas-Kienhuis A.M., van Apeldoorn A.A., Engelse M.A., Zaldumbide A., et al., 2013. Conversion of mature human beta-cells into glucagon-producing alpha-cells. Diabetes. 62(7):2471-80.

[390] Lemper M., Leuckx G., Heremans Y., German M.S., Heimberg H., Bouwens L., et al., 2015. Reprogramming of human pancreatic exocrine cells to beta-like cells. Cell death and differentiation. 22(7):1117-30.

[391] Li W.D., Cavelti-Weder C., Zhang Y.Y., Clement K., Donovan S., Gonzalez G., et al., 2014. Long-term persistence and development of induced pancreatic beta cells generated by lineage conversion of acinar cells. Nature biotechnology. 32(12):1223-U79.

[392] Herrera P.L., Huarte J., Sanvito F., Meda P., Orci L., Vassalli J.D., 1991. Embryogenesis of the murine endocrine pancreas; early expression of pancreatic polypeptide gene. Development. 113(4):1257-65.

[393] Mastracci T.L., Sussel L., 2012. The endocrine pancreas: insights into development, differentiation, and diabetes. Wiley interdisciplinary reviews Developmental biology. 1(5):609-28.

[394] Pictet R.L., Clark W.R., Williams R.H., Rutter W.J., 1972. An ultrastructural analysis of the developing embryonic pancreas. Developmental biology. 29(4):436-67.

[395] Guillemain G., Filhoulaud G., Da Silva-Xavier G., Rutter G.A., Scharfmann R., 2007. Glucose is necessary for embryonic pancreatic endocrine cell differentiation. The Journal of biological chemistry. 282(20):15228-37.

[396] McCulloch L.J., van de Bunt M., Braun M., Frayn K.N., Clark A., Gloyn A.L., 2011. GLUT2 (SLC2A2) is not the principal glucose transporter in human pancreatic beta cells: implications for understanding genetic association signals at this locus. Mol Genet Metab. 104(4):648-53.

[397] Gribble F.M., Williams L., Simpson A.K., Reimann F., 2003. A novel glucose-sensing mechanism contributing to glucagon-like peptide-1 secretion from the GLUTag cell line. Diabetes. 52(5):1147-54.

[398] Kuhre R.E., Frost C.R., Svendsen B., Holst J.J., 2015. Molecular mechanisms of glucose-stimulated GLP-1 secretion from perfused rat small intestine. Diabetes. 64(2):370-82.

[399] Parker H.E., Adriaenssens A., Rogers G., Richards P., Koepsell H., Reimann F., et al., 2012. Predominant role of active versus facilitative glucose transport for glucagon-like peptide-1 secretion. Diabetologia. 55(9):2445-55.

[400] Kokrashvili Z., Mosinger B., Margolskee R.F., 2009. T1r3 and alpha-gustducin in gut regulate secretion of glucagon-like peptide-1. Annals of the New York Academy of Sciences. 1170:91-4.

[401] Margolskee R.F., Dyer J., Kokrashvili Z., Salmon K.S., Ilegems E., Daly K., et al., 2007. T1R3 and gustducin in gut sense sugars to regulate expression of Na+-glucose cotransporter 1. Proc Natl Acad Sci U S A. 104(38):15075-80.

[402] Bauer P.V., Duca F.A., Waise T.M.Z., Rasmussen B.A., Abraham M.A., Dranse H.J., et al., 2018. Metformin Alters Upper Small Intestinal Microbiota that Impact a Glucose-SGLT1-Sensing Glucoregulatory Pathway. Cell metabolism. 27(1):101-17 e5.

[403] Abrahamsen N., Nishimura E., 1995. Regulation of glucagon and glucagon-like peptide-1 receptor messenger ribonucleic acid expression in cultured rat pancreatic islets by glucose, cyclic adenosine 3',5'-monophosphate, and glucocorticoids. Endocrinology. 136(4):1572-8.

[404] Xu G., Kaneto H., Laybutt D.R., Duvivier-Kali V.F., Trivedi N., Suzuma K., et al., 2007. Downregulation of GLP-1 and GIP receptor expression by hyperglycemia: possible contribution to impaired incretin effects in diabetes. Diabetes. 56(6):1551-8.

[405] Bergman R.N., 2007. Orchestration of glucose homeostasis: from a small acorn to the California oak. Diabetes. 56(6):1489-501.

[406] Gylfe E., Gilon P., 2014. Glucose regulation of glucagon secretion. Diabetes research and clinical practice. 103(1):1-10.

[407] Starke A., Imamura T., Unger R.H., 1987. Relationship of Glucagon Suppression by Insulin and Somatostatin to the Ambient Glucose-Concentration. Journal of Clinical Investigation. 79(1):20-4.

[408] Ishihara H., Maechler P., Gjinovci A., Herrera P.L., Wollheim C.B., 2003. Islet beta-cell secretion determines glucagon release from neighbouring alpha-cells. Nat Cell Biol. 5(4):330-5.

[409] Rorsman P., Berggren P.O., Bokvist K., Ericson H., Mohler H., Ostenson C.G., et al., 1989. Glucose-Inhibition of Glucagon-Secretion Involves Activation of Gabaa-Receptor Chloride Channels. Nature. 341(6239):233-6.

[410] Jacobson D.A., Wicksteed B.L., Philipson L.H., 2009. The alpha-cell conundrum: ATP-sensitive K+ channels and glucose sensing. Diabetes. 58(2):304-6.

[411] McCrimmon R., 2008. The mechanisms that underlie glucose sensing during hypoglycaemia in diabetes. Diabetic Med. 25(5):513-22.

[412] Miki T., Liss B., Minami K., Shiuchi T., Saraya A., Kashima Y., et al., 2001. ATP-sensitive K+ channels in the hypothalamus are essential for the maintenance of glucose homeostasis. Nature neuroscience. 4(5):507-12.

[413] Thorens B., 2011. Brain glucose sensing and neural regulation of insulin and glucagon secretion. Diabetes Obesity & Metabolism. 13:82-8.

[414] Verberne A.J., Sabetghadam A., Korim W.S., 2014. Neural pathways that control the glucose counterregulatory response. Frontiers in neuroscience. 8:38.

[415] Gylfe E., 2013. Glucose Control of Glucagon Secretion: There Is More to It Than K-ATP Channels. Diabetes. 62(5):1391-3.

[416] Rorsman P., Salehi S.A., Abdulkader F., Braun M., MacDonald P.E., 2008. K-ATP-channels and glucose-regulated glucagon secretion. Trends Endocrin Met. 19(8):277-84.

[417] Unger R.H., Cherrington A.D., 2012. Glucagonocentric restructuring of diabetes: a pathophysiologic and therapeutic makeover. The Journal of clinical investigation. 122(1):4-12.

[418] Jeng C.Y., Sheu W.H., Fuh M.M., Chen Y.D., Reaven G.M., 1994. Relationship between hepatic glucose production and fasting plasma glucose concentration in patients with NIDDM. Diabetes. 43(12):1440-4.

[419] Consoli A., 1992. Role of liver in pathophysiology of NIDDM. Diabetes care. 15(3):430-41.

[420] Scheen A.J., 2016. SGLT2 Inhibitors: Benefit/Risk Balance. Current diabetes reports. 16(10):92.

[421] Ferrannini E., Muscelli E., Frascerra S., Baldi S., Mari A., Heise T., et al., 2014. Metabolic response to sodium-glucose cotransporter 2 inhibition in type 2 diabetic patients. The Journal of clinical investigation. 124(2):499-508.

[422] Staels B., 2017. Cardiovascular Protection by Sodium Glucose Cotransporter 2 Inhibitors: Potential Mechanisms. The American journal of medicine. 130(6S):S30-S9.

[423] Deng S., Vatamaniuk M., Huang X., Doliba N., Lian M.M., Frank A., et al., 2004. Structural and functional abnormalities in the islets isolated from type 2 diabetic subjects. Diabetes. 53(3):624-32.

[424] Donath M.Y., Ehses J.A., Maedler K., Schumann D.M., Ellingsgaard H., Eppler E., et al., 2005. Mechanisms of beta-cell death in type 2 diabetes. Diabetes. 54 Suppl 2:S108-13.

[425] Low J.T., Mitchell J.M., Do O.H., Bax J., Rawlings A., Zavortink M., et al., 2013. Glucose principally regulates insulin secretion in mouse islets by controlling the numbers of granule fusion events per cell. Diabetologia. 56(12):2629-37.

Appendix

Affidavit

I hereby confirm that my thesis entitled: ***"Intestinal stem cells and the Na^+-D-Glucose Transporter"SGLT1": potential targets regarding future therapeutic strategies for diabetes"*** is the result of my own work. I did not receive any help or support from commercial consultants. All sources and / or materials applied are listed and specified in the thesis.
Furthermore, I confirm that this thesis has not yet been submitted as part of another examination process neither in identical nor in similar form.

Eidesstattliche Erklärung

Hiermit erkläre ich an Eides statt, die Dissertation: ***"Intestinale Stammzellen und der Na^+-D-Glukose Transporter SGLT1: potentielle Ansatzpunkte neuartiger Therapien für Diabetes Patienten"*** eigenständig, d.h. insbesondere selbständig und ohne Hilfe eines kommerziellen Promotionsberaters, angefertigt und keine anderen als die von mir angegebenen Quellen und Hilfsmittel verwendet zu haben.
Ich erkläre außerdem, dass die Dissertation weder in gleicher noch in ähnlicher Form bereits in einem anderen Prüfungsverfahren vorgelegen hat.

……

Ort, Datum Unterschrift

Acknowledgement

First and foremost, I would like to express my gratitude to my first supervisor PD Dr. Marco Metzger and my second advisor Professor Dr. Heike Walles. Heike and Marco, I am grateful that you provided me the opportunity to complete my thesis at the Chair of Tissue Engineering and Regenerative Medicine in Würzburg. I would like to thank both of you for the permanent support, the scientific guidance, encouragement and all the time you had for me during the last years.

My sincere thanks also goes to my third supervisor Professor Dr. Frank Edenhofer. Frank, I thank you very much for all scientific suggestions, the support from you and your laboratory members and all the inputs and feedbacks during my time as PhD student.

Besides my three thesis committee members, I would like to express my full gratitude to my “fourth” supervisor Dr. Daniela Zdzieblo. Daniela, your endless support, your knowledge and your passion for science were highly important for me to finish my PhD thesis and to become the scientist I am now. Especially your positive working attitude and the “everything is possible” mentality were inspirational and the driving force during my time in the laboratory. I also thank you for being a great person and for all the amazing moments during conferences, at TERM, on the “alte Mainbrücke” and in Würzburg.

I would like to thank all my fellow labmates and the secretary at TERM for the amazing time and for all your support. The PhD time in Würzburg was tough work but also an excellent time with many positive emotions and good people in a wonderful environment. I thank all my colleagues and the friends I found in Würzburg for this unforgettable time!

I especially want to thank Miguel Rodrigues, Davide Confalonieri, Ives Mattos-Bernardelli, Antje Appelt-Menzel, Corinna Rosenbaum, Matthias Schweinlin, Sebastian Kress, Sebastian Schürlein, Claudia Göttlich, David Fecher, Constantin Berger, Christian Lotz, Anna Schliermann, Christoph Rücker, Ram Ramkumar, Heike Oberwinkler, Renate Bausch, Alevtina Cubukova, Lina Kötzner and Dr. Joachim Nickel for all the help, the discussions during my time in the laboratory and mainly for being amazing people and friends!

I further want to thank all collaboration partners and supporters from other laboratories. Many thanks goes to Professor Dr. Roland Brock, Sander van Asbeck and Dr. Marco Favretto for the help and support during my stay in Nijmegen. In addition I want to thank Dr. Philipp Wörsdörfer and Dr. Katharina Günter from the Institute for Anatomy and Cell Biology in Würzburg. I am grateful for all good moments and all the help during my thesis while working with embryonic stem cells or for the generation of synthetic mRNAs. Furthermore, I want to thank Professor Dr. Hermann Koepsell, Dr. Alexandra Friedrich, Professor Dr. Christoph Otto and Manuela Hofmann for all their support and inputs during the preparation of the SGLT1-manuscript.

I am grateful that I got financial support from the “Bayern FIT Programm” of the Bavarian state government, Germany. Without this funding it would not have been possible to conduct my thesis here at TERM.

I deeply appreciate all the support from my friends all over the world who were always supporting me in good and bad times! Without all these people and their positive influence I would not be the person I am right now!

Last but not least, I would like to express my gratitude to my family: my parents, my two sisters, my aunt Ilse Antener and my grandparents. In particular, I would like to thank to my parents for the support throughout my life and all the love I have got. Further, I thank my grandparents and my aunt Ilse for being great personalities that I will always look up to. *Merci viu mau für aues!*

At the end, I owe my deepest gratitude to Claudia. Your happiness and unconditional love pushed me forward during the last weeks, months and years! “*Happiness is only real when shared*” – I know that we will share much more happiness together!

Grazie mille per tutto!